A STUDY OF SEISMICALLY RESISTANT ECCENTRICALLY BRACED STEEL FRAME SYSTEMS

by

KAZUHIKO KASAI

EGOR P. POPOV
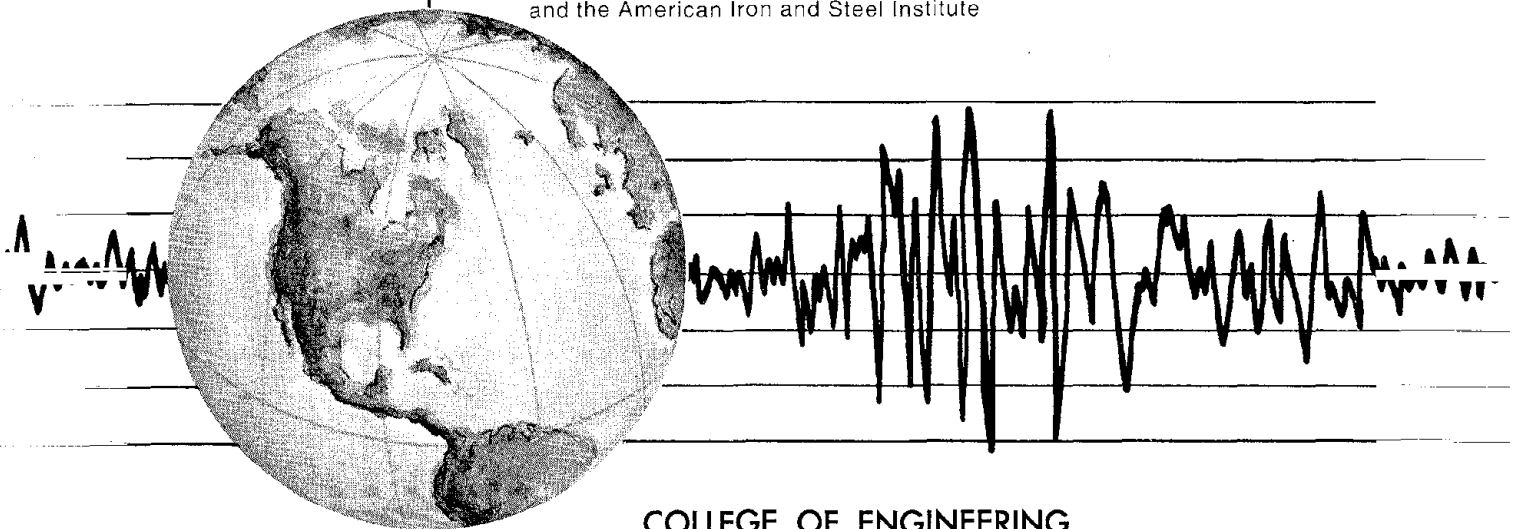
COLLEGE OF ENGINEERING

UNIVERSITY OF CALIFORNIA · Berkeley, California

For sale by the National Technical Informa-
tion Service, U.S. Department of Commerce,
Springfield, Virginia 22161.

See back of report for up to date listing of
EERC reports.

A STUDY OF SEISMICALLY RESISTANT

ECCENTRICALLY BRACED STEEL FRAME SYSTEMS

by

Kazuhiko Kasai

and

Egor P. Popov

A STUDY OF SEISMICALLY RESISTANT

ECCENTRICALLY BRACED STEEL FRAME SYSTEMS

ABSTRACT

Because of some of the inherent advantages formerly overlooked and recently pointed at, Eccentrically Braced Frames (EBFs) have been rapidly accepted in practice. A number of major buildings in California have already been constructed using this approach.

EBFs employ the braces with deliberately large eccentricities with respect to the beam-column joint. The eccentricity is introduced to provide a ductile fuse which will prevent hazardous brace buckling at extreme loads. The axial forces in the braces are transmitted to the columns through bending and shear action by a portion of the beam called the "active link". The active link provides a superior energy dissipation capability through its inelastic action. The EBF must, then, be designed so that plastic action of the active link occurs on overloading of the structure.

The first part of this report is based on a perfectly plastic idealization of EBF behavior :

Basic plastic theory for an EBF force field and ideal rigid-plastic displacement field are explained. Based on these, a simple method for obtaining the lateral load carrying plastic capacity of an EBF is proposed.

Further, the proposed plastic theory is employed for various plastic problems of EBFs, where the accuracy of the theory is demonstrated by comparing

with elasto-plastic finite element analysis results. It is shown that link length plays a dominant role in EBF plastic capacities and plastic mechanisms. The basic non-linear behavior of EBFs is summarized and important factors to be considered in determining EBF basic configuration are enumerated. Finally, a new plastic design method for EBFs is proposed. Because of the simplicity of the proposed method, it was possible to write a plastic design computer program for a general design of EBFs. Some example frames were designed by applying this program, and the accuracy of the method is demonstrated by comparisons with elasto-plastic solutions.

The second part of this report includes the effect of link inelastic deformation on both link and EBF behavior. Strain-hardening and various failures of the link are discussed :

First, the experimental program for a subassemblage simulating EBF action is described. The observed cyclic behavior of different length links tested with or without simultaneously acting axial forces are reported.

Next, the experimental results are analyzed with emphasis on the influence of the link length on the performance. Moment, shear, and axial force interaction, as well as the effect of strain-hardening on moment redistribution, energy dissipation, and flange and web buckling are considered. Based on these results, the ultimate state design for cyclically loaded links is proposed.

Further, a simple new criterion for web stiffener spacing to prevent premature cyclic web buckling is proposed using the secant modulus method based on experimental data for 30 links. The application of this criterion to an EBF ultimate state design is also discussed.

TABLE OF CONTENTS

ACKNOWLEDGEMENT

CHAPTER 6: EXPERIMENTAL STUDIES ON GENERAL BEHAVIOR OF SHEAR

LINKS

CHAPTER 7: ANALYSIS OF EXPERIMENTAL RESULTS

CHAPTER 8: CYCLIC WEB BUCKLING CONTROL FOR SHEAR LINK BEAMS

APPENDIX A: ADDITIONAL INFORMATION FROM EXPERIMENTAL STUDY

APPENDIX B: INELASTIC MODELING OF CYCLICALLY LOADED LINK

LIST OF FIGURES

LIST OF TABLES

CHAPTER 1

INTRODUCTION

1.1. General

It is now generally recognized that seismic design of buildings should satisfy at least two fundamental requirements. First, the structure must behave elastically and protect relatively brittle non-structural components against minor earthquake ground shaking. Therefore, a structure should have sufficient strength and elastic stiffness to limit structural displacements, such as interstory drift. Second, the structure must not collapse in a major earthquake. For this case, significant damage of the structure and non-structural components is acceptable. In order for a structure not to collapse and thereby minimize the loss of life, it must have large energy dissipation capacity during large inelastic deformations. In general, structural systems which exhibit stable hysteretic loops perform well under the large inelastic cyclic loadings characteristics of major earthquakes. Such stable hysteretic characteristics of a structure can be obtained provided that the structural members and joints are designed to posses sufficient ductility.

1.2. Conventional Seismic Resistant Steel Frames

For high and medium rise buildings, structural steel has been used extensively due to its excellent strength and ductility properties. In seismic design of such steel frames, either Moment Resisting Frames (MRFs) or Concentrically

Braced Frames (CBFs) were mainly used in the past.

Moment Resisting Frames (MRFs) : - Fig. 1.1 illustrates the typical configuration of a moment resisting frame (MRF). During a major earthquake, in an MRF the energy dissipation is mainly obtained through inelastic action in the beam-column joints, and such frames generally have considerable ductility if the beams and columns are proportioned to meet the so-called strong column-weak girder design concept, and proper details are implemented in the beam-column joints. As illustrated in Fig. 1.2, the deformation mechanism of an MRF consists of three major components : One is due to column flexure, another is due to beam flexure, and the other due to panel zone distortion.

It has been recognized that although the column flexure is not of significant magnitude, due to the large flexural deformation of the beams, an MRF tends to be laterally flexible in the elastic range [71]. Therefore limiting the elastic interstory drift often governs the seismic design of the frame. The commonly used solution for this problem is to increase the beam sizes, which makes this type of frame more costly and taller. Further, past experimental and analytical studies such as given in Refs. 42 and 43 indicate that due to the moment transferred from beams to columns, large shear forces are induced in the beam-column joint panel zone. Accordingly, in the inelastic range, this frame tends to show considerable panel zone shear distortions such as shown in Fig. 1.2, which create at least two serious problems. First, if the panel zone distortion is excessively large, the column flange at the beam-column connection would distort, causing large stress concentrations in the weld regions connecting beam flanges to the column flanges. Recent experimental research [72] demonstrated that this results in sudden weld fractures. Second, large inelastic panel zone distortion increases the story drift significantly. This will result

in a large P-Δ effect making this type of framing more susceptible to instability. In order to alleviate these problems, web doubler plates frequently have to be used at the beam-column panel zones, which further increases the cost of this type of frame.

Concentrically Braced Frames (CBFs) : - As Fig. 1.3 illustrates, a vertical truss system is formed in concentrically braced frames (CBFs) utilizing a set of diagonal braces placed concentrically at the joints, and the braces provide effective resistance against lateral loading during minor earthquakes. In general, CBFs have sufficient stiffness to limit elastic interstory drift, without the costs involved with MRFs discussed above. However, when overloading occurs due to a major earthquake, conventionally designed braces can buckle exhibiting the plastic mechanism such as shown in Fig. 1.4. Experimental study on the behavior of brace struts under cyclic axial loading indicated that their carrying capacity can significantly decrease under severe cyclic loads, resulting in a large loss of energy dissipation capacity, which can be well recognized from Fig. 1.5 [7]. This brace behavior directly affects the CBF global behavior, where, as illustrated in Fig. 1.6, the CBFs become unstable for a relatively small inelastic deformation level and their lateral load carrying capacity dramatically decreases as the number of cyclic excursions and/or cyclic displacements increases [52].

In order to improve the performance of CBFs, some alternative design schemes have been proposed [87] : By making the slenderness ratio of the brace larger, the decay in the compressive strength of braces under cyclic loading can be reduced. Also, for the commonly used concentric K-brace frame with braces meeting at the middle of a beam as illustrated in Fig. 1.4, the use of a larger beam to assure that it will remain elastic under severe loading

improves the behavior of such frames. However, within the economic restrictions, it is doubtful that either one of the above approaches yields sufficient improvement in the performance of CBFs for severe cyclic loadings.

1.3. Eccentrically Braced Frame System

The two basic requirements for seismic design, high stiffness at working load levels and large ductility at rare but severe overloads, are difficult to satisfy when the above conventional frames are used. On the contrary, Eccentrically Braced Frames (EBFs) offer an economical steel framing system satisfying both requirements.

A typical arrangement of this frame is shown in Fig. 1.7, and several possible types of EBFs are illustrated in Fig. 1.8, where, as indicated, they will be called *D-brace frame*, *K-brace frame*, and *V-brace frames* respectively. In all such frames, the vertical components of axial forces in the braces are held in equilibrium by shear and bending moments in short beams of length *e* — *the active links*. As shown in Fig. 1.9, these active links, which are designed to remain elastic at working loads deform inelastically on overloading of the structure, thereby dissipating large amount of energy. In this system the hazardous brace buckling can be entirely prevented since the link acts as a fuse to limit the brace axial force, which can be understood by comparing Fig. 1.9 with Fig. 1.4 where the mechanism of a CBF is shown. Also, this frame has a much greater lateral resisting capacity than that of an MRF if the beam sections used are the same.

The use of the link in spread K-braces for seismic application was studied in 1972 by Fujimoto [19]. In 1978, experimental and analytical results on diagonally braced frames were reported by Roeder and Popov [84], providing a

renewed and strong interest in this type of framing. This report showed that an EBF can be almost as stiff as a CBF when an appropriate eccentricity is assigned for the braces, and yet behaves in a very ductile manner at large cyclic overloads and the active links will dissipate great amounts of energy by inelastic action. This can be recognized from Fig. 1.10 which shows the cyclic load-deformation relationships obtained from an experiment on a one-third size EBF [54], where the remarkably stable hysteretic behavior of the EBF can be recognized and can be well contrasted with the unstable hysteretic behavior of the CBF shown earlier in Fig. 1.6. Since 1978 to date extensive research on active links and EBFs has been conducted at Berkeley resulting in numerous suggestions for implementing EBFs in practice for realistic design of earthquake-resistant structures. While the research is still in progress, a number of major buildings employing EBFs have been constructed or designed in California due to their attractive characteristics, and demand for this framing system is likely to increase in the near future. For these reasons, it is very important that a consistent design and analysis method for EBFs reflecting the most recent research should be provided. This report attempts to answer this need.

1.4. Statement of the Problem

Plastic Design and Analysis for EBFs : - Past research has shown that the active link provides a superior energy dissipating capability through its inelastic action [84,54,32,53,40]. For regions of high seismic risk, EBFs must have adequate lateral load carrying plastic capacity and must exhibit the mechanism where the plastic action of the active link occurs on overloading of the structure. Members other than links should be proportioned so as to distribute the large earthquake input energy to as many links as possible.

In order to understand EBF behavior, then, the plastic analysis of EBFs based on the active link plastic behavior is the most appropriate and logical approach to follow. The basic concept for such an analysis method was explained previously [54], and based on current development on active link ideal plastic theory and analytical study [32,40], it has been felt that a more general and yet simple method can be developed.

Also, an earlier paper by the author [40] indicated that the configuration of an EBF greatly influences its plastic behavior and performance, and, eventually, the economy of the framing system. By performing further analyses and design studies, further information on this aspect was obtained. , Therefore for the initial determination of an EBF configuration, it was considered to be of practical importance to summarize relevant relationships between frame topology and performance.

Further, since an elastic design method does not necessarily guarantee the frame plastic capacity and the mechanism sought, a direct plastic design method which proportions the members to meet the required plastic capacity and the desired mechanism is essential for EBF design. The two plastic design methods for EBFs reported earlier [54,84] require a large number of iterations for arriving at realistic member force estimates. Therefore, it was necessary to develop another approach more accurate and simple to use.

Ultimate Design and Analysis for EBFs : - Although the desired yield capacity and plastic mechanism of an EBF may be assured by the plastic design method, the behavior of active links during increasing plastic deformation should be considered for the ultimate state design. If no premature failure of the link occurs, due to the plastic deformation of the link the link capacity will increase because of the inherent material strain-hardening. Accordingly, the

capacity of an EBF may beneficially increase, however, since this also affects the redistribution of the member forces in the structure, the plastic mechanism initially obtained may be altered, and damage might be eventually concentrated on the less ductile members during further cyclic loadings. This has to be included for a good ultimate design of an EBF requiring the knowledge of the link cyclic strain-hardening behavior. In past experimental studies the cyclic strain-hardening effect on link shear capacity was well recognized and some proposals to include this for EBF design have been made [54,84]. However, the effect on link moment capacity and the manner of moment redistribution has not been investigated to-date in spite of its importance in EBF design. Therefore analytical and experimental study of this aspect was needed.

Undesirable behavior in the link and EBF may develop during increasing plastic deformation if the link is not appropriately proportioned or detailed, since there is a possibility of various premature link failure modes. Such occurrences must be prevented in order to assure ductile behavior of the link and EBF up to the required ultimate deformation level. If this is not done a substantial loss of link energy dissipation capability could occur at an early plastic deformation level of the structure and the structure may eventually collapse since EBF behavior is mostly dependent on the active link.

One of such failure modes could be local flange buckling of the link. In the instance that an active link, in addition to its usual function, is simultaneously subjected to an axial force, the possibility of such a buckling mode may become particularly acute. To date, no design recommendation has been provided for link flange buckling failure, therefore analytical and experimental studies were needed, and some ultimate state design criteria was necessary to avoid this failure as well as flange fracture.

Another possible failure mode of a link is web buckling. An active link yielding primarily in shear in the web has been mainly studied at Berkeley and used in practice. Such a link has been shown to be a much better energy dissipator than a link yielding in moment [32,40,53,54,84]. However, for such links it has been experimentally confirmed that web buckling due to poor stiffening causes a substantial loss of link energy dissipation capacity during subsequent cyclic loadings. Although a criterion for web stiffener spacing for severe cyclic loadings was proposed previously [32], it was found to lack accuracy and ease of application. Therefore, because of the importance of the web buckling problem, a more satisfactory criterion for web stiffener spacing to control cyclic web buckling was clearly necessary.

Furthermore, a dynamic analysis of EBF is much needed in order to examine the design result and reliability of the conclusions obtained based on the study of EBF behavior subjected to pseudo-static loads. An accurate analysis of such frames relies on good modeling of the active links. None of the earlier models [32,84,98] were found to be either sufficiently accurate or efficient to be used for dynamic analysis of EBFs subjected to earthquake ground motions. A new link model for simulating random cyclic strain-hardening behavior was much needed.

1.5. Objectives

As explained above, many problems which are extremely important for EBF design and analysis have remained unresolved to-date. In the present investigation, much effort was made to answer these problems. The objectives of the present study may be summarized as follows :

(1) to develop a simple analysis procedure of an EBF based on the perfectly plastic idealization of the active link,

(2) to summarize the basic nonlinear behavior of EBFs and clarify basic parameters which influence the EBF inelastic behavior,

(3) to develop an EBF plastic design method which is accurate and simple to use,

(4) to experimentally investigate the link cyclic behavior and clarify the strain-hardening effect on the plastic capacity of the link,

(5) to develop the criteria for link ultimate state design against various flange failures, including the additional effects from axial loading on the link,

(6) to study the past and present link test results and establish a new web stiffener spacing design criterion to control cyclic web buckling of a link,

(7) to develop a simple and accurate mathematical link model under random cyclic loading.

1.6. Scope

The first part of this report consists of Chapters 2 to 5, which are based on a perfectly plastic idealization of EBF behavior. The second part includes the effect of link inelastic deformation on both link and EBF behavior. Strain-hardening and various failures of the link are discussed in Chapters 6 to Chapter 8. In order to fulfill the aforementioned objectives, for each chapter, the following studies were performed:

In Chapters 2 and 3, basic plastic theory for an EBF force field and ideal rigid-plastic displacement field are explained, and based on these, a simple method for obtaining the lateral load carrying plastic capacity of an EBF is proposed. Basic differences in the plastic characteristics of various EBF types are

discussed.

In Chapter 4, the theory established in Chapters 2 and 3 is employed for various plastic problems of EBFs, where the accuracy of the theory is demonstrated by comparing with elasto-plastic finite element analysis results. It will be shown that link length plays a dominant role in EBF plastic capacities and plastic mechanisms. Based on numerous analytical results for various EBFs, the basic non-linear behavior of EBFs is summarized and important factors to be considered in determining EBF basic configuration for preliminary design are enumerated.

In Chapter 5, a new plastic design method for EBFs is proposed. Because of the simplicity of the proposed method, it was possible to write a plastic design computer program for a general design of EBFs. Some example frames were designed by applying this program, and the accuracy of the method is demonstrated by comparisons with elasto-plastic solutions.

In Chapter 6, the experimental program for a subassemblage simulating EBF action is described. The observed cyclic behavior of different length links tested with or without simultaneously acting axial forces are reported.

In Chapter 7, the experimental results are analyzed with emphasis on the influence of the link length on the performance. Moment, shear, and axial force interaction, as well as the effect of strain-hardening on moment redistribution, energy dissipation, and flange and web buckling are considered. Based on these results, the ultimate state design for cyclically loaded links is proposed.

In Chapter 8, a simple new criterion for web stiffener spacing to prevent premature cyclic web buckling is proposed using the secant modulus method based on experimental data for 30 links. The application of this criterion to an EBF ultimate state design is also discussed.

In Appendix, brief discussions are made on the general analysis of EBF's having active links appropriately stiffened against web bucklings. An accurate analysis of such frames relies on good modeling of the active links. Some shear link models previously developed are reviewed first, and a new simple and accurate shear link model for simulating random cyclic strain-hardening behavior is discussed.

CHAPTER 2

IDEAL PLASTIC THEORY FOR

EBF ANALYSIS AND DESIGN

2.1. Research Trends in Seismic Design of Buildings

Currently, the revised Japanese Seismic Code [37] requires that except for small buildings of a regular configuration , all structures designed elastically must be checked for their compliance with the required lateral load plastic carrying capacity. It is considered that the plastic capacity of a building is one of the key factors in determining the behavior of a structure under earthquake excitations.

Single-Degree-of-Freedom Modeling : - Historically, the need for ductility in seismic design was first verified by a study considering the structure as an equivalent single degree-of-freedom elasto-plastic system and analyzing its response for recorded earthquake ground motions [96]. Further development along this direction continues to-date, and in these studies, the ductility, i.e., the ratio of inelastic displacement to elastic limit displacement of the system, was related to the maximum acceleration of the system under seismic excitations depending on its natural period. By comparing these findings with the elastic spectrum analyses, some convenient rules for deriving an appropriate inelastic spectrum from the elastic spectrum were established. Since the maximum acceleration derived from the inelastic spectra can be expressed as the plastic capacity divided by the mass of the system, the above studies provide

basic information on the effect of plastic capacity on the ductility of the system under seismic excitation. Inelastic spectra have been frequently used to determine the the lateral forces to be used in a seismic design.

In some of the earlier research it was proposed to perform elastic dynamic analyses of buildings using inelastic spectra [63]. However, based on some non-linear dynamic analyses of buildings such as in Ref. 12, it has been found that simple application of the above theories does not necessarily predict well the response of buildings with many degrees-of-freedom systems whose behavior is complex. Nevertheless, in order to determine the applicability of the single degree-of-freedom approach, extensive research has been conducted in the past. From the analytical results reported in Refs. 49, 60, and 91, it appears that multi-story buildings with strong columns respond like a rigid-plastic mechanism with hinges in the beams. Recognizing this, it is shown in Ref. 91 that the drift and the corresponding ductility, as well the corresponding base shear, can be simply predicted with a remarkable accuracy by analyzing an equivalent single degree-of-freedom system subjected to a dynamic excitation. Similar modeling has been tried for rather tall buildings [68,85,91] with arbitrary strength ratios between beams and columns. Recently, for buildings with irregular distribution of stiffness and plastic capacity through the height, Moehle [57,58] proposed a rule for predicting building inelastic displacements based on the elastic response spectrum. His method was verified by analytical and experimental work.

Multi-Degree-of-Freedom Modeling : - An alternative dynamic analysis of buildings is based on the multi-degree of freedom modeling of the structure, typically with one degree-of-freedom per story. Earlier, Penzien [66] showed that the story plastic capacity distribution through the building height

influences the deformation pattern of the building. More recently, Akiyama [2] also demonstrated that the key parameters for a building deformation pattern and the damage distribution are the plastic capacity distributions along the height if strong columns are used, whereas if weak columns are employed it is the distribution of story stiffness along the height that determines the damage distribution. Based on numerous analytical studies for steel frames of selected types, he proposed some rules for predicting the damage distribution and response of buildings based on the above parameters.

Building Dynamic Behavior Prediction Using Plastic Analysis : - In all of the above approaches an estimate of building plastic capacities along the height is essential for predicting the inelastic dynamic response of a building. Either the elasto-plastic nonlinear analyses or the simpler limit analyses can be used to estimate the plastic capacity of the frames. Moreover, the use of fictitious static loadings was found to be sufficiently accurate for predicting the non-linear dynamic response.

2.2. Plastic Analysis for Seismic Design

In spite of the necessity for estimating the plastic capacity of a building indicated by the on-going research, current design practice is largely based on elastic analysis with application of the inelastic spectrum. The members of a structure are determined such that they remain elastic at the level of the lateral forces found from an inelastic spectrum which is reduced from the elastic spectrum by postulating an expected global structural ductility.

Advantage of Plastic Analysis for Seismic Design : - Even in applying this simplified method, a better design can be achieved if one knows both the plastic

capacity and the corresponding plastic mechanism of the structural frame from plastic analysis. Since the inelastic spectrum can give the relationships between the plastic capacity and the global structural ductility demand, knowing the plastic capacity of a frame results in a re-evaluation of the ductility factors initially assumed in design, and thereby a better estimate can be made for the degree of conservatism used in the design. Also, such an analysis provides a better insight as to how the plastification is distributed throughout the building at critical loading. The plastic mechanisms which form hinges in the members with poor cyclic ductility are undesirable since this can cause rapid deterioration of the plastic capacity of the structure. As stated in Refs. 50 and 70, the assumption of elastic-perfectly plastic hysteretic behavior of structural systems for obtaining inelastic response spectra makes the use of these spectra for structures with degenerate hysteretic loops questionable. The undesirable plastic mechanisms causing such behavior of a frame can be detected and avoided by re-proportioning the members if it is plastically analyzed. As discussed in the previous section, using a fictitious static loading for determining the plastic capacity is also of great value in predicting the dynamic behavior of a structure.

Conventional limit analyses have been often used in the past for estimating the plastic capacity of a frame. According to Refs. 57 and 58, a simple load pattern distributed triangularly from the top of the structure to the bottom gave a satisfactory measure of the plastic capacity of a structure and was useful for predicting the inelastic dynamic response. In the current Japanese code [37] the same lateral load distribution as in the initial elastic design is given for use with conventional plastic limit analyses.

Plastic Analysis and Design of EBFs : - For a good design of EBFs the plastic capacity should be determined requiring the knowledge of active link plastic behavior. In this chapter, the behavior of ideal-plastic active links is discussed first on the basis of previous studies. As shown by Manheim [54] in his investigations of EBF mechanisms, the strong column design with no brace buckling develops the optimum plastic capacity and stability of a structure. Such mechanism which impose plastic action in the beams can be obtained if EBFs are designed plastically as discussed in Chapter 5.

In order to discuss these desirable *energy dissipation mechanisms*, (in plastic analysis commonly known as collapse mechanisms), a first order rigid-plastic displacement field will be adopted following the conventional limit analysis procedures. Both exact and approximate formulations of such mechanisms will be given for various types of EBFs. Using this development, the methods for estimating the plastic capacity of EBFs and the plastic deformation demand on the members are proposed.

2.3. Ideal Plastic Behavior of Active Links

Basic Definition of Links and Plastic Hinges : - The performance of EBFs largely depends on the active link. As shown in Fig. 2.1, for a well-designed structure the inelastic activity is widely distributed so that a large portion of the energy generated by an earthquake can be dissipated. Based on recent analytical studies [40], the classification of ideal plastic active links given earlier in Ref. 74 is somewhat modified. It is convenient to identify three types of hinge shown in Fig. 2.1, as follows:

(1) Plastic hinges developing moment M_p [Hinges (1)].

(2) Plastic hinges developing moment larger than M_p^* and less than M_p which are simultaneously subjected to relatively high shear [Hinges (2)].

(3) Plastic hinges with moments equal to or less than M_p^* accompanied by web yielding in shear of V_p [Hinges (3)].

The basic quantities M_p^*, M_p, V_p associated with the above hinges are defined as follows:

$$M_p = \sigma_y \, Z \tag{2.1}$$

$$M_p^* = \sigma_y \, (d - t_f) \, (b_f - t_w) \, t_f \tag{2.2}$$

$$V_p = \frac{\sigma_y}{\sqrt{3}} \, (d - t_f) \, t_w \; . \tag{2.3}$$

where

M_p = plastic moment capacity of a beam,

M_p^* = plastic moment capacity of a beam reduced by shear,

V_p = plastic shear capacity of a beam,

σ_y = yield strength of steel,

Z = plastic section modulus,

d, t_f, t_w, b_f = depth, flange thickness, web thickness, and flange width of a beam, respectively.

Fig. 2.2 shows a typical moment-shear (M-V) interaction curve for a steel wide flange beam section. In terms of M_p, M_p^*, and V_p the curve can be approximated by Neal's expressions as follows [61]:

$$V \approx V_p \qquad (M \leq M_p^*). \tag{2.4}$$

$$\left[\frac{M - M_p^*}{M_p - M_p^*} \right]^2 + \left[\frac{V}{V_p} \right]^2 = 1 \qquad (M \geq M_p^*). \tag{2.5}$$

Considering the equilibrium for the link shown in Fig. 2.3 with the flanges in an axially plastic state, and the web in a shear plastic state, the *maximum shear hinge length* b^* based on ideal plastic theory is expressed as

$$b^* = \frac{2M_p^*}{V_p} \tag{2.6}$$

If a link is shorter than b^*, Figs. 2.2 and 2.3 show that link web yields in shear. Such a link is called a "shear link", and hinges formed conform to classification 3 above. In contrast with what is commonly called *moment hinge* (for example, see Ref. 80), for shear links the hinge is termed a *shear hinge* [54]. Previously [32,53,84] it was shown that shear links offer excellent ductility under cyclic loadings if appropriately sized and spaced web stiffeners are provided to prevent inelastic web buckling. Also, experimental and analytical studies [32,40] have demonstrated that shear links provide larger dissipation of energy than links whose lengths are larger than b^* in which the hinges will form in the manner described for types 1 or 2 above. A link having a hinge of type 1 is called a "moment link", whereas a link with a hinge of type 2 will be termed an "intermediate link".

It has been experimentally verified [32] that due to the high shear force which develops in a shear link most of the inelastic shear deformation is due to the inelastic shear strains in the web. On the other hand, due to the high end moments in a moment link, the inelastic axial strains in both flanges and web increase the link curvature at the ends in agreement with ordinary beam theory. The moment links are sufficiently long such that no plastic shear deformation of the web takes place. For an intermediate link, whose length is between those of the shear and the moment links, the inelastic deformation is due to both shear and moment mechanisms. For these reasons the normality rule often used in plasticity was applied in Ref. 32 to the yield surface in the M-

V space such as shown in Fig. 2.2. According to this rule, region 1 of the M-V yield surface shows that the link deformations are due to the increase of curvature conjugate with the moment, whereas region 3 suggests that most of the link deformations are due to shear deformation conjugate with the shear force.

Based on the above considerations the active links of the energy dissipation mechanisms for EBFs shown in Figs. 2.1(a) and (b) are designated types 1 through 3. In Fig. 2.1(a), the hinge on each active link with a length $e < b^*$ can be classified as type 3. The single hinge at the left end of the roof beam is of type 1 if axial force in the beam is not significant. The hinges at the left ends of the links of length e^* on the 2-nd and 3-rd floors are type 2. In Figure 2.1(b), the hinges on each active link with a length $e < b^*$ are of type 1. Column hinges at the ground level in both frames have moment capacities reduced by the axial forces. From this point of view, the kinematic fields shown in the above two figures are approximate, as they do not take into account the mechanism combining the bending and axial deformation such as discussed in Ref. 25 and 93. Since for the theories developed in this report the axial deformations concentrated at the column base plastic hinges do not play a significant role, neglecting them results in analytical simplification.

It is to be noted that the moment capacities at the two hinges of type 2 in Fig. 2.1(a) depend on the magnitude of the shear forces (see Fig. 2.2). Typically the braces interconnecting the links of length e in the floor above with the lower links of length e^* will transfer most of the shear force in the upper link to the lower link. For the lower link the required link capacity can be expected to be equal or to be somewhat greater than that for the link in the floor above. Therefore if a shear link is used at the floor above, the shear force in the lower link is approximately equal to or slightly less than the shear capacity of the lower link. Accordingly, from Fig. 2.2 it follows that the moments at type 2

hinges are M_p^* or slightly larger.

Link End Moments in the Limit State : - According to the ideal plastic theory adopted in Refs. 32 and 54, active links in the limit state should have equal end moments since the link is subjected to the same shear and both of its ends develop large plastic deformations. Equal end moments reach the same point on the M-V yield surface such as shown in Fig. 2.2. The presumably equal end moments are of great importance for limit analysis of EBFs. In designing members, additional consideration is needed for estimating link end moments. A further discussion of this problem is given in Chaper 5 as well as Chapters 6 and 7 where the strain-hardening of steel and its effect on the link end moments is considered.

Axial Force Effect on the Link Capacity : - It has been recognized that in usual EBF design the axial force in the link is small. However, as will be pointed out in Chapter 3, depending on the arrangement of the EBF bay in the global structure, a large axial force may develop in the link. For such cases, it is possible to adopt the ideal plastic solution of the moment-shear-axial force interaction proposed by Neal [62] or Kusuda [45] for determining the link capacity. However these solutions are too complex for use in actual design. As will be discussed in Chapter 6 and 7, an experimental study was undertaken to determine the axial force effect on the link capacity and a simple relationship for this effect including strain-hardening was obtained. This problem will not be discussed in this chapter, since, as will be shown later, the axial force effect is usually small.

2.4. Energy Dissipation Mechanisms and Link Deformation Demand

Limit analysis of steel frames is usually concerned with determining collapse mechanisms with plastic hinges in the assemblies of rigid-plastic members [3]. Such collapse mechanisms provide a good basis for a simplified analysis of structures. Using this approach for estimating the upper bound limit load of a structure, the designer can select a collapse mechanism which can sustain the maximum load satisfying design requirements, such as the strong-column weak-beam concept, and find the corresponding member strengths. It also enables one to estimate the member local ductility demand by studying the global displacement of a structure in the ultimate limit state [54].

In this section the rigid-plastic displacement fields of EBF's based on collapse mechanisms will be discussed, which in seismic design takes on the meaning of energy dissipation mechanisms. Previously Manheim [54] determined such a displacement field for two 3-story EBF examples of particular types. The present study offers an alternative approach which is more general and is simpler to apply. The proposed solution could be used for an EBF of any number of stories and of several types. It also includes the effect of panel zone width in beam-column joints. When the panel zone does not significantly deform in conformity with good practice [72], this method is applicable.

Rigid-Plastic Displacement Field for D-brace Frame : - Fig. 2.4 shows a rigid-plastic displacement field for a portion of the D-brace frame of Fig. 2.1. Some latitude in selecting the collapse mechanism is possible subject to kinematic constraints. For the selected mechanism to occur, the column should remain elastic except at the column bases.

Fig. 2.4(a) shows the typical mechanism at an i-th level of an N-story D-brace frame where the points A_i, B_i, C_i, D_i are, respectively, the right end of a

right link, the left end of the same link at a brace, the right end of a left link at a brace, and the left end of a left link. In order to define the geometry of this frame, the following topological parameters are required: The right link length $\overline{A_i B_i}$ is called e_i, intermediate beam length $\overline{B_i C_i}$ is called a_i, and left link length $\overline{C_i D_i}$ is called e_i^*, respectively. It is assumed that the eccentricities e_i's are sufficiently large in comparison with e_i^*'s to eliminate other hinging. The possibility of such hinges is discussed in the next chapter. Rigid end zones having lengths equal to half of the column depth are postulated. These lengths are called d_{Li} and d_{Ri}, respectively, for the left and the right columns. The constant span length between the column center lines is called L.

The angular distortions of the beam at points A_i, B_i, and D_i are called ϑ_{Ai}, ϑ_{Bi}, and ϑ_{Di} respectively, and the horizontal floor displacement at the i-th level with respect to the undeformed state is called Δ_{Bi}. Considering only the geometrical first order effects in accord with usual limit analysis, for the given plastic story drift angle ϑ_p, the expressions for ϑ_{Ai}, ϑ_{Bi}, ϑ_{Di}, and Δ_{Bi} are obtained in terms of the topological parameters enumerated above. As shown in Fig. 2.4(a), since the rigid elements $\overline{B_i D_i}$ and $\overline{C_{i-1} D_{i-1}}$ are connected by the rigid brace $\overline{B_i C_{i-1}}$, they act like a mechanism with hinges. Therefore the rotations ϑ_{Di} and ϑ_{Di-1} are related by the following equation:

$$\vartheta_{Di} = \left[\frac{e_{i-1}^*}{a_i + e_i^*} \right] \vartheta_{Di-1} \tag{2.7}$$

Using this equation in a recurrence expression, and noting that point C at the ground ($i=0$) does not move (see Fig. 2.4(b)), one obtains the following general expression:

$$\vartheta_{Di} = \left[\frac{e_{i-1}^*}{a_i + e_i^*} \right] \cdots\cdots\cdots\cdots \left[\frac{e_1^*}{a_2 + e_2^*} \right] \left[\frac{e_0^*}{a_1 + e_1^*} \right] \left[\frac{e_0^* + d_{L0}}{e_0^*} \right] \vartheta_p . \tag{2.8}$$

where $(e_0^* + d_{L0})$ is the distance of brace offset from column center line at the ground level. With the above equation the following additional recurrence formulas at the i-th floor level can be obtained for ϑ_{Ai}, ϑ_{Bi}, and Δ_{Bi}:

$$\vartheta_{Ai} = \left[\frac{L}{e_i}\right]\vartheta_p - \left[\frac{e_i^* + a_i}{e_i}\right]\vartheta_{Di} \tag{2.9}$$

$$\vartheta_{Bi} = \vartheta_{Ai} - \vartheta_{Di} \tag{2.10}$$

$$\Delta_{Bi} = \left[L - e_i - d_{Ri}\right]\vartheta_p - \left[e_i^* + a_i\right]\vartheta_{Di} \tag{2.11}$$

By using Eqs. 2.8 to 2.11, ϑ_{Di}, ϑ_{Ai}, ϑ_{Bi}, and Δ_{Bi} can be calculated beginning with the first story ($i=1$). It should be noted that when $e_0^* + d_{L0}=0$, corresponding to the case of intersecting brace and column centerlines at the ground level, ϑ_{Di} in Eq. 2.8 vanishes. Therefore ϑ_{Ai}, ϑ_{Bi}, and Δ_{Bi} in Eq. 2.9, 2.10, and 2.11 will not have any contributions from their second terms on the right hand side of the respective equations. Further, even for the case of an offset brace, as the value i increases, as can be recognized from Eq. 2.8, the ϑ_{Di} rapidly approaches zero.

As a simple example, consider a D-brace frame having $L=288$ in., $e_i=48$ in., $e_i^*=12$ in., $d_{Li}=d_{Ri}=7$ in., and $a_i=214$ in. for an i-th level. Applying Eqs. 2.8 to 2.11 gives the following result in the order from $i=1$ to N.:

$$\vartheta_{Di} = 0.089\vartheta_p, \; 0.005\vartheta_p, \; 0.000\vartheta_p, \; \dots\dots\dots, \; \approx 0, \; (rad) \tag{2.12}$$

$$\vartheta_{Ai} = 5.582\vartheta_p, \; 5.977\vartheta_p, \; 5.999\vartheta_p, \; \dots\dots\dots, \; \approx 6\vartheta_p \; (rad) \tag{2.13}$$

$$\vartheta_{Bi} = 5.493\vartheta_p, \; 5.972\vartheta_p, \; 5.999\vartheta_p, \; \dots\dots\dots, \; \approx 6\vartheta_p \; (rad) \tag{2.14}$$

$$\Delta_{Bi} = 212.9\vartheta_p, \; 231.9\vartheta_p, \; 233.0\vartheta_p, \; \dots\dots\dots, \; \approx 233\vartheta_p \; (in.) \tag{2.15}$$

As can be seen from the above, ϑ_{Di} becomes negligibly small at the higher floor levels, thereby its influence on other quantities rapidly diminishes. Eq. 2.8

indicates that the same trend develops even if e_i, e_i^*, a_i, d_{Li}, d_{Ri} vary throughout the height of the frame. Accordingly,

$$\vartheta_{Di} \approx 0 \tag{2.16}$$

$$\vartheta_{Ai} \approx \left[\frac{L}{e_i}\right]\vartheta_p \tag{2.17}$$

$$\vartheta_{Bi} \approx \left[\frac{L}{e_i}\right]\vartheta_p \tag{2.18}$$

$$\Delta_{Bi} \approx \left[L - e_i - d_{Ri}\right]\vartheta_p \tag{2.19}$$

Noting the expressions for ϑ_{Ai} and ϑ_{Bi} given by Eqs. 2.13 and 2.14, or approximately by Eqs. 2.17 and 2.18, it can be said that the energy dissipation mechanisms for EBFs require large plastic deformations of the links of length e_i. However the required plastic rotations ϑ_{Di} at the left end of links of length e_i^* are negligible. The approximate relations, Eqs. 2.16 to 2.19 can be used for the purpose of design, since they are in good agreement with the more accurate Eqs. 2.8 to 2.11.

Comparisons of D-, K-, and V-brace Frames : - Using the above approach, the mechanisms for different types of EBFs can be compared. The desirable energy dissipation mechanisms for these frames are shown in Figs. 2.5 to 2.9. Figure 2.6 shows that the K-brace frame mechanism geometrically consists of two D-brace frame mechanisms, therefore the link angular rotations and floor deformation can be obtained from either the exact or approximate equations given previously by setting L equal to $L/2$, e_i to $e_i/2$, and d_{Ri} to 0, respectively. The V-brace frame shown in Fig. 2.7 also can be said to develop two D-brace frame mechanisms. Hence the analysis can be achieved using the earlier equations by setting L equal to $L/2$, e_i^* equal to 0, and taking d_{Li} as 0. The

same approach as for this V-brace frame can be used for the V-brace frame illustrated in Fig. 2.8.

Based on the above considerations, comparisons of active link deformations and floor deformations can be made using the following approximate equations for frames of different types:

For D—brace frame: $\quad \gamma_{p\,i} = \left[\dfrac{L}{e_i}\right]\vartheta_{p\,i}, \quad \Delta_{p\,i} = \left[L - e_i - d_{\mathrm{R}i}\right]\vartheta_p \qquad$ (2.20)

For K—brace frame: $\quad \gamma_{p\,i} = \left[\dfrac{L}{e_i}\right]\vartheta_{p\,i}, \quad \Delta_{p\,i} = \left[L - e_i\right]\vartheta_p \qquad$ (2.21)

For V—brace frame: $\quad \gamma_{p\,i} = \left[\dfrac{L}{2e_i}\right]\vartheta_p, \quad \Delta_{p\,i} = \left[\dfrac{L}{2} - e_i - d_{\mathrm{R}i}\right]\vartheta_p, \qquad$ (2.22)

where $\gamma_{p\,i}$ and $\Delta_{p\,i}$ are, respectively, the average link plastic deformation angle and the horizontal plastic floor displacement measured from the undeformed position (for a D-brace frame, $\gamma_{p\,i} = (\vartheta_{\mathrm{A}i} + \vartheta_{\mathrm{B}i})/\,2$, and $\Delta_{p\,i} = \Delta_{\mathrm{B}i}$).

The above results indicate that for a given $\vartheta_{p\,i}$, the link deformation demand $\gamma_{p\,i}$ is larger if the span length L is large and/or e_i is small, whereas the floor deformation $\Delta_{p\,i}$ is mainly governed by the span length L, and is not very sensitive to a variation in e_i-magnitude. For the D- and K-brace frames, $\gamma_{p\,i}$ and $\Delta_{p\,i}$ are almost the same unless the column depth is unusually large. It is also important to note that for the V-brace frame, for links of the same lengths e_i, $\gamma_{p\,i}$ and $\Delta_{p\,i}$ are only one-half or less compared with those in the D- and K-brace frames. As will be pointed out in Chapter 4, this is an advantage of V-brace frames.

Y-brace Frame : - It also may be interesting to comment on the unique frame type shown in Fig. 2.9, called an inverted Y-brace frame [31,79]. As

shown, the mechanism of this frame is completely different from those of the other frame types. The figure suggests that the deformation demand for this link is $(h_i / e_i)\vartheta_p$, where h_i is the story height at the i-th level. Therefore, for this inverted Y-brace frame, instead of the span length L, the story height h_i becomes the key topological parameter for link deformation demand, which completely differs when compared to D-, K-, and V- brace frames. Considering the usual proportions of the frames, this frame then has an advantage in that the link deformation demand may be less than those in the D- and K-brace frames and is competitive with the V-brace frame. However, since a link directly resists lateral loading, the plastic shear capacity of this link should develop nearly the whole lateral story shear force cumulated from the top of the structure to the corresponding level. This would necessitate the use of much larger link beam sections than those needed for D-, K-, and V-brace frames (see Section 5.7) to resist the same lateral loading. Furthermore, the braces would be exposed to large bending, and since it is technically difficult to support the link and the braces laterally, there is a possibility for an out-of-plane buckling of these members. It also appears that the fabrication of this system of bracing is more complex. At Berkeley, this type of frame has not been studied either experimentally or analytically, therefore no further discussions will pertain to this frame.

2.5. Conclusion

The following conclusions based on the developments in this chapter can be made.

(1) EBF must have an adequate lateral load carrying plastic capacity and must exhibit desirable mechanism accompanied by plastic link deformation in an

overloaded structure.

(2) Based on the idealized interaction of moment and shear force of wide flange beams, three types of links can be defined according to their lengths.

(3) The rigid-plastic displacement field for an EBF representing the desired energy dissipation mechanism provides a basis for obtaining the link deformation demand and the lateral load carrying capacity for an EBF.

(4) Typically, the plastic deformation of the link of length e^* is negligibly small, and its effect on global rigid-displacement field of an EBF is extremely small. Some exceptional case is explained in Chapters 3 and 4.

(5) The link deformation in a V-brace frame is only one-half of that in the other type frames if the link lengths and the span lengths are the same.

CHAPTER 3

A METHOD TO OBTAIN EBF PLASTIC CAPACITY

3.1. General

According to previous research [54], the energy dissipation mechanisms discussed in the previous section for the various EBFs generally produce the most advantageous behavior for strength and ductility. Manheim [54] proposed a method of computing the upper bound load for EBFs based on energy dissipation mechanisms. However, using the ideal link M-V interaction described in Section 2.3 and the solutions proposed in Section 2.4 for rigid-plastic displacement fields of EBFs, a more general treatment and simplifications can be introduced for obtaining EBF plastic capacity.

3.2. Internal Virtual Work of D-brace frame

Considering the mechanism shown in Figs. 2.1(a) and 2.4 for a D-brace frame, one can obtain the following expression for the internal virtual work W_I done by the plastic virtual story drift angle ϑ_p:

$$W_I = W_{I1} + W_{I2} + W_{I3}, \tag{3.1}$$

where W_{I1} is the internal work due to the plastic shear and bending deformation of the links with lengths e_i, the expression for which combining the action of moment and shear is given in Ref. 33. W_{I2} is the internal work due to the plastic deformation concentrated at the column face of the links with length e_i^* and the

roof beam (see Fig.2.1), and W_{I3} is the internal work due to the plastic deformation of the columns at the column bases. Accordingly,

$$W_{I1} = \sum_{i=1,N} [M_{Ai} \vartheta_{Ai}^{(b)} + M_{Bi} \vartheta_{Bi}^{(b)} + V_{ABi} e_i (\vartheta_{Ai}^{(s)} + \vartheta_{Bi}^{(s)})/2] \tag{3.2}$$

$$W_{I2} = \sum_{i=1,N} [M_{Di} \vartheta_{Di}] \tag{3.3}$$

$$W_{I3} = [M_{CL1} + M_{CL2}] \vartheta_p , \tag{3.4}$$

where M_{Ai}, M_{Bi}, and M_{Di} are, respectively, the moments at A_i, B_i, D_i, at the i-th level of an N-story D-brace frame shown in Fig. 2.4, and M_{CL1} and M_{CL2} are, respectively, the right and the left column base moment. ϑ_{Ai}, ϑ_{Bi}, and ϑ_{Di} were expressed in terms of ϑ_p in the previous section. It should be noted that $\vartheta_{Ai} = \vartheta_{Ai}^{(b)} + \vartheta_{Ai}^{(s)}$ where the first term on the right hand of this equation indicates rotation due to bending at point A and the second due to shear. Similar expression is also used for ϑ_{Bi}. In Eq. 3.2, the third term on the right hand side expresses the work done due to shear deformation of the link. This expression was given in Ref. 54 based on the assumption that the shear strain in the link varies linearly over the link length. Henceforth, the properties M_p, M_p^*, V_p, and b^* of the link located at the i-th level will be called M_{pi}, M_{pi}^*, V_{pi}, and b_i^*, respectively.

Internal Work By Link of Length e : - For obtaining W_{I1}, the following procedure can be adopted. As discussed in Section 2.3, in ideal plastic theory the end moments M_{Ai} and M_{Bi} of a link with length e_i are equal in the limit state. Accepting this and a statical relation for moment and shear force,

$$M_{Ai} = M_{Bi} = \frac{V_{ABi} e_i}{2}, \tag{3.5}$$

where V_{ABi} is the shear force in the active link located at the i-th level. Substituting Eq. 3.5 into Eq. 3.2 and combining bending and shear deformation,

$$W_{I1} = \sum_{i=1,N} [\ V_{ABi} e_i (\vartheta_{Ai} + \vartheta_{Bi})/2\ ] \tag{3.6}$$

If instead of the exact Eqs. 2.9 and 2.10 for ϑ_{Ai} and ϑ_{Bi}, the approximate Eqs. 2.17 and 2.18 are substituted into Eq. 3.6, then the following expression for W_{I1} is obtained:

$$W_{I1} \approx \sum_{i=1,N} [\ V_{ABi}\ ] L\,\vartheta_p \tag{3.7}$$

This equation is very easy to apply since W_{I1} is simply the summation of the shear forces V_{ABi}'s in all links of the frame multiplied by $L\vartheta_p$. The approximate expressions for ϑ_{Ai} and ϑ_{Bi} overestimate the more accurate magnitudes given by Eqs. 2.9 and 2.10 merely a few percent at the 1-st level of the frame and provide accurate estimates for the remainder of the frame. Therefore the degree of overestimation of W_{I1} for a multi-story frame on this basis is insignificant.

According to Eq. 3.7, the magnitude of W_{I1} can be obtained if one knows the magnitude of V_{ABi}. To accomplish this it should be noted that in addition to Eq. 3.5, M_{Ai}, M_{Bi}, and V_{ABi} must also satisfy the $M-V$ interaction relationships expressed by Eqs. 2.4 and 2.5. Accordingly, when $e_i < b^*_i$ the link is a shear link with end moments less than M^*_{pi} and

$$V_{ABi} \approx V_{pi} \qquad (e_i \leq b^*_i). \tag{3.8}$$

On the other hand, when $e_i > b^*_i$, the link is categorized as an intermediate or moment link, where the end moments become larger than M^*_{pi} and equal to or smaller than M_{pi}. Therefore, substituting Eq. 3.5 into Eq. 2.5, the following equation can be obtained:

$$\left[\frac{V_{ABi} e_i/2 - M^*_{pi}}{M_{pi} - M^*_{pi}}\right]^2 + \left[\frac{V_{ABi}}{V_{pi}}\right]^2 = 1 \qquad (e_i \geq b^*_i), \tag{3.9}$$

For a given e_i, M_{pi}, M^*_{pi}, and V_{pi}, Eq. 3.9 becomes a quadratic equation for V_{ABi} and can be solved easily. Here, in contrast to Eq. 3.8, the magnitude of V_{ABi} is

less than that of V_{pi}.

Fig. 3.1 illustrates the above solution scheme showing that the magnitudes of V_{ABi} depend on e_i. If $e_i < b^*_i$, the solution point on the interaction surface lies to the left of the balance point and is identified in the figure as solution 1. For this case the V_{ABi}-magnitude is the constant V_{pi} per Eq. 3.8. By contrast, if $e_i > b^*_i$, the solution lies to the right of the balance point and is designated as solution 3 in the figure. For this case the V_{ABi}-magnitude depends on the e-magnitude per Eq. 3.9. In this manner, W_{I1} given by Eq. 3.7 can be estimated.

Internal Work By Link of Length e* : - For estimating W_{I2}, the magnitude of M_{Di} in Eq. 3.3 must be known. As discussed in Section 2.3, such magnitude depends on the shear force in the link of length e^*_i. Since the plastic rotation occurs only at one end of this link, as shown in Figs. 2.1(a) and 2.4, the end moments are not necessarily equal suggesting that the simplification used for deriving W_{I1} above cannot be used. Although general iteration procedures for obtaining forces in rigid-plastic frames under combined stresses have been proposed [25], and probably can be modified to solve the present problem, the following alternative approach, taking advantage of the special kinematics of EBFs, is proposed.

The order of magnitude of W_{I1} and W_{I2} expressed, respectively, in Eqs. 3.2 and 3.3 can be compared by examining the order of magnitude of the moments and the conjugate plastic rotations appearing in these expressions. First, as indicated in Section 2.3, the magnitude of M_{Di} of a section would be M^*_{pi} or somewhat higher, but certainly bounded by M_{pi}. Therefore, since a constant beam section is usually used throughout the span length L, the magnitude of M_{Di} should be of comparable order of magnitude with those of M_{Ai} and M_{Bi}. Second, as shown by Eqs. 2.12 through 2.14, and Eq. 2.16 through 2.18, the

magnitude of ϑ_{Di} is generally extremely small compared with those of ϑ_{Ai} and ϑ_{Bi}. Therefore

$$M_{Di}\vartheta_{Di} \ll M_{Ai}\vartheta_{Ai} + M_{Bi}\vartheta_{Bi}. \tag{3.10}$$

This leads to the conclusion that

$$W_{I2} \ll W_{I1}. \tag{3.11}$$

Therefore the internal work done by the hinges at points D_i ($i=1,N$) is negligibly small compared with that done by the plastic hinges of the links with lengths e_i.

Internal Work By Column Bases : - For estimating W_{I3} in Eq. 3.4, the magnitudes of the moments M_{CL1} and M_{CL2} at the column bases should be known. These moments depend on the axial force magnitudes in the columns since the interaction between the moment and the axial force on the column member capacity is very significant. However, using an approach similar to the above, the following approximation can be introduced.

The magnitudes of W_{I1} and W_{I3} expressed by Eqs. 3.2 and 3.4 can be compared by examining the magnitudes of the moments and the conjugate plastic rotations appearing in these expressions. As will be shown in Chapter 5, in the usual design of a D-brace frame, the column moments M_{CL1} and M_{CL2}, are of magnitudes close to those of M_{A1} and M_{B1} which occur in 1-st floor level links. Further, as indicated by Eqs. 2.17 and 2.18, ϑ_{A1} and ϑ_{B1} are approximately L/e_1 times ϑ_p. Therefore, in general,

$$(M_{CL1} + M_{CL2})\vartheta_p < M_{A1}\vartheta_{A1} + M_{B1}\vartheta_{B1}. \tag{3.12}$$

Numerical experimentation in the design and analysis of EBFs showed that typically W_{I3} is at most $2e_1/L$ times the internal work done by the links at the 1-st level. Since many links occur in a multi-story frame, W_{I3} would be much smaller than the work done by all the links, i.e.,

$$W_{I3} \ll W_{I1} .\qquad(3.13)$$

Total Internal Work : - Considering Eqs. 3.1, 3.7, 3.11, and 3.13, the following approximation can be used with very little error in estimating the internal energy of the frame.

$$W_I \approx W_{I1} \approx \sum_{i=1,N} [\; V_{ABi}\;] L\, \vartheta_p \qquad(3.14)$$

This shows that in an EBF most of the energy is dissipated by the plastic deformation of the active links. It is also interesting to note from Fig. 3.2 the physical meaning of Eq. 3.14 by displacing a D-brace frame to the right and to the left. The first mechanism will be called Mechanism 1 and the second Mechanism 2. In these mechanisms the links rotate in opposite directions. The work done by a link is simply the link shear force times the relative displacement of the link, which is approximately $L\vartheta_p$, and is the same for either Mechanism 1 or 2.

3.3. External Virtual Work of D-brace Frame

The virtual work W_E done by the external forces is given by:

$$W_E = W_{E1} + W_{E2} \;\; , \qquad(3.15)$$

where W_{E1} is the work done by the lateral loads and W_{E2} is the work done by vertical loads.

External Work By Lateral Loads : - Fig. 3.3(a) shows the lateral force distribution on an EBF exhibiting two possible Mechanism 1 and 2; for either case the W_{E1} can be expressed as

$$W_{E1} = \xi \sum_{i=1,N} [\; F_i\, H_i\;]\, \vartheta_p , \qquad(3.16)$$

where F_i and H_i are, respectively, the generalized lateral load and the distance of load application point from the ground. The parameter ξ is an unknown load factor.

External Work By Vertical Loads : - For estimating W_{E2}, first consider Mechanism 1 where the lateral load acts from the left to the right and the vertical load will produce positive external work as in Fig. 3.3(b). This mechanism is the same that would result under the condition of no vertical loads. The vertical load is modeled as a point load type and it is assumed that no vertical load acts on the link so that the shear force throughout the link length remains constant, enabling the use of the previously developed plastic theory formulation. For the case of a linearly varying shear force in the link, see Chapter 4. The work done by all the point loads at each story level can be simply expressed as the total load acting on the beam times the displacement of the centroid of the point loads. Therefore such work can be expressed for the i-th level as $w_i L \cdot \Delta_{Bi} / 2$, where, as shown in Fig. 3.3, w_i is the magnitude of equivalent uniform load and Δ_{Bi} is the vertical displacement of the point B_i. Accordingly, for an N-story D-brace frame,

$$W_{E2} = \frac{1}{2} \sum_{i=1,N} w_i L \cdot \Delta_{Bi} \, . \tag{3.17}$$

The Δ_{Bi} was previously expressed by either the accurate Eq. 2.11 or the approximate Eq. 2.19. The latter simpler equation gives a sufficiently accurate estimate for Δ_{Bi}. Hence

$$\Delta_{Bi} \approx (L - e_i - d_{Ri}) \vartheta_p \, . \tag{3.18}$$

By substituting Eq. 3.18 into Eq. 3.17, one obtains the following expression for W_{E2} in terms of ϑ_p and topological parameters:

$$W_{E2} \approx \frac{1}{2} \sum_{i=1,N} w_i (L - e_i - d_{Ri}) L \vartheta_p \tag{3.19}$$

Next, consider Mechanism 2 in Fig. 3.3 corresponding to the case where the lateral load acts from right to left. With under no vertical loads, the mechanism is analogous to the one before. For this mechanism to occur it is assumed that e_i^*'s are sufficiently small compared with e_i's and the magnitude of the vertical load is sufficiently small to cause no intermediate plastic hinge within the span. On this basis, W_{E2} can be calculated in the same way as above, but it should be kept in mind that the work done by the vertical loads is now negative, i.e.,

$$W_{E2} \approx -\frac{1}{2} \sum_{i=1,N} w_i (L - e_i - d_{Ri}) L \vartheta_p \qquad (3.20)$$

3.4. Virtual Work Solution for a D-brace Frame

Both external and internal work for a D-brace frame were expressed above for a virtual displacement ϑ_p. Since

$$W_E = W_I \quad , \qquad (3.21)$$

one can determine the unknown lateral load factor ξ. Based on Eqs. 3.14 and 3.15, the above equation yields:

$$W_{E1} + W_{E2} = W_{I1} \quad . \qquad (3.22)$$

For Mechanism 1, using Eqs. 3.16 and 3.19 for W_{E1} and W_{E2}, respectively, and Eq. 3.14 for W_{I1}, one obtains

$$\xi \sum_{i=1,N} [F_i H_i] \vartheta_p + \frac{1}{2} \sum_{i=1,N} [w_i (L - e_i - d_{Ri})] L \vartheta_p = \sum_{i=1,N} [V_{ABi}] L \vartheta_p \qquad (3.23)$$

Therefore for Mechanism 1,

$$\xi = \frac{L \sum_{i=1,N} [V_{ABi} - \frac{1}{2} w_i (L - e_i - d_{Ri})]}{\sum_{i=1,N} [F_i H_i]} \qquad (3.24)$$

For Mechanism 2, using Eq. 3.20 for W_{E2},

$$\xi = \frac{L \sum\limits_{i=1,N} \left[V_{ABi} + \frac{1}{2} w_i (L - e_i - d_{Ri}) \right]}{\sum\limits_{i=1,N} [F_i H_i]} \tag{3.25}$$

If no vertical loads are acting, by setting $w_i = 0$ in Eqs. 3.24 and 3.25 for both mechanisms, an identical simple expression for ξ is obtained:

$$\xi = \frac{L \sum\limits_{i=1,N} [V_{ABi}]}{\sum\limits_{i=1,N} [F_i H_i]} \tag{3.26}$$

Once ξ is determined, the lateral load capacity of a frame can be calculated knowing that the lateral forces are ξF_i (i = 1, N). It can be recognized from Eqs. 3.24 through 3.26, that the vertical loads will decrease the plastic capacity of the frame if the lateral loads act from left to right on the D-brace frame, and increase otherwise. As one can also recognize from the above solutions, ξ depends on the link length e_i since V_{ABi} is a function of e_i. Further discussion of these points is given in Chapter 4.

3.5. Alternative Solution for D-brace Frame Plastic Capacity

In general, a limit analysis solution based on the yield criteria of the members and assumed mechanism of a frame gives an upper bound estimate of the frame plastic capacity since the solution does not necessarily satisfy equilibrium. The solution which gives the lowest estimate of plastic capacity among all other solutions based on the various assumed mechanisms is exact. Therefore the assumption of an appropriate mechanism plays a major role in estimating the EBF plastic capacity.

In the above discussion it was assumed that the D-brace frame exhibits either Mechanism 1 or 2 which are the reverse of each other. When the lateral load acts from left to right, the solution based on Mechanism 1 would provide the most appropriate estimate for a D-brace frame capacity. With large vertical loads, it was initially felt that another mechanism with hinges in the intermediate region of the beam may occur; however, as will be discussed in Chapter 4, such a case is not likely to occur.

On the other hand, if the lateral load acts from right to left, there is a need to reconsider Mechanism 2 if the magnitudes of the vertical loads and/or of the e_i^*'s are large. A mechanism with refinements on Mechanism 2 will be referred to here as Mechanism 3, see Fig. 3.4. Similar to the the virtual work approach discussed for Mechanisms 1 and 2, the same approach can also be applied to this case. Fig. 3.4 shows that Mechanism 3 consists of three types of beam mechanisms (a), (b), and (c). The beam mechanism (a) is the same one as used previously in Mechanism 2 and is formed by the plastic deformation of link $\overline{A_i B_i}$ of length e_i, and may develop in Mechanism 3 also. The beam mechanism (b) is formed by the plastic deformation of link $\overline{C_i D_i}$ of length e_i^*. The beam mechanism (c) consists of simultaneously occurring plastic deformations in links $\overline{A_i B_i}$ and $\overline{C_i D_i}$.

Internal Work for Alternative Mechanism : - For the beam mechanisms (a) and (b) in Fig. 3.4, the internal work done by the links at the i-th level, namely $W_{I1}^{(a)}$ and $W_{I1}^{(b)}$ can be simply calculated as the link shear force times the relative link displacement $L\vartheta_p$. As explained previously for deriving Eq. 3.7 from Eq. 3.6, this can be justified since the plastic rotations at both ends of the link are of the same magnitude. Accordingly, for beam the mechanism (a),

$$W_{I1}^{(a)} = V_{ABi} L\vartheta_p ,$$

(3.27)

and for the beam mechanism (b),

$$W_{I1}^{(b)} = V_{CDi} L \vartheta_p \qquad .$$ (3.28)

For the beam mechanism (c), illustrated in Fig. 3.4, the plastic rotations of the links at both ends are not equal, thus the above simplification cannot be made, and the rotations for the link $\overline{A_i B_i}$ are expressed as

$$\vartheta_{Ai} = \left[\frac{L}{e_i}\right]\vartheta_p \,.$$ (3.29)

and

$$\vartheta_{Bi} = \left[\frac{L}{e_i} + \frac{L}{a_i}\right]\vartheta_p \,,$$ (3.30)

which is larger than ϑ_{Bi} for the beam mechanism (a). By substituting the above relations into Eq. 3.6, the work done by this link is seen to be $V_{ABi}(1+e_i/2a_i)L\vartheta_p$, larger than the work done by the beam mechanism (a) given by Eq. 3.27. The contribution to the work done by the link $\overline{C_i D_i}$ should also be included. The total work done by the two links for beam mechanism (c) is

$$W_{I1}^{(c)} = V_{ABi}(1 + \frac{e_i}{2a_i})L\vartheta_p + V_{CDi}(1 + \frac{e_i^{\bullet}}{2a_i})L\vartheta_p \,,$$ (3.31)

indicating that this beam mechanism produces much more internal work than the beam mechanisms (a) and (b).

As discussed previously, neglecting the relatively much smaller work done in other regions of the frame, the total internal virtual work can be expressed as

$$W_I \approx W_{I1} \approx \sum W_{I1}^{(a)} + \sum W_{I1}^{(b)} + \sum W_{I1}^{(c)}$$ (3.32)

External Work for Alternative Mechanism : - The equations for the external work due to the lateral load has the same form as that for Mechanisms 1 and 2. Its basis is illustrated in Fig. 3.5(a). Accordingly,

$$W_{E1} = \xi \sum_{i=1,N} [\, F_i\, H_i\,]\, \vartheta_p \tag{3.33}$$

The external work done by the vertical load can be estimated using Fig. 3.5(b). For the beam mechanism (a), the point B_i moves upward and the work due to the vertical load is negative which has the same form as Eq. 3.20, i.e.,

$$W_{E2}{}^{(a)} \approx -\frac{1}{2}\, w_i (L - e_i - d_{Ri})\, L\vartheta_p \tag{3.34}$$

For the beam mechanism (b), since the point C_i moves downward, the work due to the vertical load is positive, i.e.,

$$W_{E2}{}^{(b)} \approx \frac{1}{2}\, w_i (L - e_i^{\bullet} - d_{Li})\, L\vartheta_p \tag{3.35}$$

For the beam mechanism (c) where the point B_i moves upward and the point C_i downward, it was found that the work done by vertical load is negligibly small compared with the above estimates, hence

$$W_{E2}{}^{(c)} \approx 0 \tag{3.36}$$

Accordingly, the external work done by the vertical load in Mechanism 3 is

$$W_{E2} \approx \sum W_{E2}{}^{(a)} + \sum W_{E2}{}^{(b)} + \sum W_{E2}{}^{(c)} \tag{3.37}$$

Virtual Work Solution for Alternative Mechanism : - Based on the above discussion, ξ can be obtained using the above relationship Eq. 3.22 and to find

$$\xi = \frac{L}{\displaystyle\sum_{i=1,N} [\, F_i\, H_i\,]} \left\{ \sum^{(a)} [V_{ABi} + \frac{1}{2}\, w_i (L - e_i - d_{Ri})] \right.$$

$$\left. + \sum^{(b)} [V_{CDi} - \frac{1}{2}\, w_i (L - e_i^{\bullet} - d_{Li})] \right.$$

$$+ \sum^{(c)} \left[V_{ABi}(1 + \frac{e_i}{2a_i}) + V_{CDi}(1 + \frac{e_i^*}{2a_i}) \right] \right] \tag{3.38}$$

By comparing Eqs. 3.25 and 3.38 for Mechanisms 2 and 3, respectively, the following observation can be made: As explained previously, ξ is proportional to the magnitude of the internal work done by the links minus the external work done by the vertical loads. Since Mechanism 3 essentially has larger internal work done by the links due to the formation of beam mechanism (c), if w_i is small, ξ for Mechanism 3 is likely to be larger than that for Mechanism 2, which suggests the development of Mechanism 2. However, if w_i is large, Mechanism 3 without beam mechanism (a) and a large number of beam mechanisms (b) would have large positive external work done by the vertical load, which could result in smaller ξ compared with that for Mechanism 2, since the external work done by the vertical load for Mechanism 2 is negative and has the effect of increasing ξ. Only actually comparing the magnitude of ξ's for the assumed mechanisms, can a conclusion be reached as to which mechanism would occur. In Chapter 4, the above solutions are applied to some example cases.

3.6. Plastic Capacity of K-, and V-brace frames

Plastic Capacity of K-brace Frame : - The above discussion pertained to a D-brace frame. Fig. 3.6 illustrates the internal and the external work of an eccentric K-brace frame. Since the plastic rotation angles are the same at both ends of a link, the internal work can be calculated as the link shear force times the relative link displacement as previously explained for a D-brace frame. Accordingly,

$$W_I \approx W_{I1} \approx \sum_{i=1,N} [V_{ABi}] L \vartheta_p , \tag{3.39}$$

and for the external work done by the lateral loads,

$$W_{E1} = \xi \sum_{i=1,N} [\ F_i H_i\ ] \vartheta_p \tag{3.40}$$

It should be noted that due to symmetric configuration, the plastic capacity of the K-brace frame is the same regardless of the lateral load direction even in the presence of vertical loads. Therefore if e_i^*'s are small; Fig. 3.6(b) shows that the work done by the vertical loads is zero, i.e.,

$$W_{E2} = 0 \tag{3.41}$$

Considering the above relations, regardless of the lateral load direction,

$$\xi = \frac{L \sum_{i=1,N} [V_{ABi}]}{\sum_{i=1,N} [F_i H_i]} \tag{3.42}$$

If the vertical load and/or e_i^*'s are large, as with Mechanism 2 of a D-brace frame, due to large plastic deformation of the link with length e_i^*, the vertical load may do positive work so that ξ may be reduced. Fortunately, however, for this frame in practice e_i^* is usually kept small; thus this behavior is not expected. This problem is discussed further in Chapter 4.

Plastic Capacity of V-brace Frame : - It is interesting to comment that for the V-brace frame shown in Fig. 3.7, the internal work done by each link is only half of that in the links of other types of frames, since the plastic deformation of a link at each story level is one half that for a D- or a K-brace frame as shown earlier by Eq. 2.22 and Figs. 2.7 and 2.8. However, at each story, a V-brace frame has two links, thus the internal work of a V-brace frame becomes the same as that of a D- or a K-brace frame. Furthermore, due to symmetric configuration of this frame, the same conclusions as those for a K-brace frame follow for the external work due to the vertical loads. Accordingly the above

- 42 -

Eqs. 3.39 through 3.42 for a K-brace frame are also valid for a V-brace frame. Since no eccentricity e_i^* is present in this frame, the consideration for an alternative mechanism under vertical loading is not needed.

Comparison of Plastic Capacities of Three Frame Types : - Based on the above considerations for D-, K-, and V-brace frames, regardless of the frame type, if the beam sections, span lengths, story heights, and link lengths are the same, the lateral load carrying capacities of the frames are the same, however, in the presence of vertical loads, the D-brace frame forms an exception. It should be noted that because of the different geometries and member sections for these types of frames, their elastic stiffnesses are not the same as will be pointed out in Chapter 4.

3.7. Conclusions

The following conclusions based on the developments in this chapter can be made.

(1) Based on the special kinematics of EBFs and ideal plastic theory, a very simple formula for an EBF plastic capacity can be derived.

(2) Most of the internal energy is absorbed by the plastic action of the active links, and the contribution from the other plastic actions can be neglected and still result in a sufficiently accurate estimate for the EBF plastic capacity.

(3) The plastic capacity of an EBF depends on the link length, since shear resisting capacity of a link is length dependent when the length is larger than the maximum shear hinge length b^*.

(4) Some alternative mechanism could occur in an EBF if the vertical loads and/or e^*s are sufficiently large. Such cases can be studied using the limit analysis procedure.

(5) D-, K-, and V-brace frames have approximately the same lateral load carrying capacity if the beam sections, span lengths, story heights, and link lengths are the same, in the absence of vertical loads. Due to the symmetric configuration of the K- and V-brace frames, the capacities of these frames are less sensitive to the applied vertical loads than those of the D-brace frame.

CHAPTER 4

CONSIDERATION OF BASIC EBF BEHAVIORS IN DESIGN

4.1. General

In the previous chapter rigid-plastic mechanisms and limit analysis for obtaining the plastic capacity of EBFs were discussed. In this chapter, using nonlinear finite element analyses, general elasto-plastic behavior of various types of EBFs is considered and compared with that of the plastic mechanisms and capacities predicted by the limit analysis. By applying the limit analysis procedures general conclusions are drawn on the effect of eccentricities e and e^*'s on the link deformation demand and EBF plastic capacity. Standard steel sections are reviewed from the view point of their suitability for achieving the desired plastic capacity. A brief discussion on the effect of eccentricities on the elastic stiffness of various EBFs is also made. It is the intent of this chapter to indicate the important factors to be considered in the initial design for determining EBF configurations.

4.2. General Elasto-Plastic Behavior of EBFs

Basic Factors Considered : - In this section, the elasto-plastic behavior of various types of EBFs under the action of lateral and vertical dead and live loads on the beams is considered and compared with the case of no vertical loadings. The study presented in the previous chapter indicated that the EBF behavior under vertical and lateral loading depends on many factors such as

the type of framing, the size of beams, which is directly related to the lateral load capacity of a frame, eccentricities e and e^*'s, beam span lengths, magnitudes of vertical loads, the distribution pattern of vertical loads, direction of lateral loads for unsymmetrical frames, etc. Therefore, in order to consider these situations, the following studies of the various factors were performed:

1.- Three types of 3-story EBFs, in which the D-, V-, and K-brace frames as illustrated in Fig. 4.1 are considered.

2.- The lateral load plastic carrying capacities of these frames with $e^*=0$ and no vertical loads are either 95 or 214 kips. Since three of these frames have relatively heavy and light sections, henceforth they will be identified, respectively, as "heavy" or "light" frames. The sizes of the members for each frame type are given in Fig. 4.1, where "HD-frame" indicates a heavy D-brace frame and "LD-frame" indicates a light D-brace frame and so on. In all frames the beam sizes are the same at all floor levels.

3.- The link lengths e and e^*'s are constant at all floor levels. As shown in Fig. 4.1, for HD-frames, $e=29$ in. and $e^*=e$ or 0. For HK-frames, $e=29$ in. and $e^*=14$ in. or 0. For HV-frames, $e=29$ in. For LD-frames, $e=36$ in. and $e^*=e$ or 0. In all cases the e and e^*'s are smaller than b^* for the beam sections used, i.e., shear links were employed in all cases.

4.- The span length L for the heavy frames was 216 in., and for the light frame is 288 in. The height of each story for the heavy and light frames was 108 in. and 144 in., respectively.

5.- As shown in Fig. 4.1, the lateral load P is applied at the top of the frame. When $P>0$, the lateral load acts from left to right, and when $P<0$, it acts in the opposite direction.

6.- For all cases, a vertical floor load of 120 psf was considered. Fig. 4.2 illustrates the modeling of this load for analyses assuming that the slab is

placed on both sides of the beam in an EBF. Depending on the deck direction, the line load w on a beam of heavy frame with $L=216$ in. was calculated as either 0.06 k/in. or 0.18 k/in. The latter estimate might be somewhat conservative. For a light frame, $w=0.08$ k/in. only was considered.

7.- The above vertical loads were modeled either as uniformly distributed or equivalent point loads as illustrated in Fig. 4.3. For the D-brace frames subjected to point loads there were seven vertical load points. As can be seen from Fig. 4.3, for uniform loading the shear force in the link varies linearly, whereas the point load model generates constant shear. For the K- and V-brace frames either the uniform or the equivalent point loads were also used.

The above conditions required analyses of a total of 32 cases of three-story EBFs. The lengths of the rigid end zones d_L and d_R were kept constant at all story levels and their magnitudes are given in Fig. 4.1. For the analyses, Young's modulus, yield stress, and Poisson's ratio were set at 30,000 ksi, 36 ksi, and 0.3 respectively. Table 4.1 summarizes some of the main features for the frames considered.

Load-Deflection Behavior of EBFs : - Nonlinear finite element analyses were performed for the above frames, using the beam and column models developed by Hjelmstad [32]. These analyses take into account both the geometric and the material nonlinearity without the strain-hardening effect using the moment-shear interaction relationship given earlier by Eqs. 2.4 and 2.5 as a yield surface for the links. It should be noted that shear capacity V_p of the link beam for the present analyses was calculated using the formula given in Ref. 54 which considers the height of the beam section in calculating the shear area. Accordingly, the magnitudes of V_p for the used link sections W14x53 and W8x31

were set as 107 kips and 47.5 kips respectively. The moment-axial force interaction [32] was considered for the long main beam segments, braces, and columns in which the axial forces are prominent.

The 6-th column of Table 4.1 gives analytically obtained P_u's for all the frames which correspond to the lateral load magnitudes at an average story drift $\vartheta = 0.015$ rads. The ϑ's were calculated by dividing the top lateral displacement by the height of the frame. It should be noted that for all frames with the same beam sections, span lengths, story heights, and link lengths, approximately the same lateral load carrying capacities were obtained when no vertical load was applied. The capacities of the K- and V- brace frames were much less sensitive to vertical load than those of the D-brace frames. These observations agree with the conclusion reached in the previous chapter. For all D- and K-brace frames whose e^*'s were varied, the frames with $e^*=0$ developed slightly larger lateral load capacities than frames with $e^*\neq0$. This will be further commented upon later. The effect on the plastic capacities of frames of the vertical load modeling, whether by the point or uniform loading, was negligible. The elasto-plastic load-deflection relationships of some of the above frames are shown in Fig. 4.4 through 4.8.

Fig. 4.4 shows the relationships between the applied lateral load P and average story drift ϑ of an HD-frame with $e^*=e$. If $P>0$, the vertical load caused a decrease in the plastic capacity of HD-frames. The larger the magnitude of the vertical load, the more prominent this effect. On the contrary, when $P<0$, some increase of plastic capacity occurs.

Fig. 4.5 shows the $P-\vartheta$ relationships of an HD-frame with $e^*=0$. As in the previous case with $e^*=e$, the vertical load had the effect of increasing or decreasing the lateral load resisting plastic capacity of the frame depending on the direction of the lateral load. However the condition that $e^*=0$ resulted in

the following trend in the magnitude of P_u:

$$|P_u|_{w \neq 0} = |P_u|_{w=0} \pm \Delta P_u \qquad\qquad (4.1)$$

where the negative sign is used for the lateral load direction from left to right, and vice versa. As can be noted from Fig. 4.5 and Table 4.1, ΔP_u was about 5% of $|P_u|_{w=0}$ when $w=0.06$ k/in., and about 15% when $w=0.18$ k/in., which suggests that the magnitude of ΔP_u is proportional to the magnitude of the vertical load. This will be proved later by limit analysis.

Fig. 4.6 shows the P–ϑ relationships for the LD-frames with either $e^*=e$ or 0. These frames showed similar behavior to that obtained for HD-frames with $e^*=e$ or 0. However, it should be noted that in spite of the moderate magnitude of w considered, the variation of frame capacities was larger than that for the HD-frames. About a 40% difference in the frame capacity can be noted between the cases of $P>0$ and $P<0$. This suggests that a significant loss or gain in lateral load capacity can occur in lighter D-brace frames due to vertical loads. It also should be noted that the vertical loads on these LD-frames produced a significant initial lateral displacement of the frames.

Fig. 4.7 shows the P–ϑ relationships of HK-frames with either $e^*=0$ or 14 in., corresponding to approximately half the magnitude of e. As can be seen no significant effect from the vertical loads was found to occur even when they were of large magnitude. Also since the frame is symmetric, the behavior of the frame is the same regardless of the lateral load direction. Fig. 4.8 shows that the same conclusions can be reached for V-brace frames.

It should be noted that in the above figures the P–ϑ behavior of all frames under vertical loads whether modeled as uniform or point loads was almost identical. Therefore, only one of these loading cases was shown above for each frame.

Mechanisms and Beam Moments in D-brace frame with e* = e : - The mechanisms for HD- or LD-frames, with the condition that $e^*=e$ for large inelastic displacements are illustrated in Fig. 4.9. When $P>0$, a D-brace frame exhibits Mechanism 1 discussed in Chapter 3 regardless of the magnitude of the vertical loads considered. The illustrations in Figs. 4.9(a) and (b) physically suggest that the vertical loads aid in the formation of this type of mechanism, resulting in a lower P_u than that occurring with no vertical loading.

When $P<0$, the mechanism with no vertical load shown in Fig. 4.9(c) is merely a reversed mechanism from the one shown in Fig. 4.9(a), i.e., as recalled above it is Mechanism 2. However, in the presence of the vertical loads, when $P<0$, the mechanism shown in Fig. 4.9(d) (Mechanism 3 according to Chapter 3) occurs. Here a link of length e^* deforms considerably, whereas links of length e deform little except for the one at the 1-st floor level of the frame.

In Fig. 4.10 typical moment distributions in floor beams of a D-brace frame are shown. Since the envelopes of the moment diagrams for the uniform and the point load models agreed very closely, only the smoothed moment diagrams are drawn. Since in the analysis the brace was considered to be fixed to the beam, some concentrated moments from the brace to the beam create discontinuities in the moment at points B and C. The moment gradients in the links $\overline{AB}$ and $\overline{CD}$ are considerably higher than those in the beam $\overline{BC}$, indicating that the links are subjected to a much higher shear than in the main beam segments. When point load modeling was employed, the shear force in the link was constant over the link length, and equal to V_p of the sections used since e and e^* are smaller than b^* and the links were shear links. For uniformly distributed vertical loads, the moment gradients vary across the link length, however, since the magnitude of the V_p is much larger than the variation of the shear force produced by the uniform vertical load, the moment gradients were also

approximately V_p for all such cases. The shear forces in the beam segments adjacent to the links were only about 10% of those occurring in the links. Without the vertical loads, the moment distribution in the floor beams when $e^*=e$ is almost skew-symmetric as shown in Fig. 4.10(a) and (c). With vertical loadings some changes in this distribution occur as illustrated in Fig. 4.10 (b) and (d), where the inflection points in the intermediate beam segment shift due to the parabolic distribution of moment caused by w. The effect of the vertical load on the beam moments was as great as is shown in the figures even when the vertical load was very large and/or beam sizes were small corresponding to HD11, HD12, LD2, and LD3.

For the mechanisms and moment distributions for the beams illustrated in Fig. 4.10, the following comments may be added: From separate elastic analyses for D-brace frames subjected to vertical load only, it was found that the moment and shear force distributions in the beams are similar to those for beams fixed at the columns. On the other hand, if load $P>0$ only acts on the frame, the elastic moment and shear force distributions are skew-symmetric, similar to the one in Fig. 4.10(a). Therefore for a combined loading, both the moment and the shear force at A add up, whereas those at D tend to be reduced, which results in yielding at A causing further concentrated plastic deformation in the link $\overline{AB}$. By the same token, if $P<0$, the yielding at D and the subsequent large plastic deformation of the link $\overline{CD}$ can be explained. These conclusions confirm the predictions based on limit analysis of the formation of Mechanisms 1 and 3.

Mechanisms and Beam Moments in a D-brace frame with e* = 0 : - In contrast with the above case for $e^*=e$, for a D-brace frame, with $e^*=0$, an essentially reversing mechanism, shown in Fig. 4.11, would develop regardless of the

vertical load magnitude. Similarly to the case with $e^*\neq 0$, if $P>0$, the vertical load has the effect of aiding the formation of the mechanism shown in Fig. 4.11 (b) thereby decreasing the magnitude of P_u. If $P<0$, a typical Mechanism 2 is formed as in Fig. 4.11(c), whereas the presence of a vertical load resists the formation of this mechanism, thereby increasing the magnitude of P_u, as in Fig. 4.11(d).

As illustrated in Fig. 4.12, the moment distribution is also quite different from the case with $e^*=e$. Regardless of the vertical load magnitude, typically the moment at point C coinciding with D, since $e^*=0$, was very small. On the other hand, the large moment gradient in link $\overline{AB}$ and the large moment at A develop just as in the case with $e^*=e$. As seen from the diagrams in Figs. 4.12(a) and (c), for lateral loading only, the moment distribution in the floor beam is not skew-symmetric, and the magnitude of the moment at the center of beam segment $\overline{BC}$ is not zero. Therefore when a vertical load is applied, if $P>0$, the magnitude of this moment increases more than in the case with $e^*=e$. The significance of these moments is illustrated in Fig. 1.12(b) for the cases when the magnitudes of vertical loads are very large or the beam size is small. It is significant to note that even for these cases with very large vertical loads, the peak moments did not occur within the beam spans $\overline{BC}$ and no hinges were formed.

Mechanisms and Beam Moments in K-brace frames : - As illustrated in Fig. 4.13, the formation of mechanisms for the split K-brace frames showed some similar trends to those in the D-brace frames. When $e^*\neq 0$, the mechanisms with and without vertical load are different, and under vertical loads the plastic deformation of a link with length e^* may become large. Such plastic deformations were not very significant in the example problems due to the use of a

relatively small e^* of 14 in. When $e^*=0$, the mechanisms are the same with or without vertical load. Fig. 4.14 shows that the beam moment distribution essentially consists of the moment distribution for the beams in two D-brace frames such as illustrated in Figs. 4.10 and 4.12 and depends on the magnitude of e^*. Since the beams of the K-braced frames were supported by the braces, and the distances between the supports were much smaller in the D-brace frames, the effect even of the largest vertical loads causing parabolic moment distribution was almost negligible.

Mechanisms and Beam Moments in V-brace Frames : - The mechanisms for the V-brace frames were also the same regardless of the vertical load magnitude as illustrated in Fig. 4.15. Except some small concentrated moments, caused by the braces connected to the beams at the center of the span, the moment diagrams as illustrated in Fig. 4.16 are similar to the ones in Fig. 4.12 for the D-brace frames with $e^*=e$. As in the K-brace frame, the small distances between the supported points make the effect of vertical load on the distribution of the moment negligible.

4.3. Application of Limit Analysis

Based on the above analytical results for EBFs and the application of two types of vertical loading (the point loads and the uniformly distributed loads), it can be concluded that either type of loading would result in almost the same elasto-plastic behavior of frames. From this study and since there is a certain difficulty in obtaining solutions based on the ideal plastic theory for links under uniformly distributed loading causing different shears at link ends, the theory developed in Chapters 2 and 3 which considers a constant shear force in the

link is adopted here for investigating the effect of vertical loads on the lateral load capacity of EBFs. The limit analyses are applied here to the EBFs analyzed elasto-plastically in the preceding sections.

Limit Analysis Applications for D-brace Frames : - The basic equations for determining the plastic capacities of D-brace frame exhibiting Mechanisms 1, 2, and 3 were given, respectively, by Eqs. 3.24, 3.25, and 3.38. For the present cases, $\xi F_1 = \xi F_2 = 0$ and $\xi F_3 = |P_u|$, and the distances H_3, H_2, and H_1 are, respectively, $3h$, $2h$, and h. All other parameters are constant for all story levels. This results in the following simple expressions for $|P_u|$:

Mechanism 1: $\qquad |P_u| = \dfrac{L}{h}[\, V_p - \dfrac{1}{2} w\,(L - e - d_R)\,]$ $\qquad\qquad$ (4.2)

Mechanism 2: $\qquad |P_u| = \dfrac{L}{h}[\, V_p + \dfrac{1}{2} w\,(L - e - d_R)\,]$ $\qquad\qquad$ (4.3)

As for Mechanism 3, Eq. 3.28 shows that one must determine how the beam mechanism (a), (b), and (c) combine to form Mechanism 3. Earlier Fig. 3.4 illustrated two such possible combinations, where the left frame mechanism consists of beam mechanisms (b) and (c), and the right frame mechanism consists of beam mechanisms (a) and (c). Since in the present case, the shear resisting capacities of the links $\overline{AB}$ and $\overline{CD}$ are equal to V_p at all story levels, both frame mechanisms would have the same total internal work done by the links. However, for these two frame mechanisms, one can recognize from Fig. 3.5(a) that the total external work done by the vertical loads is positive in the left diagram, and negative in the right one. This leads to the conclusion that the left mechanism gives a lower estimate of the lateral load capacity and suggests that it is the appropriate mechanism to consider for the present case. Based on the above reasoning, and from Eq. 3.38 one has

Mechanism 3: $\qquad |P_u| = \dfrac{L}{h}[\, V_p (1 + \dfrac{e}{3a}) - \dfrac{1}{6} w\,(L - e - d_R)\,]$ $\qquad\qquad$ (4.4)

where $d_L=d_R$ and $e^*=e$ are assumed.

The above solutions can be adapted for estimating P_u's. For a D-brace frame subjected to $P>0$, regardless of the magnitude of e^*, Chapter 3 predicted the occurrence of Mechanism 1, thus Eq. 4.2 applies. For a D-brace frame under the action of a $P<0$, if $e^*=0$, the frame does not develop Mechanism 3 and Mechanism 2 occurs, thus Eq. 4.3 applies. On the other hand, if a D-brace frame is acted upon by a $P<0$, and $e^*=e$, then depending on the magnitude of the vertical loads, either Mechanism 2 or 3, as suggested in Chapter 3 become applicable. In order to determine which mechanism would occur, by equating the right hand sides of Eqs. 4.3 and 4.4, one can obtain an expression for w for which either Mechanism 2 or 3 give the same magnitudes of $|P_u|$. Naming such a w as w^*, one has

$$w^* = \frac{e}{2a(L-e-d_R)}V_p \qquad (4.5)$$

Accordingly, if $w<w^*$, the $|P_u|$ for Mechanism 2 is less than that for Mechanism 3, and Mechanism 2 should be used. If $w>w^*$, the use of Mechanism 3 is appropriate.

Limit Analysis Applications for K- and V-brace frames: - For K- and V-brace frames Chapter 3 suggests that because of the skew-symmetric mechanisms no significant effect due to w would occur. Therefore, P_u could be calculated by setting $w=0$ in either Eq. 4.2 or 4.3, and

$$|P_u| = \frac{L}{h}V_p \qquad (4.6)$$

Comparisons with Elasto-Plastic Solutions : - Based on the limit analysis solutions, P_u's for the investigated frames were calculated with the same V_p

values used for the elasto-plastic analyses explained in Section 4.2. The numerical results for such P_u are listed in the 7-th column of Table 4.1. The error estimates are given in the 8-th column, where one can recognize the very accurate predictions that are found using approximate limit analyses. In Section 4.2, it was pointed out that the elasto-plastic solutions P_u with $e^* \neq 0$ become somewhat smaller than those with $e^* = 0$. This can be explained using an accurate rigid-displacement field in the limit analysis discussed in Chapter 2, where it was indicated that if e^* is large, the magnitudes of the link deformation angles in the lower stories become smaller than if $e^* = 0$. thus, internal work done by the link, and consequently P_u become somewhat smaller.

As indicated in Table 4.1, for the case $e^* = 0$ the magnitudes of P_u estimated by the elasto-plastic analyses and those estimated by the limit analyses for the D-, K-, and V-brace frames differ by only a few percent.

For the case $e^* \neq 0$ in D-brace frame exhibiting Mechanism 1, the discrepancy of P_u estimates with the two analyses were at most 6 percent. The approximate limit analysis being used here for Mechanism 1 of D-brace frame is based on an approximate rigid-plastic displacement field which ignores the effect of non-zero e^* and d_L, thus the link deformation at the 1st story level is somewhat overestimated, and the estimated P_u becomes somewhat larger than that from elasto-plastic solution. These errors can be expected to be even smaller if the D-brace frame has a larger number of stories, since the effect of non-zero e^*s and d_Ls on its rigid-displacement field diminish at higher story level. Also, for the case $e^* \neq 0$ in D-brace frame exhibiting Mechanism 3, the discrepancy of P_u estimates with the two analyses were at most 8 percent, which indicates that the approximation employed for the limit analyses of Mechanism 3 as explained in Section 3.5 would lead to a satisfactory estimate for P_u.

It should be noted that for the K-brace frame with $e^* \neq 0$, Eq. 4.6 assumes that no work is done by the vertical loads since a skew-symmetric mechanism was used. A slight disturbance in such a mechanism occurs due to a non-zero magnitude of e^*, as discussed in Section 4.2, which results in positive work due to the vertical load (see Fig. 4.13(a)). Therefore, P_u is somewhat smaller than for the case of no vertical load.

4.4. Effect of Link Length e* on the Plastic Capacity and Mechanism

3-story D-brace Frames: - As discussed above, the limit analysis yields sufficiently accurate estimates for the plastic capacities of different types of EBFs. Accordingly, using Eqs. 4.2 through 4.5, the general relationships between the magnitudes of P_u and w for both the HD- and the LD-frames were derived and illustrated in Fig. 4.17.

For an LD-frame, P_u is quite sensitive to the magnitude of w. If $e^*=0$, either an increase or a decrease of $|P_u|$ proportional to w occurs as previously suggested by Eq. 4.1. When $w=0.16$ k/in., a relatively large magnitude of the vertical load but is a possible case in practice, the magnitude of $|P_u|$ may differ by as much as 80% between the positive lateral loading case and a negative one, resulting in Mechanisms 1 and 2, respectively. However, if $e^*=e$ and $P<0$, the figure shows that w^* in Eq. 4.5 is quite small and for most of the range of w, LD-frame develops Mechanism 3, which is quite different from the case when $e^*=0$, i.e., the $|P_u|$ under vertical load is likely to be lower than that under no vertical load.

For an HD-frame, the change in plastic capacity due to vertical load is less significant. For the negative lateral loading case of the HD-frame with $e^*=e$, Mechanism 2 would occur for w less than $w^*=0.06$ k/in, which is larger than

that for the LD-frame. However for a considerable range of $w > w^*$, Mechanism 3 would develop.

7-story D-brace Frame: - A limit analysis was also performed on a 7-story D-brace frame whose proportions are given in Fig. 4.18(a). It was assumed that four identical EBFs such as shown in Fig. 4.18(a), resist 100% of the in-plane lateral load against the whole building with a plan dimension of 96 × 96 ft. The magnitudes of the dead and live loads were assumed to be as 85 and 35 psf, respectively. Considering that the building is in a seismically most active area and satisfies the seismic lateral force requirements for Zone 4 defined in UBC [94], it was found that the base shear capacity of each EBF would be 224 kips. By considering simplified triangularly distributed lateral loads and using the design procedures to be explained in Chapter 5, it was found that the shear resisting capacities of the links would be about 28, 52, 72, 88, 100, 108, and 112 kips in order from the 7-th level to the 1-st of the EBF, i.e., unlike the above 3-story frame examples, the shear resisting capacities of the links varies through the story height.

The load factor ξ given in the table of Fig. 4.18, were obtained using the previously developed Eqs. 3.24, 3.25, and 3.38 for each of the mechanisms assumed.

When the lateral load is applied from left to right ($\xi > 0$), Mechanism 1 in Fig. 4.18(b) occurs regardless of the magnitudes of e^*'s, and ξ decreases in proportion to w. When no vertical load is applied, for the designed frame $\xi = 1$, whereas for $w = 0.16$ k/in., ξ is 0.76.

On the other hand, if the lateral load is applied from right to left ($\xi < 0$) and $e^* = 0$, Mechanism 2 would occur and $|\xi|$ increases in proportion to w. If, however, $e^* = e$, the lowest $|\xi|$ has to be found by assuming various mechanisms

such as shown in Fig. 4.18(b), where the Mechanisms 4 and 5 are variations of Mechanism 3 discussed previously. The table suggests that at a relatively small w, Mechanism 2 could occur, whereas with an increasing w, either Mechanism 3, 4, or 5 might develop, and for a magnitude of w such as 0.16 k/in., only Mechanism 3 would occur.

Recommendations for Design: - Fig. 4.19 illustrates the brace arrangements for the 7-story EBFs discussed above. If one assumes that w=0.16 k/in., for coupled EBFs with e^*=e shown in Fig. 4.19(a), the ξs are 0.76 and 1.01, respectively, thus the combined EBFs would have 88% of the required design capacity. Due to cyclic excursions likely to occur during a severe earthquake, large plastic deformations could develop in the links of either length e or e^*. Fig. 4.19(b) shows a case with e^*=0, where uncoupled EBFs have ξs of 0.76 and 1.24, thus, unlike the above case, the coupled system would satisfy a required capacity. Fig. 4.19(c) shows the case where the coupled EBFs are not arranged in a symmetrical manner, resulting in a serious problem since the coupled system now attains only 76% of required capacity. Since this arrangement has an increased capacity for lateral loads acting in the opposite direction, there arises a strong possibility for an incremental collapse of the structure during a major earthquake. Furthermore, as pointed out in Section 4.2, since the elastic lateral displacement of an EBF varies depending on the direction of the lateral loading and vertical load magnitude, this could result in additional problems.

Based on the above observations, it is necessary to reduce magnitudes of vertical loads on the beams in D-brace frames and to arrange the D-brace frames in a symmetrical manner to avoid a possible serious effect of vertical loads on plastic capacity and elastic lateral displacement. In addition, as suggested by Figs. 4.19(a) and (b) it is desirable to keep the length e^* small to

obtain good lateral load resisting capacity in coupled D-brace frames. Since this requirement still permits some offset from the column centerline, detailing for a brace-beam connection need not be so costly. Moreover, web stiffeners to assure ductility in the link e^*, would not be required and the resulting framing has an advantage in economy. It should be noted that the effect of vertical loads are large for D-brace frames with a small lateral load resisting capacity and this consideration becomes particularly important for low-rise building as well as for higher story levels of tall buildings.

Due to some architectural requirements sometimes it is possible to have only one EBF bay in the same plane of a building. In such a case, careful considerations of the above problems enumerated above must be made, and it is far better to adopt either the K- or the V-brace frames if permitted architecturally. It is also desirable to keep e^* as small as possible for K-brace frame, in order to prevent the loss of lateral load resisting capacity and concentration of plastification in the link of length e^* (see Section 4.3).

Fig. 4.20 illustrates some examples of arrangements and configurations of EBFs to be avoided in practice. The D-brace frame depicted in Fig. 4.20(a) have $e^*=0$, but as noted in Section 4.4, these frames should be placed to result in a symmetrical structure. The V-brace frame in Fig. 4.20(b) does not have a symmetric configuration. In such a case, if vertical load were supported by this frame, this frame would have the problem of different lateral deflection and loading capacity in the two directions. Figs. 4.20(c) and (d) show other cases of unsymmetric arrangement of D-brace frames. For both buildings, the initial lateral deflection caused by the vertical loading may be amplified due to the $P-\delta$ effect. The building shown in Fig. 4.20(d) would have a tendency to twist. For these frames it is advisable to use symmetric K- or V-brace frames or alternatively the vertical loads on the D-brace frames should be reduced as much as

possible.

4.5. Effect of Link Length e on Frame Plastic Capacity

Based on the above discussion, it appears that for good performance of EBFs, e^* should be small, and then for the global behavior of a frame only large inelastic deformations in the link of length e need be considered. Therefore, the internal work of an EBF becomes mainly due to the work done by the link of length e, and the lateral load capacity of an EBF becomes dependent on the links of length e.

In order to investigate this important aspect, some example EBFs such as illustrated in Fig. 4.21 were considered. The lateral load P was applied at the top of the frame, and using limit analysis, P_u was obtained for two span lengths: $L = L_0$ and $L = 2L_0$. The beam sections for both cases were set equal and it was assumed that M_p^*/ M_p is 0.75, and b^* is $L_0/6$. Fig. 4.21 illustrates the variation in P_u against the e/L ratio for the two span lengths. The plateau in the figure indicates the range of e/L where shear yielding of the link occurs. It is important to note that the shear link gives a much larger P_u than does either the intermediate or the moment link. Depending on the span length, a shear link can provide 4.5 to 9 times the lateral load resisting capacity one can obtain with MRFs which corresponds to the case of $e/L=1$, and $P_u = 2M_p/h$.

Due to the great strength of EBFs, usually only a small number of EBF bays are needed to resist the seismic loads acting on a whole structure especially when shear links are employed in EBFs. Moreover, the beam sections for EBF shear links are of a much smaller size than that for MRFs. Figure 4.21 also indicates that EBFs employing shear links have capacities P_u proportional to the span length, this can be clarified from Eqs. 3.26 and 3.42 by setting the shear

resisting capacity of the link to a constant V_p. However, EBFs employing either intermediate or moment links develop capacities P_u which for the same e/L are almost independent of the span lengths. In general, the capacity of an EBF employing a shear link can be increased by simply extending the span length with the beam sizes unchanged. The column and possibly the brace size become smaller when normalized to the same frame capacity. If the above advantages of EBFs employing shear links are incorporated into the design of a frame for the required capacity, significant economy can be achieved.

4.6. Link Length e and Deformation Demand

The link deformation angles γ_p obtained in Chapter 2 for rigid-plastic displacements on D-, K-, and V-brace frames provide a good basis for evaluating the deformation demand of the links for a given plastic story drift ϑ_p. As can be seen from Eq. 2.20 to 2.22, for a given plastic story drift angle ϑ_p, the link deformation demand is inversely proportional to the e/L ratio. Therefore it is essential that a link be made sufficiently long so that no excessive link deformation would occur. However, for obtaining large capacity of an EBF as noted in Section 4.5, the link has to be made sufficiently short so that it would primarily yield in shear. Therefore the link selection must satisfy the above two conflicting requirements. The V-brace frame appears to be particularly advantageous in satisfying these conflicting requirements since for a given e, γ_p is only one half of those in the other two basic frames.

For achieving the above design one has to know the deformation capabilities of shear links. Fortunately, in spite of the large γ_p usually imposed on shear links due to smaller e/L ratio, past experimental research [32,53,84] has demonstrated that shear links can have a greater deformation capacity than

moment links if appropriate stiffening of the web is employed to prevent prema-
ture web buckling. Accordingly, web stiffening plays a key role in shear link
design. Although such criteria were offered in the past [32,53], they have not
been found to be entirely satisfactory for practical use in design. In this report,
more accurate criteria are given in order to achieve a better ultimate state
design for shear links. For such information see Chapter 6, 7, and 8.

4.7. Statistical Surveys of Standard Steel Sections

Based on the above considerations, it appears that the shear link provides
a great advantage for the seismic design of structures. As indicated in Chapter
2, ideal plastic theory requires that for the link to be a shear link, the link
length should be less than b^*. Therefore it is important to know the practical
range of the available b^*. From this view point, 156 standard sections ranging
from the W6 to the W36 sections listed in AISC manual [1] are reviewed. Fig.
4.22(a) shows the relationships between V_p and b^* for the sections of A36 steel,
where b^* is approximately bounded by

$$15\left[\frac{V_p}{\sigma_y}\right]^{\frac{1}{2}} < b^* < 30\left[\frac{V_p}{\sigma_y}\right]^{\frac{1}{2}} \tag{4.7}$$

where σ_y is the yield strength of the steel. The above inequality suggests that
the links with larger V_p's tend to have larger b^*'s.

The relationships between b^* and cross-sectional area A of a section is
shown in Fig. 4.22(b). These quantities are strongly correlated, indicating that
sections with unusually large b^*s tend to make the beams for EBFs heavier,
hence costlier.

4.8. Link Length e and EBF Elastic Stiffness

One of the unique features of an EBF is that the elastic story stiffness can be controlled by varying the e-value at each story while maintaining its plastic capacity as long as $e < b^*$. A study was made to determine a typical range of stiffnesses is available for this purpose [40]. First, the 20-story EBFs shown in Fig. 4.23 employing three types of bracing schemes were plastically designed using the design computer program to be explained in Chapter 5. The proportions and the design lateral forces as well as the vertical forces were similar to those used in Refs. 84 and 92. Corresponding to the various values of e and $e^* = 0$, four single-story EBF panel models located at different floor levels were analyzed by eliminating the boundary effects [9,59] resulting from the roof or base boundaries.

Fig. 4.24 exhibits the analytical results for the elastic story shear drift of the panels located at the 3-rd and the 19-th story levels subjected to the corresponding plastic design loads. The horizontal axis in this figure indicates the eccentricity ratios, which are e/L for the D- and K- brace frames, and $2e/L$ for the V-brace frame to provide a comparison under the same link deformation demand. Therefore, the length of each link in the V-brace frame is half of that in the other frames. For modeling, the shear deformation of the beam was considered and rigid end zones were assumed.

From this figure, it should be noted that the shear drift of the designed EBFs is well below the UBC story drift limits [94]. In some case, it was found that maximum stiffness can be attained with non-zero e-values meaning that an EBF sometimes is stiffer than a CBF. The important point to observe is that the stiffness of the V-brace is much greater than that of the others when the eccentricity ratio is larger than 0.1. The K-brace frame is the most flexible one in

spite of the fact that the member section properties used were almost the same as those for the V-brace frame. This can be explained by comparing the elastic deformation patterns for half portions of the K- and the V-brace frames shown in Fig. 4.25, where for the same eccentricity ratio, the eccentricity lengths for half frames become the same. One end of a link in a half portion of the K-brace frame is free to rotate, whereas that in the the V-brace frame is supported by the column, thus the link rotates less, resulting in the larger stiffness of the V-brace frame. It was also found that if the eccentricity ratio of the V-brace frame is twice as those in a K-brace frames, that is, length e of the links in V-brace frame is the same as that in K-brace frame, the elastic stiffnesses of both frame types become approximately the same. Some examples of this can be seen from earlier Figs. 4.7 and 4.8.

It can be seen from Fig. 4.24 that the decrease of stiffness by increasing the eccentricity ratio is more pronounced for the 19-th floor level panels. This suggests that the stiffness of EBF with lighter sections is sensitive to eccentricity. It also should be noted that although the magnitude of the shear drift is small, for the frames such as shown in Fig. 4.23, the chord drift at the higher story levels progressively increases, which is a common behavior of slender brace frame. Some design solutions to reduce this are available in the area of tall building technology, but are not discussed here.

The elastic stiffness of the an EBF is an important factor to be considered for seismic design, since it directly influences the period of the structure which governs the seismic design force. Further studies on this aspect of the problem are being pursued at Berkeley [41].

4.9. Conclusions

From the above discussion, the following factors to be considered in EBF design may be noted.

(1) In the presence of vertical loads, D-brace frames exhibit different plastic capacities as well as different lateral deflections depending upon the direction of the lateral force. Therefore in a structure an even number of D-brace frames with braces arranged in a symmetrical manner should be used. Due to their intrinsic symmetric configuration, these problems do not arise in the K- and the V-brace frames.

(2) It is necessary to keep e^* as small as possible to minimize the loss of EBF lateral load resisting capacity due to the positive work done by the vertical loads. In this manner large inelastic deformations are largely confined to the links of length e. This also leads to an economical design since web stiffeners are needed only for the links of length e.

(3) The proposed approximate limit analyses and EBF mechanisms agree extremely well with elasto-plastic solutions. The accuracy increases when e^* is small and/or the number of EBF stories is large.

(4) It can be proved by limit analysis that the loss or gain of D-brace frame capacity due to vertical load is a function of vertical load magnitude and topological parameters of the frame. The importance of this behavior increases for the light frames occurring in low-rise buildings or in the higher stories of tall buildings, for which the vertical load should be reduced as much as possible.

(5) The plastic capacity of EBFs with shear links is much greater than of those using moment links. If a shear link is to be used prior to the detailed design process, for reasons of economy the span length L should be made

as large as possible yet retaining maximum strength.

(6) The elastic stiffness of an EBF is greatly influenced by e/L. This ratio should be small if a large elastic stiffness is required. If the member sections as well as eccentricity ratios are the same, V-brace frame is much stiffer than the K-brace frame.

(7) The link sections with large V_ps also tend to have large b^* and weight. The use of a section with an unnecessarily large b^* might make a frame uneconomical.

(8) The energy dissipation mechanism provides a good measure on the ductility demand of the links. The basic link length e should be selected using the geometric relationships between the given plastic story drift and the wanted plastic link deformation. The maximum deformation criteria for shear links is given in Chapter 8.

Based on the above considerations, e, e^*, L, and the frame type needs to be carefully chosen in EBF design. The advantages of a V-brace frame is clearly evident at least from the link deformation demand and elastic stiffness point of view. For the same link deformation demand, e in this type of a frame needs to be only one-half as large as for the other types. If so designed, the stiffness of a V-brace frame is larger, and the beam sections can have half b^*s resulting in less weight of the frame. On the other hand, for the same e the stiffness of a V-brace frame is about the same as that of a K-brace frame. However the link deformation demand in the V-brace frame is now only one half that in the K-brace frame. This effect is particularly beneficial when a relatively small shear capacity in the link is necessary. For such a shear link usually b^* is small requiring a small e. Therefore the use of an other frame type rather than V-bracing would impose too large a deformation demand on the links used.

CHAPTER 5

PLASTIC DESIGN METHODS FOR EBFS

5.1. General

Basic Principles for Ideal EBF Design : - The development of any design method requires understanding the behavior of a structure. Based on the elastic and plastic behavior of EBFs discussed in the previous chapters, it is now possible to develop a design method for EBFs. As has been repeatedly pointed out, for good performance, the EBFs should be designed such that inelastic activity is primarily confined to links of length e. For such behavior the link shear resisting capacity governs the plastic capacity of the frame as discussed in the previous chapters. Therefore the primary objective in EBF design is to select a link of an appropriate shear resisting capacity for the required plastic capacity of an EBF, and to select the other members so that they remain elastic in order to assure the plastic activity of the link. Such a task can be carried out following the three basic steps given below:

Step 1: Estimate the member force distribution likely to occur satisfying global equilibrium for an EBF in a plastic state for the design capacity load.

Step 2: Find beam sections with a capacity as close as possible to the estimated link member forces in order to attain the required EBF capacity. The selected beam sections must remain elastic in regions other than the link.

Step 3:   Select braces and columns to remain elastic by assigning reasonable safety factors on the estimated member forces.

As one can note from above, it is considered that basically a plastic design method which directly refers to the member forces in the plastic state is most appropriate for EBF design. A design method satisfying the above principles will assure the required plastic capacity and the desired energy dissipation mechanism which are essential for good EBF behavior. Once an EBF is plastically designed, the serviceability requirement of elastic behavior, such as story drift, should be checked by performing an elastic analysis. Because of their superior capacity it also should be emphasized that only shear links are considered in this chapter.

As pointed out in the previous chapter, a plastically designed EBF employing shear links usually has sufficient stiffness for the shear drift. However if an EBF has an unusually slender configuration, the chord drift may be so large that the drift limit might be exceeded. Nevertheless such a condition will not change the selection of either the beams or the braces. Since the chord drift is due to the column axial deformations, only the column size would have to be increased. An estimate of the required column axial stiffness can be made by idealizing the braced frame as a cantilever beam, and since such a method has been commonly used in practice, it is not discussed here.

Background and Proposed Design Method : - Design methods for EBFs were previously presented by Roeder [84], Manheim [54] , and Teal [92]. The first two of these methods are based on the limit analysis approach and use the lower and upper bound theorems for ideally plastic structures. However, as will be indicated in this chapter, it is very difficult to obtain a reasonable estimate of member force employing these methods. The third method is an allowable

stress design method utilizing modified safety factors based on code provisions. Since this method does not directly refer to the plastic state of an EBF and the member force estimates are not necessarily accurate, the degree of conservatism for individual member design is very difficult to assess.

Since the above design methods seem to present problems in ease of application, accuracy, or consistency, an alternative approach was developed, and will be discussed herein. Unlike the above methods, the proposed approach easily satisfies the requirements of equilibrium. Because of a straight-forward approach in the proposed design method, the member forces can be estimated very quickly with simple hand calculations. In order to minimize the design effort even further, a computer program for the basic Steps 1 through 3 given above was developed. Some example EBFs were designed using this program, and the accuracy of the developed procedure is demonstrated by comparisons with elasto-plastic solutions. Furthermore, based on this development, a simplified procedure approximating the global equilibrium yet yielding reasonable estimates of member forces was also derived and will be presented herein.

5.2. Comments on Previous Plastic Design Methods

General Concepts in Previous Plastic Design Methods : - Pioneering plastic design methods for EBFs were previously studied by Roeder [84] and Manheim [54].

The first method [84] consisted of applying the moment balancing procedure [20,34]. This technique is based on the concept that, if a structure is designed for any moment diagram which satisfies statics, the loading will be a lower bound solution for the structure. If the design is performed so as to attain also a specific mechanism, the lower and upper bound solutions are

simultaneously satisfied. However, it is immaterial how the distribution of forces and moments is attained in the moment balancing procedure. This distribution can be obtained by a good guess or by any number of iterative procedures.

In contrast to the above method, the second method [54] is based on the upper bound solution satisfying the desired energy dissipation mechanism. The procedure can be explained as follows : By assuming a desired mechanism for a structure such as shown earlier in Fig. 3.3(a), for the given plastic design lateral loads, one obtains W_E according to Eq. 3.16. Then the ratios of V_p's at all floor levels to the one at a reference floor level are assumed, and the ratios of the works done in the plastic links of length e is determined. In this manner W_I given by Eq. 3.14 is expressed in terms of one unknown, which is the V_p-value for a reference story level. On equating W_E to W_I, one can solve for V_p at a reference story level, and consequently V_p's for all the links are obtained according to the ratios assumed. The other member forces follow by applying conditions of statics.

Problems in Previous Plastic Design Methods : - Attempts were made to apply both of the above two methods for designing EBFs. The first one of these [84] starts with an assumption for the percentage of lateral force to be resisted by the braces, for which 80% was recommended. Moment balancing satisfying equilibrium to achieve appropriate kinematics involves a considerable amount of trial and error, and depends very much on intuition. On applying this method it was soon recognized that the suggested initial assumption for load distribution would not lead reasonable column moment estimates. For example, the columns in the frame would tend to develop single curvature accumulating moments from the top to the bottom of the structure. This results in very large

moments in the columns. Therefore, the assignment of 80% of the lateral force to the braces was modified and the same procedure was followed. However, again no satisfactory results were achieved and large column moments were obtained. A column moment distribution typically obtained is illustrated in Fig. 5.1(a).

Next, the second method [54] was tried. On applying it, after obtaining the link shear forces, distribution of the member forces was sought by assuming magnitudes for the redundant forces. These assumptions, satisfying statics, were varied in order to obtain reasonable member forces. However, again as in the first method, no satisfactory solutions were achieved even when the ratio of link shears in all floor levels initially assumed was changed.

In either one of the above two methods it is difficult to obtain an equilibrium solution which gives an appropriate estimate for column design moments. This stems from the initial assumptions for the link shear or brace force quantities. A relatively small perturbation of these quantities from the correct ones causes a large deviation from the acceptable shears and moments of the columns. As will be shown later, this is because in the global equilibrium, contribution of column moments are much smaller than the link shear or the brace force quantities. Either one of the above two methods for EBF design is likely to result in single curvature in columns with large moments unless a good scheme for controlling column moments by changing the link shears or brace forces is given.

If the columns were proportioned for the extraordinary large moments indicated by the above solutions, the designed frame would have a very small beam-strength-to-column-strength ratio, which suggest that the flexural behavior of the columns designed in this manner will be similar to that of coupled shear walls connected by small link beams. However, from the EBF design

point of view, this is an unrealistic solution. An optimized solution for the column moments is difficult to obtain using either one of the above two methods, and therefore a new approach was sought.

5.3. Proposed Design Approach

Basic Equilibrium Equations : - Figure 5.2 shows a free-body diagram of a D-brace frame at a typical story level. It is subjected to the lateral loads F_L and F_R on the left and on the right side of the frame, respectively. For the beams and columns, the moment, shear, and axial forces are defined by M, V, and P, respectively, with subscripts on these quantities for particular members. For example, M_R, V_R, and P_R indicate the moment, shear, and axial forces at the bottom of the right column as shown in Fig. 5.2, and M_A, M_B, V_{AB}, and P_{AB} indicate those for the link $\overline{AB}$, respectively, etc. The vertical component of the brace axial force is defined as B_V. The forces transferred from the upper story level are M_R', V_R', P_R', at the top of the right column, M_L', V_L', P_L', at the top of the left column, and B_V', the vertical component of the brace axial force form the upper story level. All of these quantities are known from the analysis of the upper floor. If the frame is located at the top of a structure, these forces are zero. As discussed in Chapter 4, it has been found that the vertical load on a beam is not likely to cause significant changes in the local member forces, thus, it is not included. Further, the brace moment magnitudes are small, and since neglecting them reduces the statical indeterminacy of the problem, they are not included in the formulation.

The task is to find both statically and kinematically admissible solutions for the frame. As discussed previously in Chapter 4, if for a given structure e^* is small enough, the desired mechanism is of only one kind being either

Mechanism 1 or 2. This means that one can assign plastic hinges deterministically for the frame.

Further, in order to reduce the statical indeterminacy of the structure and to stabilize the column moment solutions, it is necessary to assign the location of the column inflection points. The parameter defining the location of the inflection point is α_R and α_L, a ratio of the bottom end moment to the top end moment of the right and left columns respectively. α_R and α_L can be assumed as unity for a typical story except at bottom, where they should be larger than one to ensure hinging at the base. For simplicity it could be assumed that $\alpha_R=\alpha_L$. The equations for moment equilibrium for the two columns are :

$$F_R + V_R' + P_{AB} - \frac{1}{h}(1 + \alpha_R)(M_A - M_R' + V_{AB}d_R) = 0 \tag{5.1}$$

$$F_L + V_L' - P_{CD} + \frac{1}{h}(1 + \alpha_L)(M_D - M_L' + V_{CD}d_L) = 0 \tag{5.2}$$

Three force equilibrium equations can be written for the beam $\overline{BD}$

$$P_{AB} - P_{CD} + \frac{a}{h}B_V - \frac{a'}{h'}B_V' = 0 \tag{5.3}$$

$$V_{AB} - V_{CD} - B_V + B_V' = 0 \tag{5.4}$$

$$V_{AB} - B_V + \frac{1}{(a + e^*)}(M_B - M_D + e^* B_V') = 0 \tag{5.5}$$

In the above 5 equations there are 8 unknowns. However the following 3 equations should also be considered :

$$M_A = \beta_A\left[\frac{e V_{AB}}{2}\right] , \tag{5.6}$$

$$M_B = (2 - \beta_A)\left[\frac{e V_{AB}}{2}\right] , \tag{5.7}$$

$$M_D = \beta_D\left[\frac{e V_{AB}}{2}\right] , \tag{5.8}$$

where β_A and β_D, respectively, are the amplification factors for moments at A and D for the ideal equal end moments at the yield limit state for link $\overline{AB}$. The above equations can be solved if the following quantities are established.

Estimate for End Moments of Shear Link. - If one considers the limit state for a link of length e, as discussed in the previous chapters, M_A is equal to M_B, i.e., $\beta_A = 1$ in Eqs. 5.6 and 5.7. However, for column design, as will be elaborated upon in Section 5.6, the critical condition develops prior to such a limit state, especially if a shear link is used, and it is plausible [40] to set

$$\beta_A = \frac{b^*}{e} \geq 1 \tag{5.9}$$

which means that a moment M_p^* occurs at a point such as A in Fig. 5.2. As can be seen from Eqs. 5.6 and 5.7, this implies unequal end moments in the link $\overline{AB}$.

Also, β_D can be assumed to be the same as β_A in Eq. 5.9 if e^* is the same as e, since as illustrated earlier in Fig. 4.10, the moment diagram becomes approximately antisymmetric for $e^* = e$. However, since it is best to have e^* as small as possible, as illustrated in Fig. 4.12 the importance of M_D for design decreases. Based on some numerical experimentation, the following empirical equation for β_D was found to be useful :

$$\beta_D = (0.2 + 0.8 \frac{e^*}{e}) \beta_A , \tag{5.10}$$

Equilibrium Solution and Shear Link Beam Selection : - At this point, one can recognize that Eqs. 5.1 to 5.5 can be solved if β_A as given by Eq. 5.9 is known. However, b^* in Eq. 5.9 is dependent on the beam section which is not known before it is selected. Therefore for an accurate estimate of the member forces, the beam sections must be known, which depend on the member forces. This suggests a need for an iterative procedure for arriving at a solution. The

main criteria for selecting the initial beam sections are:

(1) b^* of a section must be equal to or less than the link length e.

(2) The estimated link shear force V_{AB} should be as close as possible to the V_p of the beam.

(3) The moment and axial force interaction formulas 2.4-2 and 2.4-3 specified in Part 2 of Ref. 1 for plastic design should be satisfied for the estimated moments and axial force in the beam $\overline{BC}$ in Fig. 5.2.

It should be noted that criterion 2 above neglects the axial force in the link which is usually of small magnitude (See Section 2.3 and Chapters 6 and 7 for the exceptional case). On the other hand, the axial force in the beam $\overline{BC}$ is large, and criterion 3 considers this effect.

By using the above criteria for beam selection, in order to obtain an accurate estimate of member forces, either one of the following two alternative iterative methods can be used :

First Method : - The first method starts by assuming magnitude of β_A in the range from 1.0 to 1.4. Solving Eq. 5.1 through 5.5 beam sections according to the above three criteria are selected. After that, a new β_A's are calculated using the actual b^*s for the selected sections, and the solution of Eqs. 5.1 through 5.5 is repeated. For the newly obtained member forces, the criteria 2 and 3 given above are verified. If they are violated, new sections satisfying three criteria are made and the calculations are repeated. Typically no change of sections is necessary after one or two iterations. The estimated member forces at the final iteration should be used for designing the braces and columns.

Second Method: - The second method starts by selecting a beam before solving Eqs. 5.1 through 5.5. This can be done by assuming that V_{AB} is

approximately h/L times the story shear force cumulated from top to the level in question of an EBF. This procedure will be explained in Section 5.7. During the first step the selection is based on criteria 1 and 2 only. After that, using b^*'s for the selected sections, β_A's are calculated and Eq. 5.1 through 5.5 for the member forces are solved. The remaining follows the first method outlined above. This procedure may require less effort compared to the first method.

Yielding Checks in Other Regions : - For the member forces estimated in the final iteration, it is necessary to check whether the yield criteria for the shear force in a link $\overline{CD}$ is satisfied in relation to the link $\overline{AB}$, i.e., whether

$$| V_{CD} | \leq | V_{AB} | \quad , \tag{5.11}$$

This condition is likely to be the case when the lateral load distribution smoothly varies along the height of a building and/or the e^*'s are small.

Selection of Braces and Columns : - When a beam is selected within the prescribed tolerance, the braces and columns can be proportioned based on the member forces estimated in the final iteration. In order to assure the link plastic action, these members must remain elastic.

For brace selection, the calculated axial compression forces can be used to select the brace sections employing formula 2.4-1 given in Ref. 1. For columns, the two formulas 2.4-2 and 2.4-3 for the moment and axial force interaction must be used.

It should be noted that in order to assure the elastic behavior of columns and brace, some approximate safety factors must be used in selecting the members, especially when the link beam with a V_p larger than the required V_{AB} is chosen, since then the capacities of the columns and the braces must be correspondingly upgraded. For such cases the member forces transferred from

the links to the columns and braces must be increased in the ratio of V_p / V_{AB}.

It should be emphasized that in the present discussion perfectly plastic behavior of steel is assumed. An increase in the link shear capacity due to strain-hardening should be considered in the ultimate state design, since the member forces transferred from the links to the columns and braces increase. This problem is discussed in more detail later in this report.

General Comments : - By repeating the above procedures from the top of a structure to a bottom, the design of the frame is completed. Some general comments on the design follow:

Fig. 5.3 illustrates typical variations in the beam and link forces during iterations with respect to the β_A-value. A change in β_A influences significantly the moment distribution in the link $\overline{AB}$ and the beam $\overline{BC}$ as shown in Fig. 5.3(a). On the other hand, the link shear force V_{AB} and beam axial force P_{BC} are quite insensitive to changes in β_A as shown in Figs. 5.3(b) and (c).

As explained earlier, the selection of a beam size is made by checking the shear force in the link portion $\overline{AB}$ as well as combined moment and axial force in the beam portion $\overline{BC}$. The above discussion indicates that the beam size sometimes might be changed due to a significant change in the moment in beam $\overline{BC}$, but since combined effect of moment and axial force is checked for $\overline{BC}$, such a change in the moment alone is not very influential on the design. Therefore, typically no change of member size is necessary after the first or second iteration.

The choice of α_R and α_L is rather arbitrary. It is better to assign to these quantities positive values in order that inflection points develop in the column, and moment growth along a column stack is prevented. Optimum size of column is most likely achieved by assuming $\alpha_R = \alpha_L = 1$ except at the ground level.

If the lateral load distribution over the height of a frame is not smooth, some iterations of α_R and α_L may be necessary.

It is to be noted that a solution obtained in the above manner satisfies three conditions for the correct plastic behavior of a frame, the yield criteria, kinematics and equilibrium. Therefore a design of a frame on the above basis satisfies both the upper and the lower bound solutions to this plastic problem, and inelastic activity is confined to appropriate locations.

Design of K- and V-brace Frames : - Because of the intrinsic geometrical similarities, the above procedure for designing D-brace frame is also applicable for K- and V-brace frames with some appropriate changes in the equilibrium equations.

For the K-brace frame, Fig. 5.4 illustrates the free body diagram obtained by modifying that for the D-brace frame shown earlier in Fig. 5.2. Taking advantage of the symmetry of the frame configuration, and assuming that equal lateral forces are applied on both sides of the frame, a smaller number of equilibrium equations can be obtained, i.e.,

$$F_L + V_L{}' - P_{CD} + \frac{1}{h}(1 + \alpha_L)(M_D - M_L{}' + V_{CD}d_L) = 0 \tag{5.12}$$

$$P_{CD} - \frac{\alpha}{h}B_V + \frac{\alpha'}{h'}B_V{}' = 0 \tag{5.13}$$

$$V_{AB} - V_{CD} - B_V + B_V{}' = 0 \tag{5.14}$$

$$V_{AB} - B_V + \frac{1}{(\alpha + e^*)}(M_B - M_D + e^* B_V{}') = 0 \quad , \tag{5.15}$$

and

$$M_B = \frac{e V_{AB}}{2} \ , \tag{5.16}$$

$$M_D = \left(0.2 + 0.8\,\frac{2e^*}{e}\right)\left[\frac{e V_{AB}}{2}\right] \quad (e^* < \frac{e}{2}) \tag{5.17}$$

The assumed moment magnitudes are influenced by the first term in Eq. 5.17 and also α_L only, usually no iteration is needed for this type of frame.

For the V-brace frame a similar procedure applies based on the free body diagram in Fig. 5.5, i.e.,

$$F_R + V_R' + P_{AB} - \frac{1}{h}(1 + \alpha_R)(M_A - M_R' + V_{AB}d_R) = 0 \tag{5.18}$$

$$P_{AB} + \frac{a}{h}B_V - \frac{a'}{h'}B_V' = 0 \tag{5.19}$$

$$V_{AB} - V_{CD} - B_V + B_V' = 0 \tag{5.20}$$

$$V_{AB} - B_V + \frac{M_B}{(a + e^*)} = 0 \quad , \tag{5.21}$$

where

$$M_A = \beta_A \left[\frac{e V_{AB}}{2} \right] \quad , \tag{5.22}$$

$$M_B = (2 - \beta_A)\left[\frac{e V_{AB}}{2} \right] \quad . \tag{5.23}$$

$$\beta_A = \frac{b^*}{e} \geq 1 \quad , \tag{5.24}$$

Since $M_D = 0$, the equations for this frame are simpler. However, iterations for β_A are suggested.

For both the K- and the V-brace frames the remainder of the design procedure follows that for the D-brace frame discussed previously.

5.4. Design Computer Program

The above procedures can easily be made using hand calculations. However, in order to reduce work, a design program for EBFs was developed based on the first method described in the previous section. The computer program

was written for three types of frames: the D-, K-, and V-brace frames with an iteration capability for β_A. The flow chart for the program is shown in Fig. 5.6. The program automatically calculates the lateral forces specified by the UBC[94] or ATC[4]. The lateral forces may be alternatively given as input. The basic design load condition is given as

$$\text{Design Load} = \pm\mu_1\mathbf{E} + \mu_2\mathbf{D} + \mu_3\mathbf{L} \tag{5.25}$$

where $\mathbf{E}$, $\mathbf{D}$, and $\mathbf{L}$ are the earthquake lateral, dead, and live loads, respectively, and μ_1, μ_2, μ_3 are the corresponding load factors for plastic design.

The members are proportioned using the envelopes for member force resultants. Some standard 157 wide flange beam sections for beam and brace members and 124 tube sections for brace members can be specified depending on preference. Further, some 83 sections which are mainly W14's, W12's, and W10's are available in the program for the columns.

Except for the beams, minimum weight member sections were selected. For the beams, the sections with minimum weight were chosen only from groups of sections which have V_p values close to the calculated V_{AB}. Therefore the selected beams do not necessarily have minimum weights in an absolute sense. This is because a beam section with a considerably larger V_p than V_{AB} was considered to be inappropriate, since using a such a section, the distribution of link energy dissipation throughout the story height may not vary smoothly compared with the design lateral force distribution.

The computation time necessary for the execution of this program is very short since the formulation explained above is straight-forward and due to the small memory space required even for a 40-story EBF, the use of a micro computer is possible.

5.5. Design Examples and Behavior of Plastically Designed Frames

Design Example : - In order to test the proposed design method, the frames illustrated in Fig. 5.7 were designed for lateral loads of 200 kips applied at the top of each frame. These frames could be viewed as the lowest 3 stories of a medium-rise building. The member sections for the two frames selected by the computer program are shown on the figures.

The proportion as well as the loading condition of the D-brace frame are the same as those previously designed by Roeder [77,84]. For such a frame, Fig. 5.8 shows the comparison of moment as well as axial force distribution obtained respectively by the plastic moment balancing (Roeder) and the proposed method. As can be seen there is a marked difference in the estimate for the column design moments between the two methods. As previously noted (see Fig. 5.1), this discrepancy would become even larger for taller buildings.

Elasto-Plastic Behavior of Plastically Designed Frames : - Fig. 5.9 illustrates the elasto-plastic load-deflection behavior for the two frames designed by the proposed method. It can be seen that the plastically designed frames attained the expected capacities. The large elastic stiffnesses of the frames can be recognized.

Fig. 5.10 illustrates the progress of plastic zone formation in the D-brace frame, where one can see that three links of lengths e yielded at the same time. Yielding of a rather long 1-st story link of length e^* occurred at a large story drift. In general, the figure shows that an appropriate mechanism was obtained in the designed D-brace frame.

Fig. 5.11 shows that in the V-brace frame the yielding of links developed at somewhat smaller story drift than in the D-brace frame since the beam sections are lighter having smaller M_p^*'s. However, this yielding had insignificant effect

on the global behavior as shown in Fig. 5.9. Until the links fully yield, the frame continues to resist further increments in loading. For this frame, the desired kinematic mechanism was also obtained and the required plastic capacity was attained. The plastic shear deformations of these links at considerable story drift were only about half as large as those in the D-brace frame since the same link lengths e were used in both frames (see Section 4.9).

The comparisons between the moments and axial forces for D- and V-brace frames predicted by the proposed method and elasto-plastic analysis is shown in Figs. 5.12 and 5.13. Some discrepancies, which are not significant from the design viewpoint, occur because the capacities of the selected beams somewhat exceed the design forces. The excess beam capacity was larger in the D-brace than the V-brace frame.

It is interesting to note that in the elastic range, the moments at link ends differed by ratios varying from 2 to 4, which is due to the different rotational restraint provided by the columns and the adjacent beams. Generally, the link end attached to a column develops a higher moment than at the other end because of the greater rigidity of the column compared to the beam. In a study of a 20-story EBF it was found that the ratio of link end moments was in the order of 8 or 9 near the bottom of the frame where columns are very rigid. If this ratio is of such a large magnitude an earlier yielding of the link e at a column face is likely to occur. However, as the present results for the V-brace frame show such yielding is not very important for either the stiffness or the strength of a frame.

Figs. 5.12 and 5.13 show that in general for both frames the design moments, shear forces, and axial forces are in excellent agreement with the results of the elasto-plastic analyses, leading to the conclusion that the proposed design method is very accurate.

5.6. Link End Moments for Column Design

Elasto-plastic analyses of EBF's such as discussed in the previous section suggest that the critical moments in the shear link from the column design point of view occur during the earlier stages of loading rather than the theoretical limit state explained earlier in Section 2.3. This question is elaborated upon below.

Fig. 5.14 illustrates a single story EBF with lateral load applied at the top of the structure. Corresponding to the loading path 1-2-3-4 shown in Fig. 5.14(a), the moment and shear forces at end A of an elastic-ideal plastic link follow the path such as shown in Fig. 5.14(b).

After reaching the interaction curve with shear force less than V_p, the V_{AB} continues to increase whereas M_A decreases, thus due to a relation of statics between the moment and the shear, M_B increases. When V_{AB} becomes equal to V_p at point 3, a negligibly small increase in V_{AB} occurs and the link approaches the limit state, i.e., M_A and M_B tend to equalize. The magnitude of M_A changes significantly between 3 and 4, whereas V_{AB} is almost the same.

The above considerations suggest that the moment transferred from the link to the top of the column shown in Fig. 5.14(c) would differ a great deal between the load points 3 and 4, whereas the column axial force, which is equal to link shear V_{AB}, is almost the same. Accordingly, Fig. 5.14(c) illustrates that a column designed for the theoretical link limit state point 4, is not sufficiently strong to remain elastic during the elasto-plastic loading process. The design should be done considering the most critical loading which occurs at point 3 as illustrated in the figure.

Recognizing this, unlike the earlier design methods [77,84,92] which consider equal end moments in a link, unequal end moments must be considered in

the design. On the other hand, it should be noted that for the beam $\overline{BC}$, the design based on load point 3 is less conservative than that based on point 4 since M_B is smaller at point 3 than at 4. This, however, can be considered to be acceptable since numerous trial elasto-plastic analyses indicate that loading corresponding to point 4 is not likely to occur within the practical range of EBF deformations.

A good estimate of link end moments is of great importance in design of EBF. The strain-hardening effect which has a great influence on the capacity of a link must also be considered in the design. This motivated the experimental investigation to be discussed in the next two chapters.

5.7. Approximate Solutions for Link Shear Force in EBF

Significance of Bending Moments in Global Equilibrium : - In Section 5.2 an exact equilibrium method which gives a reasonable estimate for the beam and column moments was presented. It was indicated there that during an iteration process for satisfying equilibrium, the shear and axial forces in the beams are insensitive to variations in beam moments (see Fig. 5.3). This shows that the importance of the beam (or column) moment in the global equilibrium is small in comparison with that in the shear and axial forces. One can take advantage of this fact in order to estimate the shear forces approximately in the following manner.

Approximate Analysis for D-brace Frame: - An approximate approach to obtain the link shear force can be developed based on Fig. 5.15 for the D-brace frame. In Fig. 5.15(a) is shown a typical moment distribution for an i-th level. In this development the story shear force cumulated from the top to the i-th

level will be called V_{CUM}. Fig. 5.15(b) illustrates a D-brace frame panel at the i-th level where for simplicity it is assumed that on the left the brace intersects at the column centerline. Using the same notation for the moment, shear, and axial forces as used in Section 5.2, and by setting the horizontal component of the brace force as V_B, for equilibrium one has

$$V_{CUM} = V_{L}{}' + V_{R}{}' + V_B{}'. \qquad (5.26)$$

It is to be noted that the moments $M_L{}'$ and M_L are opposing each other and could be expected to be of the same order of magnitude. In any event the significance of these column moments compared with that of $V_{AB}L^-$ is very small, therefore the relative magnitude of the term $(M_L\text{-}M_L{}')$ is is likely to be extremely small in the sense of global moment equilibrium. Therefore, neglecting this term,

$$(V_L{}' + V_B{}')h \approx V_{AB}L^- + P_{AB}h \qquad (5.27)$$

Further, making a summation of moments around the bottom of the right column, and neglecting the term $(M_R\text{-}M_R{}')$ as above, one has

$$V_R{}' \approx V_{AB}(L - L^-) - P_{AB}h \qquad (5.28)$$

Substituting Eqs. 5.27 and 5.28 into Eq. 5.26 gives,

$$V_{CUM} \approx \frac{V_{AB}L^-}{h} + P_{AB} + \frac{V_{AB}(L - L^-)}{h} - P_{AB} \qquad (5.29)$$

Accordingly, one can obtain an extremely simple formula stating that

$$V_{AB} \approx \frac{h}{L} V_{CUM} \qquad (5.30)$$

Approximate analysis for the K- and V-brace Frame : - For K-brace frame, due to symmetry of the configuration, the left portion of the above free body diagram can be used for modeling left half of a K-brace frame, and P_{AB} can be

set at zero both in Fig. 5.15 and Eq. 5.27. Therefore, Eq. 5.30 remains valid for the K-brace frame.

By following a similar procedure, one can reach the conclusion that Eq. 5.30 also holds for V-brace frame.

Design Applications : - Unlike the exact equilibrium method developed in Section 5.2, Eq. 5.30 was derived from approximate equilibrium conditions. Nevertheless the estimated link shear forces are in reasonably good agreement with the accurate solutions, even for the cases where braces are offset. It can be expected that this accuracy will hold as long as the difference in the column moments at the top and bottom is not very large, and would apply whether the frame is in an elastic or plastic condition. In design application, the beam sections may be chosen by calculating V_{AB}'s using Eq. 5.30. Iterations satisfying the equilibrium conditions as in Method 2 of Section 5.2 could then be performed if desired.

5.8. Comments on Allowable Stress Design Method

An alternative approximate procedure for estimating member forces in EBFs has been proposed by Teal [92]. By modifying the allowable stress approach given in the specifications [1], the members are proportioned for the calculated forces.

Estimation of Member Forces : - The method begins by calculating the base shear V for allowable stress design [94]:

$$V = ZIKCSW,$$ (5.31)

where W is the total weight of a building, and Z, I, K, C, and S respectively are

the coefficients depending on the zone, importance of the building, type of building frame, period of building, and soil properties.

In the approach developed by Teal [92] the member forces are calculated by iterating the magnitudes of the link shear forces assuming the inflection points in the middle of each link and approximately maintaining the equilibrium conditions. However, since this implies equal link end moments, according to Section 5.6 this procedure underestimates the link moment at A and overestimates it at B. Although not explicitly stated in Ref. 92, the above approach seems to try to predict the elastic member force distribution, and in such a case according to the discussions in Section 5.5, the error in link end moment estimates would be usually very large.

Furthermore, due to an inaccurate basic assumption employed, the iterations for obtaining the correct link shear force is no better than the simple estimate given by Eq. 5.30, which, in fact is used in the above method to provide an initial estimate for the link shear forces prior to iteration.

Safety Factor in Allowable Shear Stress Design: - Since the specifications [1] and the code [94] were not written with EBFs in mind, several modifications had to be introduced in the above allowable stress design approach [92]. For example, the code specifies that all members in braced frame shall be designed for 1.25 times the force determined on the basis of Eq. 5.31. This factor is intended to compensate for a lack of ductility in compression members loaded with axial forces. However in Ref. 92 it is assumed that for an EBF, this should apply only to the columns, braces, and beam connections but excludes the beam from this requirement.

The standard codes also allow a 1/3 increase in the allowable stresses except for the connection stresses. Therefore, the usual allowable shear stress

of $0.40F_y$ is modified to be

$$F_v = (0.40F_y)(1.33) = 0.53F_y \ , \tag{5.32}$$

where F_y is the yield stress of the steel, and F_v is the average shear stress taken on the area dt_w [1] for obtaining the allowable shear force. As given by Eq. 2.3, the plastic shear capacity V_p is calculated herein using yield shear stress $F_y / \sqrt{3} \approx 0.58F_y$ and the shear area $(d-tf)t_w$. As will be commented upon in Section 7.2, the authors feel that the use of the shear area $(d-2t_f)t_w \approx 0.95dt_w$ would represent an actual V_p more closely. Thus using the latter area, Eq. 5.32 provides a safety factor

$$\text{S.F.} = \frac{(0.58)(0.95)}{0.53} = 1.04 \ , \quad \text{for allowable shear stress.} \tag{5.33}$$

Therefore an EBF designed for such an F_v would have a base shear capacity V_u only 1.04 times the code specified V given by Eq. 5.31, i.e.,

$$V_u = 1.04 \, V \ , \quad \text{by allowable stress design.} \tag{5.34}$$

On the other hand, if the plastic design method is applied, the frame must be designed with a load factor of 1.3 [1,94]. This load factor is compatible [3] with the safety factors for the allowable axial and flexural stresses in the specifications [1], i.e.,

$$\text{S.F.} = 1.30 \ , \quad \text{for allowable flexural and axial stresses.} \tag{5.35}$$

and

$$V_u = 1.30 \, V \ , \quad \text{by plastic design.} \tag{5.36}$$

Although code provisions are not as yet available for EBF's, if the plastic design method is used for such frames, designed EBF's would have a story shear capacity 1.3 times V. Comparing Eqs. 5.34 and 5.36, one can recognize that methods result in about a 26% difference in the base shear capacity. This stems from the

relatively small S.F. for the allowable shear stress in the code as Eq. 5.33 indicates. Using the above allowable stress design it is asserted in Ref. 92 that since the code does not consider the ductile nature of EBFs and assigns a large K-factor for CBFs in Eq. 5.31 the design base shear V is overly conservative, and the small S.F. such as given by Eq. 5.33 is acceptable. However, it appears that the current code development activity tends to categorize EBFs as ductile seismic resistant frames having a reduced K-factor. In that case, it is necessary to revise the allowable shear stress so that S.F. will become about 1.3 since the smaller safety factor than 1.3 would give EBFs a smaller capacity than is normally expected for the other types of frames.

Based on this more consistent approach, from Eq. 5.33 the allowable stress in shear including one-third increase in stress, would be

$$F_v = \frac{(0.58F_y)(0.95)}{1.3} = 0.42F_y \ . \tag{5.37}$$

The allowable shearing stress without the one-third increase would be

$$F_v = \frac{0.42F_y}{1.33} = 0.32F_y \ . \tag{5.38}$$

For seismic loads by using the allowable shearing stress given in Eq. 5.37, V_u for EBFs would be consistent with that determined from Eq. 5.36 for plastic design.

Lastly, it is also important to clarify how the magnification factor of 1.25 noted above should be applied in the EBF design. According to Ref. 92, this factor should be used in the design of columns and braces, This consideration is quite good in assuring the desired mechanism for an EBF. However, the following should be also noted : The 1.25-factor used in practice for CBFs has the effect of increasing their capacity thereby improving their seismic performance of CBF, and if such a factor is also used in the design of EBFs, it may be

interpreted to mean that the EBF capacity must also be increased by a load factor of 1.25. In such a case,

$$V_u = (1.25)(1.3) V = 1.63 V \qquad (5.39)$$

As one can see by comparing Eq. 5.34, 5.36, and 5.39, very different base shear capacities for EBFs are required depending on the interpretation of the code. It is hoped that these remarks will prove useful in development of the code provision for EBFs.

5.9. Conclusions

Based on the development in this chapter the following conclusions can be made.

(1) In order to assure the required plastic capacity and desired energy dissipation mechanism, a plastic design method is essential in EBF design.

(2) The previously developed plastic design methods present some problems in accuracy and ease of application.

(3) It is believed that the new fully developed plastic design method is both direct and simple to apply. The predictions of EBF mechanisms, capacities, and member forces appear to agree well with elasto-plastic solutions.

(4) It is advisable to take into account that link end moments occurring prior to link limit state are not equal leading to a critical condition in column design. An equalization of end moments in a shear link was not observed in elasto-plastic analyses of EBFs for reasonably large deformations. It is believed that if a moment link is used, the end moments can be expected to equalize.

(5) Due to a special equilibrium field for EBFs, unless the distribution of column moments is very different from the assumed, the shear force in a link can be estimated simply as h/L times the story shear cumulated from the top of a frame to the level being investigated. This approach is reasonably accurate whether the EBF is in an elastic or plastic state.

(6) An approach for estimating member forces given in Ref. 92 is somewhat cumbersome, and the assumption employed for determining moment distribution is not in general correct.

(7) The allowable shear stress given in the codes [1,94] provides a smaller safety factor than is used for the other allowable stresses. Since EBFs depend on the shear capacity of the links, it is very important to revise this factor to correspond with others if the allowable stress design is to be permitted.

It should be strongly emphasized that this chapter is based on ideal plastic behavior of links, and can be considered as the basis for further design developments where the effect of cyclic strain-hardening on the moment and shear capacities of the links must be included. In order to obtain the needed information on this aspect, an experimental study on link cyclic behavior was carried out, and will be discussed in the following two chapters.

CHAPTER 6

EXPERIMENTAL STUDIES ON

GENERAL BEHAVIOR OF SHEAR LINKS

6.1. General

Fig. 6.1(a) illustrates a typical wide flange eccentric beam link of length e for an EBF. As discussed earlier, in such active links the vertical components of the brace axial forces are principally transmitted to the columns through bending and shear. Extensive experimental studies were carried out at Berkeley on cyclic inelastic behavior of isolated active link models. It was concluded that active links proportioned to yield primarily in shear provide excellent energy dissipation under the severe cyclic loading characteristic of earthquake excitation. Such shear links must be appropriately sized and reinforced with web stiffeners [32,53], and a criteria for stiffener spacing design are to be given in Chapter 8. Experimental and analytical studies have demonstrated that well stiffened shear links provide larger dissipation of energy than links forming only end plastic moments [32,40,53,84].

A shear link is usually exposed to high end moments and large shear in both the elastic and inelastic states. To-date, no investigations have been conducted on the cyclic performance of links under the action of unequal end moments and the manner of inelastic moment redistribution. In spite of the practical importance of this problem for design and analysis of EBFs as pointed out at Section 5.6, past studies have not addressed this issue since ideal plastic

theory was used for moment-shear interaction and the inherent strain-hardening effect was neglected. Furthermore, so far no realistic studies have been carried out on the exceptional but important situation where the links are simultaneously subjected to large axial forces. The present experimental investigation of active link cyclic behavior was undertaken to obtain some basic data on the foregoing problems. Unlike experiments carried out in the past, the subassemblage test setup designed for EBF behavior simulation made it possible to examine moment redistribution of the cyclically loaded link and its behavior with or without the application of an axial force. The results of tests on seven link beams subjected to monotonic and cyclic excitations are reported herein. Based on these and past research results, some new proposals for the design and analysis of links are made.

6.2. Preliminary Remarks

Prediction of Link End Moments By Ideal-Plastic Theory : - If a link in an EBF is placed next to a column, the elastic link moment at the column is generally much larger than at the other end of the link as shown in Fig. 6.1(a). The basic question is how these moment will redistribute in the the link in the inelastic state. In order to describe this behavior lower bound solutions using moment-shear interaction curves based on perfect plastic theory were often used in the past [32,53,54]. Fig. 6.1(b) shows one of such curves.

Following ideal plastic theory, as discussed for a single-story EBF in Section 5.6, the arrows shown in Fig. 6.1(b) indicate the ideal elasto-plastic behavior of the shear link in Fig. 6.1(a) for a typical story level of an EBF. The ideal theory predicts that after reaching the interaction curve, the moment in the yielded region decreases until equalization of moments at both ends occurs.

This concept was used in the previous design methods [84,92] as well as in the development of a finite element model for the link beam [32]. However, since complete reliance on such procedures can be questioned as suggested in Chapter 5, a statically indeterminate system was devised to investigate experimentally the actual link moment redistribution with a high shear force in the web under monotonic and cyclic loadings.

Effect of Large Axial Force on Link Performance : - In some EBF framing arrangements, the active links may also be subjected to axial forces P that are nearly proportional to link shear forces V. If the ratio $\rho=P/V$ is small, the effect of P may be neglected. However, there are times when the ratio ρ may be large. This is explained with the aid of Fig. 6.2. This figure shows an approximate relationship between the link shear force and the lateral force acting on the EBF as estimated by Eq. 5.30. The distribution of lateral force is assumed as triangular type. An upper bound estimate of the axial force in each link is obtained by assuming that the entire lateral force assigned to each floor level is transmitted axially through the link. With these assumptions, the ρ calculated for the link at each story level is shown in Fig. 6.2. It is apparent that ρ is the largest at the highest story level and becomes progressively smaller for the lower levels except at the 3-rd story where, as a result of the framing arrangement, the cumulated story shear forces above this level are concentrated on the link. It is also apparent that $\rho=L/h$ is the largest upper bound value of ρ for any link in this frame, although this large value occurs in only a few links.

Up to today, no information was available on the behavior of links subjected simultaneously to cyclic shear, moment, and axial force. Such a case was studied experimentally in this investigation.

Effect of Link Length on Performance : - The experimental setup for study-ing the behavior of a link was based on the kinematics of energy dissipation mechanisms of typical EBFs such as shown in Fig. 6.3(a). Using the plastic dis-placement δ_p, plastic rotation γ_p, and plastic story drift angle ϑ_p shown in the figure, from geometry, as discussed earlier in Section 2.4, it follows that

$$\delta \approx \delta_p = L \, \vartheta_p \qquad\qquad (6.1)$$

$$\gamma \approx \gamma_p = \frac{\delta_p}{e} = \frac{L}{e} \vartheta_p , \qquad\qquad (6.2)$$

in which δ and γ include the elastic components. Approximations as above can be used for large link deformations as in Ref. 40. The two diagrams in Fig. 6.3(a) suggest that a subassemblage with displacements controlled in the manner shown in Fig. 6.3(b) can represent the inelastic behavior of a typical beam in an EBF. An axial force synchronized with link shear simulates the behavior of axially loaded links.

In the tests, links of various lengths e were investigated for the same cyclic δ-history. Therefore from Eq. 6.2, it follows that γ is larger if e is smaller or vice versa. On the other hand, one can conclude from statics, that the sum of the end moments for a longer shear link must be larger to achieve the same shear yield, meaning that such a link would develop larger bending strain demand at the ends. Therefore for different lengths e, shear and bending deformation demands were also studied.

6.3. Experimental Modeling of Active Links

Design of Test Setup : - The setup shown in Fig. 6.4(a) was constructed to develop the mechanisms shown in Figs. 6.3(a) and (b). The west end of a remov-able link was connected to a large steel plate girder support, and the east end

to a long beam of the same cross section as the specimen. The rotation compatibility between the link end plates and these supports was securely maintained by means of A490 bolts of 1.25 in. diameter. Steel blocks with bolts in direct contact with the end plates prevented slip (See also Appendix A.1). The detail of the connection is shown in Fig. 6.4(b). This arrangement permitted replacement of the specimen link after each test.

Cover plates of 0.25x3.5x15 in. were fillet-welded to the west flanges of the long beam after yielding of the beam was noted in the first experiment. As to be explained in Appendix A.1, due to the span length selected for this stiffened beam, the rotational stiffness at the west end was approximately 9 times larger than on the east end, which corresponds to some typical cases in EBF design with strong columns. Accordingly, the initial elastic link end moments are unequal, and the experimental setup simulates well not only the rigid-plastic but also the initial elastic displacement field.

As can be seen from Figs. 6.5 and 6.6, the whole system was supported by three wide Teflon coated pads to prevent out-of-plane rotation. The friction forces due to these supports were found to be negligible.

Instrumentation : - The specimen displacements were monitored with linear potentiometers, and linear variable differential transformers (LVDTs) were used to obtain the rotations of the link ends as well as the beam ends (Fig. 6.6). Strain gages were attached to the beam to determine whether it remained elastic, and to provide a check on the rotations and resultant forces. The specimens were whitewashed to aid in observing the yielding pattern and its progression. All the reaction forces on the three oil jacks were monitored by means of load cells. With these forces known, moment and shear force at any point in the beam and specimen link could be obtained from static equilibrium.

Displacement and Axial Force Control : - The equal in-plane displacements of the beam were imposed by Jacks 1 and 2, whose movements were automatically controlled by the use of a pseudo-static option of an on-line pseudo-dynamics experimental computer program [88]. When the axial force was to be applied, Jack 3 was activated (Fig. 6.3(b)) such that its force is equal to the shear force in the link. This was made possible by taking the difference of output voltages from the load cells mounted on jack 1 and 2 and using it simultaneously as an input voltage for the force control of jack 3. According to the upper bound for link axial force estimate in Section 6.2, it was concluded that $\rho = P/V = 1$ is appropriate to investigate this rare but critical case in link loading.

6.4. Specimens

Section and Material Properties : - All link specimens were of W8×10 sections, which is approximately half scale of the W18×35 section used earlier in link tests [32] as well as in the full-size 6 story building model test at Tsukuba [18,24,97]. The measured section properties of the specimen are given in Table 6.1 where they are compared with the values given in the AISC Manual [1]. All specimens were made of ASTM A36 steel. The initial material properties were determined in uniaxial tension tests and are presented in Table 6.2, where σ_y = the yield stress, σ_u = the ultimate stress, ε_{sh} = the strain at onset of strain hardening, ε_u = the strain corresponding to σ_u, and E = Young's modulus. Table 6.3 gives the plastic section constants. In the first row, the values were obtained by using the different yield stress values obtained for web and flanges. In the second row, the average value of the above stresses was used. Since V_p and $M_p{}^*$ depend directly on the web and flange yield stresses, respectively, and the M_ps by the above two methods are within 3%, it was considered more

accurate to use the values in the first row. Unless noted otherwise, all future references to plastic section constants refer to these values.

Design of Specimens : - As can be seen from Table 6.4, links 1 to 4 are all medium length links, links 5 and 6 are relatively long links, and link 7 is a short link. The behavior of the link reinforced with web stiffeners prior to web buckling was of particular interest. Although in this investigation unequal end moments were developed, the stiffener spacing criteria given in Ref. 32 was used, and equally spaced stiffeners on only one side were fillet welded to the web and both flanges. For all the specimens, a was selected such that a/t_w ratio was between 21 to 23. The number of panel zones created by the stiffeners , a, and a/t_w are given for each specimen in Table 6.4. All stiffeners were 0.25 in. thick conforming to the criterion given in Refs. 53 and 74.

6.5. Loading Programs

As indicated in Table 6.4, the applied loadings were varied for different specimens: monotonically increasing displacement was applied to Specimen 1, and cyclic displacements were applied to all other specimens. In addition, an axial force P of magnitude equal to the applied shear V was applied to Specimens 4 and 6. The cyclic displacement history consisted of one cycle at $\delta=\pm0.25$ in. (6.5 mm) and two cycles at $\delta=\pm0.5$ in. (13 mm), ±0.75 in. (19.5 mm), ±1.0 in. (25 mm) ...., until failure of the specimen occurred. Each cycle consisted of two excursions from a point of zero shear, one in a southerly direction (S), followed by one in a northerly direction (N). For sign convention, see Fig. 6.3(b) for δ and Fig. 6.4(b) for M_A, M_B, M_C, and V. All of these force quantities were obtained at the displaced positions and the effect of beam rotations and

elongations (see Appendix A) on the tilting of oil jacks were considered.

6.6. Observed Results

Test 1 : - The first specimen was initially subjected to a monotonically increasing southerly displacement to 3 in. The link length was medium and three transverse stiffeners were provided with equal spacing of 4.5 in. Fig. 6.7 shows the appearance of the link after this test, and Figs. 6.8 through 6.10 show respectively shear-displacement $(V-\delta)$, moment-displacement $(M-\delta)$, moment-shear $(M-V)$ relationships of the specimen. The intersection of the tangent lines drawn from the initial elastic region and the initial strain hardening region of the load-displacement curve gives a yield shear of 44.5 kips, which is a mere 4% below V_p. With increasing δ, the link continued to deform in the form of a parallelogram bounded by the end plates and flanges (Fig. 6.11). At $\delta=2.5$ in., the west web panel (at A) began to buckle causing deterioration of shear. Subsequently, a severe flange distortion at A occurred as can be seen from Fig. 6.11. During this initial loading, the flange buckling wave was apparent in the longitudinal direction only without twisting. That is, it was *symmetric* with respect to the web plane. As can be seen from Fig. 6.9, the moment at A (M_A) shown by solid line deteriorated just after web buckling occurred.

It should be noted that the rotation and strain reading of the supporting beam indicated early nonlinearity at C due to residual stress. The tangent lines drawn as above for the moment-rotation curve at C gave an experimental moment capacity of 460 k-in., 7% below the theoretical one listed in Table 6.3. This value for a low shear condition can be considered as the experimental moment capacity for the link, since both the link and the beam were cut from the same stock.

The M-V relation shown in Fig. 6.10 was approximately linear until the M_A-V curve reached a point corresponding to M_p and V_p, indicating no significant interaction between M and V. This is completely different from the prediction given by the ideal plastic theory discussed earlier in connection with Fig. 6.1(b). With a further increase in V, M_A slightly decreased but then began to increase at a much slower rate than during the elastic stage, whereas M_B continued to increase at a fast rate. After δ reached 3 in., the specimen was unloaded.

After completely relaxing the specimen, displacement was imposed in the opposite northerly direction starting from the position of the unloaded state in above test and ending in the original position of $\delta=0$ in. At the early stage of this loading, the north flange at A started to buckle, whereas the significant buckling wave of the web panel at A seen in the previous southerly loading started to vanish. When displaced by about 1.5 in., *unsymmetric flange buckling* accompanied by twisting occurred and became more severe upon further loading. At the end of the loading, slight symmetric buckling of the south flange at B was seen, and the web panel at A became fairly flat: no buckling in the other panels was observed. Note the apparent difference of flange buckling patterns between above two loadings.

It should be noted that because of the experience with this test, the flanges of the beam adjoining the link were reinforced for the subsequent experiments.

Test 2 : - In Test 2, the cyclic loading program explained in Section 6.5 was used. The specimen was medium length, identical with the one examined in Test 1. The test was accidentally terminated at the completion of the 1-st half cycle of southerly excursion (1S), and the specimen was unloaded resulting in approximately +0.12 inches permanent deformation. The test was restarted from this condition, and the experiment was completed with almost identical

results to those of Test 3. Accordingly, further experimental observation and analysis are described under Test 3.

Test 3 : - The cyclic loading explained in Section 6.5 was applied to this test specimen of medium length, identical with the ones used in Test 1 and 2. Figs. 6.14 through 6.16 illustrate respectively $V-\delta$, $M-\delta$, and $M-V$ relationships of the specimen. In these figures, remarkably stable hysteretic behavior of the specimen can be recognized.

Yielding of the specimen occurred at the 1-st cycle evidenced by fine cracks in the whitewash in all the web panels. The yield shear force was 43.5 kips, 2% lower than that of Specimen 1. At cycle 3S, cracks in the whitewash on the south flange at A were noted. A symmetric flange buckling at A was apparent from the 4-th cycle on (see for example Fig. 6.17(a) and (b)). However, such buckling was moderate and did not have an appreciable effect on the $V-\delta$ and $M-\delta$ relations, as Figs. 6.14 and 6.15 show. It is also interesting to note from Figs. 6.15 and 6.16 that M_A remained constant with the magnitude of M_p for further cyclic excursions. This will be discussed in Section 6.7 and further in Chapter 7. At later cycles, the cracks in the whitewash appeared to be the most severe in the web at region A, whereas the two inner panels showed much less cracking, suggesting that in addition to shear force, moment also contributes to web yielding of a shear link.

When the link was displaced for the 8-th cycle of $\delta=\pm1.25$ in., slight web buckling at region A was recognized, and this caused slight deterioration of V and M_A as seen in Figs. 6.14 and 6.15. The diagonal tension field formed after the web buckling became apparent at the peak of cycle 10S ($\delta=1.5$ in.) and also induced the severe symmetric flange buckling at A (Fig. 6.17(c)). However, Figs. 6.14 and 6.15 show that deterioration of V was not so large, since although M_A

deteriorated, M_B increased significantly. After the loading was reversed and before cycle 10N was completed, tearing occurred in the west panel originating from the perimeter of the transverse web stiffener. This resulted in a further increase of symmetric flange buckling amplitudes, as seen in Fig. 6.17(d).

Fig. 6.18 shows the severity of flange yielding and buckling at regions A and B. It is apparent that yielding and buckling at region A is much more severe than at region B.

Test 4 : - In Test 4, in addition to the same cyclic displacement history as used for Tests 2 and 3, an axial force of the same magnitude as the shear force in the link was simultaneously applied through the third oil jack. When the link is displaced in the southerly direction, the shear force is positive, and the axial force in the link was a tension force. The link was subjected to compression axial force when displaced in the opposite northerly direction. The specimen was of medium length and identical with the ones used in Test 1 to Test 3.

Figs. 6.20 through 6.22 illustrate respectively $V-\delta$, $M-\delta$, and $M-V$ relationships of the specimen. These figures indicate that up to cycle 3N the hysteretic behavior of the specimen was stable and almost the same as those without application of axial force. The yield shear force of the specimen was 42.0 kips, only 3% less than that of the Specimens 2 and 3, tested without axial force. At cycle 3S, large inelastic tension stress on the north flange at region A was recognized since the whitewash cracked severely (see Fig. 6.23(a)).

At cycle 3N, due to the compression axial force, the unsymmetric buckling of the north flange at A occurred as shown in Fig. 6.23(b), whereas the diametrically opposite flange showed very little cracking in the whitewash and remained flat. Fig. 6.21 clearly shows that this unsymmetrical buckling lead to deterioration of M_A, whereas M_B kept increasing. Thus, V still increased as Fig. 6.20

illustrates. At cycle 4N, with increased δ=-0.75 in., the web panel at region A no longer appeared as a parallelogram but began to show trapezoidal form, where the shorter side was created by the severely buckled flange and web, and the longer side was essentially straight. On the other hand, the other web panels were essentially flat and formed parallelograms with less cracking of whitewash. It should be noted that for each southerly excursion, the buckled flange was straightened because of the tension axial force.

When the specimen was displaced to δ=-1.0 in. (cycle 6N), the south flange at region B also started to buckle severely and the trapezoidal form was seen in the buckled web panels at both regions A and B. As Figs. 6.20 and 6.21 show, V started to deteriorate due to deterioration of both M_A and M_B. For the interior web panels, the parallelograms formed in the previous southerly excursion were never reversed, suggesting that the link shear force was no longer large enough to cause web yielding. For further southerly excursions, the flanges compressed in the previous excursions never straightened (see for example Fig. 6.23(c)). When δ=-1.25 in. (cycle 8N) was applied, the distortion appearing in the previous cycles increased in severity as Fig. 6.23(d) illustrates. During cycle 9S, tearing initiated from the welded region of the severely buckled flange and propagated to the buckled web panel at region A, where experiment was terminated.

Fig. 6.24 shows the the severity of flange yielding and buckling at regions A and B. Compared with the identical specimen tested without axial force (Fig. 6.18), the damage on the flanges was quite unique. The regions damaged with severe unsymmetric flange bucklings and those undamaged can be clearly contrasted in this figure.

Test 5 : - Unlike the specimens in the previous tests, a long shear link was used in this test. In order to keep same a/t_w ratio as for the medium length links, the number of web panels was increased to five. The cyclic displacement history employed was the same as in previous three tests and no axial force was applied. Figs. 6.26 through 6.28 illustrate respectively $V-\delta$, $M-\delta$, and $M-V$ relationships of the specimen. These figures indicate that this long shear link performed quite well. The number of the cycles prior to failure was the largest among all the specimens.

Yielding occurred at the 1-st cycle, where fine cracking in the whitewash in all the web panels was recognized. At cycle 2S, whitewash on the flanges at region A also showed some cracking. At the 4-th cycle, symmetrical flange buckling at region A initiated. Similar to the medium length specimens previously discussed, Figs. 6.26 and 6.27 show no appreciable effect of this buckling on $V-\delta$ and $M-\delta$ relationships. Also, as Figs. 6.27 and 6.28 show, M_A remained bounded by the magnitude of M_p, which is the same behavior as obtained for the medium length link. However, due to the large length of this specimen, M_B was the largest among all the specimens, and M_A and M_B equalized. At the 6-th cycle of $\delta=\pm 1.0$ in., slight symmetric buckling of the flanges at region B was observed, in addition to that at region A (Fig. 6.29(a) and (b)). At the 8-th cycles of $\delta=\pm 1.25$ in., cracking of whitewash on the web panels at both ends of the link was apparently more severe than that on the inner three web panels. At cycle 10S (Figs. 6.29(c) and (d)), where δ was increased to +1.5 in., slight web buckling at region A was recognized, and grew substantially larger at the opposite peak (10N). Accordingly, flange buckling at A became severe and M_A, bounded by M_p up to this cycle, began to deteriorate. M_B increased, since, at region B, no web buckling occurred although moderate symmetric flange buckling was observed. Before the next cycle of the same δ-magnitude, a weld

fracture initiated at the connection between the north flange and the end plate at A, after which tearing of the web panel occurred. The experiment was terminated at this point.

Fig. 6.30 shows the severity of flange yielding and buckling at regions A and B. Compared with the medium length link shown in Fig. 6.18, the flange damage at both regions A and B was greater. Also, from Fig. 6.25, one can see that web damage was primarily concentrated at both end regions. This can be contrasted to Fig. 6.13 where damage was more uniformly distributed on the web of the medium length link.

Test 6 : - The loading method in this test was the same as that used for Test 4, i.e. axial force was simultaneously applied in addition to the imposed cyclic displacement history. The specimen used was a long link, same as the one used in Test 5. Based on the results of Test 5, this test was expected to show the most critical case for flange damage among those tested. The short link under the axial force, therefore, was not tested in this series of experiment.

Figs. 6.32 through 6.34 illustrate respectively $V-\delta$, $M-\delta$, and $M-V$ relationships of the specimen. The hysteresis loops of this specimen were the smallest among all the specimens, thus the amount of the dissipated energy by this specimen was the smallest, which will be explained in Chapter 7. A yield shear force of 41.0 kips was observed, which is 6% lower than the specimen in Test 1. The manner of damage development in this specimen was same as that in Test 4. Much cracking of the whitewash on the north flange at region A was seen at the very early cycle 2S. At cycle 3N, unsymmetric buckling appeared in this flange, which resulted in slight deterioration of M_A as shown Fig. 6.33. However, as can be seen from Fig. 6.35(a), the buckled flange was restraightened at cycle 4S. At cycle 5N, the buckling amplitude of this north flange at A increased, being

accompanied by slight unsymmetric buckling of the south flange at B. At opposite cycle 5S, the north flange at A never restraightened, whereas the south flange at B became straight.

At cycle 6N with δ=-1.0 in., as Fig. 6.35(c) shows, the flange buckling at both regions became severe and the corresponding web panels buckled and deformed into the trapezoidal shape. Accordingly, the deterioration of M_A, M_B, and V became apparent, as seen in Figs. 6.32 and 6.33. The buckled flanges were never restraightened at further cycles (Fig. 6.35(d)). At cycle 8S prior to the peak δ of 1.25 in., a similar failure as the one seen in Test 4 occurred, and the test was stopped.

Fig. 6.36 shows the the severity of flange yielding and buckling at regions A and B. The damage patterns were approximately same as those seen in the medium link in Test 4 (see Fig. 6.24). However, it should be noted that by comparing Fig. 6.31 with 6.19, concentration of damage on the end regions is much more prominent in the long link.

Test 7 : - The short link was examined using the same cyclic displacement history as used in the previous tests. No axial force was applied. The number of web panels was three resulting in the same a/t_w ratio as those for the links of other lengths.

Figs. 6.38 through 6.40 illustrate respectively $V-\delta$, $M-\delta$, and $M-V$ relationships of the specimen. The number of cyclic excursions of this link prior to failure was the smallest of all links tested. Yield shear force was determined as 43.7 kips, almost the same as in Test 1. At the 1-st cycle, all the web panels showed cracking of whitewash. Upon further cyclic loading, it appeared that the whitewash cracking in this specimen was more severe compared with the longer links, since γ for the same δ is the largest for the short link. At cycle 4N,

the slight symmetric buckling of the north flange at region A occurred as Fig. 6.41(b) shows. It also became clear that deformation demand on the exterior panels was greater than on the interior panel. Bounding of M_A at the magnitude of M_p also occurred in this link (Fig. 6.39). With increased δ-magnitude at cycle 6S, the web at region A began to buckle, which also induced severe symmetric buckling of the flanges, as Fig. 6.41(c) shows. Accordingly, M_A deteriorated, whereas M_B kept increasing. At cycle 7N, due to the severe diagonal tension field which formed, tearing initiated from the perimeter of the stiffener closest to region A.

Fig. 6.42 shows the severity of flange yielding and buckling at regions A and B. Compared with the longer links shown in Figs. 6.18 and 6.30, the flange damage at both regions A and B was the smallest. Also, from Fig. 6.37, one can see that a much more uniform distribution of damage on the web was obtained in this link compared with the longer links shown in Figs. 6.13 and 6.25.

6.7. Summary of Significant Behaviors

Cyclic Tests Without Axial Force : - Specimen 3, 5, and 7 were subjected to the same displacement history although their lengths differed. (14.5, 17.5, and 11.5 in., respectively.) By comparing Figs. 6.26 through 6.28 with Figs. 6.38 through 6.40, one can see that the performance differs greatly between the long link (Specimen 5) and the short link (Specimen 7). Although both links showed about the same yield shear close to V_p, by inducing larger γs more rapidly, larger shear strains in the web were evident in the short link at a smaller number of cycles by exhibiting severe cracking of the whitewash. The west web panel buckling of the long and short link was observed at cycles 10S and 6S, respectively. In both links moderate symmetric buckling of the flanges at

region A was apparent from the 4-th cycle on. For the long link additional buckling in the flanges at region B appeared at the 6-th cycle, when M_B reached M_p and end moment equalization occurred. In contrast, the M_A and M_B of the short link showed great inequality throughout the test and no buckling of the flange at region B was observed due to the small magnitude of M_B.

Figs. 6.26 and 6.38 show that moderate flange buckling did not have an appreciable effect on the V-δ relations. Figs. 6.27 and 6.39 illustrate the M-δ relations at both ends of the links, and indicate the very interesting result that the magnitude of M_A remained essentially constant in both links after reaching M_p. This behavior was seen in most cycles regardless of the development of a moderate symmetric flange buckling at A indicating that such buckling does not have a particularly detrimental effect on moment capacity. The moment M_B having initial magnitude smaller than M_A kept on increasing during cycling. No noticeable effect of symmetric flange buckling at B on the moment capacity was observed in the long link.

Figs. 6.28 and 6.40 show the M-V relations for the two test links, where one can see that with an increasing number of cycles and displacement amplitudes, M_A reaches its bound with an ever lower value of V and thereafter remains almost constant. No apparent relationship between the above curves and the interaction surface suggested in Fig. 6.1(b) is observed.

As noted earlier, the links were subjected to the same δ-history, therefore the γ-histories for the two links differed significantly due to their different lengths e. Figs. 6.43(a) and (b) show the V-γ histories for the long and the short link. The number of cycles for the long link when the web buckled was much larger than for the short link due to the smaller increments of γ used. These figures demonstrate the important result that regardless of the manner in which γs are incremented, the links buckled at almost the same $\overline{\gamma_B}$ measured

from the most recent zero shear to the point of buckling. This issue will be discussed later in Chapters 7 and 8. Due to proper stiffening of the web, present specimens deformed through very large γ's.

Cyclic Tests With Axial Force : - When in addition to transverse forces an axial force also acts on a link, the flange behavior becomes more critical. In order to examine this behavior, a medium length link and a long link were tested (Specimen 4 and 6, respectively). for the long link. By considering Fig. 6.20 through 6.22 with 6.32 through 6.34, it should be noted that the long link deteriorated faster than the medium length link, opposite to that of the case with no axial force. As noted earlier, the axial force was in tension during the southerly excursion and in compression for the northerly. For both excursions, the northwest and the southeast flanges experienced much larger normal stresses than the diametrically opposite flanges, since the stresses from bending and axial forces having the same sign combine.

As the above figures show, the behavior of the axially loaded link had essentially three stages. For the *first stage*, very similar behavior was observed to that of the identical link with no axial force. During the *second stage*, severe *unsymmetric* flange buckling at end A caused marked deterioration in M_A. Nevertheless a substantial increase in M_B, up to about two times M_A, developed, since no buckling occurred at the end B. This permitted V to increase, and the usual shear deformation pattern was observed. The *third stage* was accompanied by severe flange buckling at both ends when both M_A and M_B deteriorated and V decreased. It is to be noted that unstable hysteretic loops were observed for northerly excursions only when the compressive axial force amplified flange buckling. For southerly excursions the tensile axial force tended to reduce flange buckling and thereby to stabilize the hysteretic loop.

At this stage of loading the northerly excursions caused concentration of flange damage in the end regions, and shear yielding was terminated because the end moment capacities were insufficient to maintain the high shear force. The southerly excursions continued to develop web shear yielding because the end moments were sufficiently large.

The medium length link survived a larger number of cycles and tended to deform more in shear compared with longer link. This suggests that for a medium length link the flanges deteriorate slower and have a smaller bending rotation demand at the ends. The ultimate end moment capacities appear to be almost the same as for the long link. For both links, the web buckling induced by the severe flange buckling were the final failure modes.

6.8. Conclusions

Based on the above observations, the following conclusions are noted.

(1) A shear link with properly stiffened web, even with initially unequal end moments, can deform through large cyclic γs. One sided stiffeners appear to be satisfactory.

(2) The monotonic and cyclic test results indicate that no significant interaction exists between M and V such as predicted by ideal plastic theory.

(3) The bounding of moment at end A occurred in all the links supported elastically. Accordingly, with increasing link shear force due to strain hardening, the moment at B increased.

(4) Symmetric local flange buckling with an unbuckled web did not have any deleterious effect on either shear or moment capacities of the link.

(5) Web buckling is the direct cause of link hysteretic behavior deterioration. The diagonal tension field formed in the post-buckling range induces

severe symmetric flange buckling, and both shear and moment capacity decreases, soon followed by web tearing.

(6) The tests with an axial force indicate the importance of preventing unsymmetric local flange buckling in order to avoid premature failure. Web buckling was induced by this type of flange buckling.

(7) The link shear resisting capacity does not deteriorate unless the moment capacities of both ends of the link deteriorate.

(8) The test results indicate that regardless of the manner in which γs are incremented, the links buckled at almost the same γ measured from the most recent point of zero shear to the point of buckling.

CHAPTER 7

ANALYSIS OF EXPERIMENTAL RESULTS

7.1. General

The experimental investigations on cyclic behavior of beam links can be subdivided into two categories. Those dealing with statically determinate tests, and those dealing with statically indeterminate cases. For a statically determinate system such as a cantilever, the M/V ratio in the test beam remains constant, which is a typical radial loading, and the M-V relationship plots as a straight line in the M-V space. In this case no moment redistribution can take place, and no indication of yielding can be found from the diagram.

On the other hand, experiments on statically indeterminate systems enable one to study moment redistribution in the post yielding stage. The recorded link behavior projected onto the M-V space offers pertinent information on the strain hardening effect which readjusts moments and modifies the shape of the yield surface. Although some monotonic tests for continuous beams under concentrated load were made in the past using indeterminate systems, very few were concerned with shear yielding [63,99], and no cyclic tests have been reported.

In the experiments discussed in Chapter 6, a statically indeterminate system was employed in order to provide basic information on redistribution of link end moments due to strain hardening under cyclic loads. These test results are interpreted in this chapter emphasizing several link characteristics such as elastic stiffness, strain hardening behavior and its effects on the yield surface, energy dissipation, and flange and web buckling behavior.

severe symmetric flange buckling, and both shear and moment capacity decreases, soon followed by web tearing.

(6) The tests with an axial force indicate the importance of preventing unsymmetric local flange buckling in order to avoid premature failure. Web buckling was induced by this type of flange buckling.

(7) The link shear resisting capacity does not deteriorate unless the moment capacities of both ends of the link deteriorate.

(8) The test results indicate that regardless of the manner in which γs are incremented, the links buckled at almost the same γ measured from the most recent point of zero shear to the point of buckling.

CHAPTER 7

ANALYSIS OF EXPERIMENTAL RESULTS

7.1. General

The experimental investigations on cyclic behavior of beam links can be
subdivided into two categories. Those dealing with statically determinate tests,
and those dealing with statically indeterminate cases. For a statically deter-
minate system such as a cantilever, the M/V ratio in the test beam remains
constant, which is a typical radial loading, and the M-V relationship plots as a
straight line in the M-V space. In this case no moment redistribution can take
place, and no indication of yielding can be found from the diagram.

On the other hand, experiments on statically indeterminate systems enable
one to study moment redistribution in the post yielding stage. The recorded
link behavior projected onto the M-V space offers pertinent information on the
strain hardening effect which readjusts moments and modifies the shape of the
yield surface. Although some monotonic tests for continuous beams under con-
centrated load were made in the past using indeterminate systems, very few
were concerned with shear yielding [63,99], and no cyclic tests have been
reported.

In the experiments discussed in Chapter 6, a statically indeterminate sys-
tem was employed in order to provide basic information on redistribution of
link end moments due to strain hardening under cyclic loads. These test
results are interpreted in this chapter emphasizing several link characteristics
such as elastic stiffness, strain hardening behavior and its effects on the yield
surface, energy dissipation, and flange and web buckling behavior.

7.2. Elastic Behavior and Yield Limit State

Elastic Behavior : - The elastic behavior of the test links were compared with the well established beam theory including shear deformation. The web area was used in making shear calculations. Good correlation with experimental results was obtained for both loading and unloading conditions.

Moment-Shear Force Interaction : - In order to predict the inelastic link behavior, it is essential to know the M-V interaction surface. The profile of such a surface can be found by plotting the initial yield points for the specimens on the M-V space. In order to construct such a surface numerous points are required for various M/V ratios. Fortunately, together with the present test data, additional data were available from previous Berkeley tests [32,84]. Fig. 7.1 shows a plot for 26 specimens normalized by their respective M_p and V_p which were calculated in the same manner as in Chapter 6 using the reported coupon test results. For comparison, the typical theoretical solutions by Hodge [33] and Neal [61] are also indicated on the diagram by the dashed lines.

The experimental data indicate essentially no M-V interaction which is similar to the upper bound solution by Leth [48]. Whereas the theoretical lower bound solutions, which assume no strain hardening and constrain the stresses by imposing equilibrium and yield condition such as the von Mises criterion, are very different from the experimental results. In reality, the link ends could be under very high normal and shear strains so that strain-hardening could occur at a very high rate after yield [3], resulting in added strength without significant loss of link global stiffness. Further, it has been shown [84] that due to warping restraint provided at the link ends, the flange shear may be relatively large so that the web shear could become smaller, allowing the web moment to increase in the end regions. In order to overcome the gap between

experiment and theory, a new theory on kinematics and stress distribution for the end regions needs to be developed. Since this is not available, the rectangular yield surface bounded by M_p and V_p based on experimental evidence is adopted here. Although Eq. 2.3 which considers $(d - t_f)t_w$ as the shear area was used to calculate V_p, based on Fig. 7.1, the use of the web area $A_w = (d - 2t_f)t_w$ as in Ref. 45 may be more appropriate for design.

Moment-Shear-Axial Force Interaction : - It is also important to establish M-V-P interaction for the cases where the links are called upon to transmit axial forces. Thus, considering the initial yield state obtained in Tests 4 and 6 in Chapter 6, the following equation as suggested in Ref. 54, was considered,

$$\left[\frac{P}{P_y}\right]^2 + \left[\frac{V}{V_p}\right]^2 = 1 , \qquad (7.1)$$

In this relation a uniform stress distribution through the link cross section due to the axial force is assumed. Alternatively, assuming no significant interaction between M and V, the well-known equation for M and P [1,3] was examined, i.e.,

$$\frac{P}{P_y} + \frac{M}{1.18 M_p} = 1 , \quad M \leq M_p \qquad (7.2)$$

The yield limit of the link could be predicted by using Eqs. 7.1 and 7.2, whichever gives the lower yield load. This approach was applied to the present test results and to Kusuda's short cantilever monotonic tests [45]. For the present tests, the calculated link shear forces at yield limit had a discrepancy with experimental results of only 5%. In Kusuda's tests, M, V, and P were radially applied to three different W10×29 beams with P/P_y ratios of 0.13, 0.19, and 0.37 to reach the yield limit state. For his results the maximum error in applying Eqs. 7.1 or 7.2 was also only 5%. If the web area A_w is used in calculating V_p instead of Eq. 2.3 as noted above, the discrepancy between experimental and

analytical results is even smaller. Considering these small discrepancies, the above approach of neglecting the M-V interaction is believed to be satisfactory for predicting the the yield capacity of the wide flange beams under the action of M, V and P. Kusuda's analytical solution also suggests that the M-V interaction for large P is negligible.

7.3. Comments on EBF Design.

The ideal plastic theory predicts that for a yield shear V_p, the magnitude of either end moment must be $e V_p/2$, which for the medium length link is 335 k-in., whereas the actual M_A and M_B in the monotonic test were 480 and 183 k-in., respectively, resulting in a ±43% error. Such large errors may frequently occur if the ideal plastic theory is applied in design. There would be no such discrepancies if the yield surface were assumed to be a rectangle as proposed above.

For an EBF with a link attached to the column as shown in Fig. 6.1(a), the link moment estimate is of great importance in selecting and detailing the columns. The earlier design methods for EBFs [84,92], underestimate the column moment and overestimate the moments for the neighboring beam. Therefore it is necessary to use the proposed yield surface in the design. For the ultimate state, the following considerations apply.

7.4. Postyield Behavior

Formation of Moment Hinge and Shear Hinge : - The behavior of shear links in the post yield range is of particular importance in seismic design. In all the tests the increase in V due to strain-hardening occurred until the development

of severe buckling. The links become very flexible after shear yielding of the web. Most of the inelastic deformations are due to web inelastic shear strains, which cause the formation of a parallelogram bounded by web stiffeners and flanges, i.e., a shear hinge is formed. Due to progressive web yielding the link shear stiffness decreases. However as clearly seen from the short link cyclic test, the moment ratio M_A/M_B did not change significantly until M_A became bounded (Fig. 6.40). The monotonic test (Fig. 6.10) revealed that after M_A reached M_p, the ratio M_A/M_B significantly changed, since the increase in M_A became much smaller than that in M_B due to the drastic decrease of rotational stiffness at A. The above points indicate that whether a *shear hinge* is already formed or not, a *moment hinge* develops whenever the end moment reaches M_p. This conclusion is in agreement with the test results reported in Ref. 28.

The bounding of M_A occurred especially early in the cyclic tests for the medium length and the long links since the initial elastic M_A/M_B ratios were larger than for the short link (see Figs. 6.16 and 6.28). The deformation mechanism consists of a moment hinge at A and a shear hinge. For such kinematics, the moment hinge rotation at A would not be large, and M_A would remain bounded. In order for a link to develop a higher shear due to strain-hardening, the more rigid end B must develop an ever increasing moment. A W12×19 link currently being tested [81] with a similar kinematic setup shows analogous behavior.

In the monotonic test, the second moment hinge was formed early at C in the unstiffened beam. The end C region in the test corresponds in a prototype to the reinforced brace-beam region such as shown in Fig. 6.1(a). Therefore the cyclic tests with stiffened beam was considered to be more appropriate for modelling purposes. For cyclically loaded long link, the second moment hinge was formed at B in the very late phase of the cyclic loading.

Strain-hardening Effect on Moment and Shear Force : - Based on the above observations, the schematic M-V diagram shown in Fig. 7.2(a) can be used to illustrate the three possible cases of shear link behavior. Case 1 corresponds to the condition of equal end moments and the slopes of OJ and OJ' are identical during both loading and unloading processes. Case 2 is for a situation with a moderately large M_A/M_B ratio which does not change significantly even after shear yield (lines EH and E'H'). The bounding of M_A occurs after M_A reaches M_p (lines HI and H'I'), due to the formation of a moment hinge at A and a shear hinge. If further loading were imposed, two end moment hinges would form and M_A could increase along the line IJ. Case 3 illustrates the result for a very large M_A/M_B ratio where M_A reaches M_p at F. Since this link is expected to yield in shear soon thereafter, the plastic rotation at A would not grow large enough to cause significant moment increase, and M_A would be bounded by line FI. Similarly to Case 2, paths IJ and I'J' could also develop. In all of the above three cases, no matter where the link is unloaded, the unloading path is parallel to the original elastic path. Fig. 7.2(b) illustrates the sequences of hinge formation for the above three cases.

Tests 4 and 6 indicated that prior to buckling, similar trends can be expected in the presence of an axial force except that the moment bounds would be smaller.

7.5. Simple Shear Link Modelling for Cyclic Action.

As illustrated by Figs. 6.16, 6.28, and 6.40, in a shear link, the expansion of an M-V loop due to strain-hardening occurs primarily in the V-direction whereas it is bounded in the M-direction through many excursions. This means that no significant change in the end moment capacity occurs even with very

large plastic shear deformations. It may also be reasonable to assume that the link shear capacity cannot be increased by the localized plastic bending rotation. This leads to the conclusion that in the strain-hardening range the cross-coupling effect between M and V is negligible. Furthermore, if the normality law for plastic flow is adopted for the M-V space using the rectangular yield surface proposed above, a simplified analytical approach for the link cyclic behavior can be developed. Namely, all the constitutive relations for both the moment-rotation and the shear-shear deformation can be established without considering the coupling effect between them for the entire inelastic range. Based on such a concept, an analytical model for predicting the global cyclic link behavior was developed by the authors, using a new cyclic constitutive model to accurately simulate random cyclic behavior. This is further discussed in Appendix B.

7.6. Maximum Shear Hinge Length.

Maximum Shear Hinge Length Without Axial Force : - The maximum shear hinge length b^* proposed in Ref. 32 and 54 given by Eq. 2.6, or $1.15b^*$ proposed in Ref. 53 have to be modified in view of the above discussion. The rectangular interaction surface suggests that M_p instead of M_p^* must be used to establish the maximum shear hinge length b_{max} as

$$b_{max} = \frac{2M_p}{V_p} \tag{7.3}$$

If the length $e = b_{max}$, two end moment hinges form at shear yield.

However if such a length were used for large rotation angles γ between ± 0.03 and ± 0.08 radians encountered in EBF design, excessive flange strain would develop at the link ends due to large end moments and steep strain

gradients. From the data for the W16×26 section with $e=0.92b_{max}$ reported in Ref. 32, the strain was 4% when end moment was at about M_p, and premature buckling occurred in the unstiffened web. However had this link been stiffened for larger γ noted above, a further increase in shear and end moment would have caused a larger strain. Ref. 53 also reports a link with a highly stiffened web, developing the largest end moments among all the links of the same section tested, which failed in the flange welds. These results suggest the need for limiting end moments to prevent low cycle fatigue weld failure. Earlier on an empirical basis Lay suggested for monotonically loaded beams that for A36 steel $1.4M_p$ may be an acceptable upper bound for the moment [47]. Since this is not entirely conclusive and yet flanges must be conservatively designed to prevent premature failure, the newly obtained data for shear link suggest that $1.2M_p$ may be adopted as a reasonable upper bound for the maximum moment for cyclic loadings. The accumulated data also show that the shear might reach $1.4V_p$ to $1.5V_p$ at the ultimate state defined by the web buckling. Therefore by limiting the end moment to $1.2M_p$ for a shear of $1.5V_p$ requires that

$$e \leq 0.8b_{max} = \frac{1.6M_p}{V_p} \; . \tag{7.4}$$

By examining the data in Ref. 32, it can be concluded that the length e limited by Eq. 7.4 can reduce the moment hinge rotation demand throughout cyclic loading by keeping the end moment relatively smaller.

Maximum Shear Hinge Length With Axial Force : - By substituting the relation, $P=pV$, into Eqs. 7.1 and 7.2, the reduced shear and moment capacity for a link with an axial force can be expressed in terms of ρ, M_p, V_p, A, and the web area A_w. Using the relations so found in Eq. 7.3, and neglecting the P-δ effect, the reduced b_{max} expression is found to be approximately

$$b_{max} = \left[1.15 - 0.5 \rho \frac{A_w}{A}\right] \frac{2M_p}{V_p}, \quad \text{for} \quad \rho \frac{A_w}{A} \geq 0.3, \text{ otherwise use Eq. 7.3 (7.5)}$$

It should be noted that because of the inequality above, very few cases are likely to arise where the reduction of b_{max} due to an axial force in an EBF would be necessary. Prior to a buckling failure, the test links with axially applied forces showed very similar behavior to the links without such an axial force. If σ_y's in the web and flange are significantly different, one should consider this effect on M_p and V_p in Eqs. 2.1, 2.3, 7.3, and 7.4, and a slight modification of Eq. 7.5 should be made.

7.7. Energy Dissipation

With the exception of Specimen 1, the energy dissipation of the links was calculated in relation to the imposed cyclic displacements up to a tearing failure as a measure of their performance. The three energies measured are: E_e = elastic energy stored by the link at yield, E_p = the energy that would have been dissipated during a cycle by an elastic-perfectly plastic system having the same yield as the virgin specimen going through the same inelastic displacement, and E_* = the actual energy dissipated during each cycle. The displacement ductility μ, the ratio of the link maximum relative displacement at each cycle against the initial theoretical link yield displacement, was also calculated.

Fig. 7.3 shows E_* vs. N, where N is the number of half cycles. For the short link (No.7), γ is larger for the same imposed δ-history than for the longer links resulting in a more rapid strain-hardening and a larger energy dissipation E_*. Until the flange buckling occurred at both ends, the specimens with axial force dissipated only slightly less energy than the specimen to which no axial force was applied. Fig. 7.4 shows $\sum E_*$ vs. N relations. It is interesting to note that in

spite of a larger E_*s for the short link No. 7, the link deteriorated very early due to web buckling. The magnitude of $\sum E_*$ at web buckling for this link was less than half of that for the long links No. 2 and 3. The figure also indicates that the links subjected to axial force (Nos. 4 and 6) deteriorated very early after flange buckling occurred. The difference of the energy dissipating capacity between the axial load case (No. 6) and the no axial case (No. 5) was the greatest in the long link test.

Fig. 7.5 shows E_*/E_a vs. N relations. It is interesting to note that the curves for both the axial load case (Nos. 5 and 6) and the no axial load case (Nos. 3 and 4) coincide in the initial part of the test. This as well as the examination of the hysteretic loops lead to the conclusion that the cyclic behavior of links with axial load are analogous to the ones without axial load until severe flange buckling occurs at both ends of a link.

Fig. 7.6 shows $\sum E_*/E_a$ vs. $2\sum(\mu\text{-}1)$ relations for the test specimens, where for a perfectly plastic system, $\sum E_*/E_a = 2\sum(\mu\text{-}1)$. The specimens Nos. 2, 3, 5, and 7 without axial force dissipated more energy than the perfectly plastic systems over a large range of cumulated cyclic ductility. Refs. 32 and 53 proposed a constant relationship between $\sum E_*/E_a$ and a/t_w at the occurrence of web buckling, however no such correlation is evident from this diagram.

Fig. 7.7 shows E_*/E_p vs. N, where for a perfectly plastic system $E_*/E_p = 1$. Except for the earlier cycles of small δ, $E_*/E_p > 1$ for the specimens without the axial forces. For such a case the web buckling was the direct cause of energy absorption deterioration. For specimens with axial forces, the deterioration in energy after flanges buckle is more severe for the longer specimen than for the others. Due to the compressive axial forces, less energy was dissipated in the northerly excursions than in the southerly ones.

7.8. Flange and Web Buckling.

Unsymmetric Local Flange Buckling : - The tests with an axial force indicate the importance of preventing severe *unsymmetric* local flange buckling in order to avoid premature failure, and an estimate of the flange yield zone length as it relates to the end moment is essential. Due to the unique features of the shear link compared to an ordinary beam with no shear yielding in the web, some special considerations have to be introduced in order to derive this length. The proposed approach is illustrated in Fig. 7.8 where e_i is the distance between the end of a link and the inflection point. It is assumed that the critical distance from the end is sufficiently long to make the customary idealization that flange is resisting moment and web the shear force. This idealization is in conformity with the experimentally observed link deformation pattern and analysis using the sandwich beam theory [69,84], indicating that a portion of the shear taken by the web rapidly increases as the distance from the end is increased thereby reducing the warping restraint of the flanges. Accordingly, it can be shown that on neglecting the second order geometric effects the flange yield length l_Y can be expressed as

$$l_Y = e_i \left[1 - \frac{M_p^{\ *}}{M_A} \right] + \rho \frac{M_p^{\ *}}{P_y}, \quad l_Y \geq 0, \tag{7.6}$$

where the first term is the contribution from bending and the second from the axial force. This equation is believed to be conservative. Its application with $\rho=0$ to the test links in Refs. 32 and 53 resulted in good agreement with the strain data.

For deriving the flange buckling condition, the two available derivations by Haaijer [26,27] and Lay [46,47] include the web restraining effect against flange twisting. However their methods for obtaining the web restraint stiffness could

not be directly applied to the link, since the complicated distribution of normal and shear stresses occur in the plastic web and the effect of the web stiffeners also plays a role. Since the flange has to be conservatively designed so as not to induce premature web buckling, in the discussion that follows no web restraint is assumed. Such an assumption has been used often to derive a conservative bound on the solution for ordinary beams [3,26,46]. Using Haaijer's plastic buckling equation in the strain hardening range for plates of finite length compressed longitudinally with one unloaded edge simply supported, and the other free, the flange stress σ_B at unsymmetric flange buckling is given as

$$\sigma_B = \left[\frac{2\,t_f}{b_f}\right]^2 \left\{\frac{\pi^2 D_x}{12}\left[\frac{b_f}{2\,l_H}\right]^2 + G_t\right\} , \qquad (7.7)$$

where l_H, D_x, G_t are, respectively, half wave length, plastic plate modulus in longitudinal direction, and plastic plate shear modulus.

The magnitudes of D_x and G_t in Eq. 7.7 were experimentally obtained by Haaijer [26,27], and were 3,000 ksi and 2,400 ksi, respectively. Lay [46] developed a theoretical relationship between G_t and uniaxial strain-hardening modulus of steel considering a slip plane in the yielded flange plate. The magnitude of G_t obtained by Lay was 3,080 ksi based on his empirical assumption that strain-hardening modulus for A36 steel is 1/33 times the elastic modulus, which corresponds to 880 ksi. However, as Lay comments [46], there is insufficient data for a firm evaluation of the strain-hardening modulus. Using Lay's theory, Haaijer's G_t corresponds to the strain-hardening modulus of 670 ksi, which lies within the range of expected values for A36 steels. Furthermore based on Ref. 3, even for a steel of higher yield strength, this strain-hardening modulus would not be far off the actual one. Therefore Haaijer's values for D_x and G_t were adopted for the steels of any yield strength.

In applying Eq. 7.7 to the present problem, the following procedure was considered: Typically the flange buckling of a shear link shows only one full wave length due to the high moment gradient compared to a conventional beam. Therefore if l_Y lies inside of the link end and the nearest web stiffener, one could assume $l_H = l_Y/2$ in Eqs. 7.6 and 7.7. The flange buckling possibility of the link could be checked by comparing σ_B and σ_{AV} [46], where σ_{AV} is the average normal flange stress along l_Y. In Ref. 46 and 47, for a conventional beam the maximum flange stress was expressed as $\sigma_y M_A/M_p$, and σ_{AV} was taken as $\sigma_y(1+M_A/M_p)/2$. Such an assumption was considered to be reasonable for the case at hand, since on studying Ref. 100, it can be concluded that the stress block at a cross section of a beam under large cyclic loadings reverts to a rectangular one commonly used in calculating an M_p. However for a shear link, from the strain data in Ref. 32, it appears that the maximum stress should be increased by approximately 10%. Accordingly $\sigma_{AV} = \sigma_y(1+1.1 M_A/M_p)/2$ was assumed in the present study. The shear force was conservatively set at 1.5 times V_p. For the postyield state $e_i = e/2$ was assumed in the calculation. When the axial force is present, the reduction of V_p and M_p due to $P = \rho V$ is taken into account by using Eqs. 7.1 and 7.2, respectively.

Possibility of Flange Buckling in Standard Steel Sections : - Based on the above approach the possibility of flange buckling was checked for 156 sections varying from W6 to W36 beams listed in Ref. 1. The conditions checked were for the combinations of $e = 0.8 b_{max}$ and b_{max}, $\rho = 0$ and 1, and $\sigma_y = 36$, 42, 45, 50, and 55 ksi. The value of b_{max} was reduced according to Eq. 7.5 when $\rho = 1$.

The results of calculations are shown in Figs. 7.9 and 7.10. In these figures, σ_{AV}/σ_B calculated for each section is plotted with respect to b_f/t_f ratio. On these figures the limits for b_f/t_f specified by AISC [1] are also shown for comparison. A section with σ_{AV}/σ_B larger than one is likely to have flange buckling.

From these figures, one can see the common trend that the possibility of flange buckling increases with larger b_f/t_f ratios and/or larger σ_y. Furthermore, the following influence of link length and axial force magnitude should be noted. For $e=0.8b_{max}$ and $p=0$ (Fig. 7.9(a)), no flange buckling was indicated for the above range of σ_y's for the majority of the sections satisfying the b_f/t_f ratio limits of Part 1 in Ref. 1 for 'compact cross sections'. However if $p=1$ (Fig. 7.9(b)), the more stringent b_f/t_f limit given in Part 2 of Ref. 1 for plastic design need to be adhered to especially for σ_y stresses of 45 ksi or larger. On the other hand, for $e=b_{max}$ (Fig. 7.10(a) and (b)) some sections satisfying even the b_f/t_f limits in Part 2 indicate the possibility of flange buckling. The number of such sections increases for $p=1$ as shown in Fig. 7.10(b) even though reduced b_{max} using Eq. 7.5 is considered. Based on these results and, since σ_y is usually larger than the nominal σ_y, it is advisable to use the b_f/t_f ratios specified in Part 2, and limit e according to Eqs. 7.4 and 7.5.

Comments on Specimens 4 and 6 : - The Eq. 7.7 derived for monotonic loading gives reasonable results for the the cyclically loaded links with axially applied forces (Specimen 4 and 6). In these cases, l_Y was larger than the stiffener spacing a, therefore l_H was taken as $a/2$ and σ_{AV} was calculated over the length a. The b_f/t_f ratio of the present test specimen series using the nominal σ_y satisfied Part 1 of Ref. 1, but if the actual $\sigma_y=52.4$ ksi would have been used, the section would be classified as non-compact. The thin flanges selected for these experiments however, were considered appropriate since the whole process of inelastic flange buckling and the subsequent failure modes could be studied. Similar behavior is assumed to occur for thicker flanges with longer e or larger p.

Web Buckling : - Refs. 32 and 53 proposed a constant relationship between E_*/E_e as well as $\sum E_*/E_e$ at web buckling and a/t_w. This finding is contradicted by the present more comprehensive tests. The experimental results shown in Fig. 7.5 for specimens 2, 3, 5, and 7 indicate that at web buckling the magnitude of E_*/E_e predicted by the earlier theory were 1.81 to 2.63 times larger than found in the tests. Similar large discrepancies of 2.23 to 3.19 times the magnitude of $\sum E_*/E_e$ at web buckling can be seen from Fig. 7.6.

Furthermore, as discussed in the previous section, $\sum E_*/E_e$ at web buckling differed greatly among the specimens although their a/t_w ratios were about the same. The number of full cycles applied to the links up to web bucklings differed being 6, 8, and 10, respectively, for short, medium length, and long specimens, resulting in different γ-histories. However, it should be noted that the measured $\overline{\gamma}_B$ from the most recent zero shear to the point of buckling were all about 0.14 to 0.16 radians (for the monotonically loaded link, $\overline{\gamma}_B$ was 0.17). This suggests a relation between the stiffener spacing and $\overline{\gamma}_B$ regardless of the number of cycles, the γ-history, or the amount of energy dissipated. Previously, a similar trend was reported for flange buckling of ordinary beams cyclically loaded, and it was concluded that the beam rotation limit is the same regardless of the number of cycles applied unless they are excessively large [95]. For cyclic web buckling an accurate relation between $\overline{\gamma}_B$ and a/t_w as well as d/t_w was found and is discussed in Chapter 8.

7.9. Conclusions

The following conclusions based on the above results may be reached. Most of them are of great importance for a correct design and analysis of EBFs.

(1) Because of the strain-hardening no reduction of link moment capacity due to high shear need be considered and the link yield limit state can be defined by a rectangular yield surface bounded by V_p and M_p.

(2) The proposed equations for reduction of V_p and M_p due to axial force seem to agree well with the available experimental data. No interaction between V_p and M_p need be considered even in the presence of an axial force.

(3) The concept of end moment equalization based on ideal plastic theory can lead to large errors in end moment estimates, which may be critical in EBF design.

(4) For cyclic loading no coupling effect between bending deformation and shear deformation need be considered for the modification of the yield surface in the strain hardening range.

(5) The bounding, increase, and equalization of end moments can be rationalized by the sequential formations of moment and shear hinges caused by strain-hardening.

(6) The limit proposed for the shear link length seems to be reasonable for avoiding various failure patterns due to excessive bending demand, and for assuring inelastic shear deformation.

(7) For a large axial force, the flange buckling can become a potential cause of premature failure. This possibility can be reduced by selecting a small b_f/t_f ratio and short link length.

(8) Web buckling cannot be predicted on the basis of energy as given in Ref. 32. A relation between the critical γ and web stiffeners spacing exists regardless of the amount of energy dissipation, γ-history, or the number of cycles applied unless they are excessively large.

(9) It is to be noted that in all experiments to-date, the ends of shear links were connected to stiff elements. Therefore it is recommended to design

the column panel zones to have small shear distortions [72].

CHAPTER 8

CYCLIC WEB BUCKLING CONTROL FOR SHEAR LINK BEAMS

8.1. General

Based on the experimental studies on one-third scale 3-story EBF's [54,84], together with analytical studies in Chapter 4, Fig. 8.1(a) show the typical energy dissipation mechanisms for EBF's under severe cyclic loadings, characteristics of strong earthquake excitation, where the active links designed to remain elastic at small loads, deform inelastically on overloading of the structure (Fig. 8.1(a) and (b)), thereby dissipating large amounts of energy. The active links therefore play a cardinal role in the proper functioning of the system.

In order to determine the active cyclic link behavior, in the majority of the experimental investigations the link beams were isolated from the remainder of the framing systems [32,53]. These studies showed that the links which yield primarily in shear (shear links) are more effective energy dissipaters than those which yield primarily in bending (moment links). For shear links it was recognized early that plastic web buckling causes a significant drop in the load carrying capacity and energy dissipation for subsequent link displacements, and that such a reduction in the link capability could be prevented by transverse web stiffeners. This behavior is illustrated in Fig. 8.2 where the hysteretic loops for the shear force vs. displacement for an unstiffened and a stiffened shear link beam of identical section are compared [32]. Based on the above findings, equal link stiffener spacing as shown in Figs. 8.1(b) and 8.2(b) was suggested.

Since the lateral load carrying capacity of EBFs is governed by the link capacity [40,54], the link has to be detailed so that no premature link failure would occur. In shear links web buckling must be prevented up to a link design deformation level (Fig. 8.1). If a proper spacing of the stiffeners is not made, Fig. 8.2(a) suggests that web buckling would lead to a large loss of EBF capacity and could even cause a collapse of the structure.

The first criterion for spacing stiffeners for delaying web buckling in order to sustain large cyclic deformations usually encountered in EBF design was proposed in Ref. 32, assuming that there is a constant relationship between the energy dissipated up to web buckling and the ratio a/t_w, where a is stiffener spacing and t_w is web thickness. However, Chapters 6 and 7 in this report questioned the accuracy of this assumption and suggested a new formulation for the stiffener spacing on the basis of the required deformation angle γ_p such as shown in Fig. 8.1(a). With this as the motivation, this chapter presents a re-analysis of 30 shear links tested at Berkeley [32,53,81] including those investigated in Chapter 6 and 7. After examining these shear links subjected to a variety of loading histories, a relationship between the link web deformation angle and the web panel aspect ratio as well as beam depth-to-web-thickness ratio is proposed. The application of such a relationship for EBF seismic design is then discussed.

8.2. Description of Link Specimen and Tests

Test Specimens : - As shown in Fig. 8.1(b), a shear link under an overload deforms into a parallelogram bounded by flanges and stiffeners, and most of the link deformation is due to web inelastic shear strains [32]. To develop this mechanism the link must be sufficiently short so that although the link end

moments are relatively small, the web shear yields due to a high shear force. The maximum link length for such shear links was proposed in the past [32,40,53,54,84], and has been refined in Chapter 7.

Most of the links tested at Berkeley were shear links. Table 8.1 lists 30 shear links tested to date, where the specimen series A,B, and D, respectively, correspond to the ones reported in Refs. 32, 53, and 81, and specimen series C corresponds to the ones studied in Chapter 6 and 7. Shear links which failed prematurely at the end connections prior to web buckling were excluded. The sections for the specimens varied from W8 to W18. The mechanical material properties of the webs of the specimens are given in Table 8.2, where a wide variation in the yield stresses σ_y can be observed, ranging from 39.5 ksi. to 60.6 ksi. although the steel was A36 grade throughout. In this table, σ_y = yield stress, σ_u = ultimate stress, ε_{sh} = strain at onset of hardening, ε_u = ultimate strain, E_h^* = slope of a straight line drawn between the point of onset of strain-hardening and point σ_u in the monotonic stress-strain curves; E = Young's modulus. The ratio σ_u/σ_y ranged from 1.22 to 1.54, and E_h^* varied from 66.7 ksi. to 146.2 ksi., suggesting that the strain hardening characteristics of specimens differed greatly.

The 3-rd and 4-th columns of Table 8.1 give, respectively, the values of the *web panel aspect ratio* α and *the web panel height-to-thickness ratio* β defined as

$$\alpha = \frac{a}{b} \qquad (8.1)$$

$$\beta = \frac{b}{t_w} = \frac{(d - 2t_f)}{t_w}, \qquad (8.2)$$

where d, b, and t_f are, respectively, beam depth, panel height, and flange thickness ; as before, a = stiffener spacing, t_w = web thickness. The value of α

varied widely from 0.42 to 2.40. Most specimens had multiple panels. In some cases they were of different sizes. Since the prominent buckling occurred typically in the panel of the largest α, only such an α is listed in Table 8.1. The shear tab region was excluded in calculating α. The stiffeners were typically welded to the web and flanges, either on both sides of the web or only on one side. Specimens B21 and B26 were different : in the former, the one-sided-stiffeners terminated at a distance k (See Ref. [1]) from one of the flanges, in the latter, the one-sided-stiffeners were not attached to either of the link flanges.

The β values ranged from 40.1 to 57. For the numerous sections listed in the AISC Manual [1], the maximum β is about 60, with the smallest β-values commonly used for beam sections at about 40. For reasons of economy, the sections meeting the shear link capacity requirements tend to have a large β. Moreover, since it is necessary that the beam regions adjoining the link (Fig. 8.1(a)) should remain elastic under large axial forces and moments, economy is best achieved by selecting a deeper beam. For these reasons the range of β's considered in this study adequately covers the cases likely to be encountered in practice.

Testing Methods : - Experimental setups for the Berkeley link tests are schematically illustrated in Fig. 8.3. The links in Refs. 32 and 53, (Fig. 8.3(a)), were tested by fixing the link ends. As explained in Chapter 6, the subassemblage setup shown in Fig. 8.3(b) consisted of a link, an adjoining beam, and a simulated column to study the interaction between these structural components. In Ref. 81, (Fig. 8.3(c)), the main concern was the slab-link interaction, although two bare links were also tested. In all of the above tests, one could clearly see the links deforming into parallelograms bounded by flanges

and stiffeners, and

$$\gamma = \frac{\delta}{e} \tag{8.3}$$

was considered as the measure of the link deformation angle. In a few exceptional cases, the rotation of link support was of some significance especially when γ was small, therefore a correction for γ was made in Eq. 8.3. The length e corresponded to the clear length of the link. If shear tabs were welded to the link web, e was measured from the edge of the tab.

The loading schemes in the above tests can be categorized into two basic categories: In the one, the cyclic γs are symmetrically imposed up to web buckling *(S-loading)*, and in the other the imposed γs are unsymmetrical *(U-loading)*. Depending on the manner of increasing or decreasing the peak γ's, the S-loading types were categorized into ten groups. Load types S-4 and S-8 are illustrated in Fig. 8.4(a) and (b). In S-8, the cyclic γ-history consisted of one cycle at $\gamma=\pm0.022$ and two cycles at $\gamma=\pm0.044$, ±0.066, ±0.088, ..., until failure of the specimen occurred. In S-4, several initial elastic and inelastic cycles with small γ, were applied first, followed by cycles similar to S-8 with the γ-magnitudes of 63% of the former case. In load types S-1, S-2, S-3, S-9, and S-10, respectively, 88%, 81%, 63%, 76%, and 92% of the γ-magnitude of the load type S-8 were applied at each cycle. For type S-7, 107% of the γ-magnitude for load type S-4 were induced. Accordingly, the number of cycles in the tests differed in arriving at the same γ-magnitudes. In some cases, they differed by a factor of about two. The random load types S-5, S-6, U-1 are illustrated in Fig. 8.4(c), (d), and (e), respectively. A large single pulse loading was considered to be of the load type U-2. The 10-th and 11-th columns of Table 8.1 give N, the number of inelastic half cycles applied up to buckling for each specimen, and load type. For detailed descriptions of specimen behavior, see Refs. 32, 53, and 81.

8.3. Analysis of Test Results

Web Cyclic Buckling and Energy : - In an earlier paper [32] empirical equations relating the stiffener spacing to the amount of energy dissipated due to the shear force and link inelastic deformation were given in two different forms as

$$\frac{a}{t_w} = 90 - 9 \ln \frac{E_\Sigma^*}{E_e} \tag{8.4}$$

$$\frac{a}{t_w} = 94 - 14 \ln \frac{E^*}{E_e}, \tag{8.5}$$

where E_e, E^*, E_Σ^*, respectively, are the elastic energy stored by a link at yield, the energy absorbed during the largest prebuckling cycle, and the total energy dissipated prior to buckling. These equations were based on the test results of 15 specimens including moment links, where S-type loads were employed, and it was proposed [32,74] that the stiffener spacing should be less than a/t_w given by either Eq. 8.4 or 8.5.

Eqs. 8.4 and 8.5 include the topological parameter of the web panel such as the stiffener spacing distance a and web thickness t_w, but lack another parameter, the panel height b, which is not in agreement with the classical plate buckling theory. Moreover, as explained in Chapter 7, more recent tests by the author showed a considerable discrepancy from Eqs. 8.4 and 8.5. It was also found that if one applies different loading histories, E_Σ^*/E_e differs greatly. This indicates that Eq. 8.4 derived from the result with the same loading history is not applicable for other loading histories.

On the other hand, regardless of the number of cycles applied, energy dissipation, or γ-history, the links of the same section with almost the same stiffener spacings exhibited web buckling at approximately the same γ (Section

7.8) Although this finding was based on a limited variety of loading histories, it does suggest that instead of the energy criterion, the shear link deformation angle limit is a more reliable parameter for predicting the cyclic web buckling. Previously a similar conclusion was reached for flange buckling of cyclically loaded beams [95].

Proposed Approach for Cyclic Web Buckling Problem : - The test data obtained for the 30 shear links were reduced, where instead of the energy criterion, the *deformation-angle* $\bar{\gamma}$ was used as the main parameter for buckling. As shown in Figs. 8.5, the value of $\bar{\gamma}$ was measured from the farthest point of zero shear reached during the entire previous history to a current point. This approach for measuring $\bar{\gamma}$ was adopted since it was found that regardless of N, the $\bar{\gamma}$ and the shear forces at buckling of symmetrically cycled links were nearly the same as those for the links of identical sections and stiffener spacings which were unsymmetrically loaded (See Table 8.1 for Specimen C3 vs. C1 and C2, A8 vs. B16, and B24 vs. A9, B17, B20, B21, and B25, where N varied from 1 to 18). This approach appears to be also applicable for the flange buckling problem [95].

The deformation-angle at buckling denoted by $\bar{\gamma}_B$ is generally the maximum $\bar{\gamma}$ attained prior to web buckling. Typically web buckling corresponds to the largest $\bar{\gamma}$ in the entire prebuckling history. In a limited number of cases web buckling was observed at a magnitude of $\bar{\gamma}$ somewhat smaller than the maximum attained in the previous half cycle. For such cases it can be surmised that slight web buckling must have occurred at the peak of the previous half cycle. Therefore for such a case, the maximum $\bar{\gamma}$ attained in the previous half cycle was adopted for $\bar{\gamma}_B$.

Although a complicated stress distribution can be expected to develop in the web [32], in an approximate sense, the average web shear stress τ can be defined (Fig. 8.5) as

$$\tau = \frac{V}{A_w},$$

(8.6)

where V, A_w are, respectively, the link shear force and the web area. The *buckling-shear-stress* τ_B is defined by Eq. 8.6 at $\bar{\gamma}_B$. The quantities τ_B and $\bar{\gamma}_B$ for the specimens studied are listed in Table 8.1.

Cyclic Web Buckling Solution : - To date, with the exception of Eqs. 8.4 and 8.5, no solutions have been proposed for the plastic cyclic web buckling of wide flange shear beams, and only solutions for plastic monotonic plate buckling with idealized stress and strain distributions are available [6,8,21,22,23,29,36,90] However, considering the similarity of the web buckling modes [32] to the ones of plates under shear loading, the plastic plate shear buckling theory can be applied to the present problem. The relevant earlier theories for the plastic plate buckling problem were based on an analogy to the elastic buckling problem, and the theoretical plastic buckling shear stress τ_B was obtained from elastic buckling solutions. Following the formalism of such theories, it was hypothesized that the present plastic buckling problem can be expressed as

$$\tau = \eta(\tau)\, \tau_E$$

(8.7)

where η is a *plastic-reduction-factor*, a function of plate strain-hardening history, and τ_E is an elastic buckling stress for a plate given as

$$\tau_E = \frac{\pi^2 E}{12(1-\nu^2)}\, K_s(\alpha) \left[\frac{1}{\beta}\right]^2,$$

(8.8)

where ν is Poisson's ratio, and K_s is a plate-buckling-coefficient which is a function of the aspect ratio α and the boundary conditions [5,8]. It should be noted

that Eq. 8.7 is non-linear. However, the topological plate parameters α and β have the same meaning for the plastic solutions as for the elastic buckling solutions.

In order to solve Eq. 8.7, the expression for η should be known. In the present investigation, an empirical approach based on the 30 shear link tests was used to derive the expression for η. This approach is similar to the one developed by Gerard [21,22,23] for the plate problem. Experimental values of η at buckling follow from Eq. 8.7 by calculating τ_B/τ_E. As pointed out in Ref. 53, since shear links are relatively short and are laterally braced at both ends, for the usual rolled sections it would appear that the flange provide significant restraint along the longitudinal edges of the web. Therefore it seems reasonable to assume a clamped end condition for estimating τ_E. Accordingly, τ_E in Eq. 8.8 was calculated using K_s for clamped end conditions [8], i.e.,

$$K_s(\alpha) = \begin{cases} 8.98 + \dfrac{5.60}{\alpha^2} & (\ \alpha \geq 1\ ), \\ 5.60 + \dfrac{8.98}{\alpha^2} & (\ \alpha \leq 1\ ) \end{cases} \tag{8.9}$$

Also following Gerard, the secant modulus G_s for the shear link was defined (Fig. 8.5) as

$$G_s = \frac{\tau}{\bar{\gamma}} \tag{8.10}$$

By substituting τ_B and $\bar{\gamma}_B$ into Eq. 8.10, the value of G_s at buckling was obtained for each specimen. Using the above equations, together with $G=E/2(1+\nu)$ and ν of 0.3, η and G_s/G were calculated for each specimen at buckling and plotted in Fig. 8.6. Remarkably, regardless of the cyclic histories applied to the links, the wide range of σ_y's and E_h^*'s, and a variety of α's and β's, an excellent correlation between η and G_s/G was obtained. The linear relation between these two quantities suggests that for the postyield state, regardless of the loading

histories,

$$\eta = 3.7 \frac{G_s}{G} \quad (\eta \leq 0.3) \tag{8.11}$$

Using Eq. 8.11 with Eq. 8.7 for determining plastic plate buckling leads to good agreement with experimental results. The expression for η is purely a function of strain-hardening of the material and is independent of the topological parameters α and β. Regardless of the wide range of the nonlinear characteristics of the materials used in the experiments, the same expression applies. Moreover the wide range of σ_y, σ_u/σ_y and E_h^* suggests that the relation between η and G_s/G given by Eq. 8.11 is generally applicable for A36 steel. As for elastic buckling, the solution depends on parameters α and β.

It would further appear that Eq. 8.7 can be applied even to the link cyclic web buckling problem. This suggests that cyclic web buckling is strongly related to the web plate plastic modulus. Substituting Eqs. 8.10 and 8.11 into Eq. 8.7, with $\tau=\tau_B$ and $\gamma=\bar{\gamma}_B$ at a buckling stage results in

$$\tau_B = 3.7 \frac{\tau_B}{\bar{\gamma}_B \, G} \tau_E \tag{8.12}$$

It should be emphasized that this solution based on the secant modulus has a great advantage since it can be recast into a direct equation for $\bar{\gamma}_B$ by cancelling τ_B in Eq. 8.12 leading to

$$\bar{\gamma}_B = 3.7 \frac{\tau_E}{G} \tag{8.13}$$

Using Eq. 8.8 with $\nu=0.3$, a further simplification of Eq. 8.13 can be made, yielding

$$\bar{\gamma}_B = 8.7 \, K_s(\alpha) \left[\frac{1}{\beta}\right]^2 \tag{8.14}$$

Eq. 8.14 is an extremely simple relationship showing that $\bar{\gamma}_B$ is merely a function

of two topological parameters α and β. Fig. 8.7 shows the relationship between $\beta^2 \bar{\gamma}_B$ and α, where excellent correlation between Eq. 8.14 and the test data can be seen.

Based on Eq. 8.14, if the aspect ratio α is the same, $\bar{\gamma}_B$ for a beam with $\beta=40$ is more than double the one for a section with $\beta=60$. This is confirmed by experimental results. For example see data for Specimen A8 and A11 in Table 8.1 and the corresponding plots in Fig. 8.7. Alternatively, for the same magnitudes of β, $\bar{\gamma}_B$ increases for smaller α's. For instance, although Specimens A1 through A4 had identical sections, their α's ranged from 1.66 to 0.42, since the number of equally spaced stiffeners varied from none to three. As can be seen from Table 8.1 and Fig. 8.7, compared to the unstiffened Specimen A1, $\bar{\gamma}_B$'s for A2, A3, and A4 were about 1.9, 3.3, and 5.8 times larger in close conformity with the predictions by Eq. 8.14.

Comparison with Plate Buckling Problem : - Earlier plastic buckling solutions for monotonic loadings were derived from elastic solutions for plates, and theoretical expressions for η were based on different loading and boundary conditions. Various theoretical expressions for η were proposed by Bijlaard [6], Ilyushin [36], Stowell [90], Handelman and Prager [29] etc. Typically, the parameter η was expressed as a function of the uniaxial plate tangent modulus E_t and the secant modulus E_s. These solutions were based either on the deformation or the incremental theory of plasticity with or without consideration of the strain reversal.

Gerard [21,22,23] reported that the above theories gave much higher estimates for the buckling stress compared to the test data for the plates in uniform shear, and proposed an empirical expression for η as a function of G_s/G, where G_s is the secant modulus in shear. The maximum errors by this approach

in estimating plastic buckling shear stresses and strains for his specimens in Ref. 21 were about 15% and 60%, respectively. The expression for η given by Eq. 8.11 was obtained in a manner similar to that used by Gerard. It is to be noted that due to completely different proportions of the plates tested in his experiments, the critical shear strains were on the order of 0.01 radians, whereas in the present study $\bar{\gamma}_B$'s were from 0.03 to 0.18. The experimentally obtained η's in Gerard's study mostly were in the range of 0.3 to 1.0, whereas in this study 29 links out of 30 had η's under 0.3. Moreover, his solutions were derived for very long plates where dependence on α is suppressed.

None of the earlier theories are conclusive, and Gerard's empirical solution based on a limited number of tests may not be sufficiently general. Moreover, the experimentally observed non-uniformity of stresses and strains in the actual shear links [32] indicates further unresolved theoretical problems. Therefore, since the present test results strongly correlate with the proposed Eq. 8.11, in the discussion that follows, Eq. 8.14 is adopted.

Effect of Stiffener Rigidity : - It should be noted that no significant effect of stiffener rigidity and detail on the proposed solution was observed. According to Refs. 9, 83, and 89, it may be concluded that the stiffeners used in the shear link experiments were much more rigid than necessary to achieve maximum τ_B and $\bar{\gamma}_B$. However, the large rigidity of the stiffeners appears to be necessary to prevent a rapid deterioration of the links in the post-buckling stage [53].

8.4. Link Cyclic Behavior and Web Buckling

Prebuckling Behavior : - Figs. 8.6 and 8.7 indicate that regardless of different loading histories applied to the links, the $\bar{\gamma}_B$ limit was stable and can be simply expressed by Eq. 8.14. As can be seen from Fig. 8.2(b), the cyclic V-γ

relationship of the link prior to web buckling was very stable generating hysteretic curves analogous to the one for uniaxial loading. However, for specimens such as B18, on applying nine identical full cycles with a $\bar{\gamma}$ of 86% of theoretical $\bar{\gamma}_B$, hysteretic loops were identical up to the 6th cycle, then a small deterioration in the loops was observed with the development of slight web buckling. This suggests that a large number of excursions with magnitude of $\bar{\gamma}$ near $\bar{\gamma}_B$ may initiate web buckling.

Post Buckling Behavior (Case 1) : - Fig. 8.8 shows two examples of envelopes for V-γ link hysteretic loops up to buckling. An envelope for symmetric loops is shown in Fig. 8.8(a) and for some extreme unsymmetrical one-sided loops in Fig. 8.8(b). If further loading is applied with the γ's exceeding such envelopes, unstable loops of the type shown in Fig. 8.2(a) would develop. The deterioration in capacity is more likely to occur in the less stiffened links where typically the loop pinching develops due to flange buckling when the web buckles. In such cases the flanges became severely compressed when a diagonal tension field forms in the web. The less stiffened links provide less support for the flanges, and thereby permit deterioration to occur more rapidly. Lateral-torsional buckling of a link may also be induced due to such failures [32]. For a link with a large number of stiffeners, instead of gradual deterioration after buckling, a sudden tearing failure may develop along the perimeter of the link panels due to stress concentrations created by the buckled web. The prediction of post-buckling behavior of links exceeding the envelopes discussed above is very complex and eventually can result in hazardous lateral torsional buckling and tearing. Therefore, since an EBF greatly depends on link capacity and behavior, one cannot rely on the link performance in such a range of loading. Accordingly, as asserted in Ref. 32, it would be appropriate to consider web

buckling as the shear link design ultimate limit state.

It should be noted that links with β's much smaller than the ones considered in this investigation tend to show remarkably stable behavior accompanied with increase of shear capacity even in the post-buckling stage, and web buckling may not be an appropriate ultimate state. See Refs. 19 and 84 for this behavior of sections having $\beta=29.8$ and 23.8.

Post-Buckling Behavior (Case 2) : - In contrast to the above case, if after buckling further cycles do not exceed but fall within the buckling hysteretic loop envelop such as shown in Fig. 8.8, an alternative type of link post-buckling behavior occurs. Specimens B16 and B20 with such a loading showed that the subsequent hysteretic loops were essentially stable and the ductile nature of the link behavior was retained during further cycles not exceeding the envelop. It can be said that if the severe web buckling does not occur i.e., if $\bar{\gamma}$ at the buckling excursion is not much larger than $\bar{\gamma}_B$, the stable post-buckling behavior can be maintained for the subsequent loadings within the buckling hysteretic loop envelop. These considerations suggest that regardless of when the largest loading excursion occurs, web buckling as an ultimate limit state can be safely adopted. This behavior is similar to the flange buckling cyclic behavior of ordinary beams [95].

8.5. Stiffener Spacing for Seismic Design

Story Drift and Link Deformation : - Fig. 8.9(a) shows two typical relationships between the cumulated story shear force F and the story drift angle ϑ for a typical EBF. In general,

$$\vartheta = \vartheta_e + \vartheta_p .$$
(8.15)

where ϑ_e is the elastic and ϑ_p is the plastic story drift. For the usual magnitude of the ϑ considered in design, ϑ_e is of such a magnitude that it cannot be neglected [40], as can be seen from Fig. 8.9(a). In this figure a realistic F-ϑ relationship for an EBF panel is contrasted with the one for an ideal elasto-plastic model. Although ϑ_e for these two cases may differ (compare ϑ_e and ϑ_e^*, in Fig. 8.9(a)), for simplicity the elasto-plastic model is used herein, and ϑ_e defines the elastic story drift. The ϑ_e includes elastic flexural and axial deformations of beams, columns, braces, and, a small contribution from the links. On the other hand, ϑ_p is due almost entirely to the link plastic deformation angle γ_p as illustrated in Fig. 8.1(a), whence from geometry,

$$\gamma_p = \frac{L}{e}\,\vartheta_p \tag{8.16}$$

Since γ_p in an EBF ultimate state design is much larger than the elastic link deformation angle γ_e, the total link deformation angle $\gamma = \gamma_e + \gamma_p$ can be approximated by γ_p [40]. Hence applying Eqs. 8.15 and 8.16 for cyclic action, at a given peak values of ϑ,

$$\gamma \approx \frac{L}{e}\,(\,\vartheta \pm \vartheta_e\,), \tag{8.17}$$

where the negative sign should be used for a positive ϑ and vice versa. This is schematically illustrated in Fig. 8.9(b) based on experimental results for a 3-story EBF [54]. As can be seen from this figure, Eq. 8.17 provides a reasonable estimate of γ for the inelastic excursions. The somewhat conservative estimate for γ is due to neglecting the increase in ϑ_e in the strain-hardening loading range and support rotations at link ends.

Design for Seismic Load : - For a well designed EBF the inelastic link deformation is largely responsible for the non-linear response of the frame during an

earthquake. The remarkably stable behavior of the shear links prior to web buckling has been recognized and modeled by the authors (see Appendix B), and should be useful in performing non-linear dynamic analyses of EBFs. The unstable postbuckling behavior of the links is difficult to model, and at this stage of the development only the EBF with stable link behavior should be used in design.

Since no unique earthquake motion can be selected for any given site, and because of the considerable cost involved in the time-history analyses in practical design of EBFs, one either turns to a response spectrum approach or simply to the structural code provisions [4,70,94]. For the response spectrum application, there is some question on its applicability for structures with degenerate hysteretic loops [70]. In EBF applications such behavior would occur if the link web severely buckles causing lateral torsional buckling of a beam or web tearing in the link [32].

In current seismic code development activity EBFs are classified as a ductile seismic resistant system, and thereby benefit from a substantial reduction in the design lateral force. In order either to assure the reliability for the response spectrum approach, as well as to satisfy the code requirement for a ductile system, the links must be appropriately stiffened to prevent web deformation at the required *ultimate story drift* angle ϑ_u. In applying either one of the above two approaches no information on the type of cyclic loading to be expected is given, and therefore it becomes essential to satisfy the ductility requirement for the drift of $|\vartheta_u|$, for which the link web does not buckle. Clearly by substituting $\vartheta = |\vartheta_u|$ into Eq. 8.17, the required *ultimate* link deformation angle $|\gamma_u|$ can be calculated.

Proposed Stiffener Spacing Formula : - In Eq. 8.14, the web buckling deformation angle $\bar{\gamma}_B$ was expressed with two parameters: the panel web aspect ratio α, and the web panel height-to-thickness ratio β. In the actual design of a link it is more convenient to rewrite this relation in terms of γ_u. On reviewing the V-γ hysteretic loops of the links tested, it can be concluded that $2\gamma_u$ is only about 5% to 10% larger than $\bar{\gamma}_B$. Furthermore, instead of using $\beta = b/t_w$ as in Eq. 8.2, it is more convenient to approximate this by a *beam-depth-to-web-thickness-ratio* d/t_w, where for typical beams d/t_w is only about 5% to 8% larger than β. Also since it has been pointed out that the web stiffeners are effective in reducing the possibility of lateral torsional buckling [32], a maximum permissible spacing of $a/d = 1$ is adopted. Considering these factors, for the range of γ_u from 0.03 to 0.08 radians, a conservative approximation for Eq. 8.14 in the following form can be established:

$$\frac{a}{t_w} + \frac{1}{5}\frac{d}{t_w} = C_B \qquad (a \le d), \tag{8.18}$$

where the constant C_B = 56, 38, and 29, respectively, for γ_u = 0.03, 0.06, and 0.09. For other values of the γ_u, C_B can be linearly interpolated. In Table 8.1 columns 7 and 8 provide a comparison between the experimentally determined γ_u's and the calculated γ_u^{th} using Eq. 8.18. It is believed that the correlation is remarkably good with slight conservatism for most of the cases (see column 9).

Effect of Random Loading on Design : - For the various loading types investigated, the above formula for web stiffener spacing for γ_u is quite reliable. For general loadings, considering the symmetric loop envelopes bounded by $\pm\gamma_u$ as in Fig. 8.8(a), it has been asserted that, if the link hysteretic history lies within the loop, no web buckling would occur. In order to justify this further, experimental investigations employing random types of loading history are necessary.

Fortunately, some information recently became available to clarify this issue.

A full-scale 6-story, two-bay steel structure with eccentric bracing (see right hand Fig. 8.1(a)) recently was tested using the pseudo-dynamic method [18,24] at Tsukuba, Japan. This structure was subjected to a simulated Taft earthquake with the maximum ground acceleration scaled to 0.5g. Fig. 8.10(a) shows the ϑ-history from this test for the 1-st story EBF panel [18]. Based on Ref. 18 and Eq. 8.17, it was estimated that about 16 to 20 inelastic half cycles were imposed to the link located at the 2-nd floor level with maximum and minimum γ's of 0.06 and -0.035, respectively. For the W18×40 shear link employed having stiffeners spaced at $a=7.25$in., using Eq. 8.18, γ_u is estimated to be 0.072. Therefore the random link excursions were well within the envelope bounded by $\pm\gamma_u$ and as to be expected, no web buckling was observed during the test. Inasmuch as in the Tsukuba tests it was decided to determine the ultimate strength of the structure, additional "final" tests were performed by applying sinusoidal motions schematically shown in Fig. 8.10(b). During the second test, the peak ϑ reached 0.011, and the corresponding γ's including support rotations were about ±0.08 [18]. It is reported that during this test the web was about to buckle [18]. However, due to failure at the brace-beam connection, no further loading was imposed on the link, therefore no actual buckling could be observed. Considering the conservatism of Eq. 8.18 for estimating γ_u, it is believed that this shear link would have sustained the initially planned on random excursions.

At Berkeley several subassemblage tests of the type shown in Fig. 8.3(c) simulating the Tsukuba framing were run by Ricles [81] with W12×19 links having $a=6.75$in. In these experiments the a/t_w ratio of the web panels was larger and d/t_w ratio was smaller than those in the Tsukuba test, and according to Eq. 8.16, γ_u should attain 0.066. Several of the links were subjected to a random

history of load reversals, and the loading applied to one of the links simulated the effect of a scaled 0.5g Taft earthquake as in the Tsukuba tests. These experimental results confirmed that Eqs. 8.14 and 8.18 are applicable for severe random loadings.

8.6. Conclusions

Based on the results of experimental and analytical studies discussed in this paper, the following conclusions may be reached.

(1) In spite of the various loading histories and energies dissipated, it appears that the onset of web buckling can be reasonably well predicted by the link deformation angle $\bar{\gamma}$ for either symmetric or unsymmetric loadings.

(2) Experimental results strongly suggest that the classical monotonic plastic plate buckling theory provides guidance for shear link cyclic web buckling, therefore the aspect ratio α and the height-to-thickness ratio β play a similar role as in the elastic buckling solution.

(3) Buckling link deformation angle $\bar{\gamma}_B$ can be simply expressed in terms of parameters α and β only. This relationship appears to be independent of the variation in the material nonlinear characteristics of the available tests, and it is similar to Gerard's empirical plastic buckling solution utilizing the secant modulus as the plastic reduction factor.

(4) The proposed solution for $\bar{\gamma}_B$ appears to be valid not only for the loading types investigated, but also for other types of random loadings.

(5) Web buckling is the direct cause of link hysteretic behavior deterioration for the sections commonly used for EBF applications. Since postbuckling behavior and final failure are difficult to predict, and since stable link action is essential in EBF design, link web buckling is the most appropriate

state to consider for EBF ultimate design.

REFERENCES

[1] AISC, "Specifications for the Design, Fabrication and Erection of Structural Steel for Buildings with Commentary", *Manual of Steel Construction*, 8th ed., American Institute of Steel Construction, 1980.

[2] Akiyama, H., "Damage Distribution Law of Steel Rigid Frames Under Earthquakes", *Trans. of A.I.J.*, No. 309, Nov., 1981 (In Japnese).

[3] ASCE-WRC, "Plastic Design in Steel", *ASCE Manual 41*, 2nd ed., Welding Research Council and American Society of Civil Engineers, New York, 1971.

[4] ATC-3 (Applied Technology Council), *Tentative Provisions for the Development of Seismic Regulations for Buildings*, National Bureau of Standards, U.S. Dept. of Commerce, Washington, D.C., June, 1978.

[5] Basler, K., "Strength of Girders under Combined Shear and Bending", *Journal of the Structural Division*, ASCE, Vol.87(ST7), 1961.

[6] Bijlaard, P. P., "Theory and Tests on the Plastic Stability of Plates and Shells.", *J. Aeronaut. Sci.*, vol. 16, no.9, Sept. 1949, pp.529-541.

[7] Black, R.G., Wenger, W.A.B., and Popov, E.P., "Inelastic Buckling of Steel Struts Under Cyclic Load Reversals", *EERC Report, 80-40*, Univ. of Calif., Berkeley, CA., Oct., 1980.

[8] Bleich, F., "Buckling Strength of Metal Structures", 1st edition, McGraw-Hill Book Company, Inc., New York, 1952.

[9] Blume, J.A., "Structural Dynamics of Cantilever-type Buildings", *Proceedings, World Conference in Earthquake Engineering*.

[10] Chen, P.F.S., "Generalized Plastic Hinge Concepts for 3D Beam-Column Elements", *Ph. D Thesis*, University of California, Berkeley, 1981.

[11] Ciampi, V., Elingehausen, R., Bertero, V.V., and Popov, E.P., "Analytical Model for Concrete Anchorages of Reinforcing Bars under Generalized Excitations", *EERC Report*, 83-19, Univ. of Calif., Berkeley, CA., Dec. 1982.

[12] Clough, R.W., and Penzien, J., "Dynamics of Structures", McGraw-Hill Book Company, Inc., New York, 1975.

[13] Cowper, G.R., "The Shear Coefficient in Timoshenko's Beam Theory", *Journal of Applied Mechanics*, Vol.33(6), 1966.

[14] Dafalias, Y.F.,and Popov, E.P., "A Model for Nonlinearly Hardening Materials for Complex Loadings", *Acta Mechanica*, Vol.21, 1975.

[15] Dafalias, Y.F.,and Popov, E.P., "Plastic Internal Variables Formalism of Cyclic Plasticity", *Journal of Applied Mechanics*, Vol.98(4), 1976.

[16] Drucker, D.C., "The Effect of Shear on the Plastic Bending of Beams", *Journal of Applied Mechanics*, Vol.23(4), 1956.

[17] Filipou, F.C., Popov, E.P., and Bertero, V.V., "Effects of Bond Deterioration on Hysteretic Behavior of Reinforced Concrete Joints", *EERC Report, 83-19*, Univ. of Calif., Berkeley, CA., 1983.

[18] Foutch, D.A., "Phase 2 Final Tests Preliminary Report of Observations", (Private Communication).

[19] Fujimoto, M., Aoyagi, T., Ukai, K., Wada, A., Saito, K., "Structural Characteristics of Eccentric K-Braced Frames", *Trans. of A.I.J.*, No. 195, May 1972 (in Japanese).

[20] Gaylord, E.H., "Plastic Design by Moment Balancing", *Steel Structures Symposium*, University of Illinois, Urbana (October 1966).

[21] Gerard, G., "Critical Shear Stress of Plates above the Proportional Limit", *J. Appl. Mechanics*, vol. 15, no. 1, pp.7-12, March, 1948.

[22] Gerard, G., "Introduction to Structural Stability Theory", McGraw-Hill Book Company, Inc., New York, 1962.

[23] Gerard, G. and Becker, H., "Handbook of Structural Stability. Part1 - Buckling of Flat Plates", *NACA TN 3781*, 1957.

[24] Goel, S.C., and Foutch, D.A., "Preliminary Studies and Test Results of Eccentrically Braced Full-Size Steel Structure", *Report, 16-th Joint Meeting U.S.-Japan Panel on Wind and Seismic Effects*, National Bureau of Standards, Washington, D.C., May 15-18, 1984.

[25] Grierson, D.E., and Abdel-Baset, S.B., "Plastic Analysis under Combined Stresses", *Proc., J. of Eng. Mech. Div.*, ASCE, Vol. 103, No. EM5, Oct., 1977.

[26] Haaijer, G., "Plate Buckling in the Strain-Hardening Range.", *J. Eng. Mech. Div.*, ASCE, Vol. 83, No. EM2, April, 1957.

[27] Haaijer, G. and Thurlimann, B. "On Inelastic Buckling in Steel.", *J. Eng. Mech. Div.*, ASCE, Vol. 84, No. EM2, April, 1958.

[28] Hall, W.J., and Newmark, N.M., "Shear Deflections of Wide-Flange Steel Beams in The Plastic Range.", *Transactions, ASCE*, Vol.122, Paper No. 2878, 1957, p.666.

[29] Handelman, G.H., and Prager, W., "Plastic Buckling of a Rectangular Plate Under Edge Thrusts", *NACA Rep. 946*, 1949.

[30] Hilmy, S.I., "Adaptive Nonlinear Dynamic Analysis of Three-Dimentional Steel Framed Structures with Interactive Computer Graphics", *Dept. of Civil Eng. Report*, No. 84-8, June, 1984, Program of Computer Graphics and Department of Structural Engineering, Cornell University.

[31] Hisatoku, T., et. al., "Experimental Study on the Static Behavior of the Y-typed Bracings", *Report of Takenaka Technical Institute*, No. 12, August, 1974.

[32] Hjelmstad, K.D., and Popov, E.P., "Seismic Behavior of Active Beam Links in Eccentrically Braced Frames", *EERC Report 83-24*, Univ. of California, Berkeley, CA, 1983.

[33] Hodge, P.G., "Plastic Analysis of Structures", McGraw-Hill Book Company Inc., New York, 1959.

[34] Horne, M.R., "A Moment Distribution Method for the Analysis and Design of Structures by the Plastic Theory", *Proceedings, Institude of Civil Engineers 3*, No.1(April 1954).

[35] Horne, M.R., "Full Plastic Moments of Sections Subjected to Shear Force and Axial Load", *British Welding Journal*, Vol.5, 1958.

[36] Ilyushin, A.A.,"The theory of Elasto-Plastic Strains and Its application", *Bull. Acad. Sc., URSS, Sec. Tech. Services*, June 1948, pp 769-788.

[37] "Japanese Revised Aseismic Design Code - 1980", Ministry of Construction, Japan, July 14, 1980.

[38] Jennings, P.C., "Response of Simply Yielding Structures to Earthquake Excitation", *Report No. 6360*, California Institute of Technology, Pasadena, CA., June 1963.

[39] Kaba, S.A., and Mahin, S.A., "Interactitive Computer Annalysis Methods for Predicting the Inelastic Cyclic Behavior of Structural Sections", *EERC Report 83-18*, University of California, Berkeley, CA., 1983.

[40] Kasai, K., and Popov, E.P., "On Seismic Design of Eccentrically Braced Steel Frames", *Proceedings 8WCEE*, San Francisco, CA., Vol. 5, July 21-28, 1984, pp.387-394.

[41] Kasai, K., and Popov, E.P., "Design and Dynamic Characteristics of Eccentrically Braced Frames", *EERC Report*, University of California, Berkeley, CA., (In preparation).

[42] Krawinkler, H., "Shear in Beam-Column Joints in Seismic Design of Steel Frames", *AISC Eng. Journal*, Vol. 15, No.3, 1978.

[43] Krawinkler, H., Bertero, V.V., and Popov, E.P., "Inelastic Behavior of Steel Beam-to-Column Subassemblages", *EERC Report, 71-17*, Univ. of Calif., Berkeley, CA., Oct., 1971.

[44] Krivetsky, A., "Plasticity Coefficients for the Plastic Buckling of Plates and Shells.", *J. Aeronaut. Sci.*, vol.22, pp.432-435, 1955.

[45] Kusuda, T., and Thurlimann, B., "Strength of Wide-Flange Beams Under Combined Influence of Moment, Shear, and Axial Force", *Report No. 248.1*, Fritz Eng. Laboratory, Lehigh Univ., Bethlehem, Pa., 1958.

[46] Lay, M.G., "Flange Local Buckling in Wide-Flange Shapes.", *J. Struct. Div.*, ASCE, Vol. 91, No. ST6, Dec., 1965.

[47] Lay, M.G., and Galambos, T.V., "The Inelastic Behavior of Beams Under Moment Gradient", *Report No. 297.12*, Fritz Eng. Laboratory, Lehigh Univ., Bethlehem, Pa., 1964.

[48] Leth, C.F., "Effect of Shear Stresses on the Carrying Capacity of I-Beams", *Technical Report NO.A-11-107*, Brown University, 1954.

[49] Lu, L.W., "Seismic Damage Analysis of The Morisada Building", *Proceedings, Annual Technical Session*, Structural Stability Council, 1984, pp.281-290.

[50] Mahin, S.A., and Bertero, V.V., "An Evaluation of Inelastic Seismic Design Spectra", *J. of Str. Div.*, ASCE, Vol. 107, No. ST9, Sept, 1981.

[51] Ma, S.Y.M, Bertero, V.V., and Popov, E.P., "Experimental and Analytical Studies on the Behavior of Reinforced Concrete Rectangular and T-Beams", *EERC Report*, 76-2, Univ. of Calif., Berkeley, CA., May 1976.

[52] Maison, B.F.and Popov, E.P., "Cyclic Response prediction for Braced Steel Frames", *J. Struct. Div.*, ASCE, 106, No.ST7, Proc.Paper 15534, 1401-1416 (July 1980).

[53] Malley, J.O., and Popov, E.P., "Design Considerations for Shear links in Eccentrically Braced Frames", *EERC Report 83-24*, Univ.of Calif., Berkeley, CA., 1983.

[54] Manheim, D.N., "On the Design of Eccentrically Braced Frames", *D.Eng. thesis*, University of California, Berkeley (Feb.1982).

[55] Matzen, V.C., and McNiven, H.D., "Investigation of the Inelastic Characteristics of a Single-Story Steel Structures Using System Identification

and Shaking Table Experiments", *EERC Report*, 76-20, Univ. of Calif., Berkeley, CA., Aug., 1976.

[56] Menegotto, M., and Pinto, P., "Method of Analysis for Cyclically Loaded Reinforced Concrete Plane Frames Including Changes in Geometry and Nonelastic Behavior of Elements under Combined Normal Force and Bending", *Final Report, IABSE Symposium on Resistance and Ultimate Deformability of Structures Acted on by Well-Defined Repeated Loads*, Lisbon, 1973.

[57] Moehli, J.P., "Strong Motion Drift Estimates for R/C Structures", *J. of Str. Eng.*, ASCE, Vol.110, No.9, Sept.,1984, pp.1988-2001.

[58] Moehli, J.P., "Seismic Response of Vertically Irregular Structures", *J. of Str. Eng.*, ASCE, Vol.110, No.9, Sept.,1984, pp.2002-2014.

[59] Muto, K., "Aseismic Design Analysis of Buildings", Maruzen, Tokyo, Japan.

[60] Mueller, P., "On a Seismic Design", *Proceedings 8WCEE*, San Francisco, CA., Vol. 5, July 21-28, 1984, pp.411-418.

[61] Neal, B.G., "Effect of Shear Force on the Fully Plastic Moment of an I-Beam", *Journal of Mechanical Engineering Science*, Vol.3(3), 1961.

[62] Neal, B.G., "The Effect of Shear and Normal Force on the Fully Plastic Moment of a Beam of Rectangular Cross Section", *Journal of Applied Mechanics*, Vol.28(2), 1961.

[63] Newmark, N.M., and Hall, W.J., "Earthquake Spectra and Design", EERI (Earthquake Engineering Research Institute), Berkeley, CA.

[64] Ortiz, M., and Popov, E.P., "Distortional Hardening Rules for Metal Plasticity", *J. Eng. Mech.*, ASCE, Vol.109, No.4, Aug., 1983.

[65] Pauley, T., "Deterministic Seismic Design procedures for Reinforced Concrete Buildings", *Engineering Structures*, Vol.5, No.1, 79-86 (Jan.1983).

[66] Penzien, J., "Elasto-Plastic Response of Idealized Multi-Story Structures Subjected to a Strong Earthquake", *Proc., 2WCEE*, 1960.

[67] Petersson, H., and Popov, E.P., "Constitutive Relations for Generalized Loadings", *J. Eng. Mech.*, ASCE, Vol.103, No. EM4, Aug., 1977.

[68] Pique, J.R., "On the Use of Simple Models in Nonlinear Dynamic Analyses", *MIT Dept. of Civil Eng. Report*, R 76-43, Massachusetts Inst. of Tech., Cambridge, Mass., 1976.

[69] Plantema, F.J., "Sandwich Construction: The Bending and Bucking of Sandwich Beams, Plates, and Shells", John Wiley and Sons Inc., New York, 1966.

[70] Popov, E.P., "Seismic Behavior of Structural Subassemblages", *J. of Str. Div.*, ASCE, Vol. 106, No. ST7, July, 1980.

[71] Popov, E.P., "Recent Research on Eccentrically Braced Frames", *Proceeding*, Structural Engineers Association of California, Coronado, Sept. 1981, pp. 69-80. Republished in *Engineering Structures* (Butterworth & Co.ltd.), Vol.5, No.1, 3-9 (Jan.1983).

[72] Popov, E.P., Amin, N.R., Louie, J.J.C., and Stephen, R.M., "Cyclic Behavior of Large Beam-Column Assemblies", *Earthquake Spectra*, Vol.1, No.2, Feb. 1985, pp. 3-38.

[73] Popov, E.P., and Bertero, V.V., "Seismic Analysis of Some Steel Building Frames", *J. of Eng. Mech. Div.*, ASCE, Vol. 106, No. EM1, Feb., 1980, pp.75-95.

[74] Popov, E.P., and Malley, J.O., "Design of Links and Beam-to-Column Connections for Eccentrically Braced Steel Frames", *EERC Report No.83-03*, Univ. of Calif., Berkeley, CA., 1983.

[75] Popov, E.P., and Ortiz, M., "Macroscopic and Microscopic Cyclic Metal Plasticity", *Proceedings, Third Engineering Mechanics Division Speciality Conferenece*, ASCE, Austin, Texas, Sept. 17-19, 1979, pp.303-330.

[76] Popov, E.P., and Petersson, H., "Cyclic Metal Plasticity: Experiments and Theory", *J. of Eng. Mech.*, ASCE, Vol.104, No. EM6, December , 1978.

[77] Popov, E.P., and Roeder, C.W., "Design of an Eccentrically Braced Frame", *AISC Engineering Journal*, Third Quarter, 1978.

[78] Popov, E.P. and Stephen, R.M., "Cyclic Loading of Full-Size Steel Connections", *EERC Report, 70-3*, Univ. of Calif., Berkeley, CA., July 1970.

[79] Popov, E.P., Takanashi, K., and Roeder, C.W., "Structural Steel Bracing Systems: Behavior Under Cyclic Loading", *EERC Report No. 76-17*, Univ. of Calif., Berkeley, CA., 1976.

[80] Prager, W., and Hodge, P.G., Theory of Perfectly Plastic Solids, John Wiley and Sons, Inc, New York, 1951.

[81] Ricles, J.M., "Cyclic Behavior of Composite Shear Links", *CE 299 Report*, Dept. of Civil Engrg., Univ. of California, Berkeley, CA., 1985.

[82] Ramberg, W., and Osgood, W., "Description of Stress-Strain Curves by Three Parameters", *Technical Note*, No. 902, NACA, July 1943.

[83] Rockey, K.C., and Cook, I.T., "Shear Buckling of Clamped Infinitely Long Plates - Influence of Torsional Rigidity of Transverse Stiffeners", *Aeronautical Quarterly*, Vol. 16, February, 1965, pp. 92-95.

[84] Roeder, C.W., and Popov, E.P., "Inelastic Behavior of Eccentrically Braced Steel Frames Under Cyclic Loading", *EERC Report No.77-18*, Univ. of Calif., Berkeley, CA., 1977.

[85] Saiidi, M., and Sozen, A.M., "Simple and Complex Models for Nonlinear Seismic Response of Reinforced Concrete Structures", *Civil Eng. Studies, Structural Research series*, No. 465, Univ. of Illinois at Urbana, Illinois, 1979.

[86] Saisho, M., "Effects of Axial Deformations and Forces of the Columns on the Dynamics Collapse of Steel Frames under Strong Ground Motions", *Proceedings 8WCEE*, San Francisco, CA., Vol. 6, July 21-28, 1984, pp.161-168.

[87] SEOANC (Structural Engineers Association of Northern California), "Earthquake Resistant Design of Concentric and K-Braced Frames", *Report*, (20 July 1982).

[88] Shing, P.B., and Mahin, S.A., "Psuedodynamic Test Method for Seismic Performance Evaluation: Theory and Implementation", *EERC Report No.84-01*, Univ. of Calif., Berkeley, CA., 1984.

[89] Stein, M., and Fralich, R.W., "Critical Shear Stress of an Infinitely Long Simply Supported Plate with Transverse Stiffeners", *NACA TN 1851*, 1949.

[90] Stowell, E.Z., "A Unified Theory of Plastic Buckling of Columns and Plates", *NACA Rep. 898, 1948*.

[91] Takizawa, H., Umemura, H., "Dynamic Response of Reinforced Concrete Buildings", *Structural Engineering Documents*, International Association of Bridge and Structural Engineering (IABSE), Zurich, 1982.

[92] Teal, E., "Practical Design of Eccentrically Braced Frames to Resist Seismic Forces", *Structural Steel Education Council*, Sanfrancisco/El Monte, CA., 1979.

[93] Tsuboi, Y., "Theory of Elasticity and Plasticity for Buildings", *Kenchikugaku-Taikei*, Shokoku-Sha, Tokyo, Japan (in Japanese).

[94] UBC, *Uniform Building Code*, International Conference of Building Officials, Whittier, CA., 1982.

[95] Udagawa, K., Takanashi, K., Tanaka, H., "Restoring Force Characteristics of H-shaped Steel Beams Under Cyclic and Reversed Loadings", *Trans. of A.I.J.*, No. 264, Feb. 1978 (in Japanese).

[96] Veletsos, A.S., and Newmark, N.M., "Effect of Inelastic Behavior on the Response of Simple Systems to Earthquake Motions", *Proceedings 2WCEE*, Vol. 2, Tokyo, Japan, 1960., pp.895-912.

[97] Yamanouchi, H., Midorikawa, M., Nishiyama, I., and Watabe, M., "Experimental Results on a K-Braced Steel Structure Under Seismic Loading

Utilizing Full-Scale Six-Story Test Structure - U.S./Japan Cooperative Research Program - ", *Proceedings, Annual Technical Session*, Structural Stability Research Council, San Francisco, CA., 1984.

[98] Yang, M.S., " Shaking Table Studies of an Eccentrically X-Braced Frame", *Ph.D Thesis*, Univ. of Calif., Berkeley, CA., 1982.

[99] Yang, C.H., and Beedle, L.S., "Behavior of I and WF Beams in Shear", *Report No.205B.21*, Fritz Engineering Laboratory, Lehigh University, Bethlehem, Pa., 1951.

[100]

Yoshimura, K., "Inelastic behavior of Steel members Subjected to Alternating Loads", *Doctor of Engrg. Thesis*, Kyushu Univ., Fukuoka, Japan, 1973.

TABLES

Frame Type	Link Length		Vertical Load		Lateral Load		
	e (in)	e^* (in)	w (k/in)	Type	$P_u{}^*$ (k)	$\|P_u{}^{**}\|$ (k)	$\dfrac{\|P_u{}^{**}\|}{\|P_u{}^*\|}$
(1)	(2)	(3)	(4)	(5)	(6)	(7)	(8)
HD- 1	29	29	0.	-	±204	214	1.05
HD- 2	29	29	0.06	point	+194	203	1.05
HD- 3	29	29	0.06	point	-211	225	1.07
HD- 4	29	0	0.	-	±214	214	1.00
HD- 5	29	0	0.06	point	+202	203	1.00
HD- 6	29	0	0.06	point	-224	225	1.00
HD- 7	29	29	0.06	unif.	+192	203	1.06
HD- 8	29	29	0.06	unif.	-209	225	1.08
HD- 9	29	0	0.06	unif.	+201	203	1.01
HD-10	29	0	0.06	unif.	-221	225	1.02
HD-11	29	29	0.18	point	+172	182	1.06
HD-12	29	29	0.18	point	-217	218	1.00
HD-13	29	0	0.18	point	+180	182	1.01
HD-14	29	0	0.18	point	-242	246	1.02
LD- 1	36	36	0.	-	±90	95	1.06
LD- 2	36	36	0.08	unif.	+72	75	1.04
LD- 3	36	36	0.08	unif.	-92	94	1.02
LD- 4	36	0	0.	-	±94	95	1.01
LD- 5	36	0	0.08	unif.	+72	75	1.04
LD- 6	36	0	0.08	unif.	-110	114	1.04
HK- 1	29	14	0.	-	199	214	1.08
HK- 2	29	14	0.06	point	195	214	1.10
HK- 3	29	0	0.	-	209	214	1.02
HK- 4	29	0	0.06	point	209	214	1.02
HK- 5	29	14	0.18	point	197	214	1.09
HK- 6	29	0	0.18	point	208	214	1.03
HK- 7	29	14	0.18	unif.	194	214	1.10
HK- 8	29	0	0.18	unif.	207	214	1.03
HV- 1	29	0	0.	-	214	214	1.00
HV- 2	29	0	0.06	point	214	214	1.00
HV- 3	29	0	0.18	point	213	214	1.00
HV- 4	29	0	0.18	unif.	209	214	1.02

* Obtained from elasto-plastic analysis at $\vartheta = 1.5\%$
** Obtained from approximate limit analysis.
Note: For HD-,HK-,HV-frames, L=216 in., and for LD-frames L=288 in.

Table 4.1 Summary of Nonlinear Analyses for 32 Eccentrically Braced Frames.

Section	d (in.)	t_w (in.)	b (in.)	t_f (in.)	A (in.^{2})	I (in.^{4})	Z (in.^{3})
Specimen	7.97	0.17	3.96	0.208	2.98	31.6	9.07
W8×10	7.89	0.17	3.94	0.205	2.96	30.8	8.87

Table 6.1. Specimen Section Properties

Location	σ_y (ksi.)	σ_u (ksi.)	ε_{sh} (in./in.)	ε_u (in./in.)	E (ksi.)
Web	60.6	79.9	0.031	0.163	30,001
Flange	52.4	70.7	0.026	0.198	31,118

Table 6.2. Specimen Material Properties

σ_y Web	σ_y Flange	P_y (k.)	V_p (k.)	$M_p^{\,*}$ (k–in.)	M_p (k–in.)	$b^{\,*}$ (in.)	b_{max} (in.)
60.6	52.4	167.1	46.2	321	498	13.9	21.6
56.5 (averaged)		168.4	42.6	346	513	16.2	24.1

Table 6.3. Specimen Plastic Properties

Specimen No.	e (in.)	Panel zones Number	Panel zones a (in.)	Panel zones a/t_w	Loading
1	14.5	4	3.63	21.3	Monotonic (twice)
2	14.5	4	3.63	21.3	Cyclic
3	14.5	4	3.63	21.3	Cyclic
4	14.5	4	3.63	21.3	Cyclic + Axial force
5	17.5	5	3.50	20.6	Cyclic
6	17.5	5	3.50	20.6	Cyclic + Axial force
7	11.5	3	3.83	22.5	Cyclic

Table 6.4. Test Specimens

Speci-men (1)	Section (2)	α (3)	β (4)	τ_B (ksi) (5)	$\tilde{\gamma}_B$ (rad) (6)	γ_u (rad) (7)	γ_u^{sh} (rad) (8)	$\dfrac{\gamma_u}{\gamma_u^{sh}}$ (9)	N (10)	Load Type (11)
A 1	W 18x40	1.66	53.6	25.5	0.032	0.018	0.018*	1.00	3	S- 2
A 2	W 18x40	0.83	53.6	30.4	0.082	0.033	0.030	1.10	4	S- 1
A 3	W 18x40	0.55	53.6	34.8	0.106	0.056	0.055	1.02	11	S- 1
A 4	W 18x40	0.42	53.6	39.1	0.184	0.096	0.074	1.30	18	S- 1
A 5	W 18x40	0.65	53.6	32.5	0.105	0.056	0.046	1.22	8	S- 1
A 6	W 18x40	0.50	53.6	38.1	0.114	0.061	0.060	1.02	8	S- 1
A 7	W 18x35	0.55	52.3	37.5	0.117	0.062	0.057	1.09	11	S- 2
A 8	W 18x60	2.13	40.1	35.0	0.060	0.034	0.030*	1.13	9	S- 3
A 9	W 18x40	0.71	53.6	32.5	0.078	0.042	0.041	1.02	9	S- 3
A 10	W 16x26	2.40	57.0	31.2	0.040	0.022	0.015*	1.47	4	S- 3
A 11	W 18x35	2.13	52.3	28.6	0.032	0.019	0.018*	1.06	4	S- 3
A 13	W 16x26	0.80	57.0	34.3	0.056	0.031	0.027	1.15	7	S- 3
A 14	W 18x35	0.71	52.3	33.5	0.076	0.042	0.043	0.98	10	S- 3
B16	W 18x60	2.13	40.1	38.4	0.060	0.033	0.030*	1.10	3	U- 1
B17	W 18x40	0.71	53.5	34.0	0.075	0.040	0.041	0.98	8	S- 4
B18	W 18x60	2.13	40.1	35.4	0.047	0.028	0.030*	0.93	12	S- 5
B20	W 18x40	0.71	53.5	34.5	0.077	0.041	0.041	1.00	4	S- 6
B21	W 18x40	0.71	53.5	35.2	0.082	0.044	0.041	1.07	13	S- 4
B22	W 18x40	0.67	53.5	35.2	0.101	0.054	0.045	1.20	15	S- 7
B23	W 18x40	0.67	53.5	35.2	0.081	0.045	0.045	1.00	14	S- 7
B24	W 18x40	0.71	53.5	35.3	0.090	0.049	0.041	1.20	1	U- 2
B25	W 18x40	0.71	53.5	33.5	0.073	0.040	0.041	0.98	13	S- 4
B26	W 18x40	0.50	53.5	40.1	0.134	0.072	0.059	1.22	19	S- 4
C 1	W 8x10	0.48	44.4	51.6	0.172	0.092	0.084	1.10	1	U- 2
C 2	W 8x10	0.48	44.4	48.4	0.160	0.086	0.084	1.02	18	U- 3
C 3	W 8x10	0.48	44.4	48.4	0.160	0.086	0.084	1.02	18	S- 2
C 5	W 8x10	0.46	44.4	45.9	0.136	0.075	0.087	0.86	19	S- 3
C 7	W 8x10	0.51	44.4	50.6	0.135	0.073	0.080	0.91	11	S- 8
D 1	W 12x19	0.60	44.7	39.5	0.118	0.063	0.066	0.95	11	S- 9
D 2	W 12x19	0.60	44.7	40.8	0.121	0.063	0.066	0.95	11	S-10

* Obtained from Fig. 8.7 $(a > d)$.

Table 8.1. Shear Link Cyclic Test Results

Test (1)	Section (2)	σ_y (ksi) (3)	σ_u (ksi) (4)	ε_{sh} (in/in) (5)	ε_u (in/in) (6)	$\dfrac{\sigma_u}{\sigma_y}$ (7)	E_h^* (ksi) (8)	E (ksi) (9)
A	W 16x26	48.3	67.2	0.026	0.24	1.39	88.3	30150
	W 18x35	46.7	68.9	0.020	0.20	1.47	123.3	28650
	W 18x40	39.5	60.1	0.018	0.22	1.52	102.0	28300
	W 18x60	44.4	68.4	0.019	0.21	1.54	125.7	28600
B	W 18x40	48.0*	64.0*	0.02**	0.26*	1.33	66.7	29000**
	W 18x60	44.4	68.4	0.019	0.21	1.54	125.7	28600
C	W 8x10	60.6	79.9	0.031	0.163	1.32	146.2	30001
D	W 12x19	54.3	66.4	0.036	0.175	1.22	87.1	28730

* From mill tests
** Estimated

Table 8.2. Specimen Web Material Properties

FIGURES
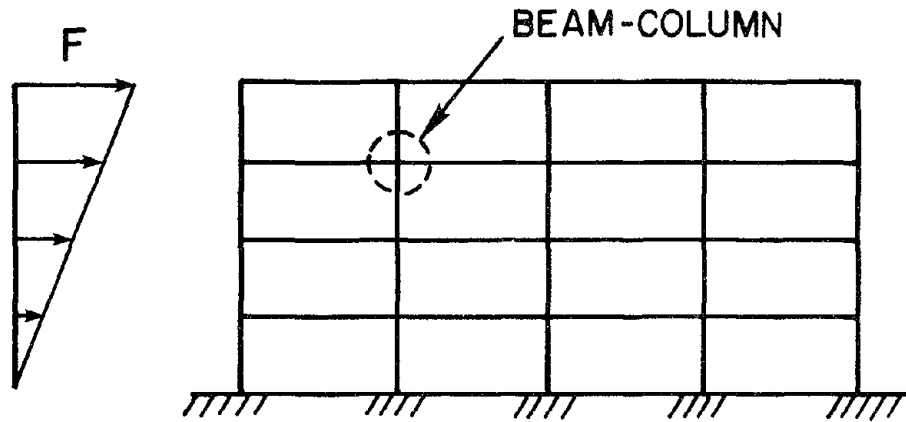
Fig. 1.1   A Typical Moment Resisting Frame (MRF).
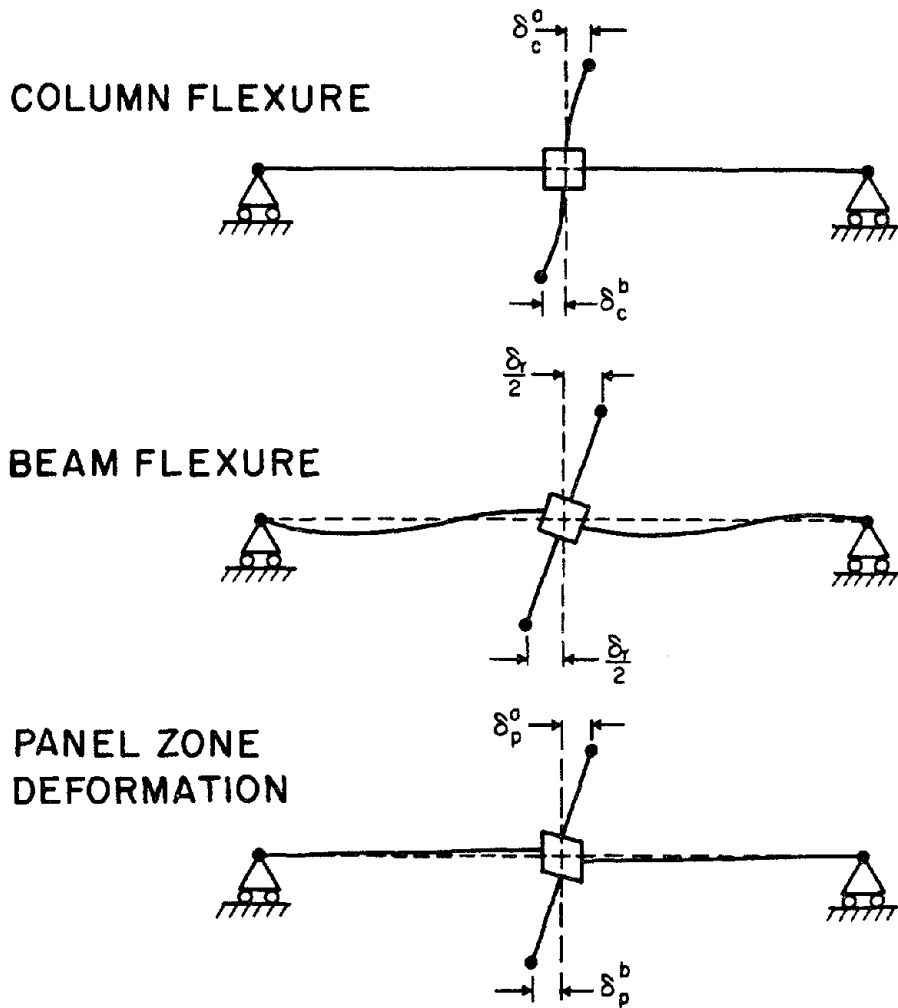
Fig. 1.2   Lateral Displacement Components of MRF.
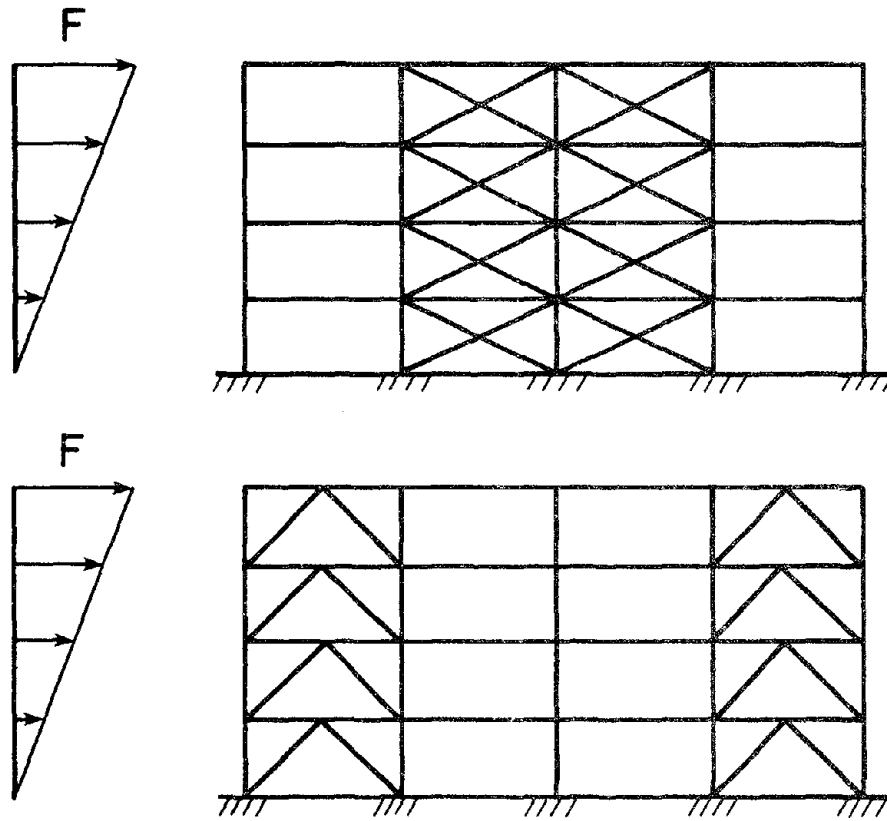
Fig. 1.3   Typical Arrangements for Concentrically Braced Frames (CBFs).
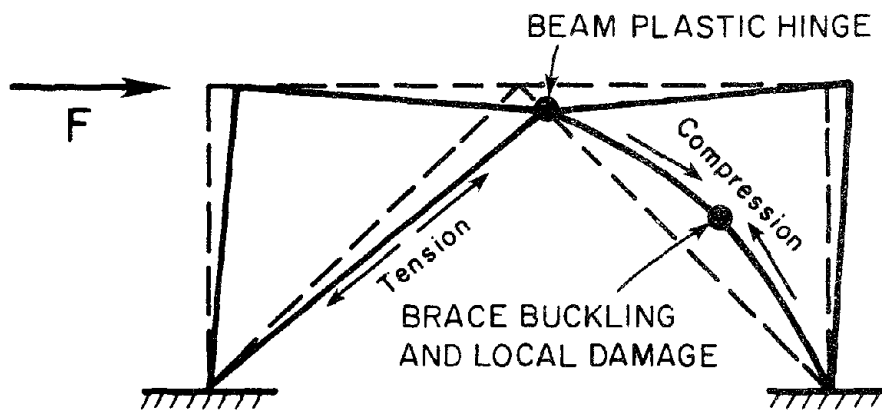
Fig. 1.4   Severe Plastic Deformation of a Concentric K-braced Frame.
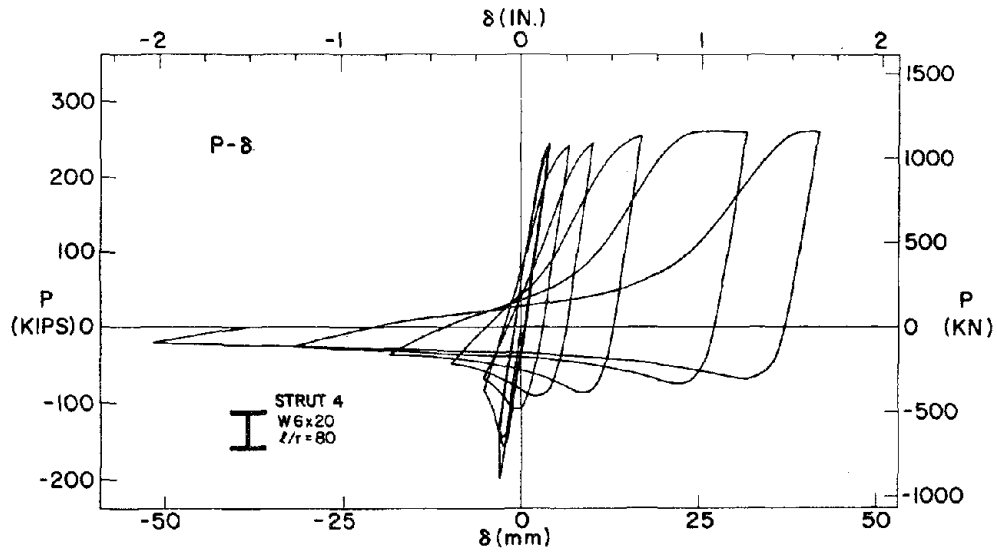
Fig. 1.5   Hysteretic Loops for Axial Force v.s. Axial Displacement
             of a Pin-Ended Brace Strut [7].
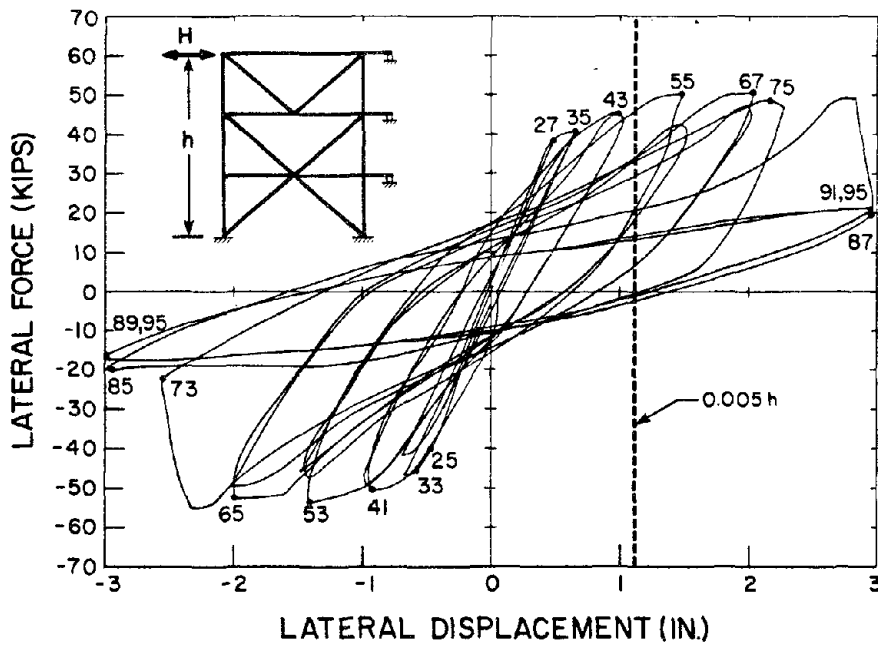
Fig. 1.6   Hysteretic Loops for One-third Size Concentric K-brace Frame [52].
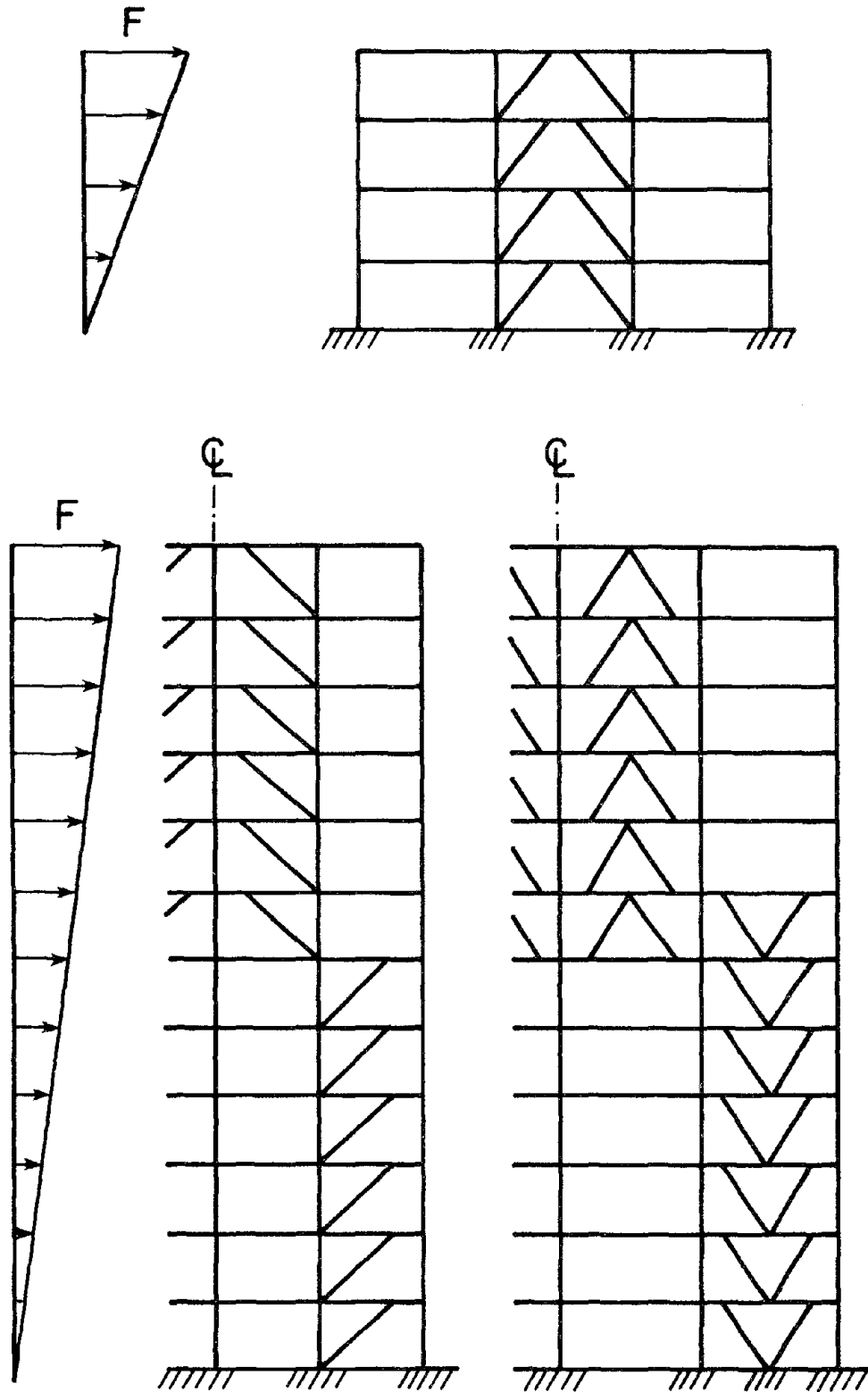
Fig. 1.7   Typical Arrangements of Eccentrically Braced Frames (EBFs).
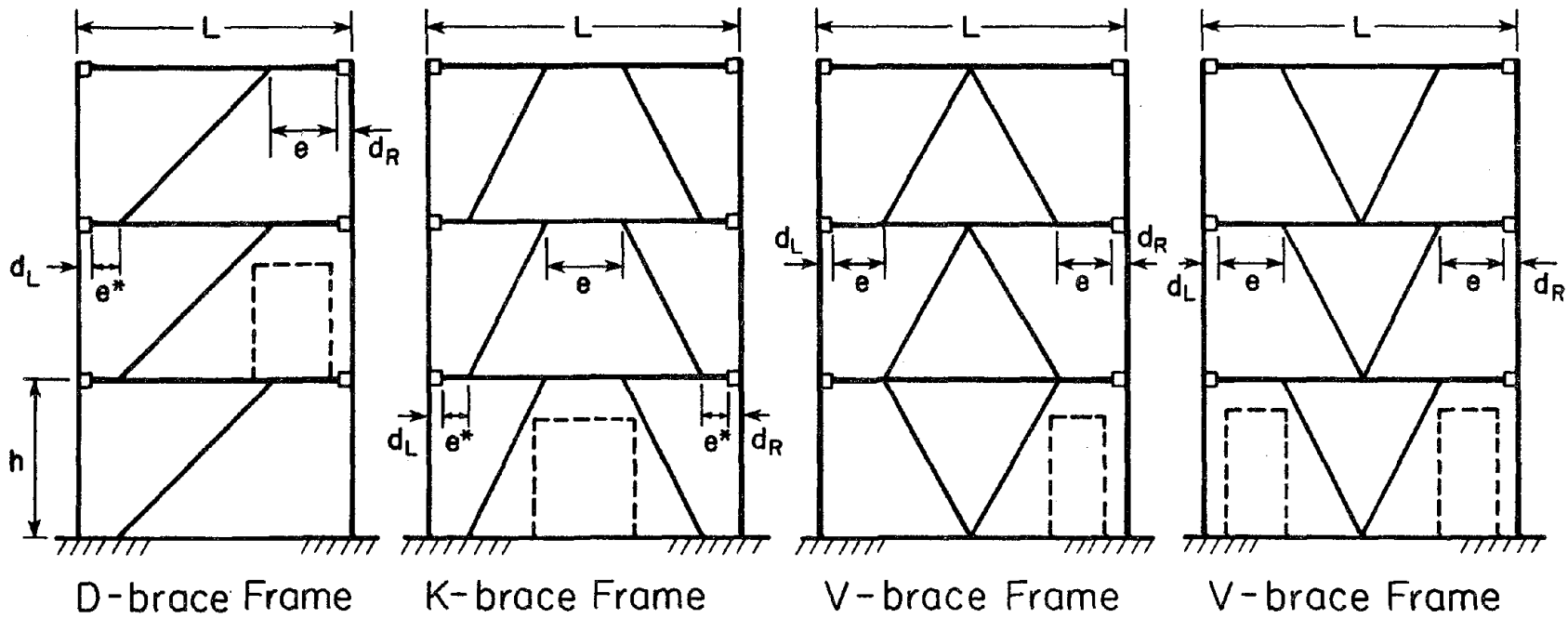
Fig. 1.8   Various Types of EBFs [40].

ACTIVE LINK

F

e
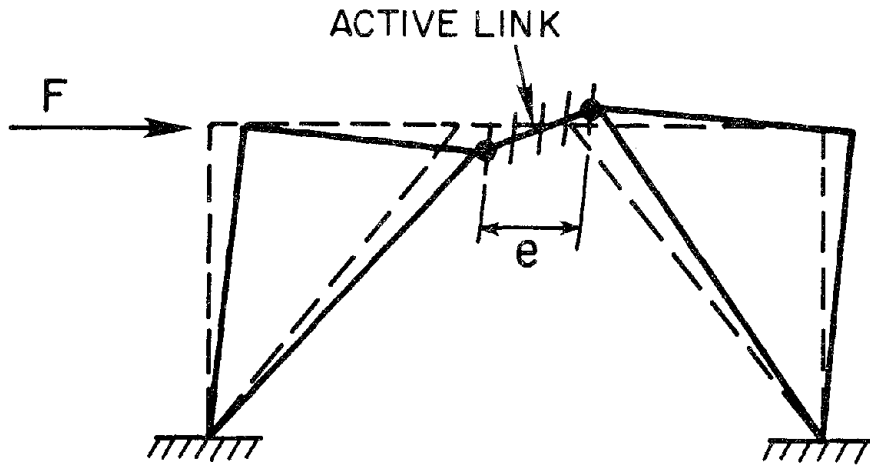
Fig. 1.9   Typical Plastic Deformation of Eccentric K-braced Frame.
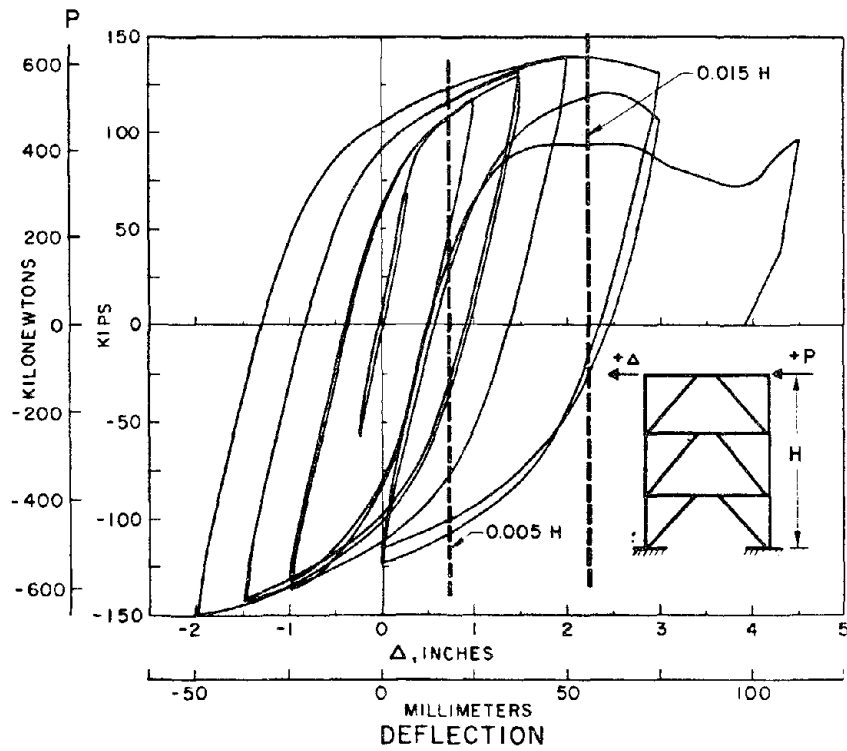
Fig. 1.10   Hysteretic Loops for One-third Size EBF [54].

(b)

HINGE (2)

$e > b^*$

(a)

HINGE (1)   HINGE(3)

HINGE (2)

$e^* < e < b^*$

$e < b^*$
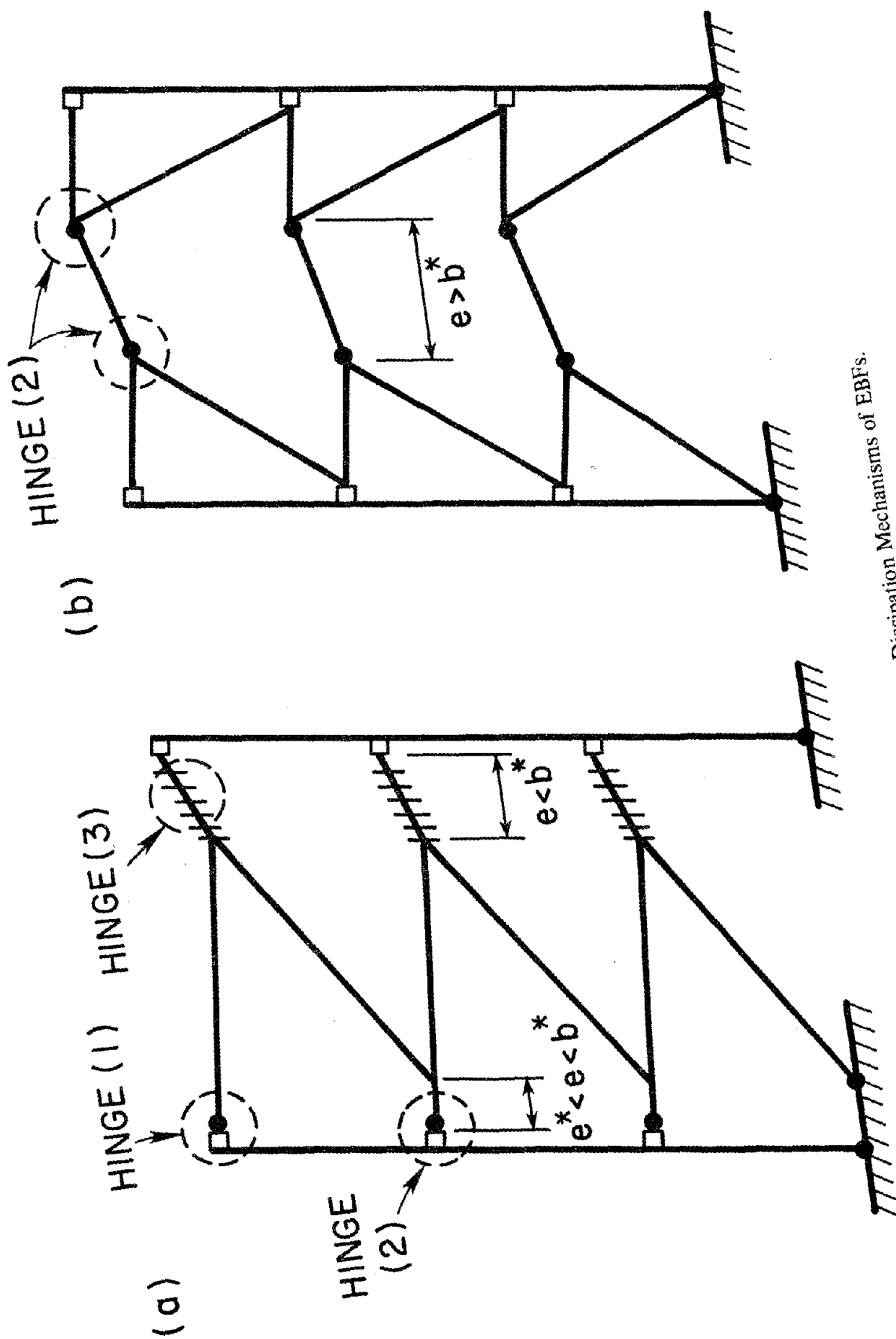
Fig. 2.1   Energy Dissipation Mechanisms of EBF's.
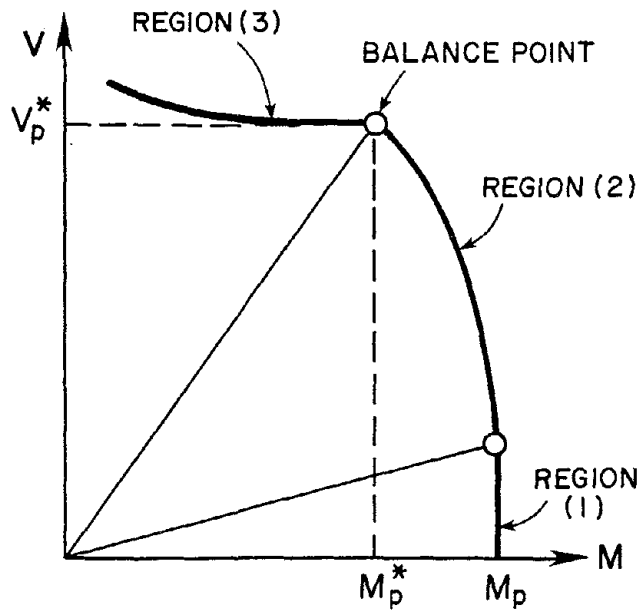
Fig. 2.2 $M-V$ Interaction Curve
for Wide Flange Beams.
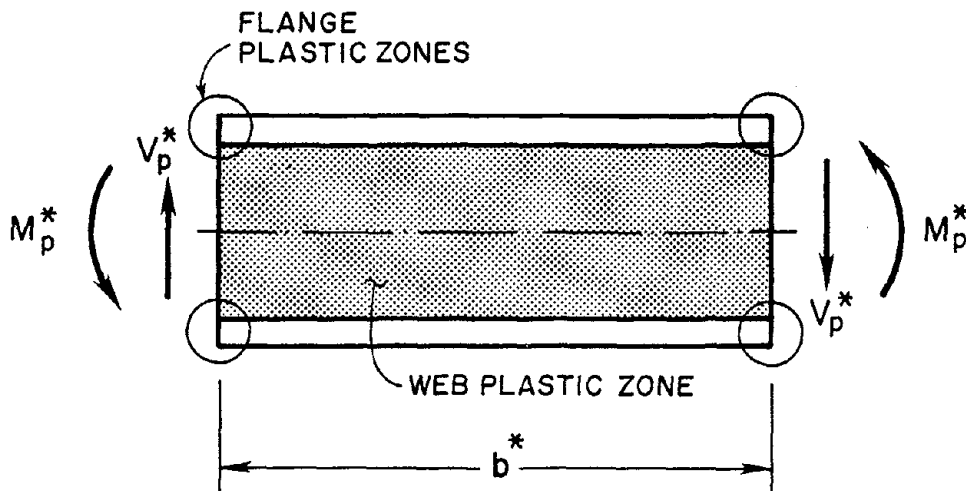
Fig. 2.3   Maximum Shear Hinge Length
of Ideal Plastic Link.
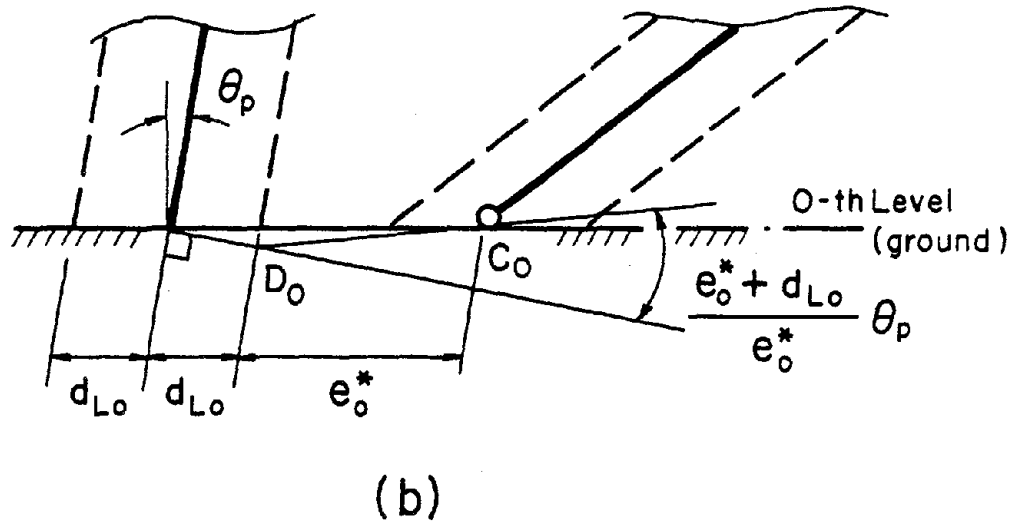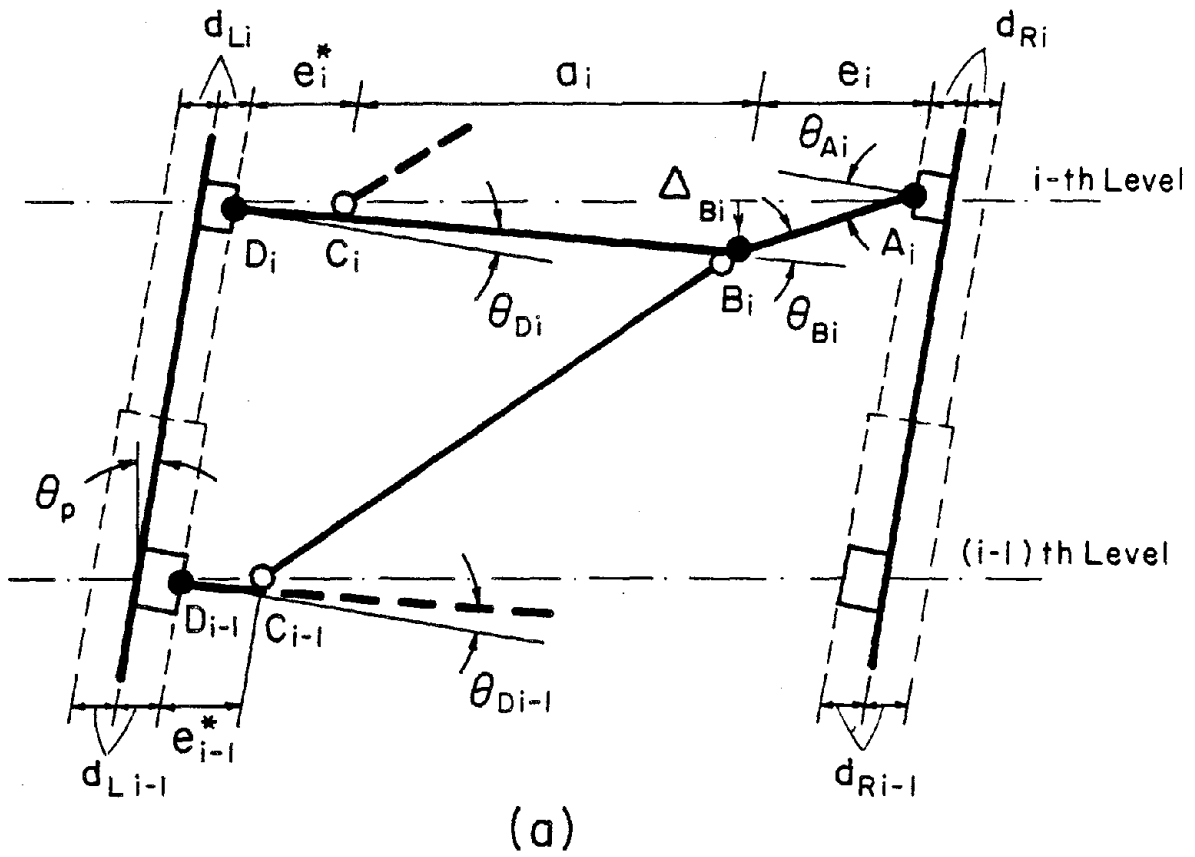
Fig. 2.4   Rigid-Plastic Displacement Field of an EBF.
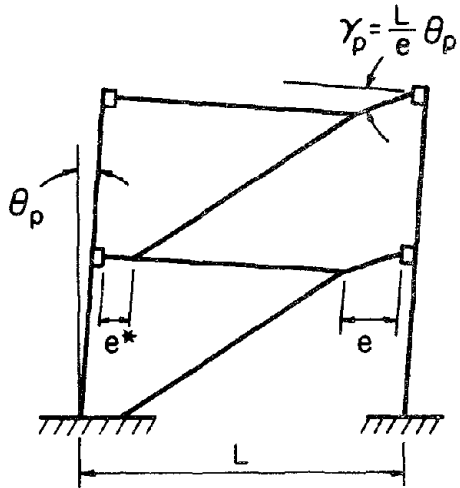
Fig. 2.5   D-brace Frame Mechanism.
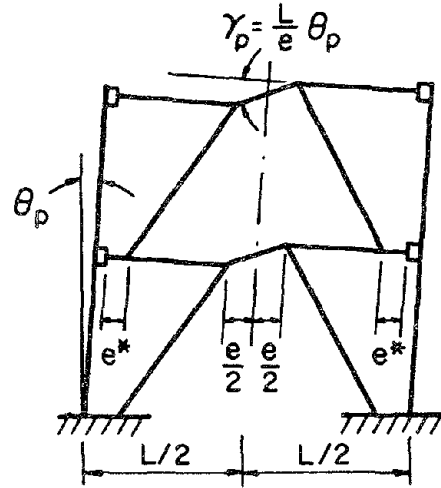
Fig. 2.6   K-brace Frame Mechanism.
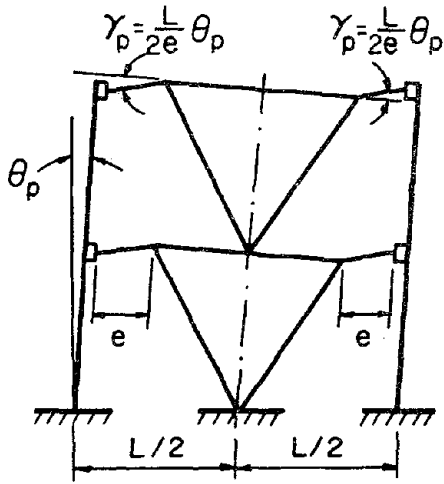
Fig. 2.7   V-brace Frame Mechanism.
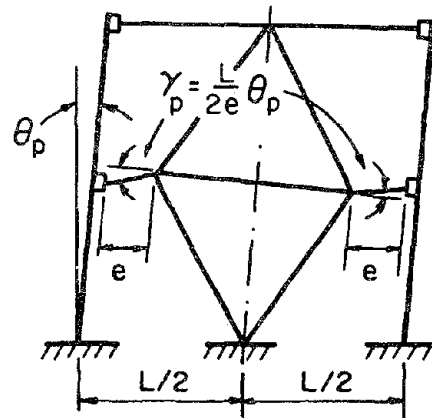
Fig. 2.8   Alternative V-brace
Frame Mechanism.
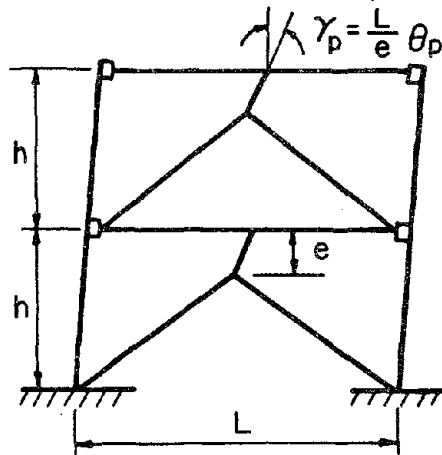
Fig. 2.9   Inverted Y-brace Frame Mechanism.
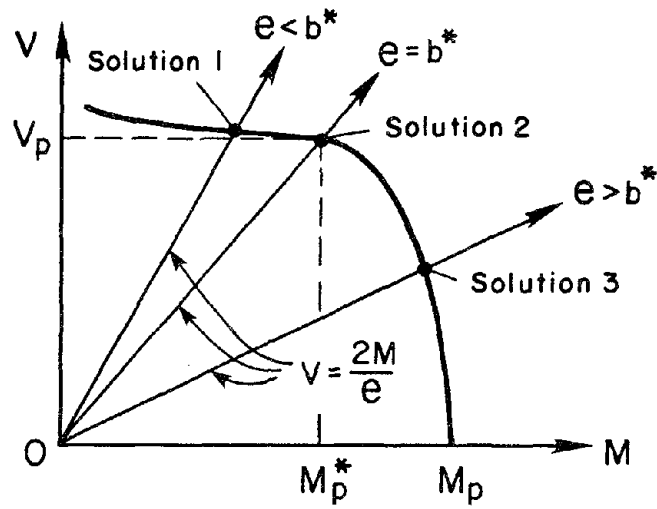
Fig. 3.1   Schematic Illustration for Obtaining V for Given e.

MECHANISM I

MECHANISM 2

$$W_I \simeq W_{II} \simeq \sum_{i=1}^{3} V_{ABi} \, L\theta_p$$

Fig. 3.2   Internal Virtual Work in D-brace Frame for Mechanisms 1 and 2.
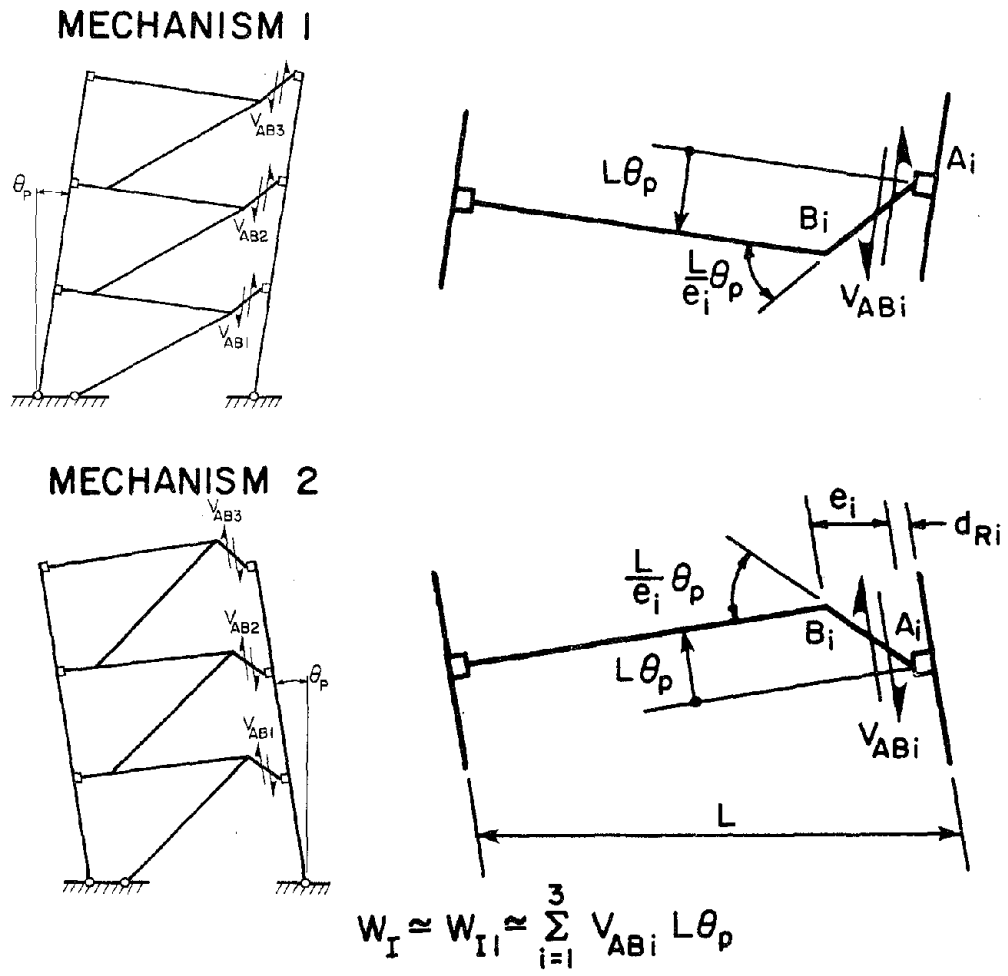
MECHANISM 1   MECHANISM 2

(a) Work Done By Lateral Load.

(WORK > 0)

TOTAL WEIGHT

$$= w_i \; L$$

(WORK < 0)
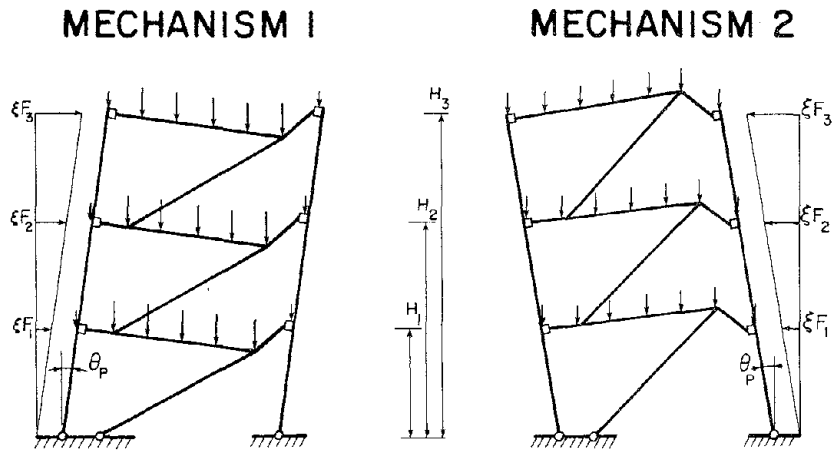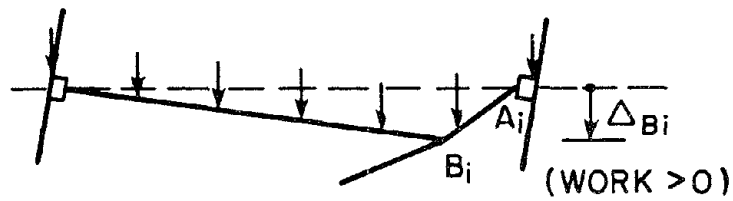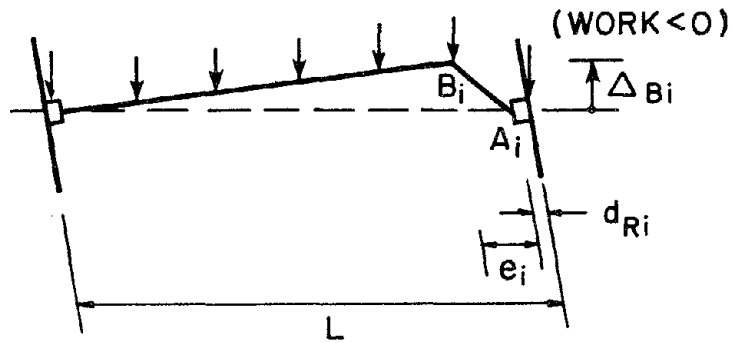
$$W_{E2} \simeq \pm \frac{1}{2} \sum_{i=1}^{3} w_i \; \Delta_{Bi} L \qquad \Delta_{Bi} \simeq (L - e_i - d_{Ri}) \, \theta_p$$

(b) Positive and Negative Work Done by Vertical Loads.

Fig. 3.3   External Virtual Work in D-brace Frame for Mechanisms 1 and 2.

VARIATIONS OF MECHANISM 3
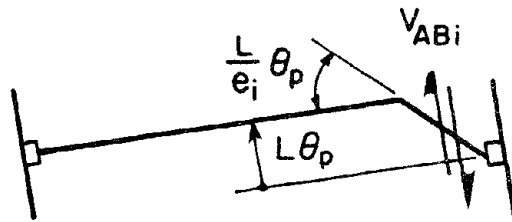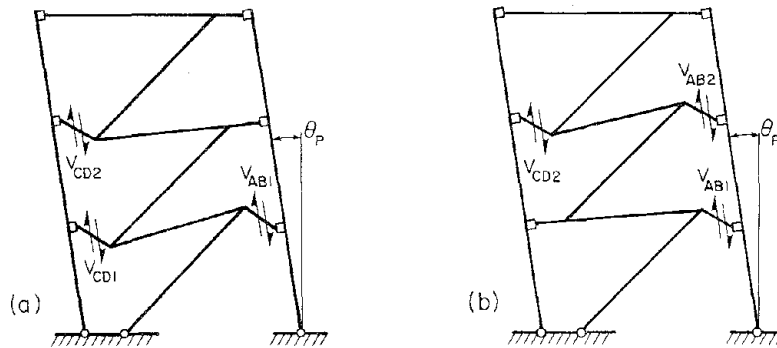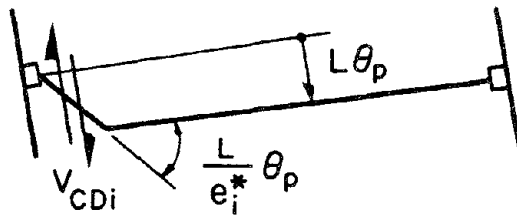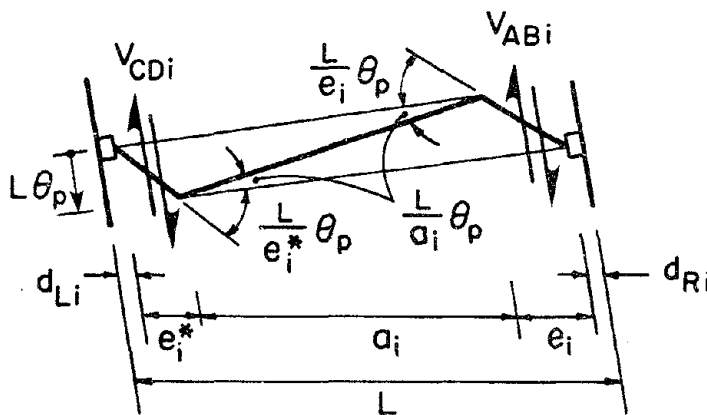
$$W_I \simeq W_{II} \simeq \Sigma W_{II}^{(a)} + \Sigma W_{II}^{(b)} + \Sigma W_{II}^{(c)}$$

Fig. 3.4   Approximate Estimates of Link Deformation Angles and Internal Virtual Work in a D-brace Frame for Mechanism 3.

MECHANISM 3
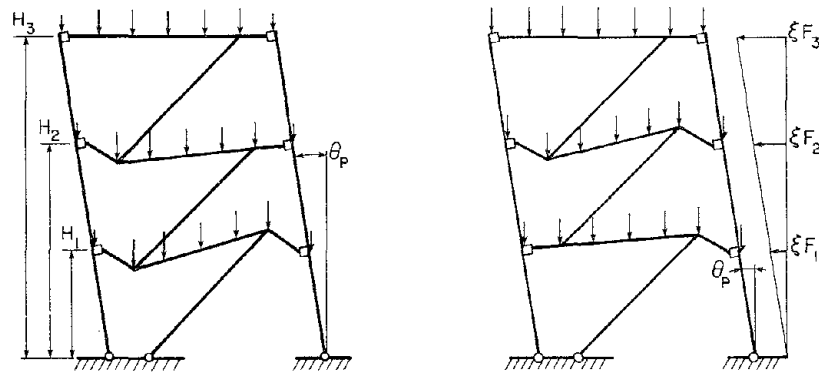
(a) Work Done by Lateral Load.
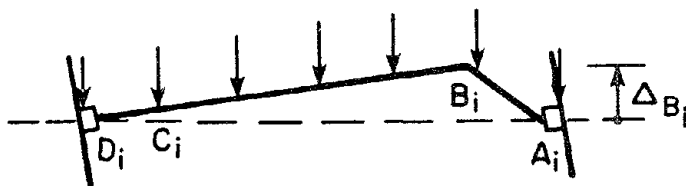
beam mechanism (a)

$$W_{E2}^{(a)} \simeq \frac{-1}{2} w_i \, \Delta_{B_i} L$$

$$\Delta_{B_i} \simeq (L - e_i - d_{Ri}) \theta_p$$
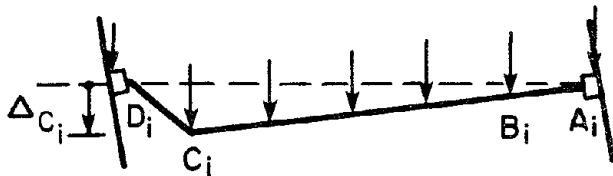
beam mechanism (b)

$$W_{E2}^{(b)} \simeq \frac{1}{2} w_i \, \Delta_{C_i} L$$

$$\Delta_{C_i} \simeq (L - e_i^* - d_{Li}) \theta_p$$
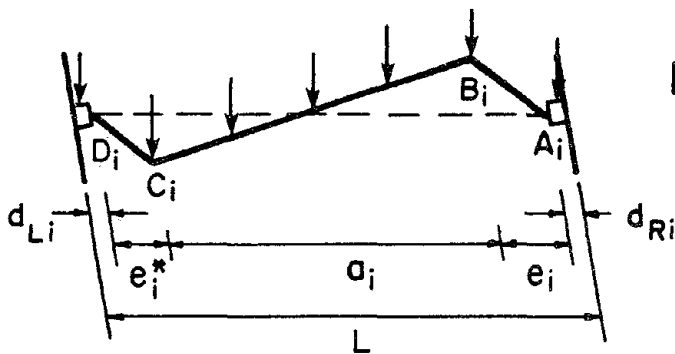
beam mechanism (c)

$$W_{E2}^{(c)} \simeq 0$$

$$W_{E2} \simeq \Sigma W_{E2}^{(a)} + \Sigma W_{E2}^{(b)}$$

(b) Work Done by Vertical Loads.

Fig. 3.5   External Virtual Work in a D-brace Frame for Mechanisms 3.
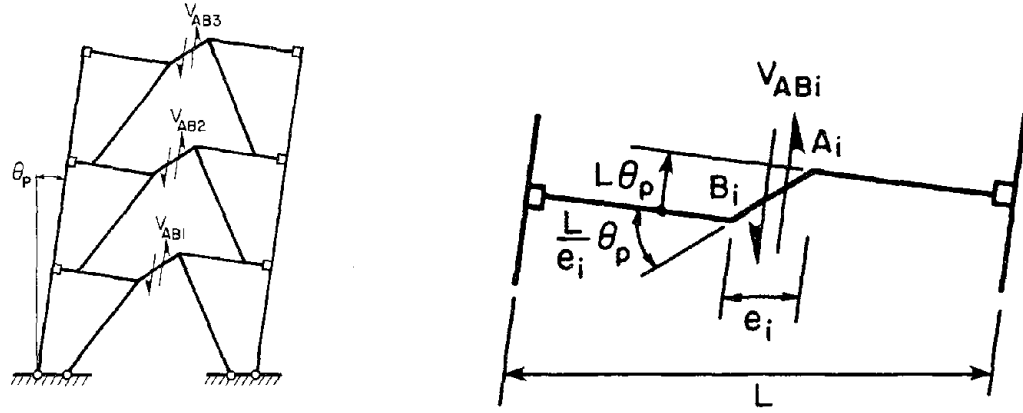
$$W_{II} = \sum_{i=1}^{3} V_{ABi} L\theta_p$$

(a) Internal Work for K-brace Frame.
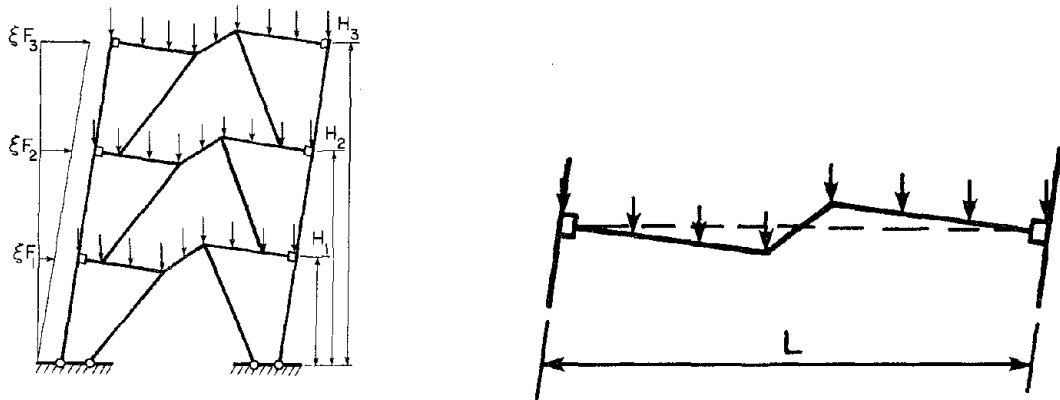
$$W_{EI} = \xi \sum_{i=1}^{3} F_i H_i \theta_p \qquad\qquad W_{E2} = 0$$

(b) External work for K-braced Frame.

Fig. 3.6   Internal Work and External Work for K-brace Frame.
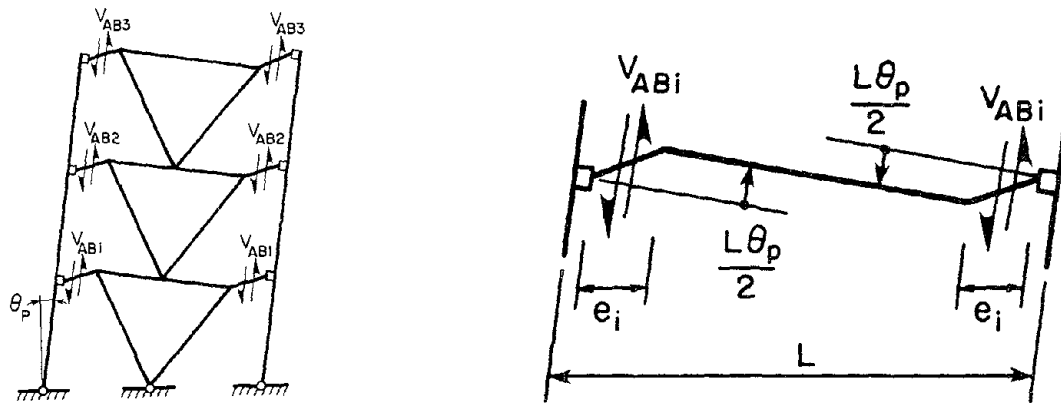
$$W_{II} = \sum_{i=1}^{3} V_{ABi} \, L\theta_p$$

(a) Internal Work for V-brace Frame.
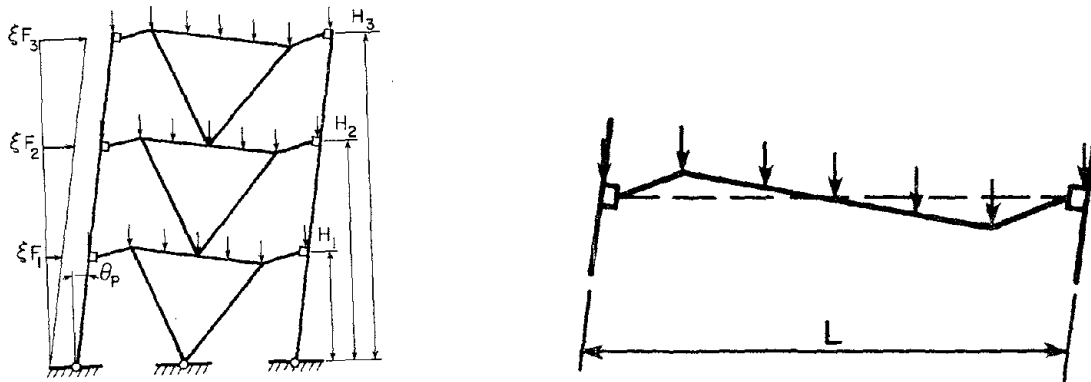
$$W_{EI} = \xi \sum_{i=1}^{3} F_i \, H_i \qquad\qquad W_{E2} = 0$$

(b) External work for V-braced Frame.

Fig. 3.7   Internal Work and External Work for V-brace Frame.
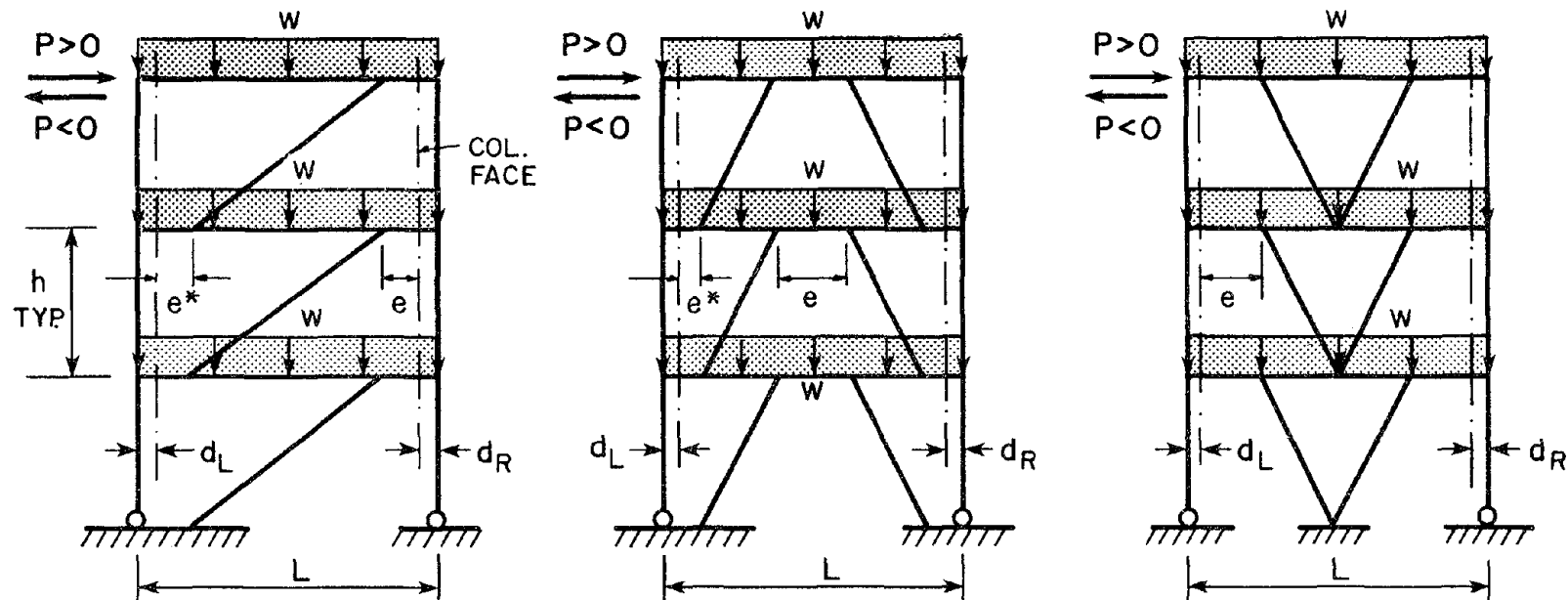
FRAME TYPES	L (in)	h (in)	e (in)	e* (in)	d_L, d_R (in)	BEAM	BRACE	COLUMN
HD	216	108	29	29 or 0	7	w14 x 53	8x8x5/16	w14 x 82
HK	216	108	29	29 or 0	7	w14 x 53	8x8x1/4	w14 x 82
HV	216	108	29	--	7	w14 x 53	8x8x1/4	w14 x 82
LD	288	144	36	36 or 0	7	w 8 x 31	8x8x1/4	w14 x 48

Fig. 4.1   Basic Parameters for EBF Analyses for Lateral and Vertical Loads.
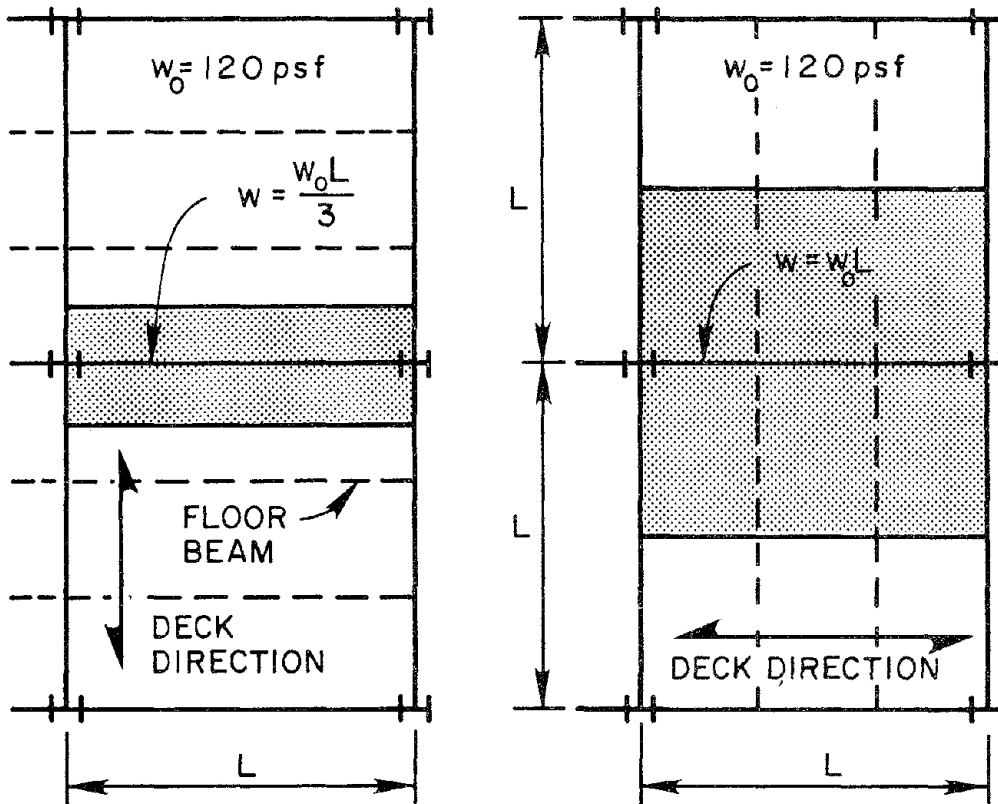
Fig. 4.2   Two Cases of Vertical Loading.
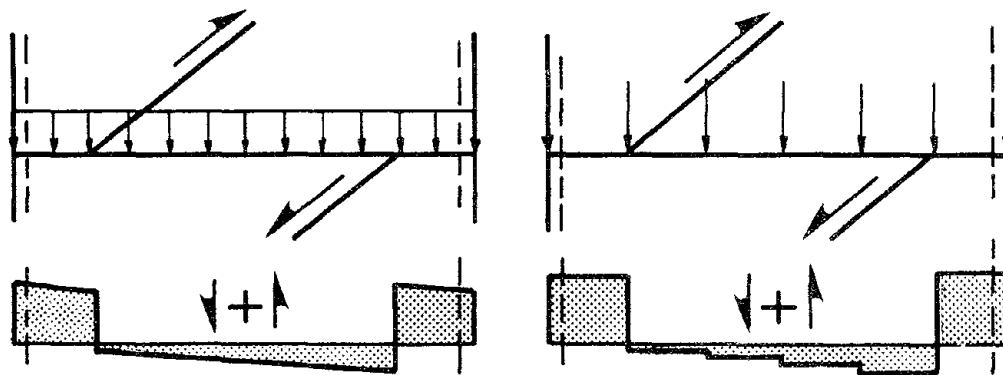
Fig. 4.3   Modeling of Distributed Load by Point Loads
and Shear Force Distributions in a Beam.
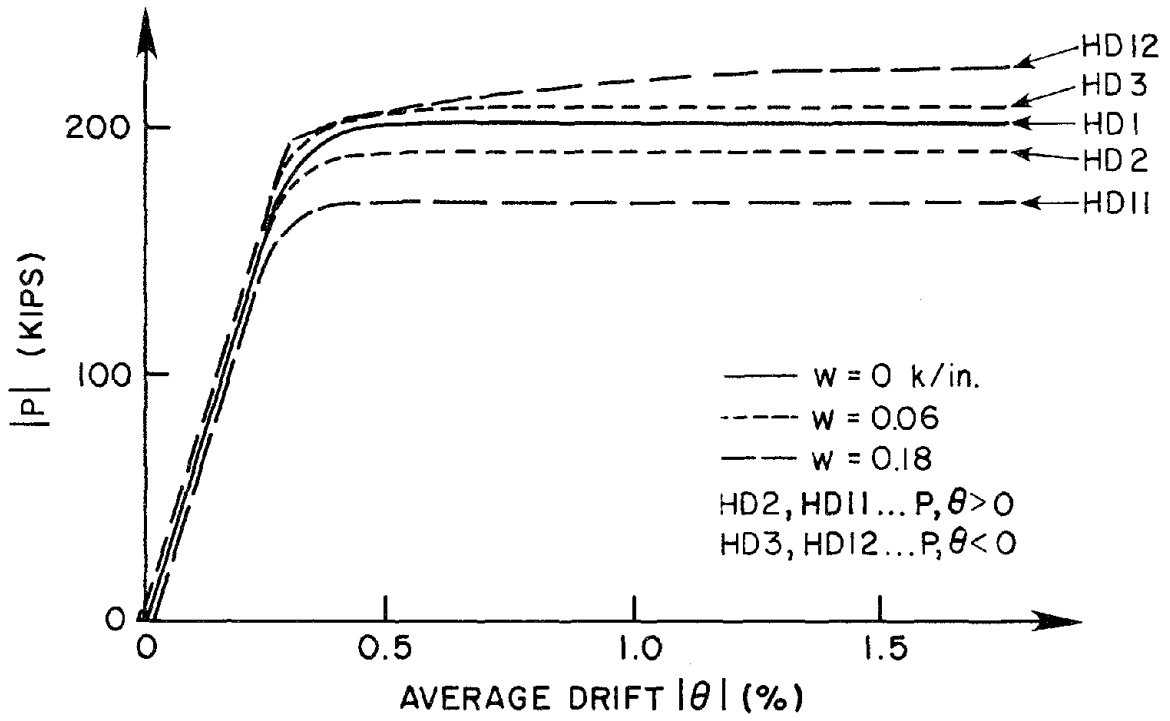
Fig. 4.4   Load-Deflection Relationships for HD-frames with $e^* = e$.
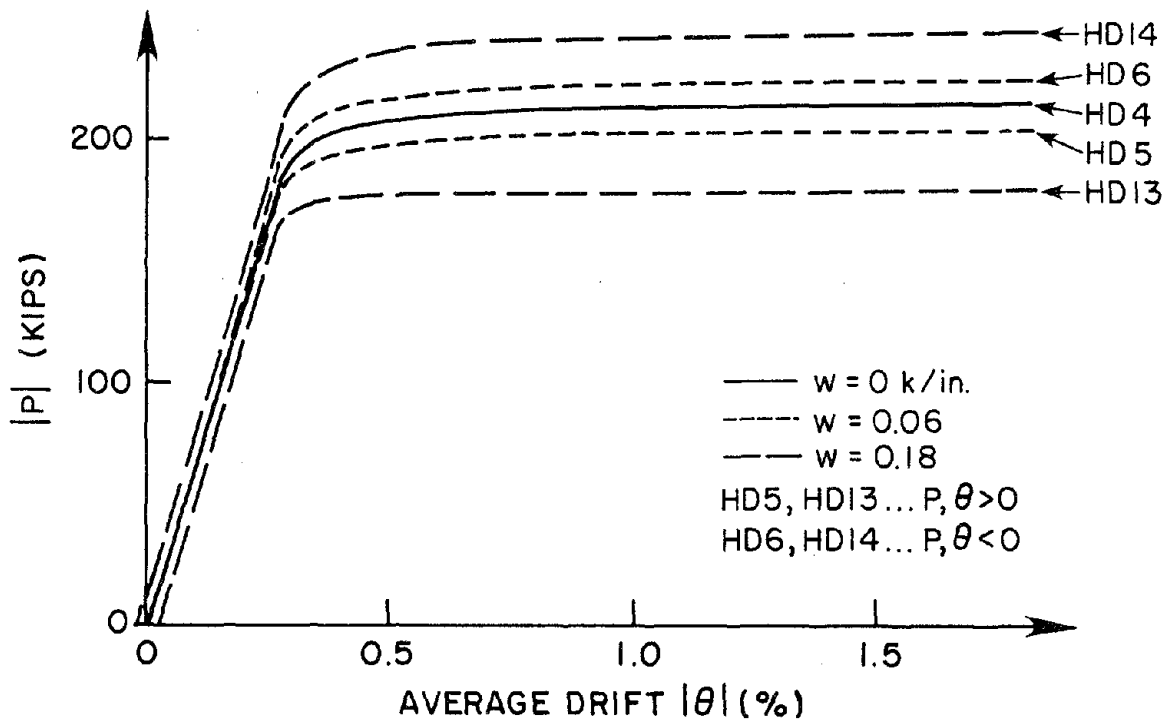
Fig. 4.5   Load-Deflection Relationships for HD-frames with $e^* = 0$.
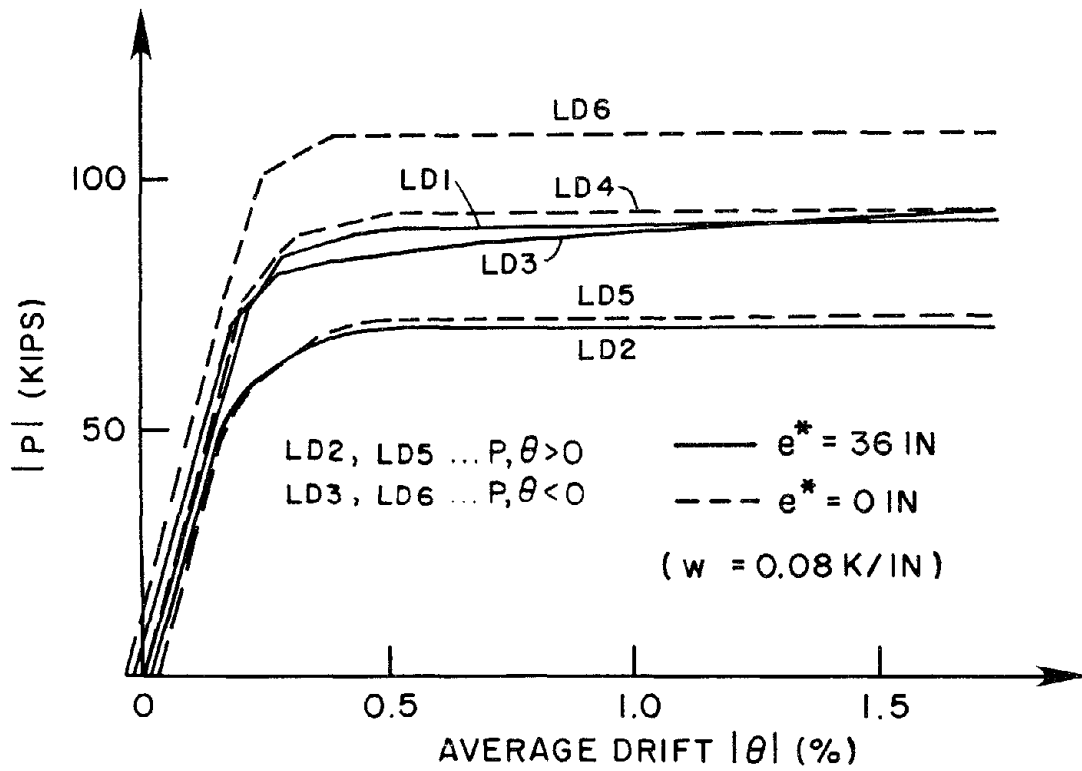
Fig. 4.6　　　　Load-Deflection Relationships for LD-frames.
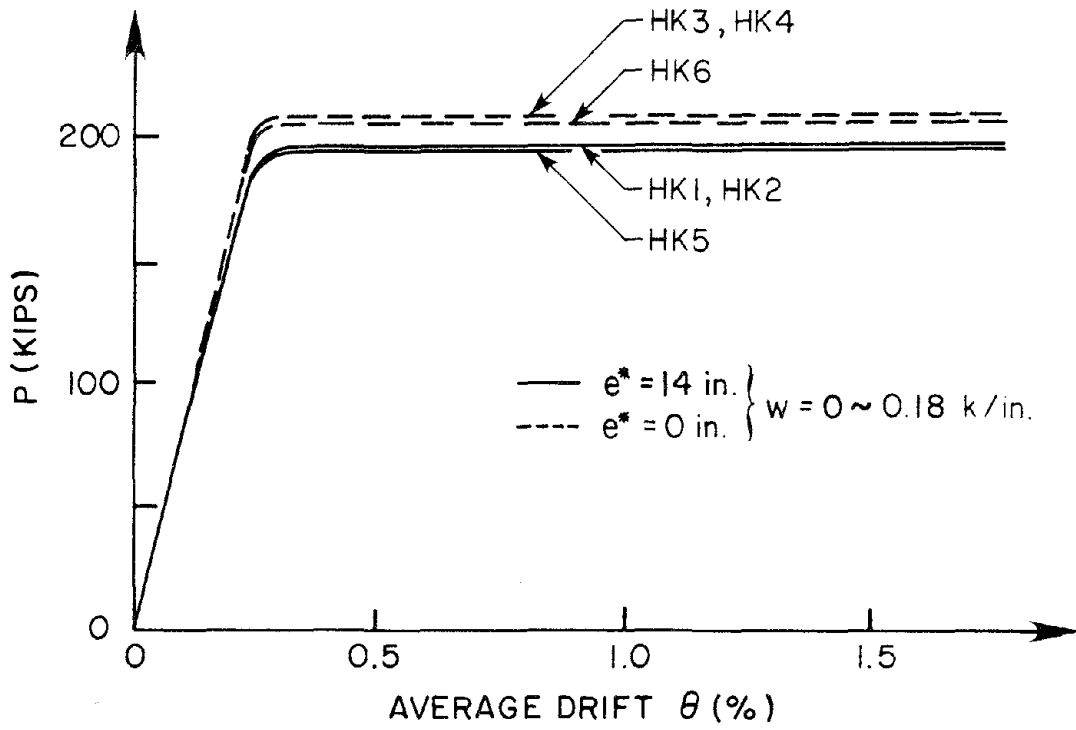
Fig. 4.7   Load-Deflection Relationships for HK-frames with $e^* \approx e/2$ and $e^* = 0$.
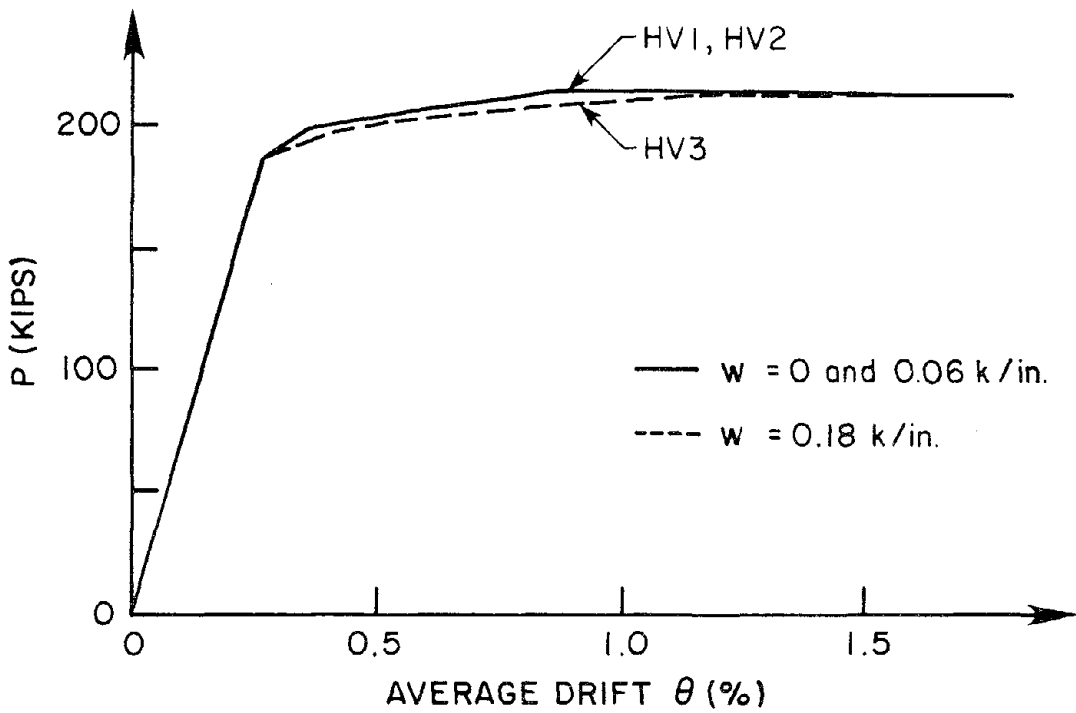
Fig. 4.8   Load-Deflection Relationships for HV-frames.
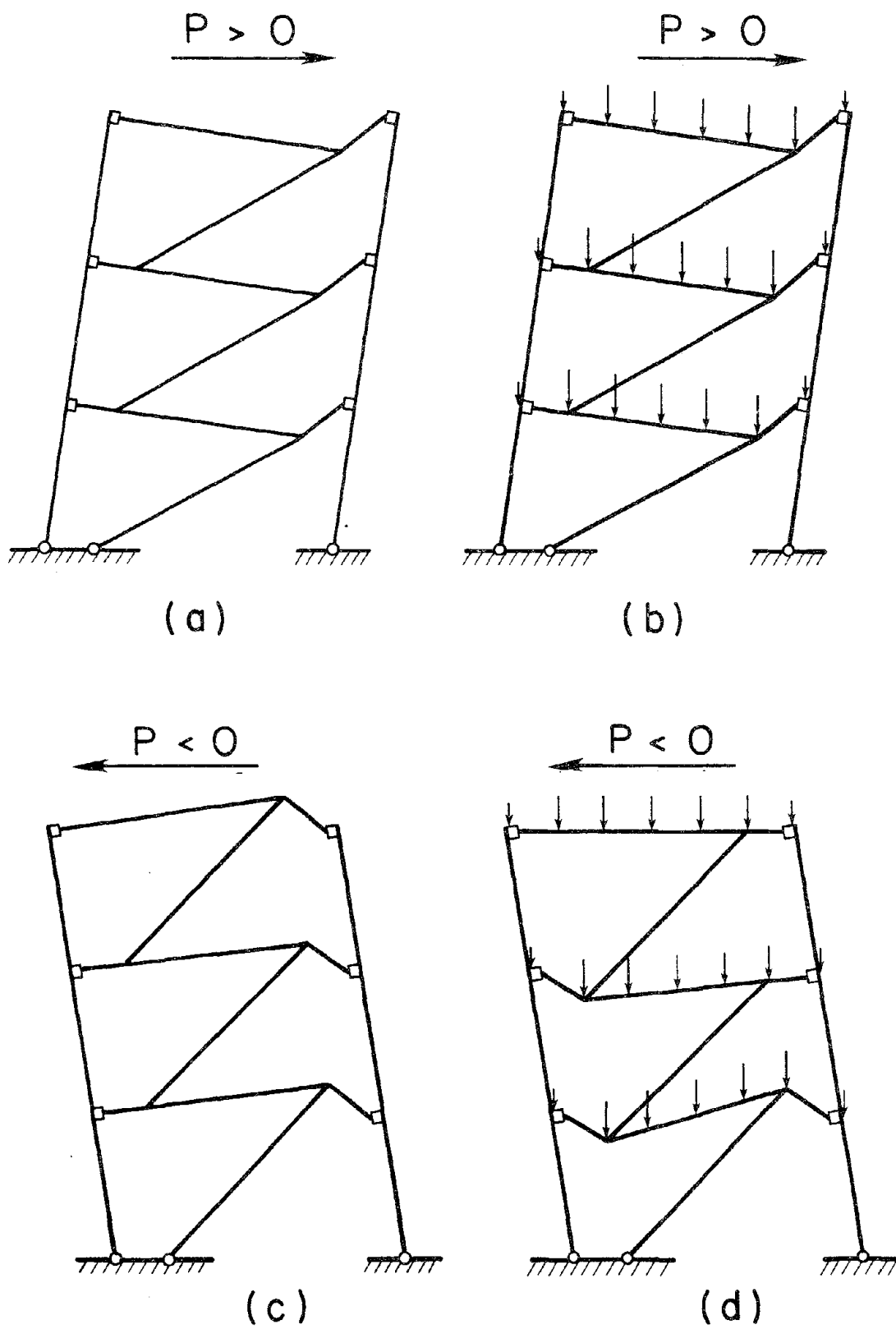
Fig. 4.9　　Mechanisms for a 3-story D-brace Frame with large e^*.
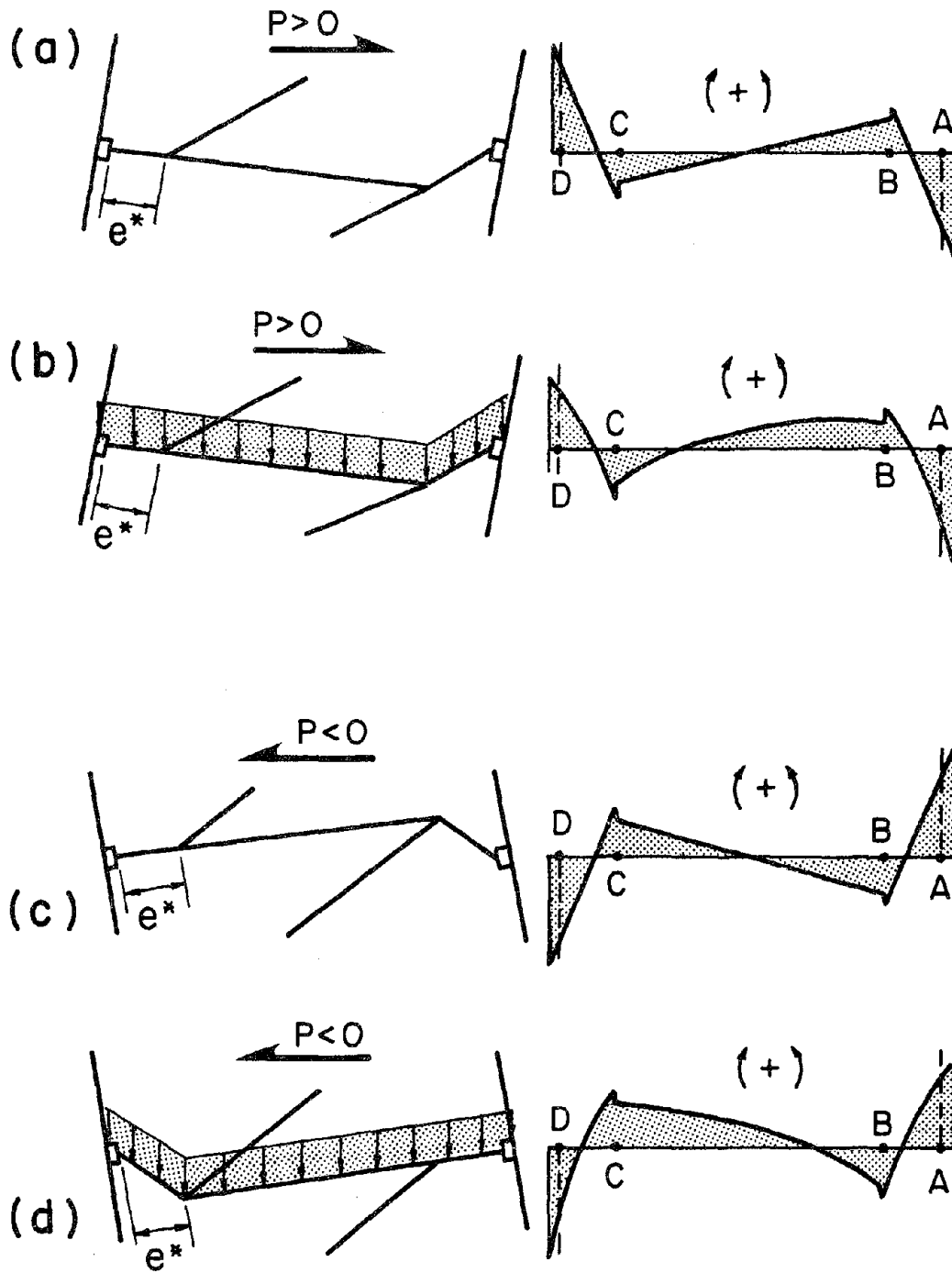
Fig. 4.10   Typical Behavior of Beams in a D-brace Frame with Large e^*.
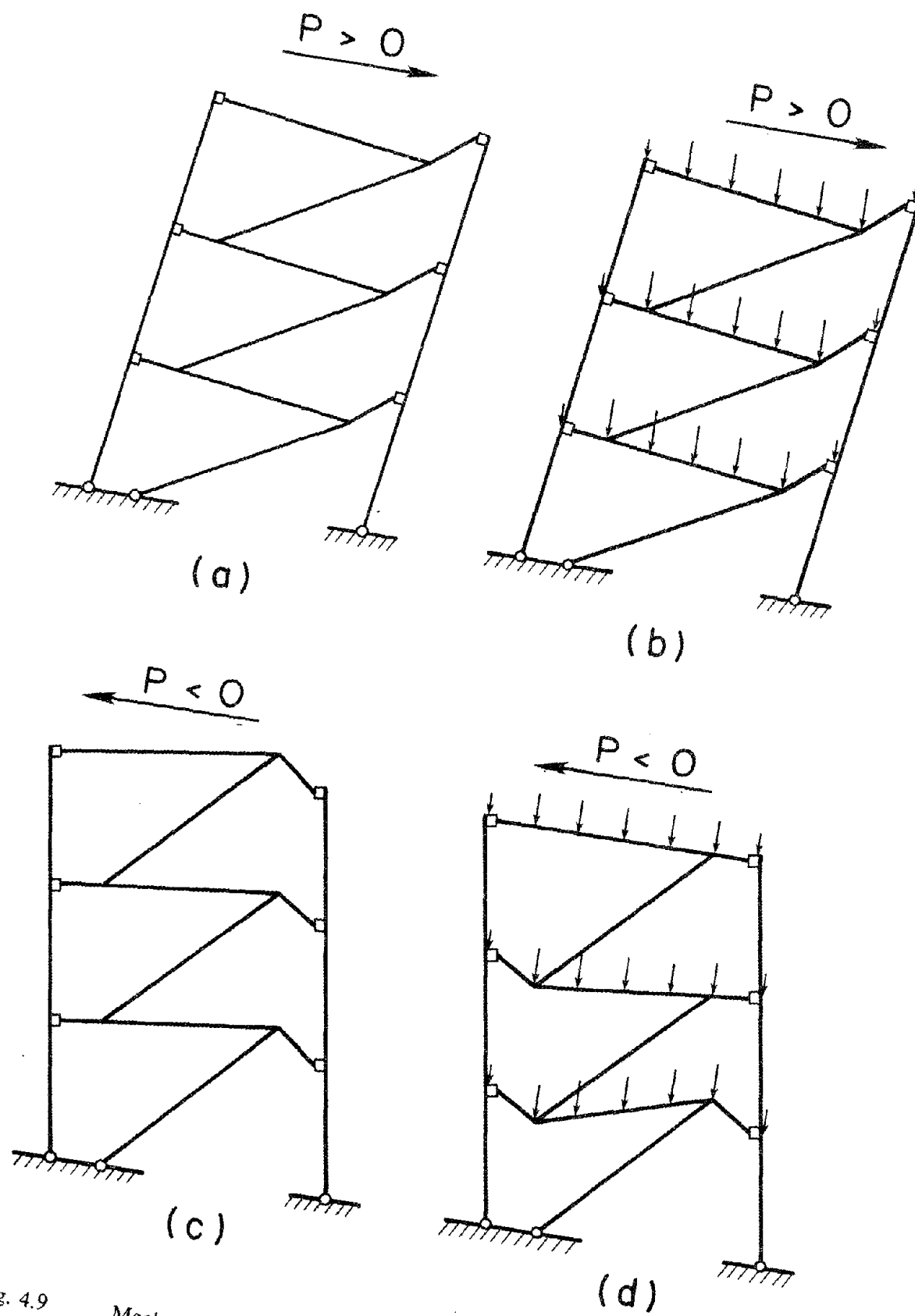
Fig. 4.9   Mechanisms for a 3-story D-brace Frame with large e^*.
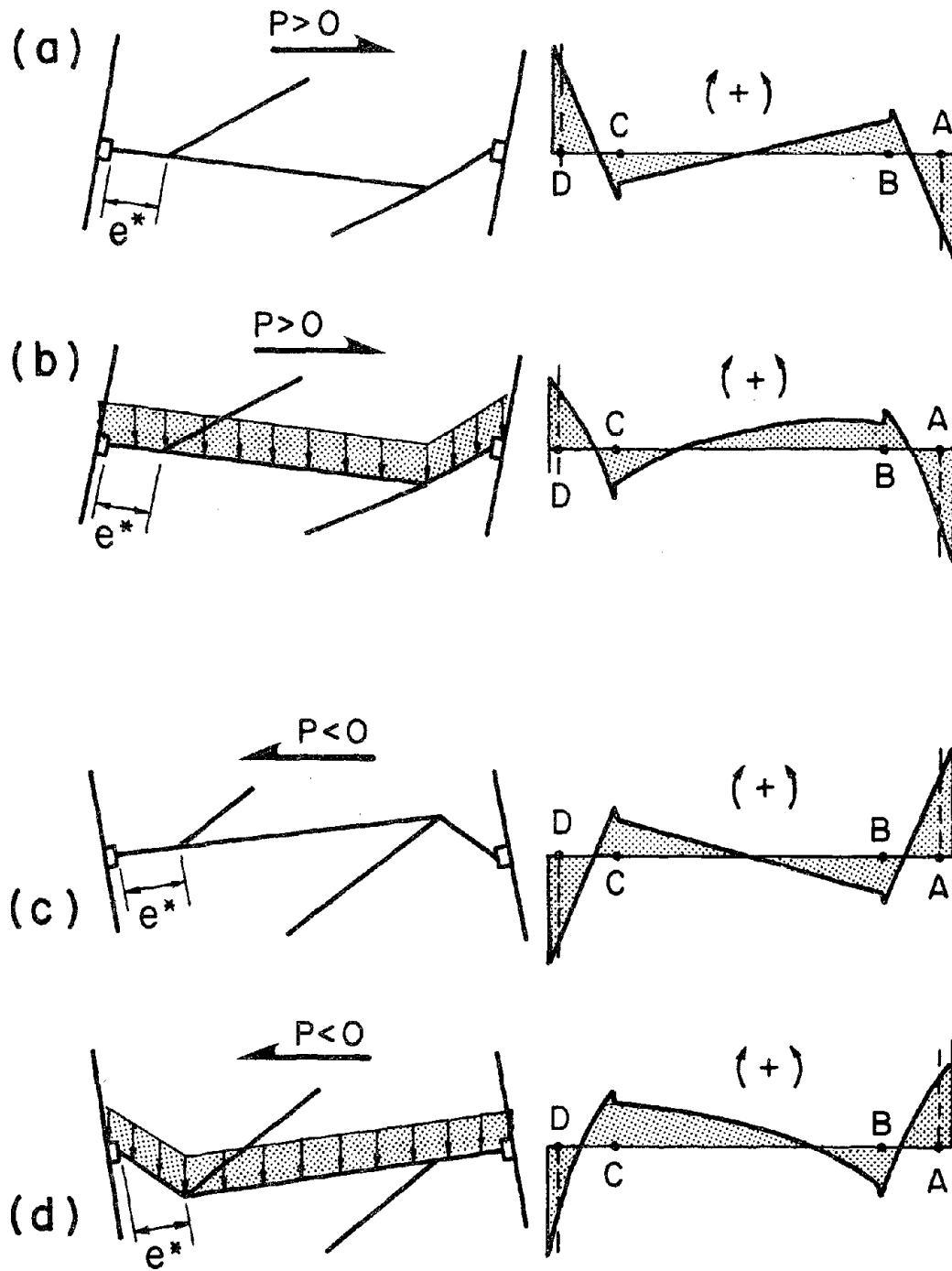
Fig. 4.10   Typical Behavior of Beams in a D-brace Frame with Large e^*.
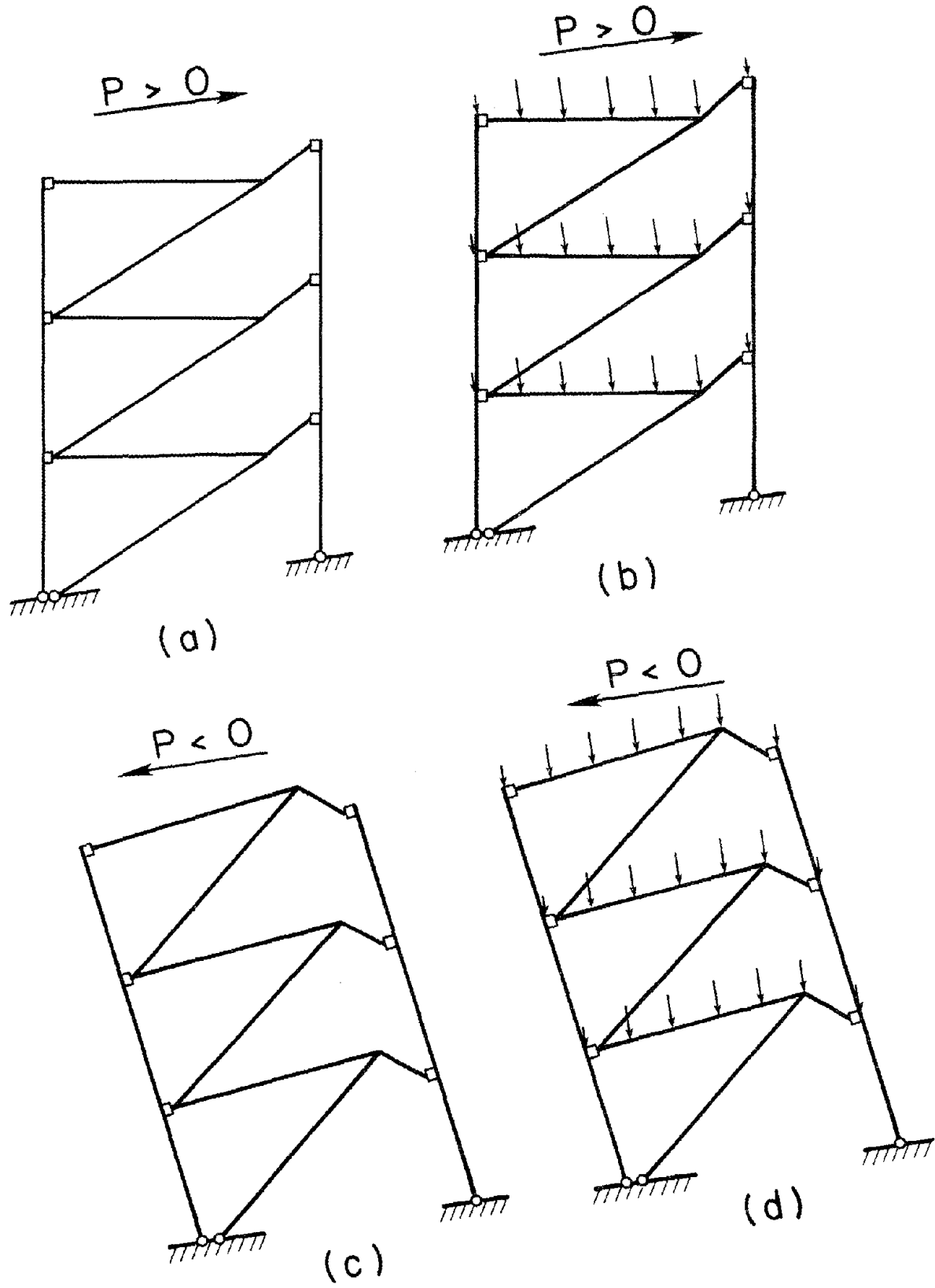
Fig. 4.11   Mechanisms for a 3-story D-brace Frame with $e^* = 0$.
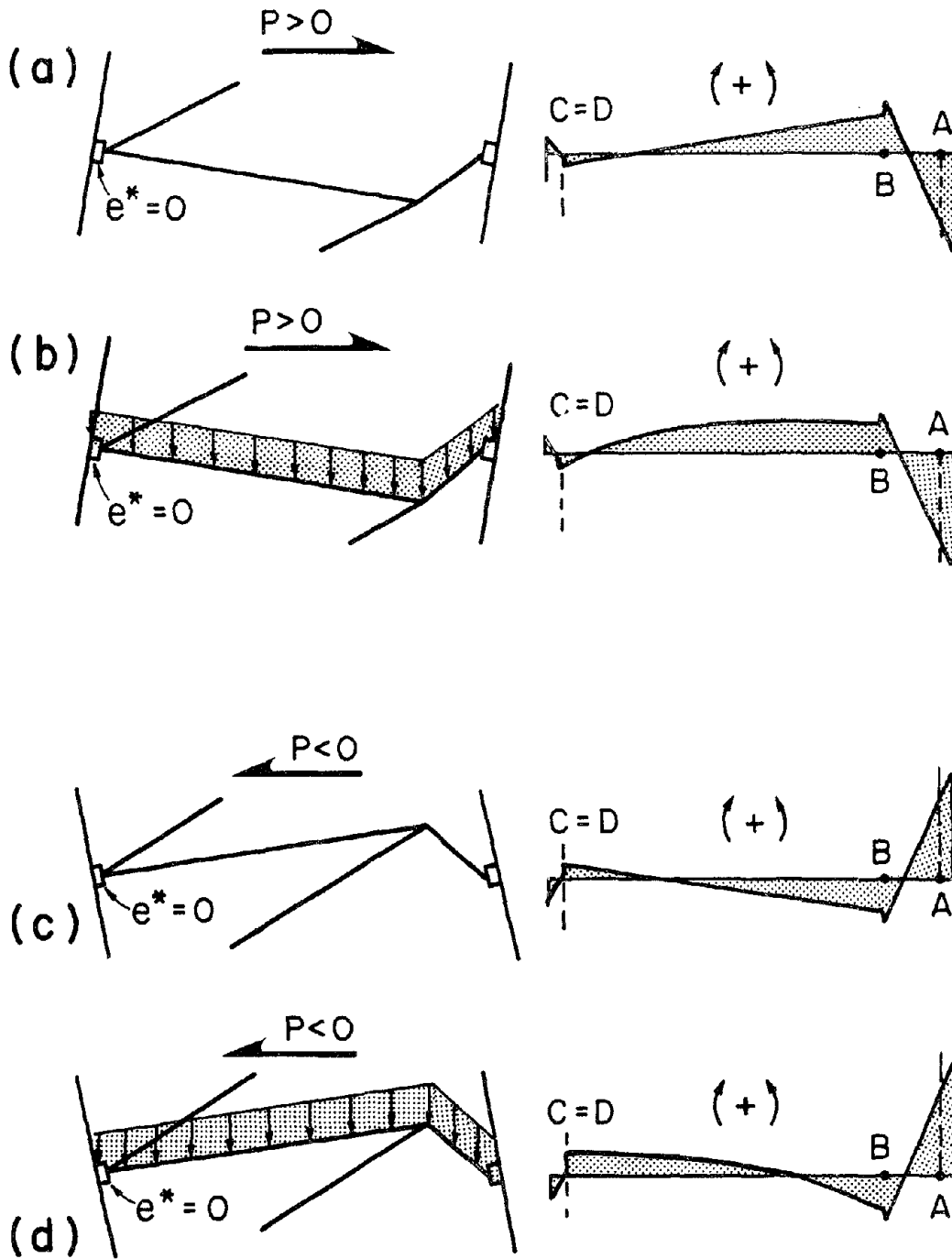
Fig. 4.12   Typical Behavior of Beams in a D-brace Frame with $e^* = 0$.

(a)

(b)
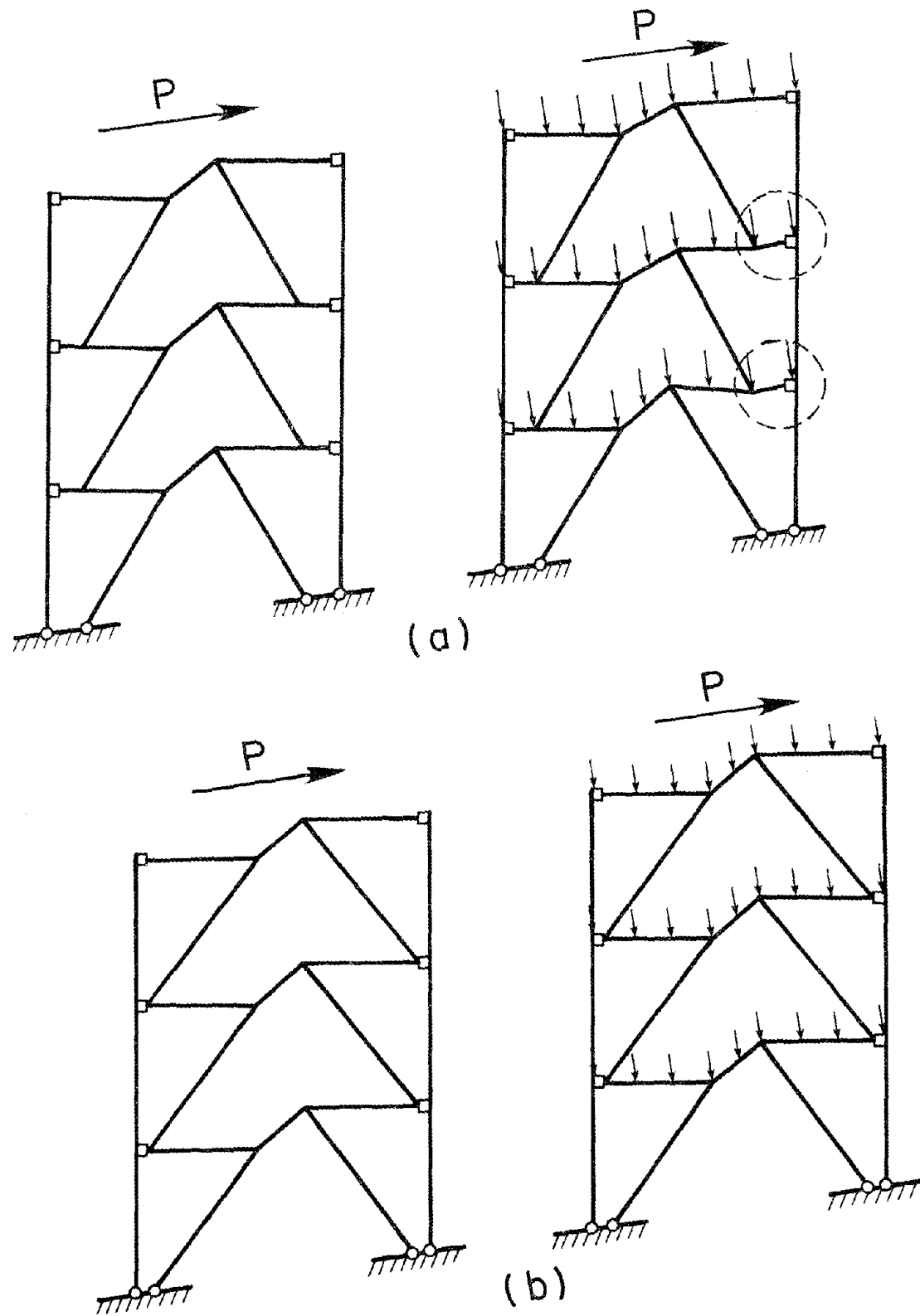
Fig. 4.13   Mechanisms for a 3-story K-brace Frame with (a) $e^* \approx e/2$, and (b) $e^* = 0$.
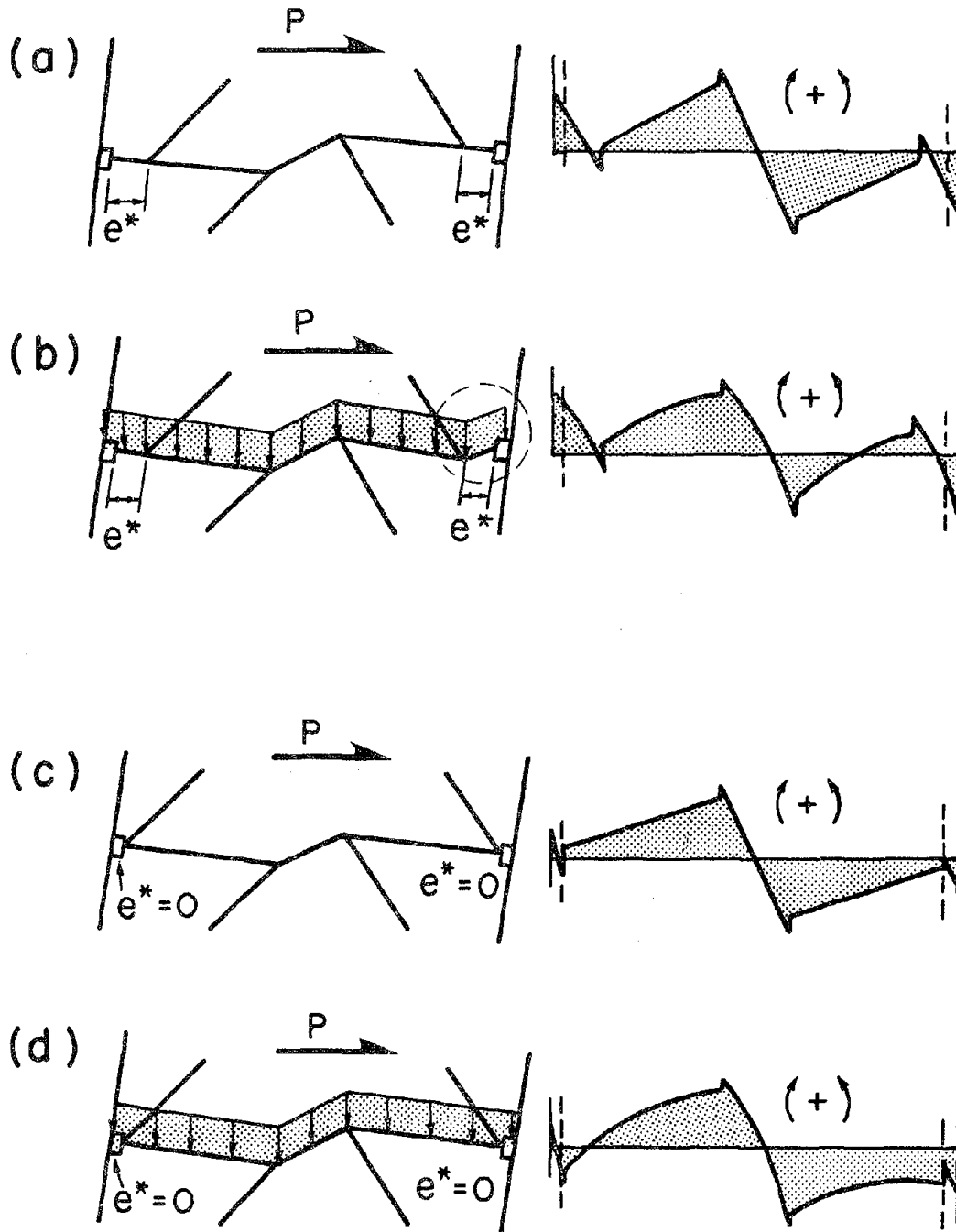
Fig. 4.14   Typical Behavior of Beams in a K-brace Frame with $e^* \approx e/2$, and 0.
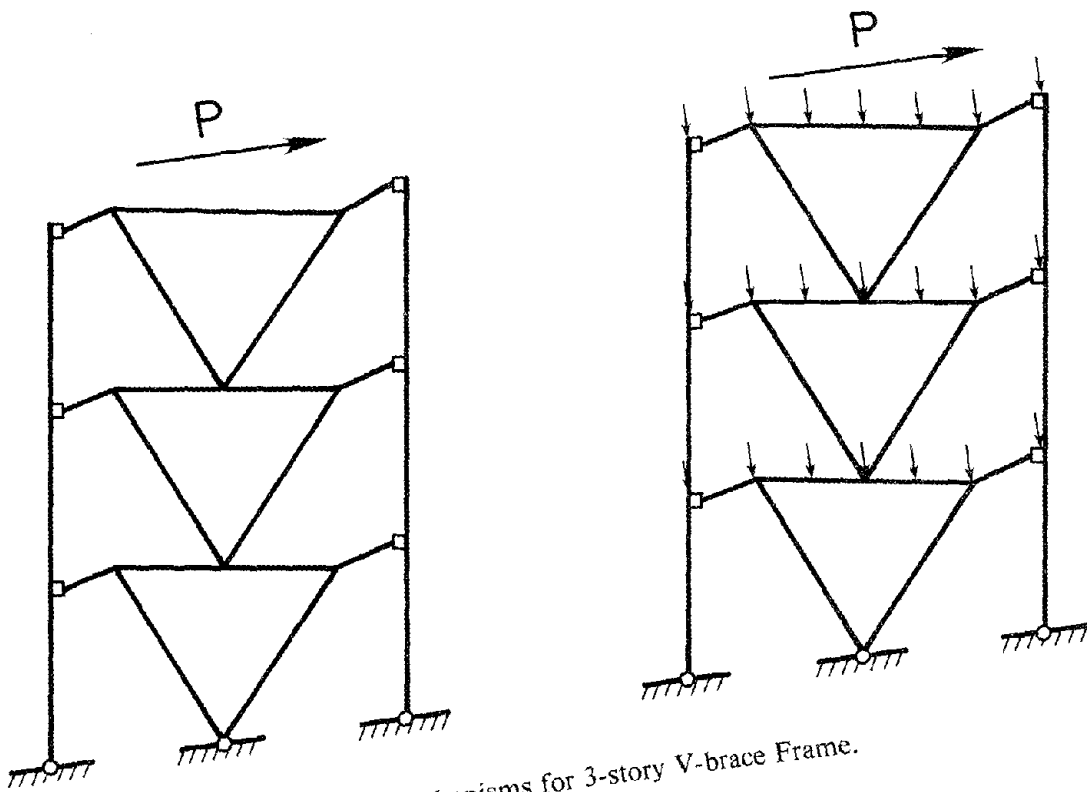
Fig. 4.15   Mechanisms for 3-story V-brace Frame.
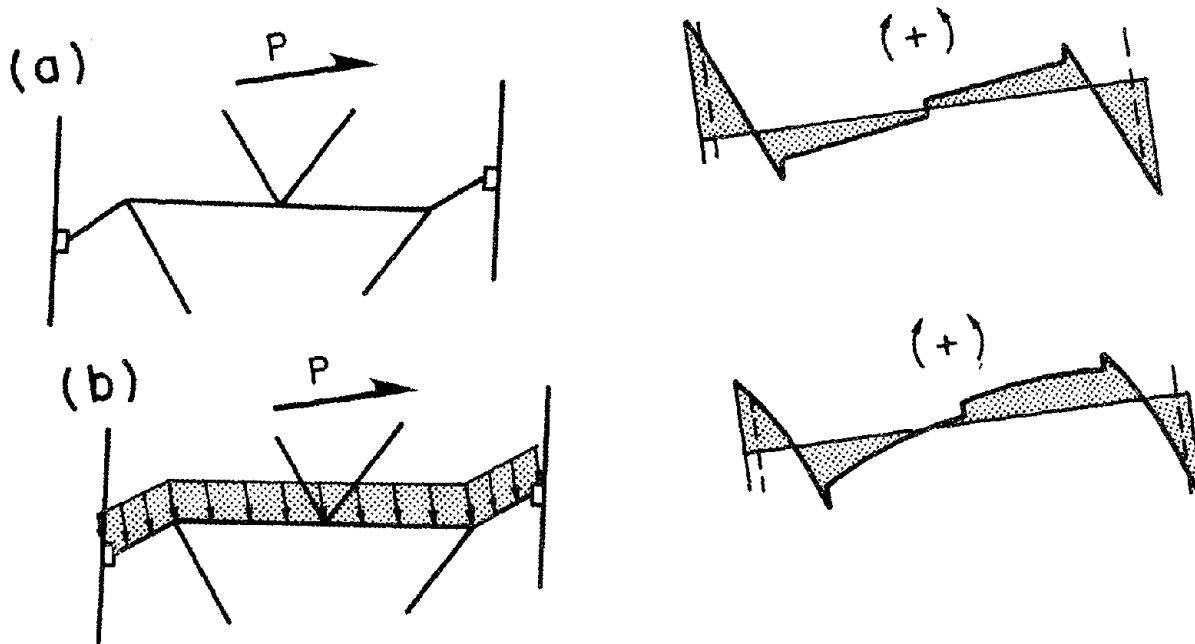
Fig. 4.16   Typical Behavior of Beams in a V-brace Frame.
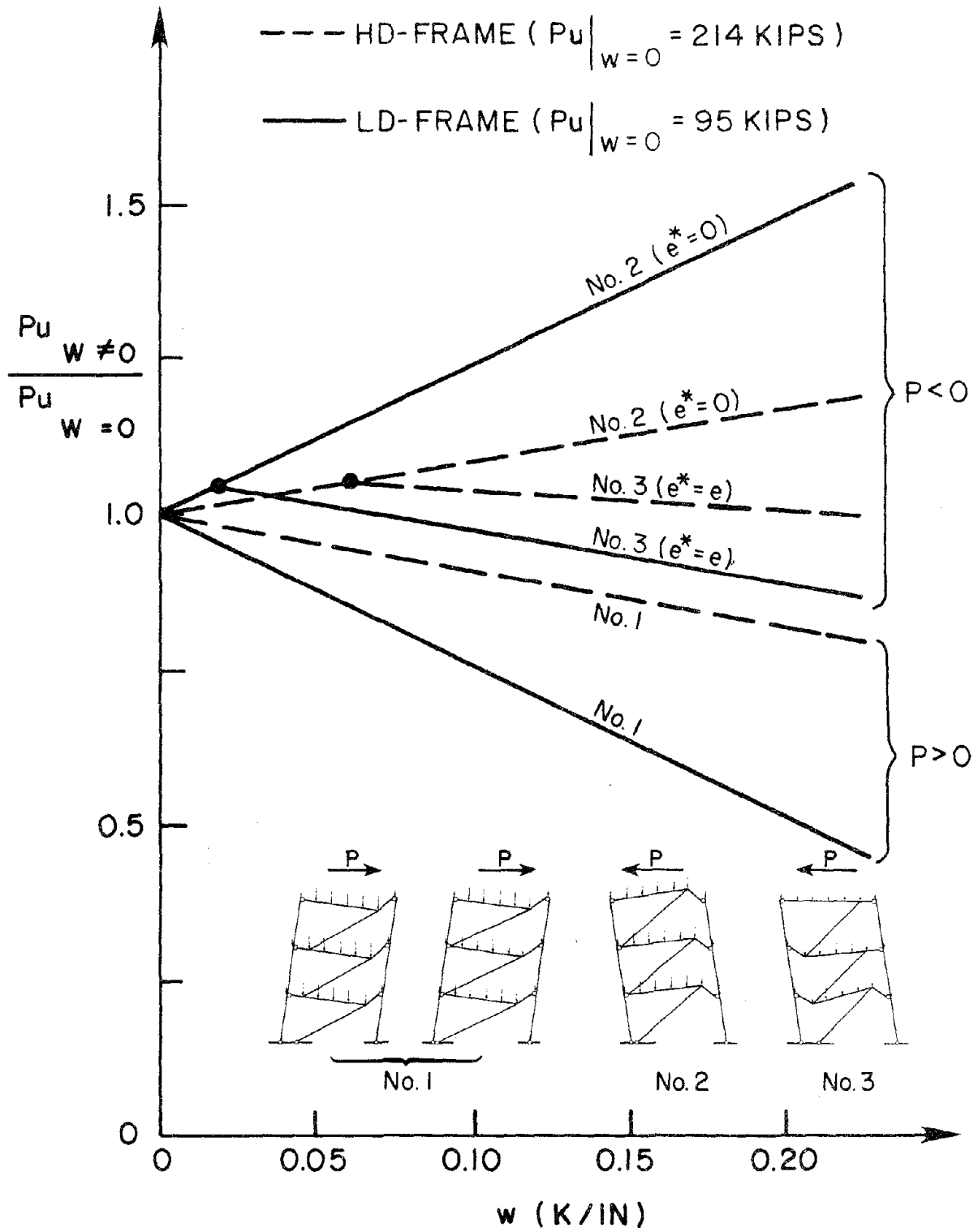
Fig. 4.17   Variation of Lateral Load Carrying Capacities and Mechanisms for 3-story
HD- and LD-frames Due to Vertical Load Magnitudes.

(a)

56 ξ

48 ξ

40 ξ

32 ξ

24 ξ

16 ξ

8 ξ

288"

144" Typ.

7" — 7"

e = 36"

e* = 36" or 0"

ξ F_i (kips)

V_base = 224 ξ (kips)

(b)

MECHANISM 1   2   3   4   5

-193-
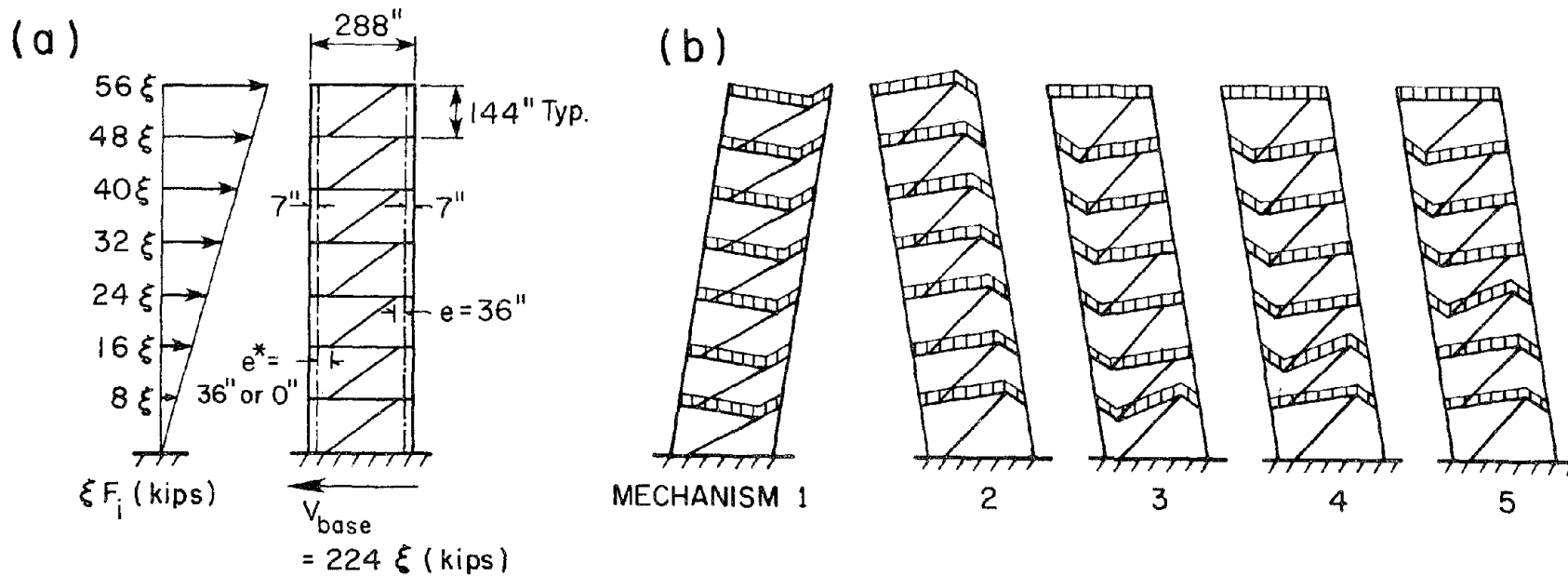
SOLUTION FOR e* = 0
SOLUTION FOR e* = e

$w(k/in)$	Mechanism		$w(k/in)$	Mechanism			
	1			2	3	4	5
0.00	$\xi = 1.0$		0	$\xi = -1.00$	$\xi = -1.19$	$\xi = -1.19$	$\xi = -1.15$
0.08	$\xi = 0.88$		0.08	$\xi = -1.12$	$\xi = -1.10$	$\xi = -1.13$	$\xi = -1.14$
0.16	$\xi = 0.76$		0.16	$\xi = -1.24$	$\xi = -1.01$	$\xi = -1.07$	$\xi = -1.13$

Fig. 4.18   Variation of Lateral Load Carrying Capacities and Mechanisms for 7-story D- brace Frames Due to Vertical Loads.
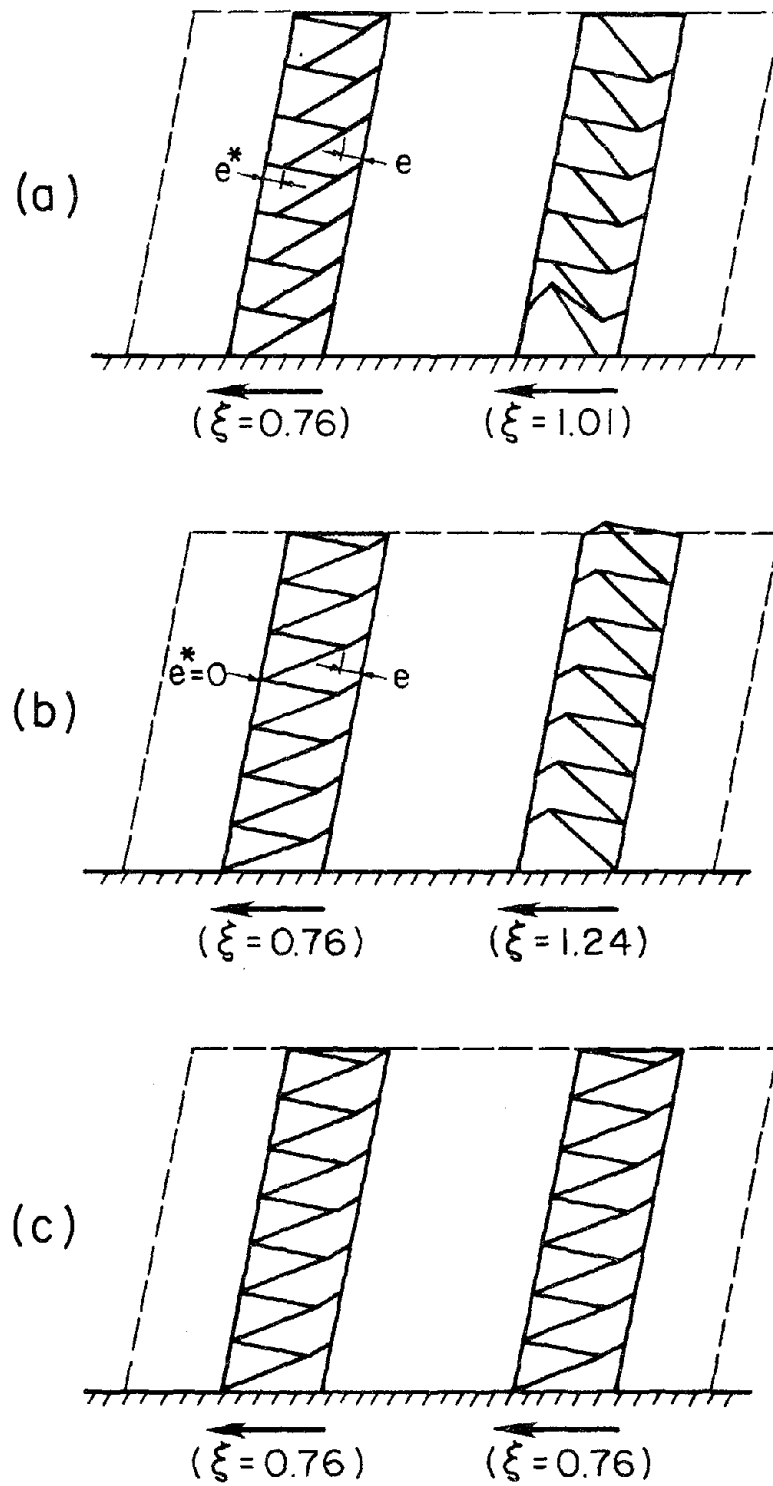
Fig. 4.19　Some D-brace Frame Arrangements and Variations in Plastic Capacities Due to Vertical Loads.
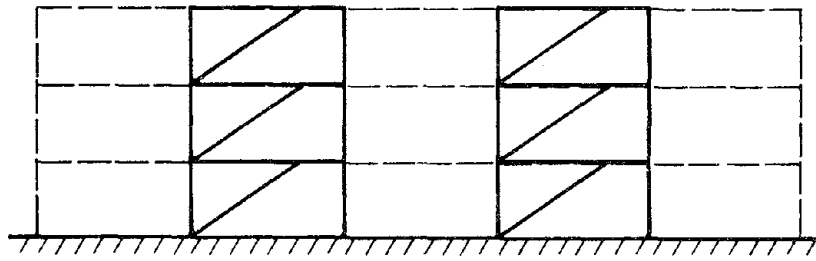
(a)
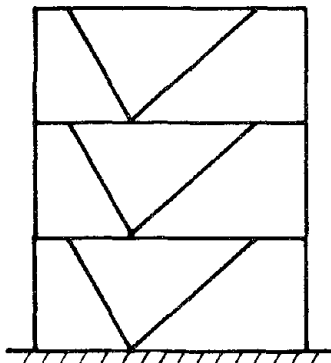
(b)
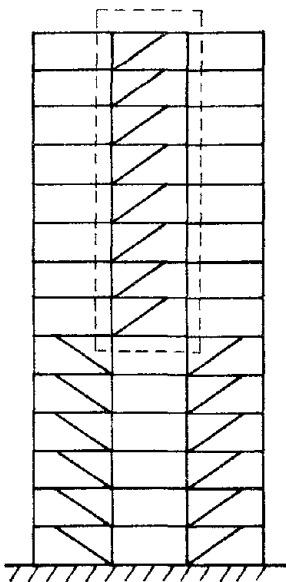
(c)
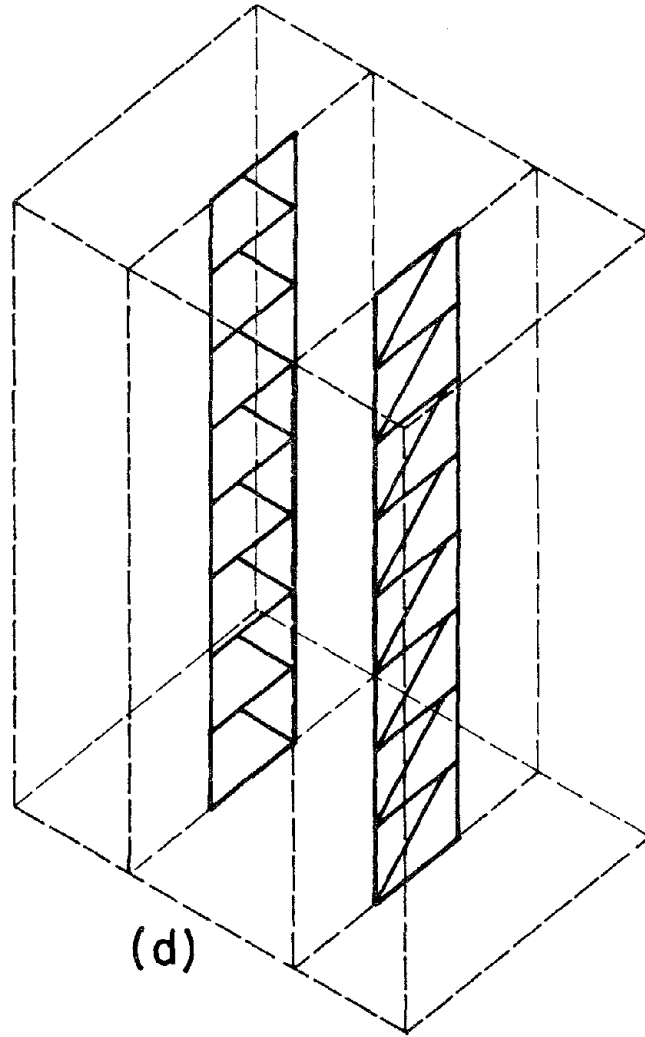
(d)

Fig. 4.20   Some Undesirable Configurations and Arrangements
for EBFs with Large Vertical Loads.
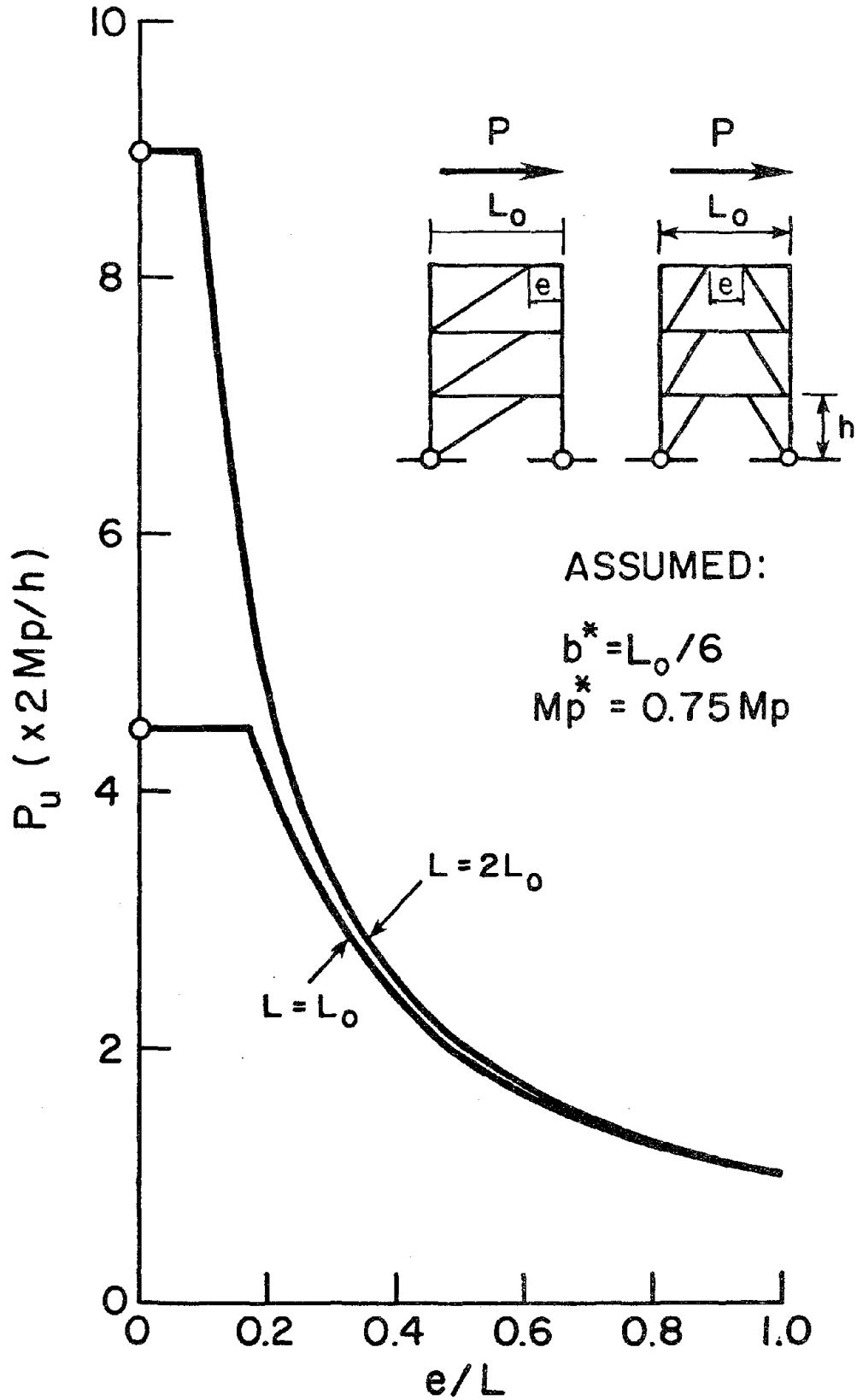
Fig. 4.21   Variation of Frame Plastic Capacity as a Function of Link Length e.
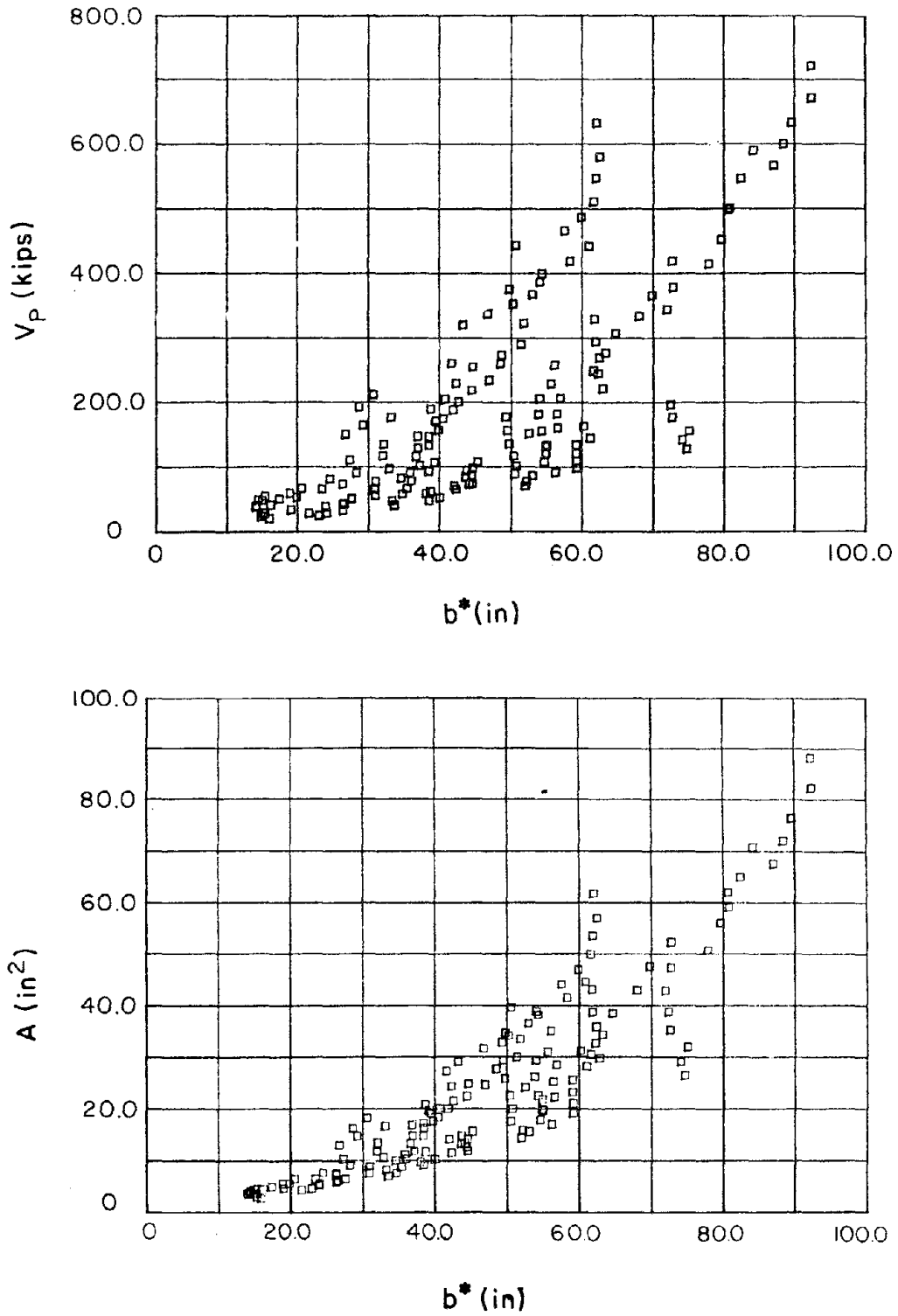
Fig. 4.22   Trends of Section Properties for Standard Steel Sections.

71 KIPS

110
146
181
214
244
273
299
324
346
367
385
401
415
428
438
446
452
456
458 KIPS

PLASTIC DESIGN
STORY SHEAR

288"

20TH
FLOOR

144"
TYP

15TH

10TH

5TH
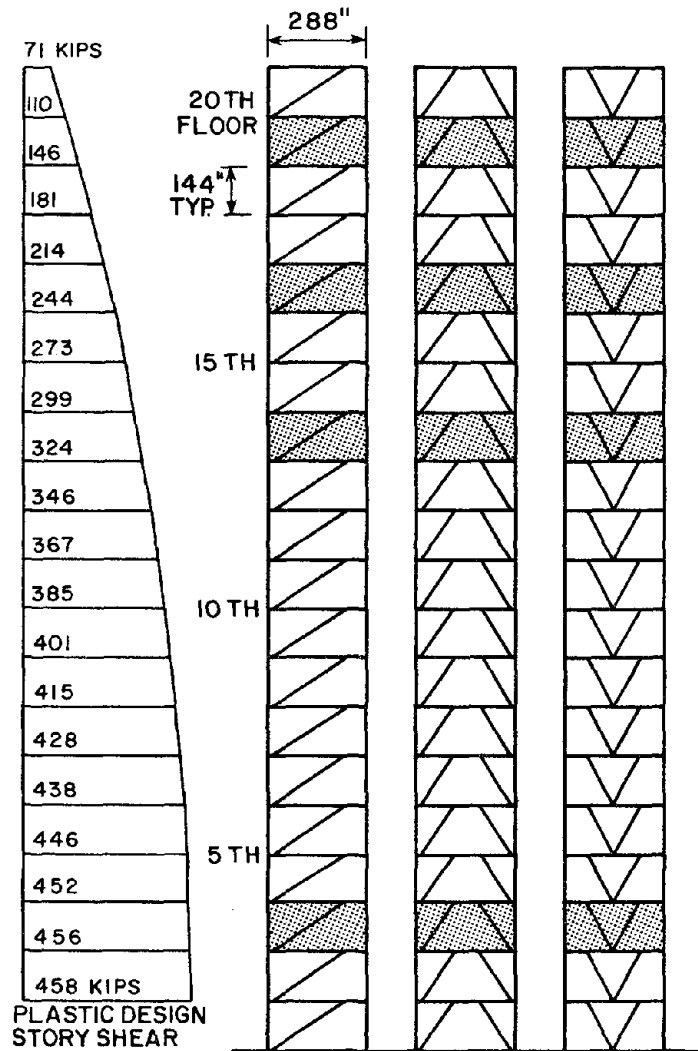
Fig. 4.23   Plastic Design of 20-story EBFs.

UBC LIMIT EQUIV.

———— D- BRACE
— — — K- BRACE
- - - - - V- BRACE

3rd STORY PANEL

19th STORY PANEL

SHEAR DRIFT ($\times 10^{-2}$)

0.5
0.4
0.3
0.2
0.1
0

0   0.1   0.2

ECCENTRICITY RATIO
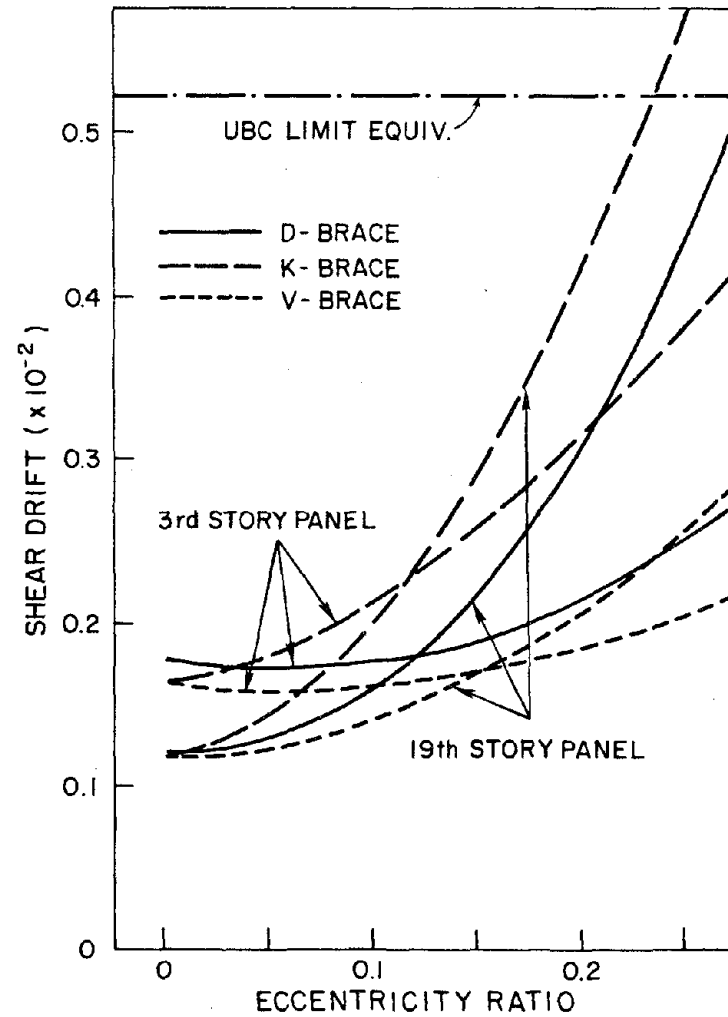
Fig. 4.24   Dependence of EBF Elastic Stiffness
on Basic Parameters.
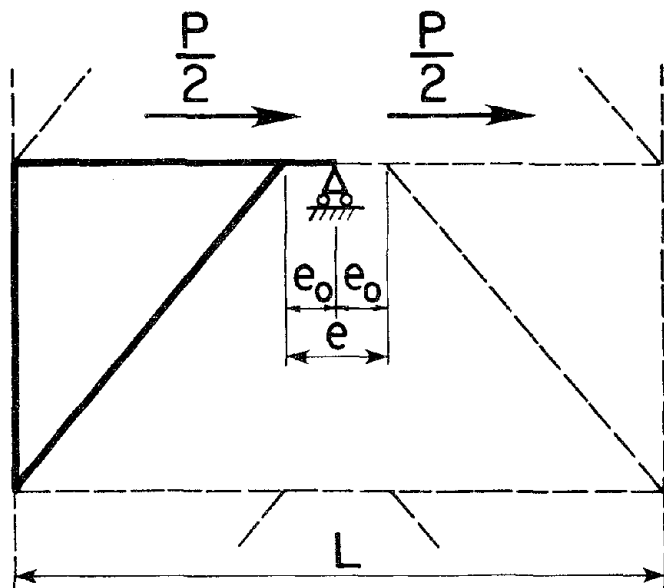
(a) K - brace Frame
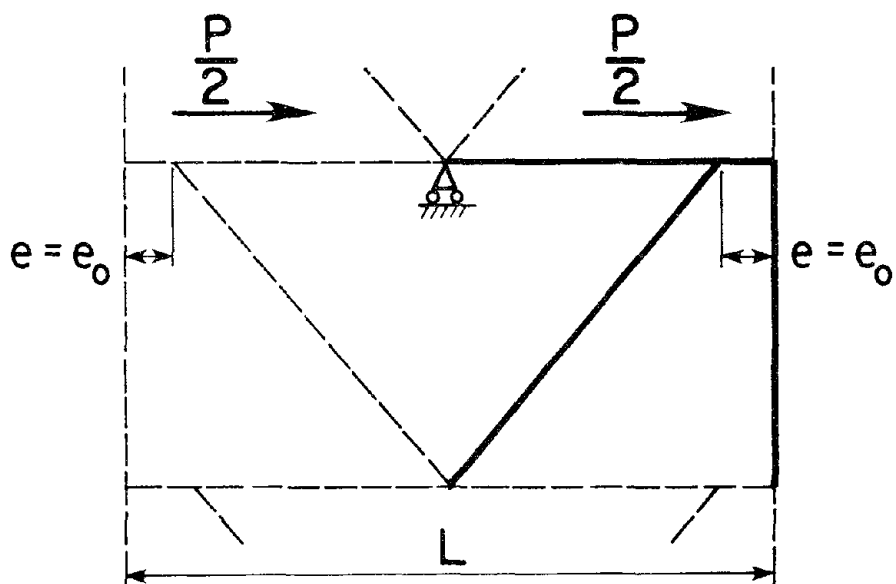
(b) V - brace Frame

Fig. 4.25   Comparison of Elastic Stiffness Characteristics for K- and V-brace Frames with Same Eccentricity Ratio.
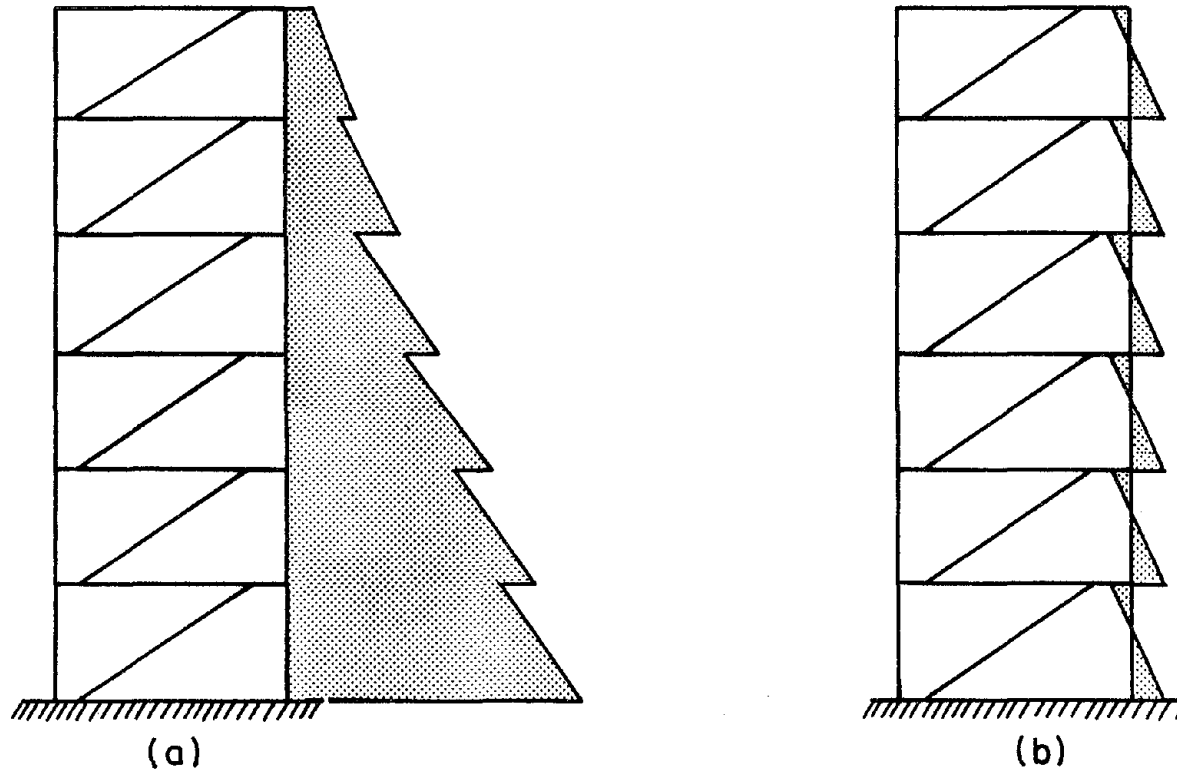
Fig. 5.1   Estimates of Statically Admissible Member Forces from
(a) Previous, and (b) Proposed Plastic Design Methods.
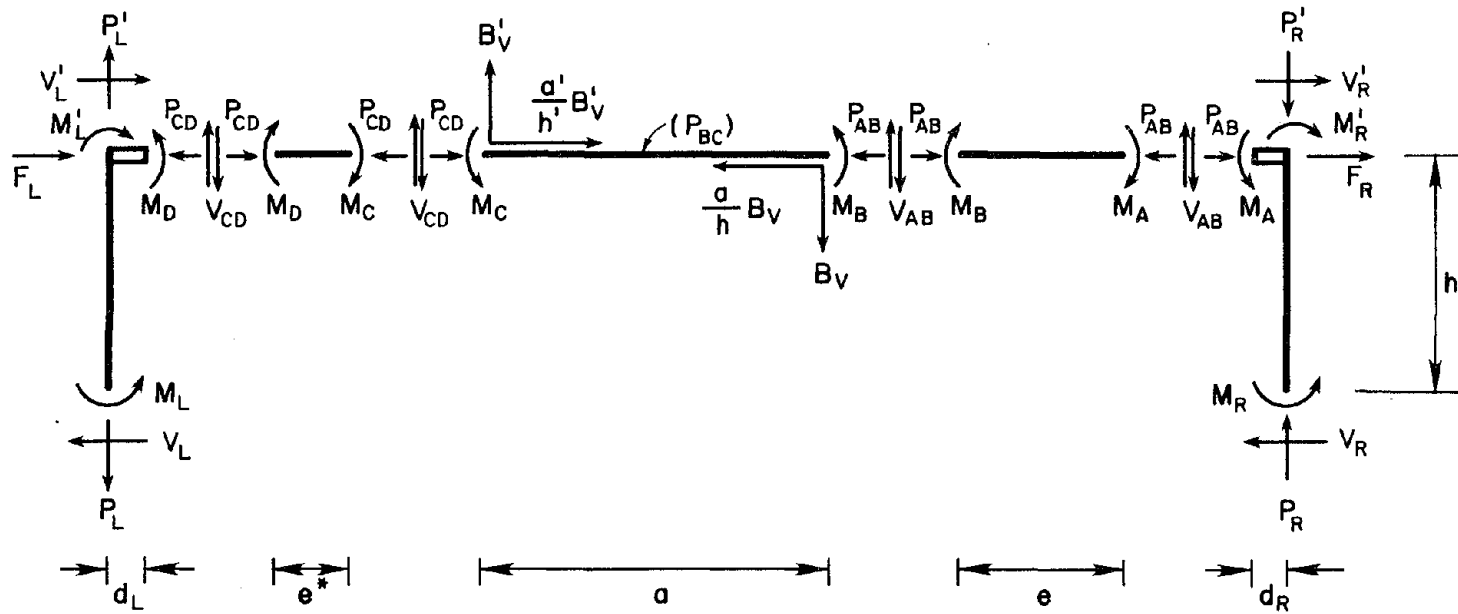
Fig. 5.2 Free-Body Diagram for a D-brace Frame used for Proposed Design Method.
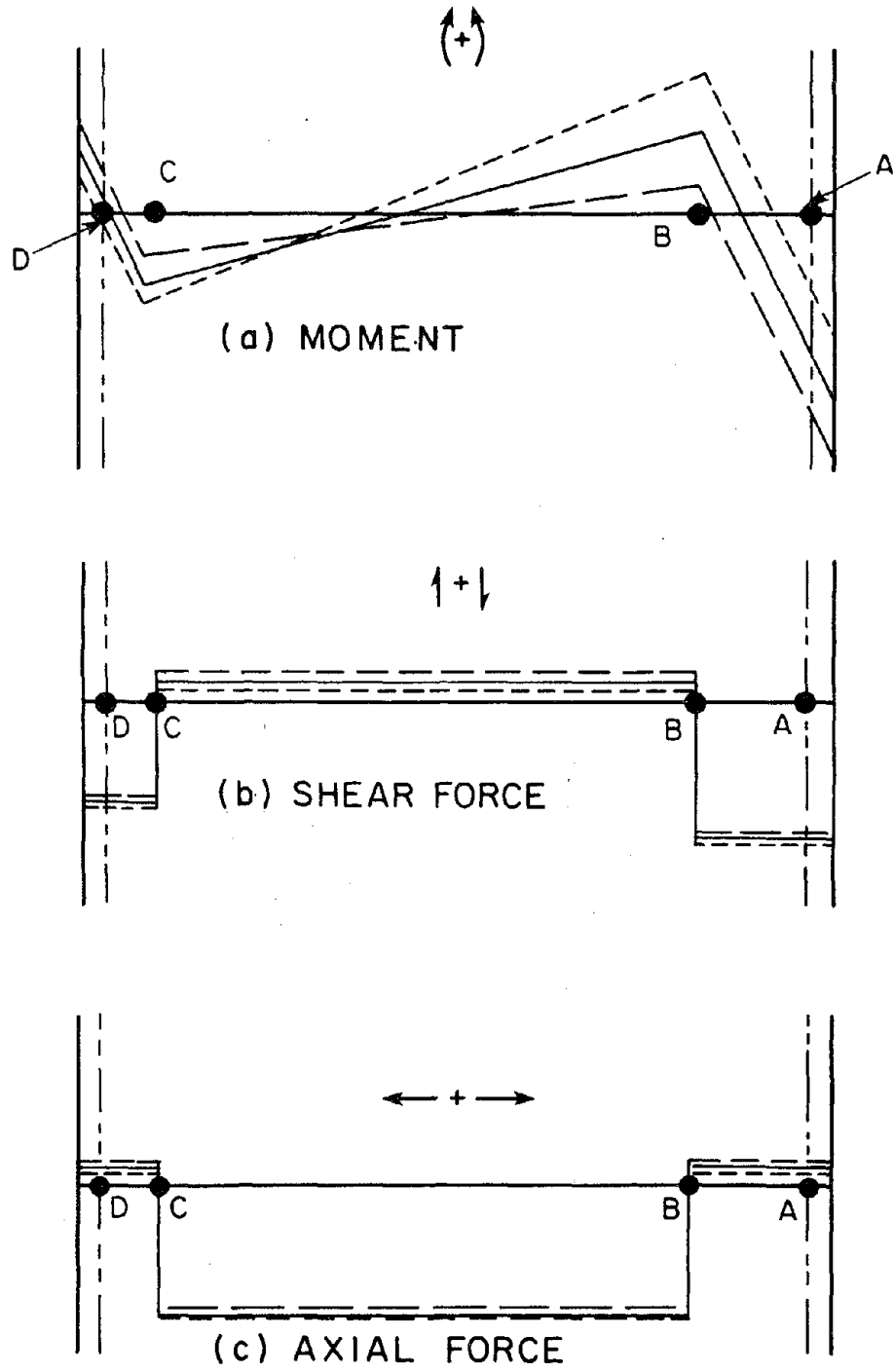
Fig. 5.3   Examples of Variations in Beam and Link Forces During Iterations.
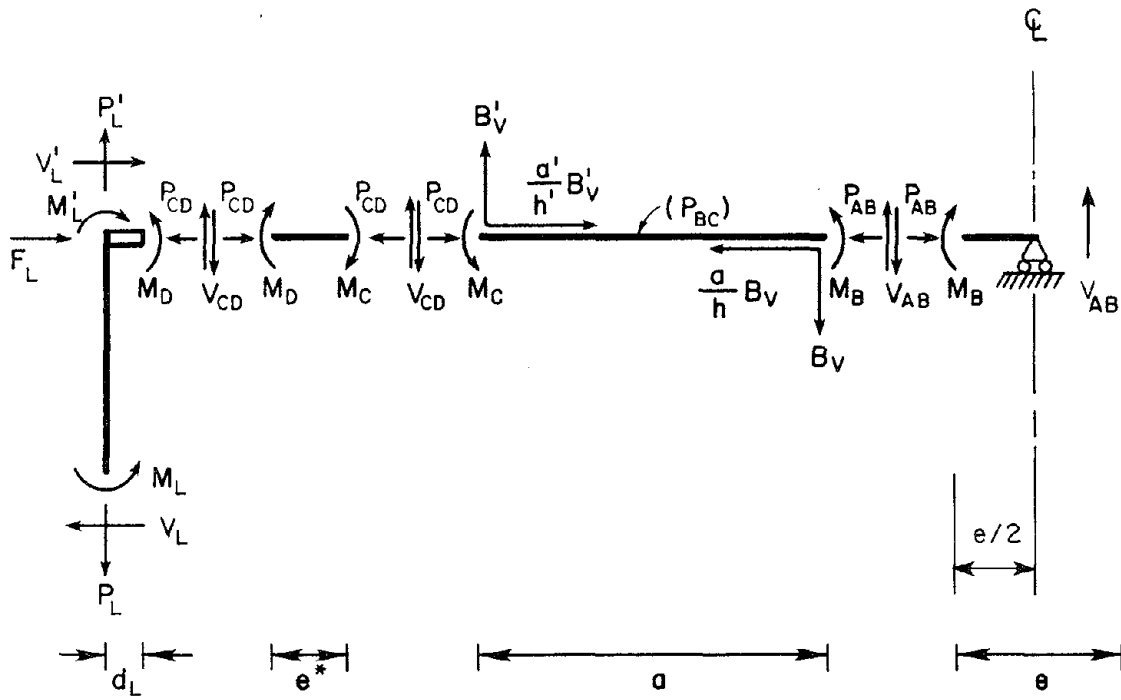
Fig. 5.4   Free-Body Diagram for a K-brace Frame used for Proposed Design Method.
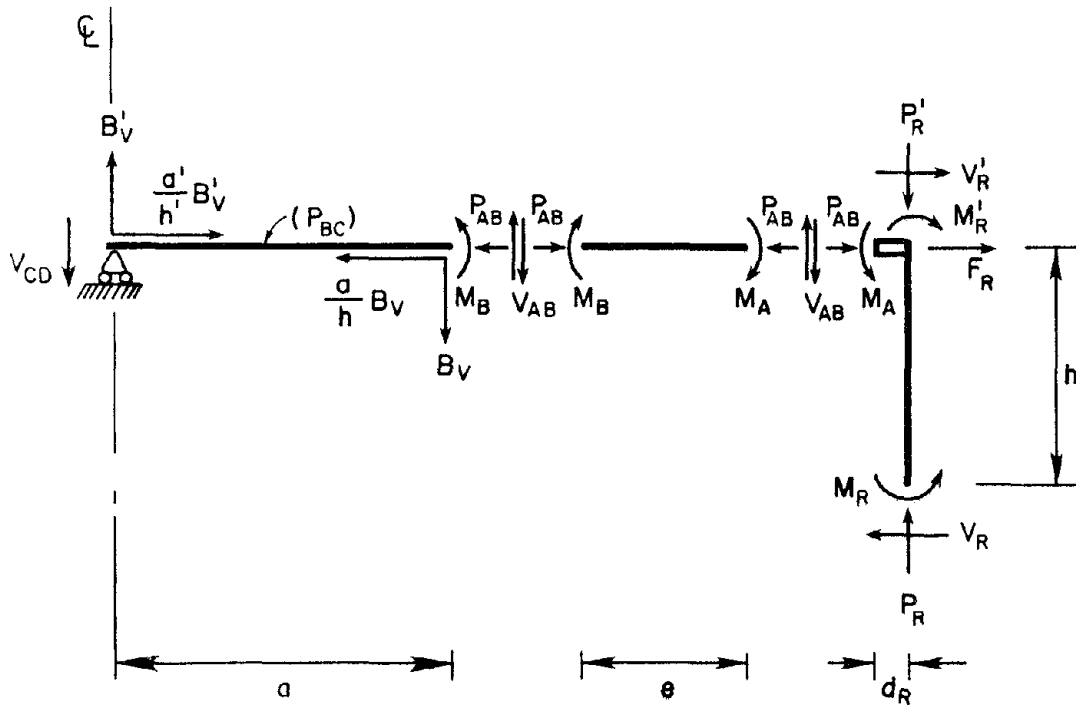
Fig. 5.5   Free-Body Diagram for a V-brace Frame used for Proposed Design Method.
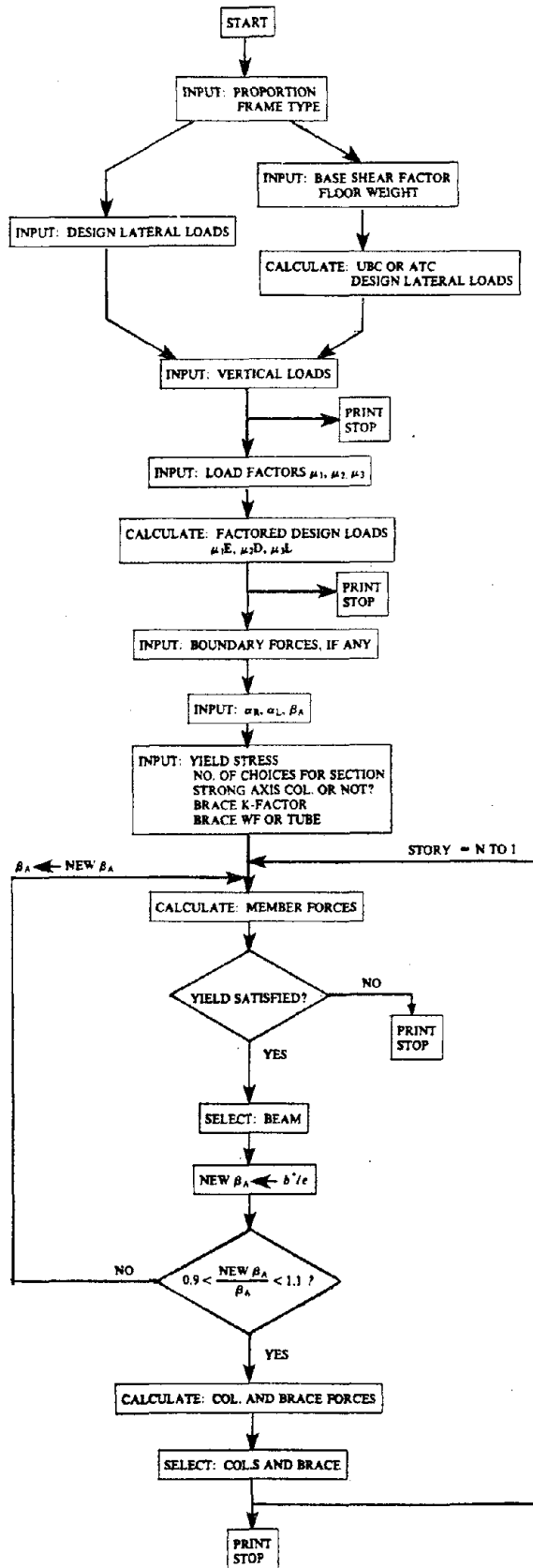
Fig. 5.6   Flow Chart of EBF Design Computer Program.
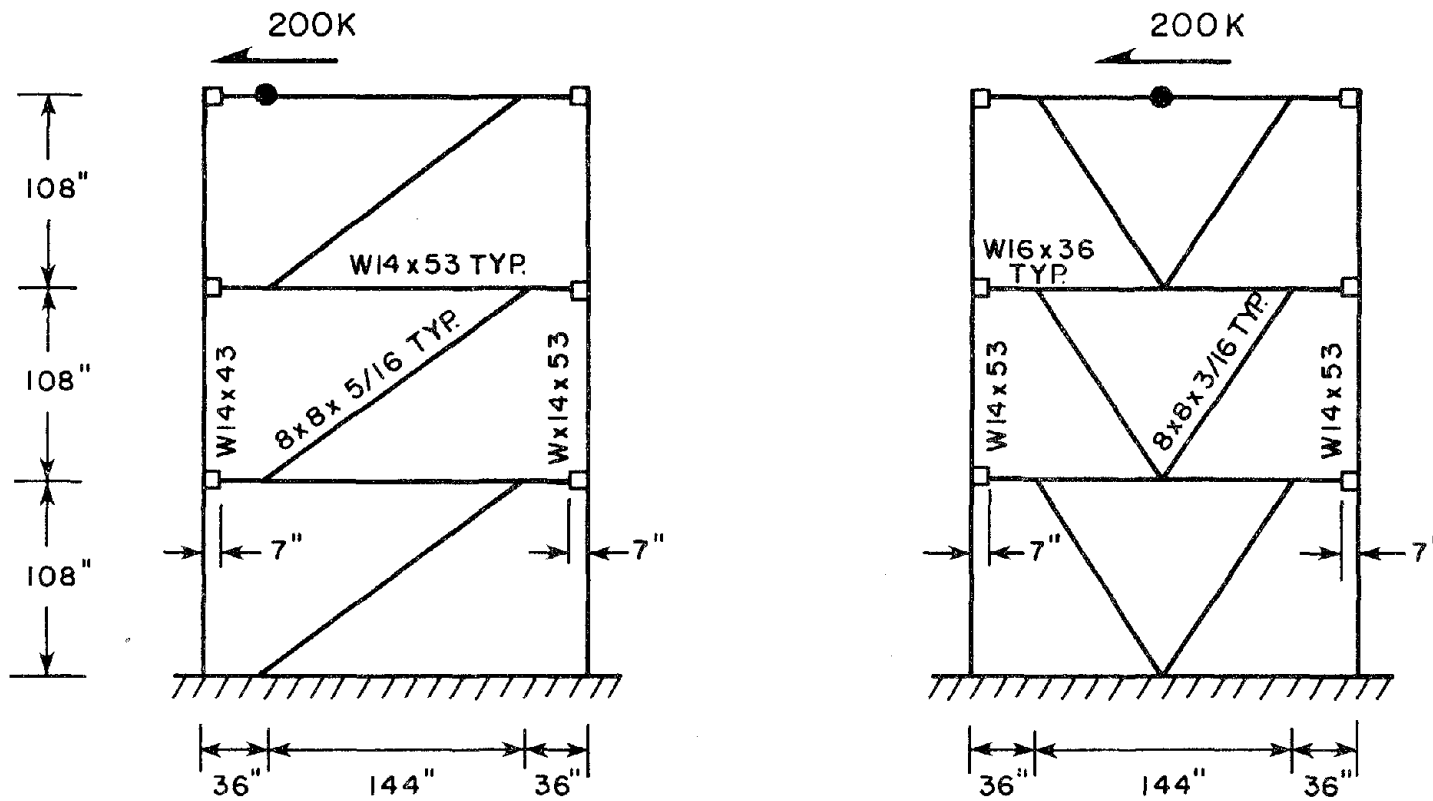
Fig. 5.7   Proportions and Member Sections for EBFs.

MOMENT (k-ft.)   AXIAL FORCE (kips)
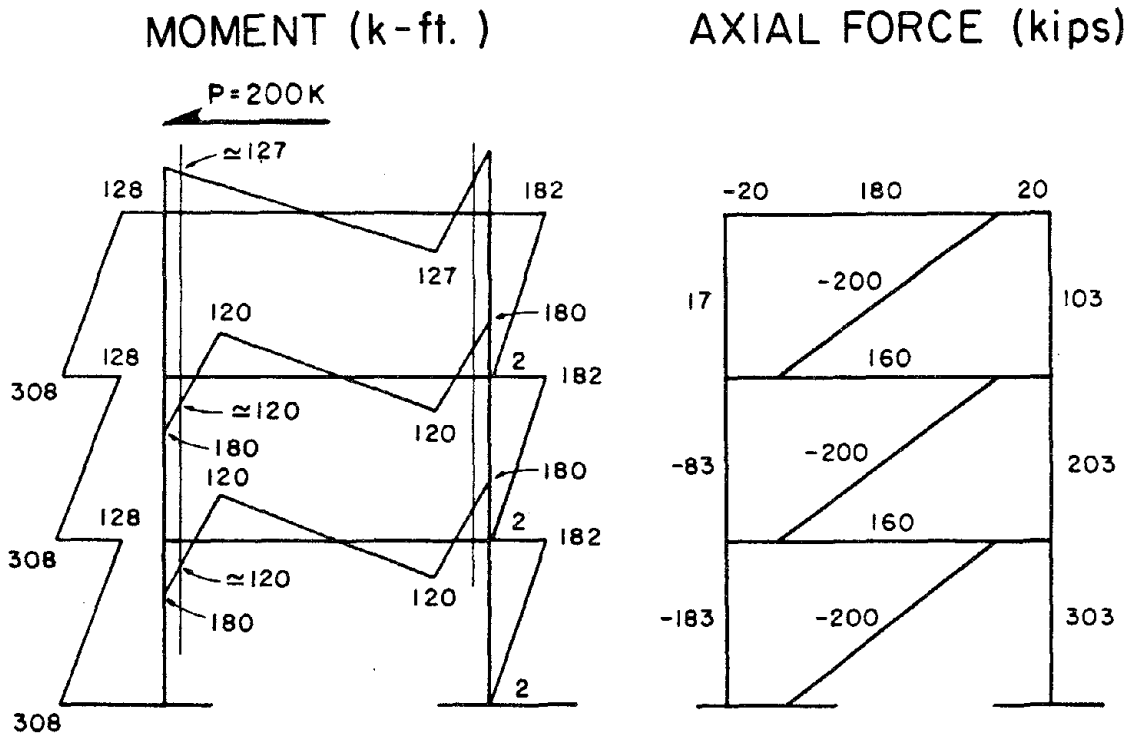
(a) MOMENT BALANCING METHOD
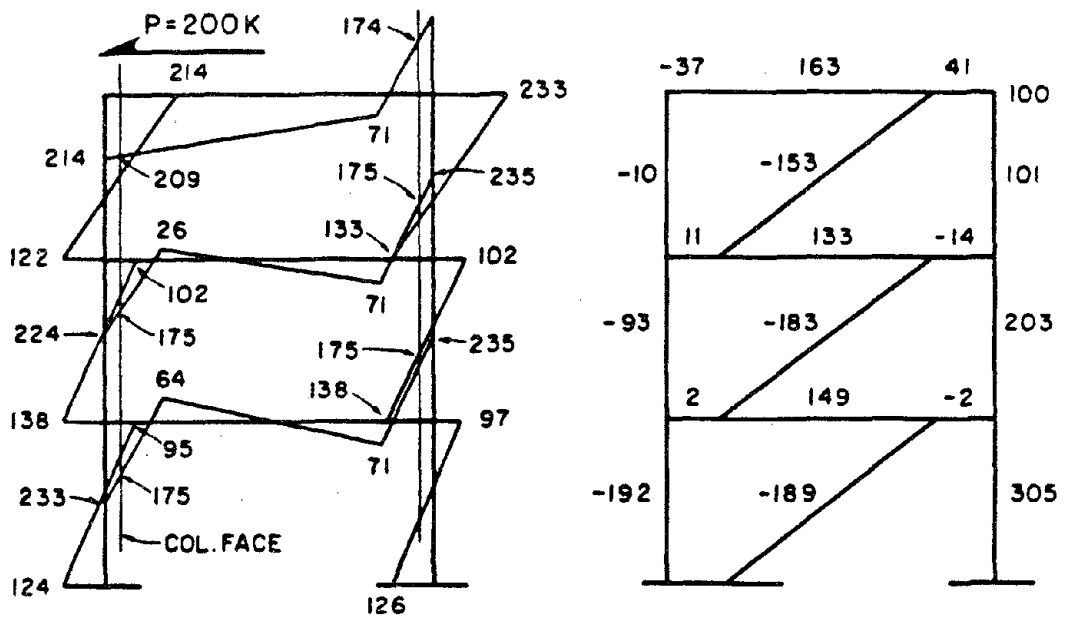
(b) PROPOSED METHOD

Fig. 5.8   Comparison of Member Force Estimates Between (a) Plastic Moment Balancing Method, and (b) Proposed Method.
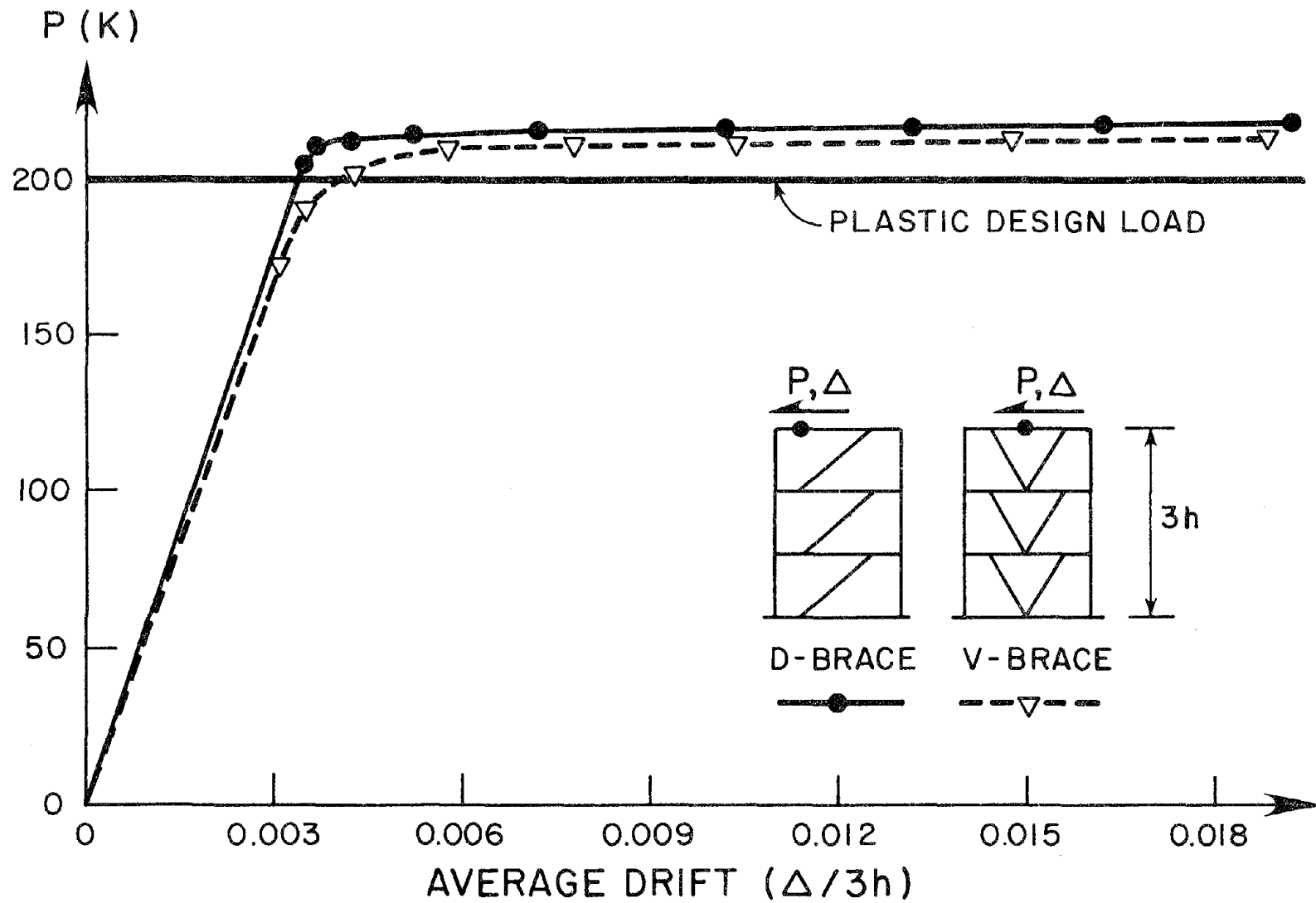
Fig. 5.9   Load-Deflection Behaviors of Plastically Designed EBFs.

(1)

F = 205.5 k
θ = 0.35 %

(2)

F = 213.1 k
θ = 0.52 %

(3)

F = 214.9 k
θ = 0.72 %

(4)

F = 218.0 k
θ = 1.62%
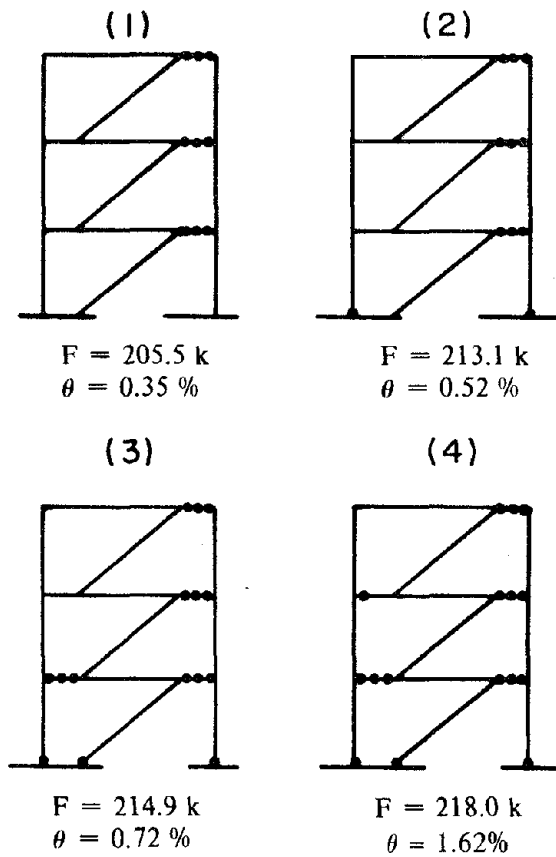
Fig. 5.10   Development of Yield Zones
in Designed D-brace Frame.

(1)

F = 85.8 k
θ = 0.31 %

(2)

F = 92.2 k
θ = 0.34 %

(3)

F = 97.1 k
θ = 0.38 %

(4)

F = 103.0 k
θ = 0.48%

(5)

F = 105.1 k
θ = 0.58 %

(6)

F = 105.5 k
θ = 0.78 %
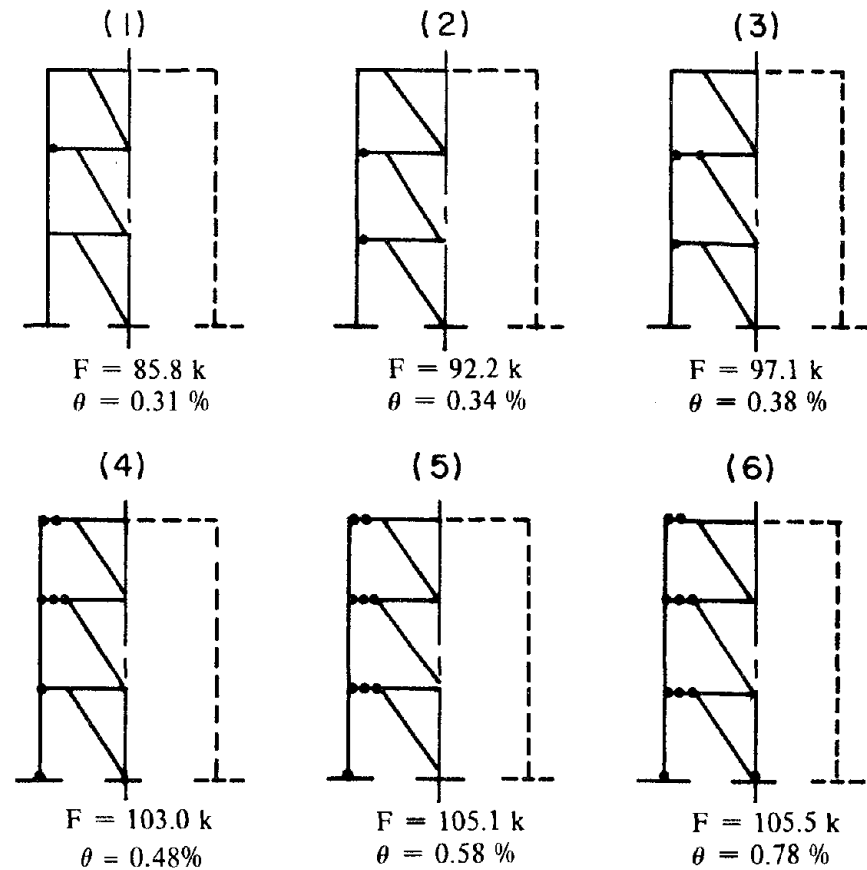
Fig. 5.11   Development of Yield Zones
in Designed V-brace Frame.

MOMENT (k-ft)   AXIAL FORCE (kips)

(a)

(b)
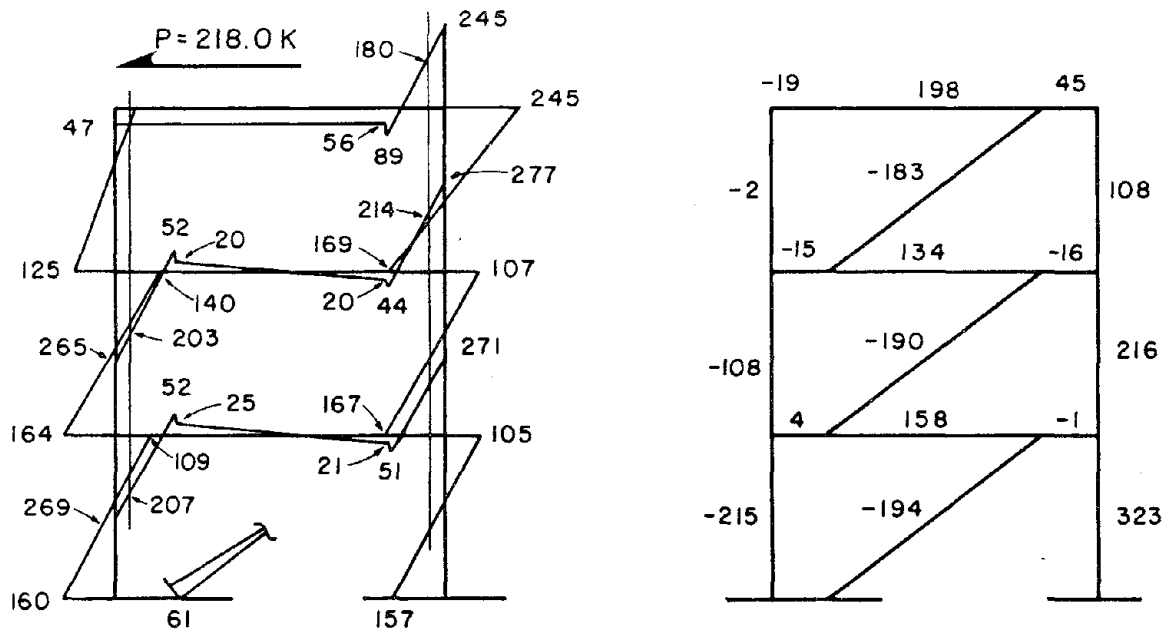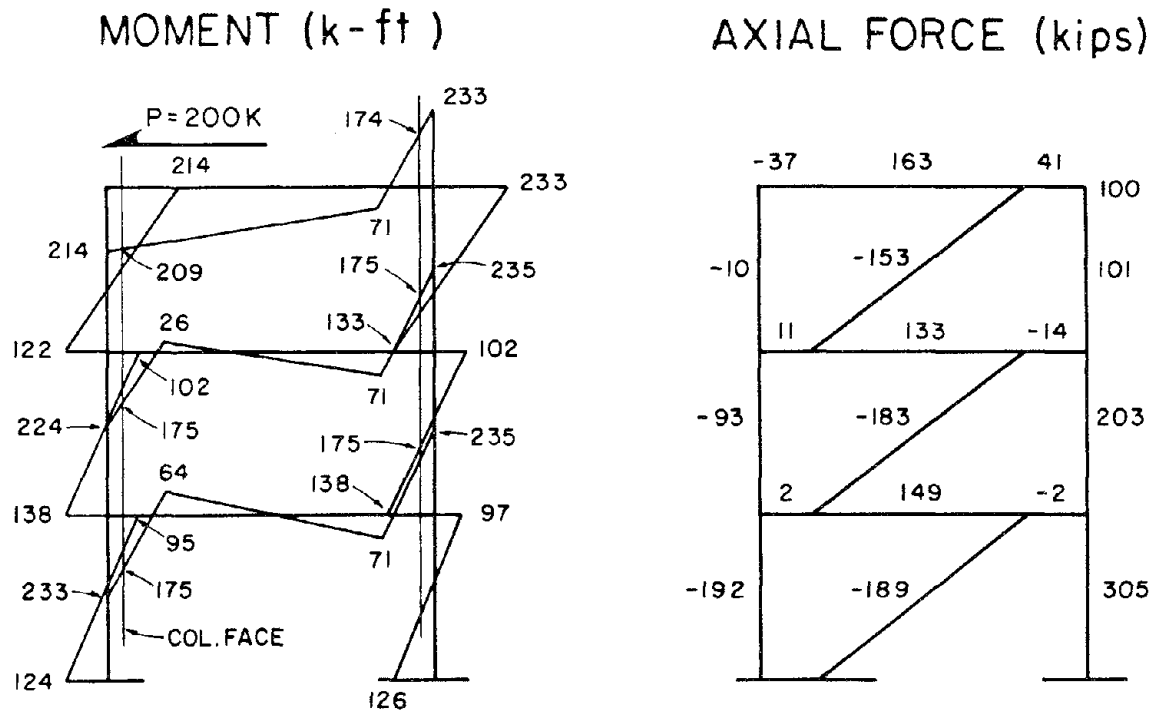
Fig. 5.12   Comparison of D-brace Frame Member Forces Obtained from
(a) Proposed Design Method, and (b) Elasto-Plastic Analysis.
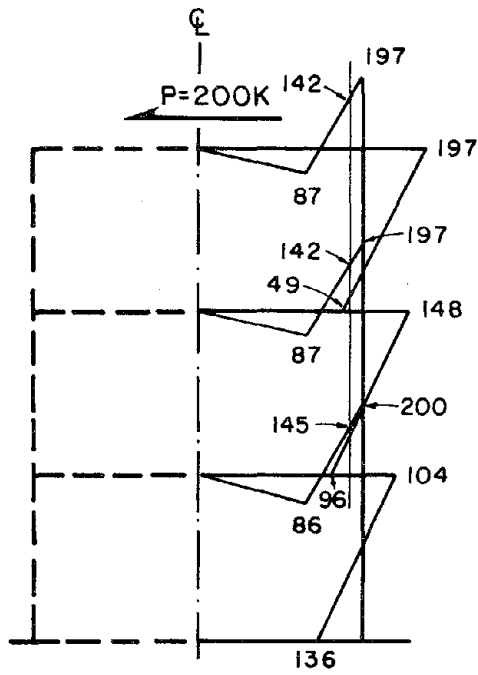
MOMENT (k-ft)   AXIAL FORCE (kips)
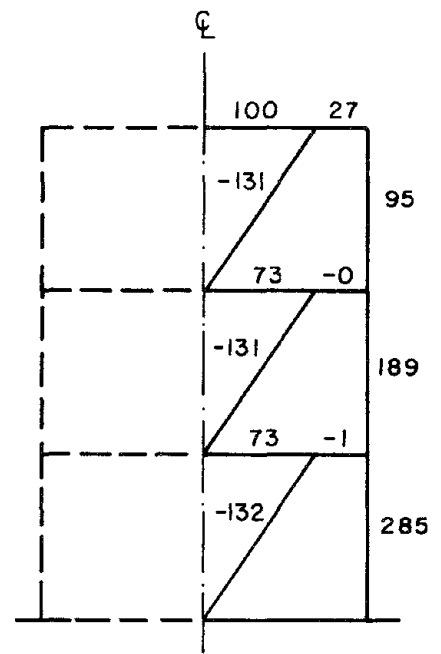
(a)
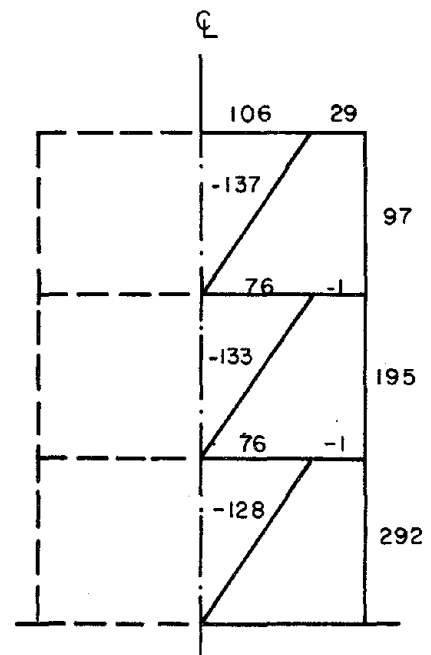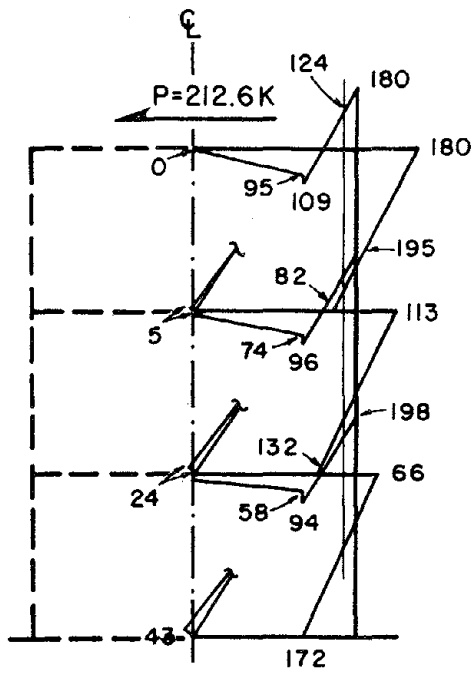
(b)

Fig. 5.13   Comparison of V-brace Frame Member Forces Obtained from
(a) Proposed Design Method, and (b) Elasto-Plastic Analysis.
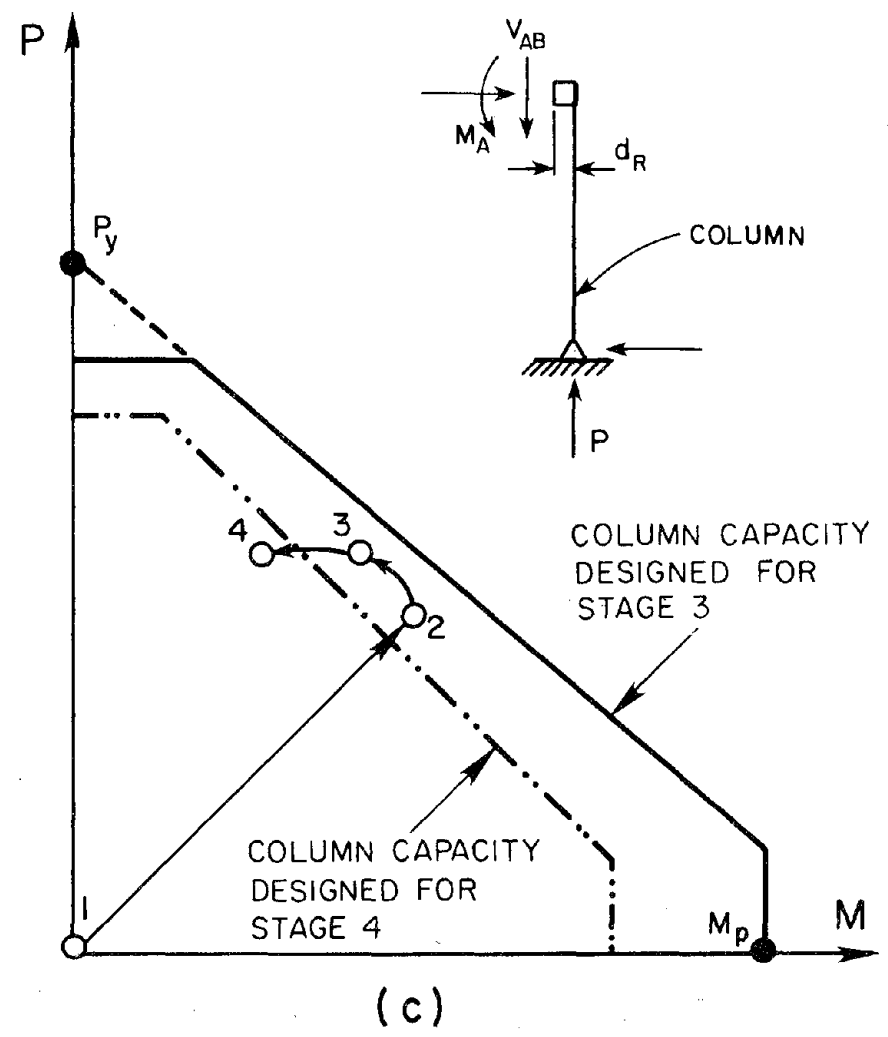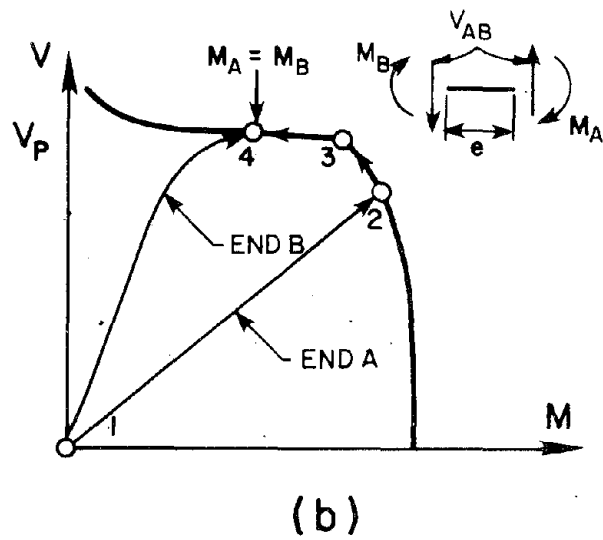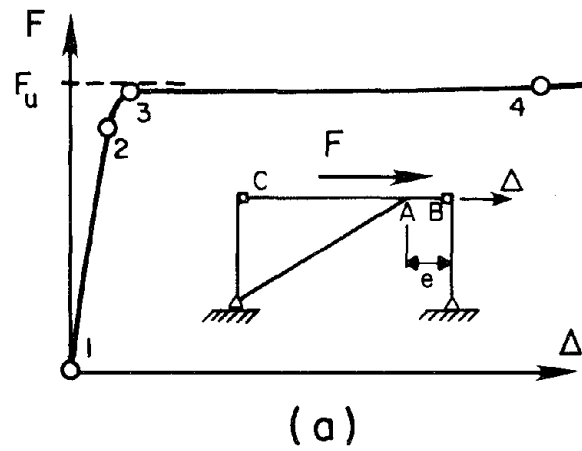
Fig. 5.14   Global and Local Behavior of EBF Based on Ideal Plastic Theory. (a) Load-Deflection Diagram,
(b) Link Moment-Shear Interaction Diagram, and   (c) Moment-Axial Column Force Interaction Diagram.
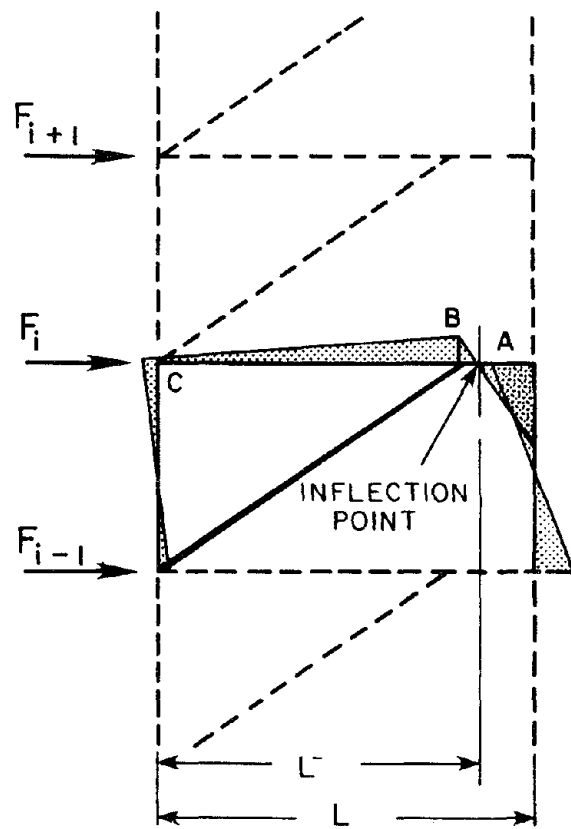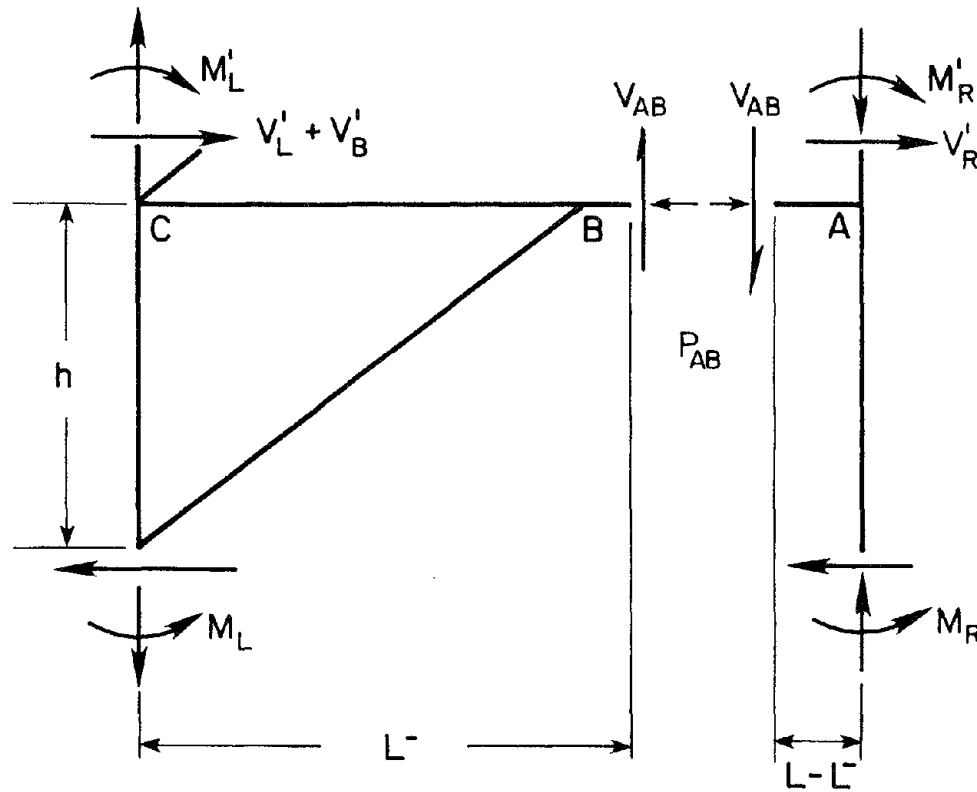
Fig. 5.15   Free-Body Diagram of a D-brace Frame Panel for Approximate Analysis Method.
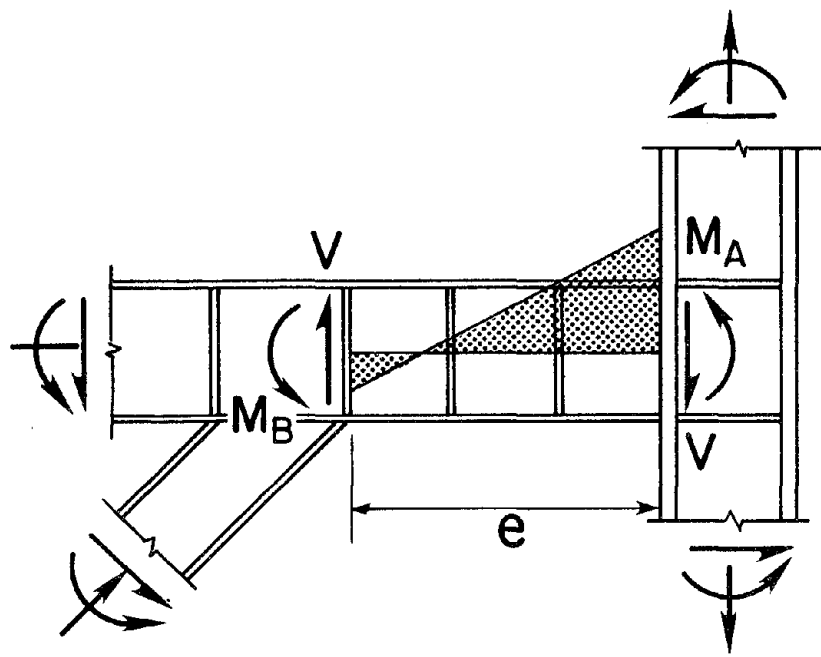
(a)
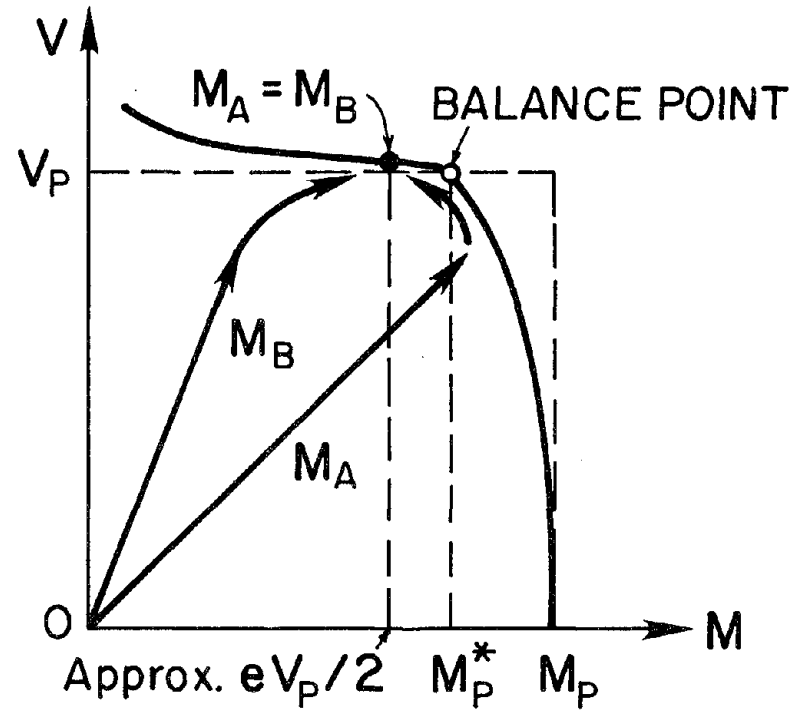
(b)

Fig. 6.1   (a) Typical Elastic Beam Link Moment at column, and
(b) Behavior of An Ideal Plastic Link.

EBF EXAMPLE STORY FORCE

STORY LEVEL	LINK AXIAL FORCE P	LINK SHEAR FORCE V	ρ ($=P/V$)
6	$6F_0$	$6F_0\,\dfrac{h}{L}$	$1.00\,\dfrac{L}{h}$
5	$5F_0$	$11F_0\,\dfrac{h}{L}$	$0.45\,\dfrac{L}{h}$
4	$4F_0$	$15F_0\,\dfrac{h}{L}$	$0.27\,\dfrac{L}{h}$
3	$18F_0$	$18F_0\,\dfrac{h}{L}$	$1.00\,\dfrac{L}{h}$
2	$2F_0$	$20F_0\,\dfrac{h}{L}$	$0.10\,\dfrac{L}{h}$
1	F_0	$21F_0\,\dfrac{h}{L}$	$0.05\,\dfrac{L}{h}$
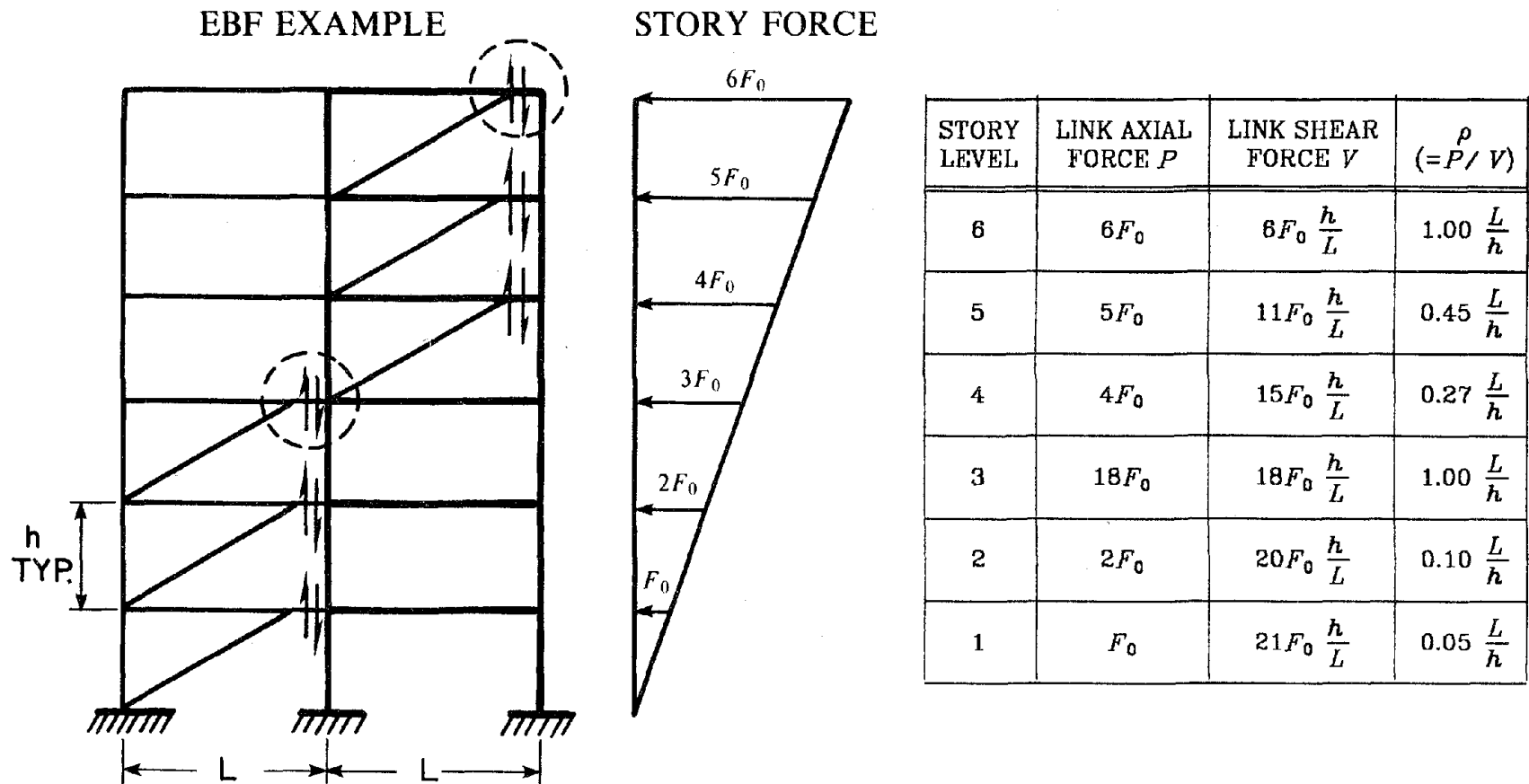
Fig. 6.2   Approximate Relationship of Link Shear and Axial Forces.
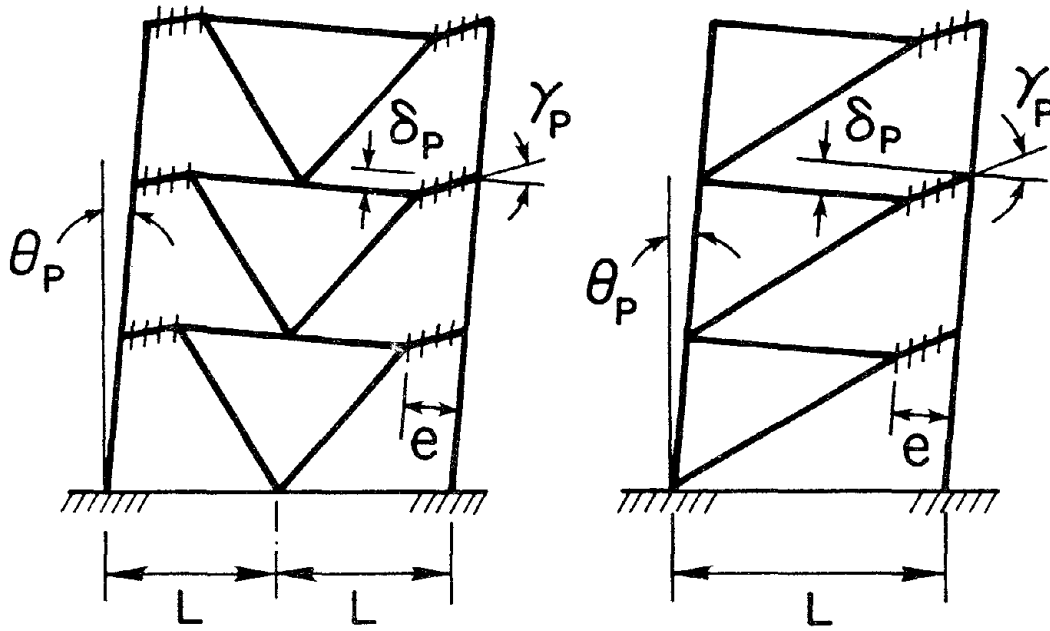
(a) Energy Dissipation Mechanism of EBFs.
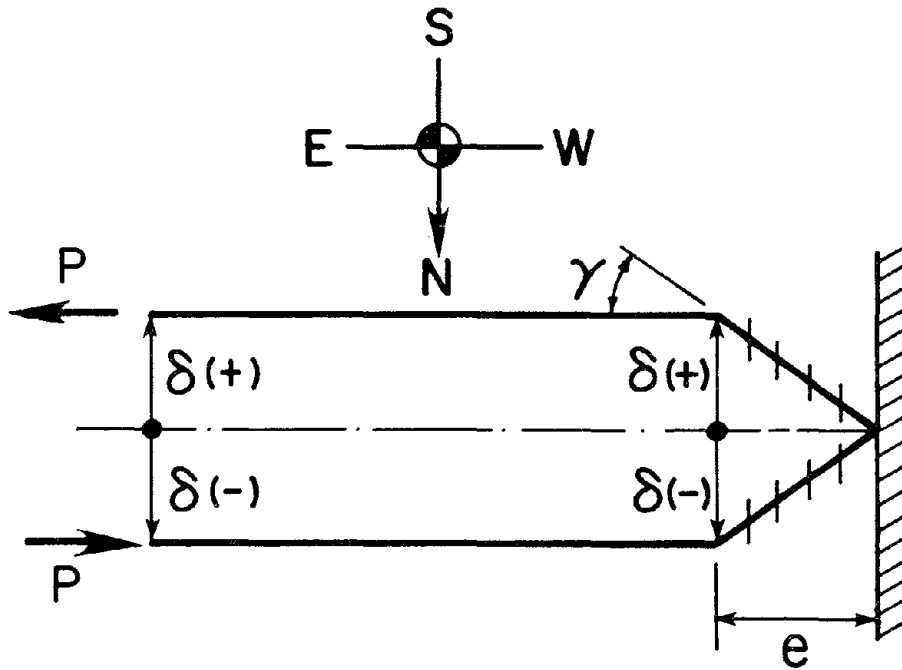
(b) Displacement and Axial Force Control.

Fig. 6.3   Experimental Simulation of Beam Deformation in EBF.
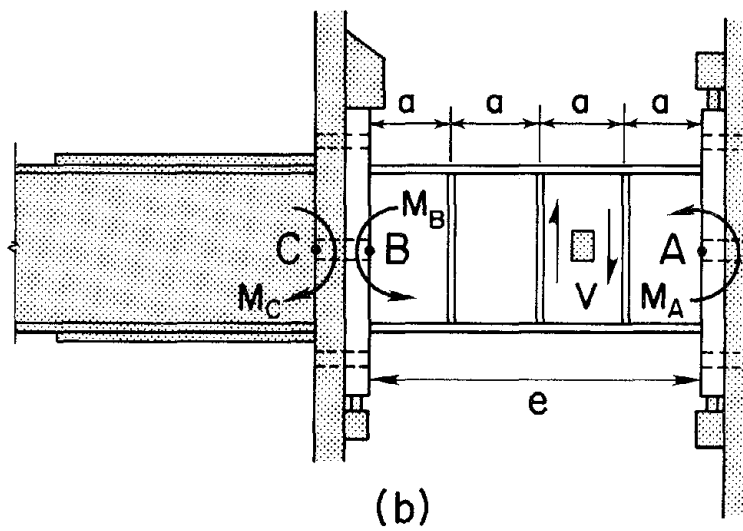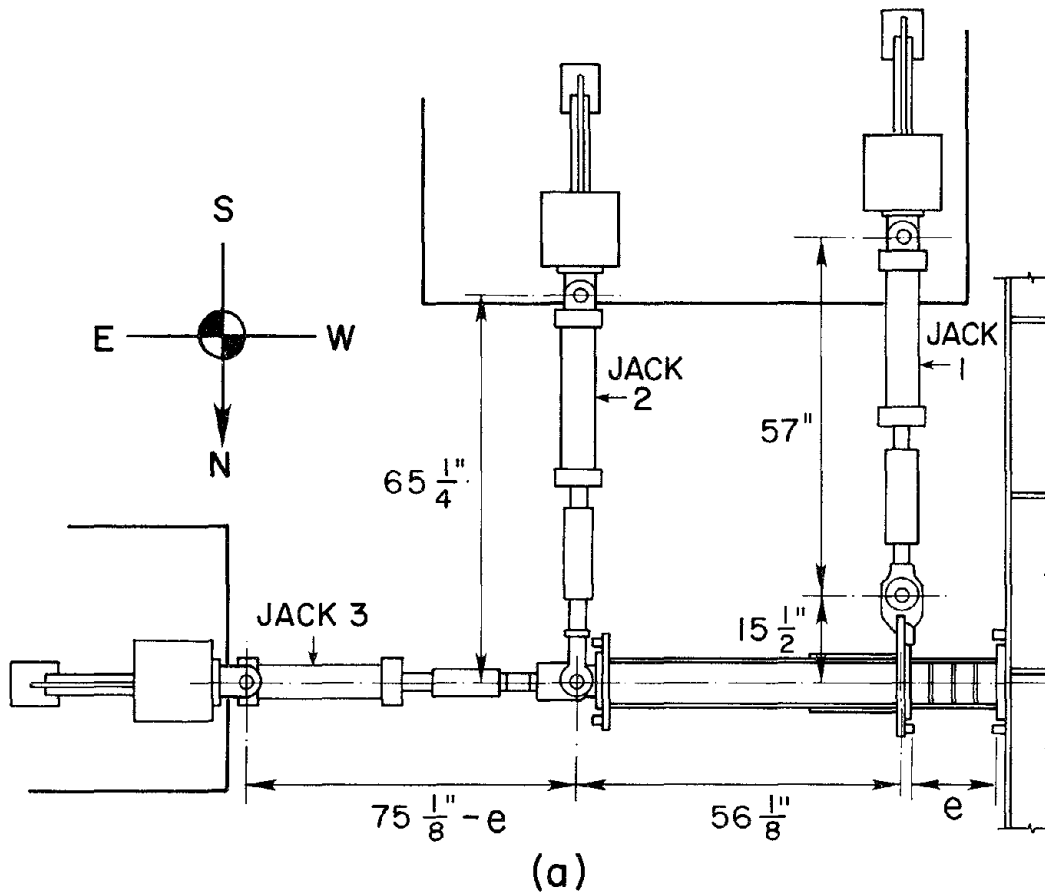
Fig. 6.4   Experimental Setup.
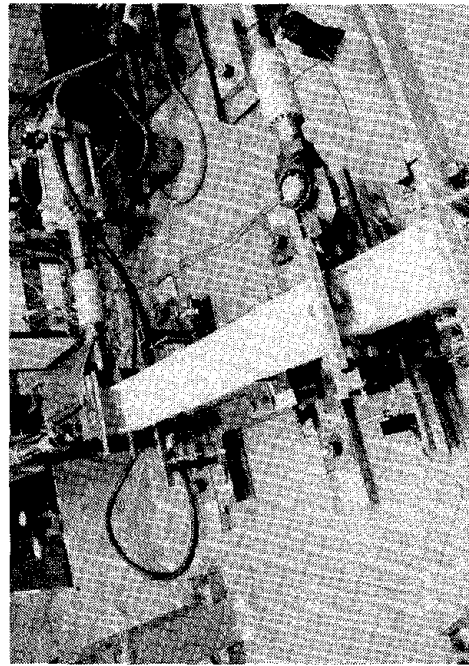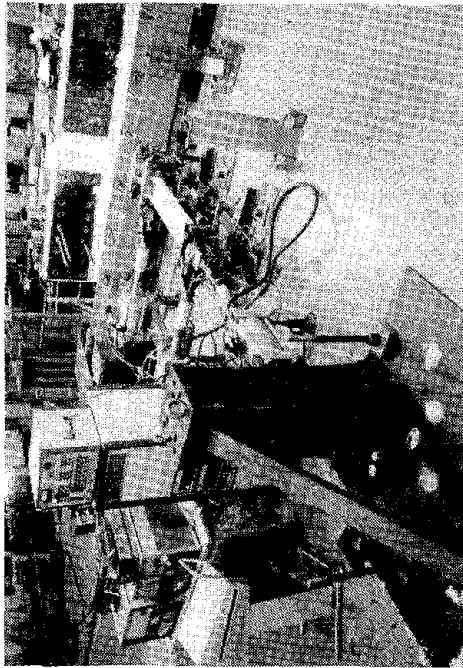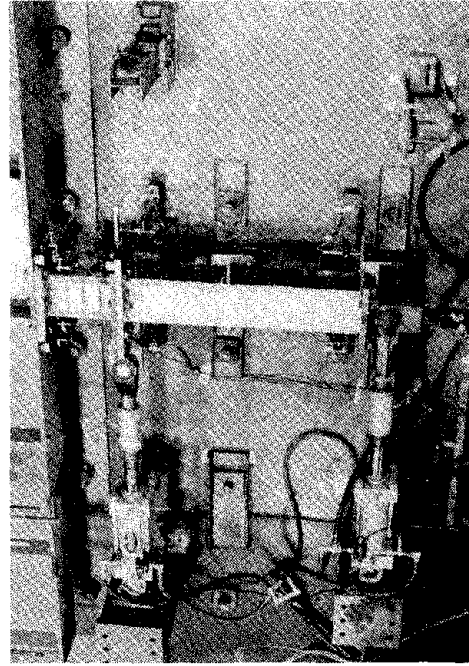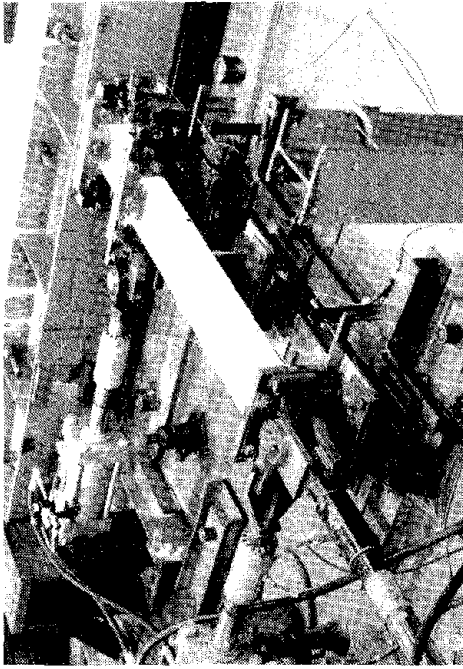
Fig. 6.5   Global View of Actual Experimental Setup.
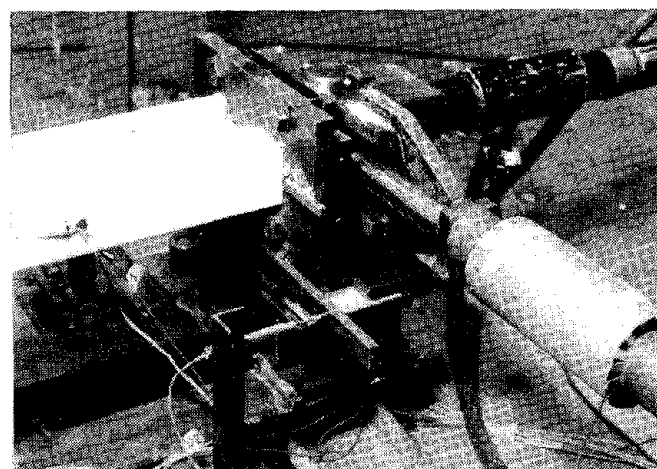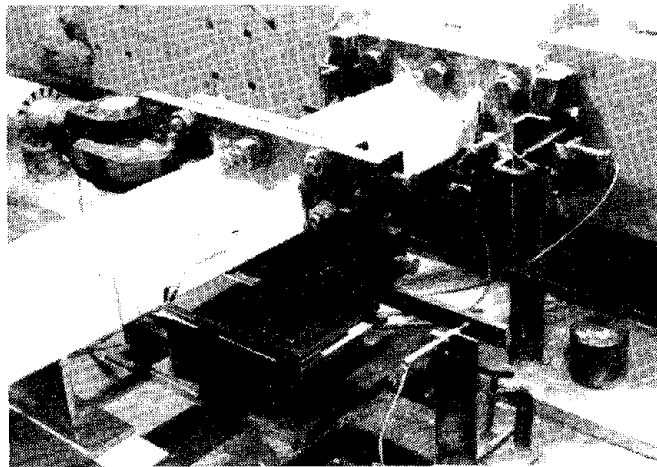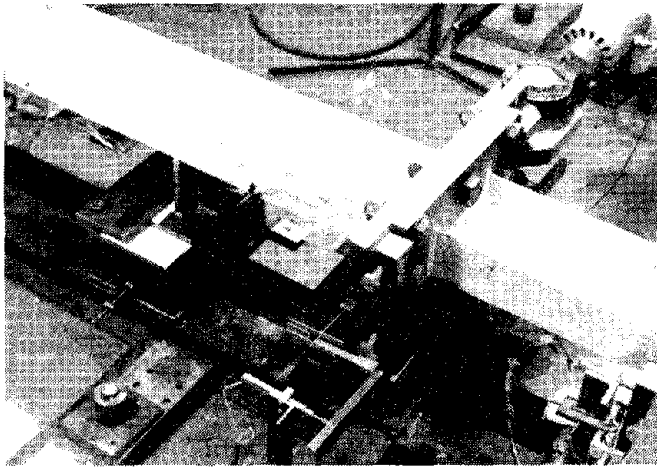
Fig. 6.6   Photos of Supports, Connections, and Instrumentation for Rotation Measurements.
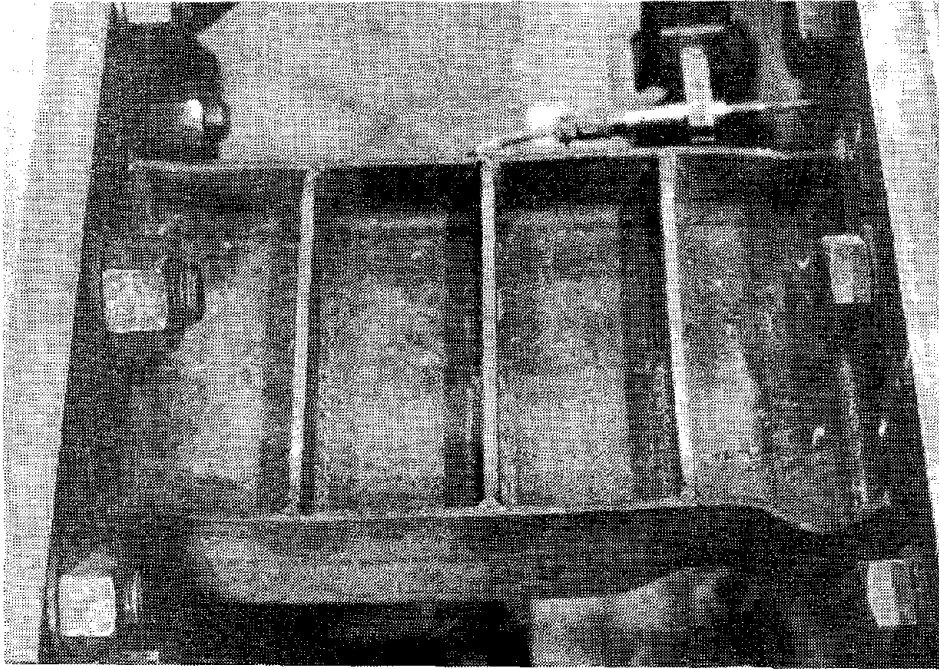
Fig. 6.7   Photo of Specimen 1 at the End of Testing.
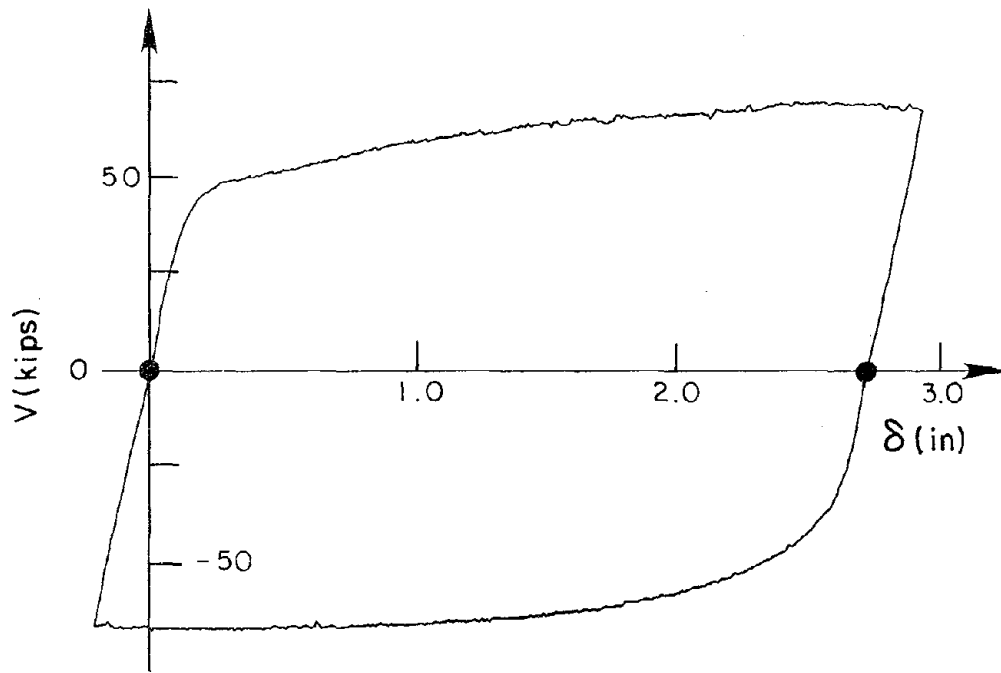
Fig. 6.8   Shear-Displacement Relationship of Specimen 1.
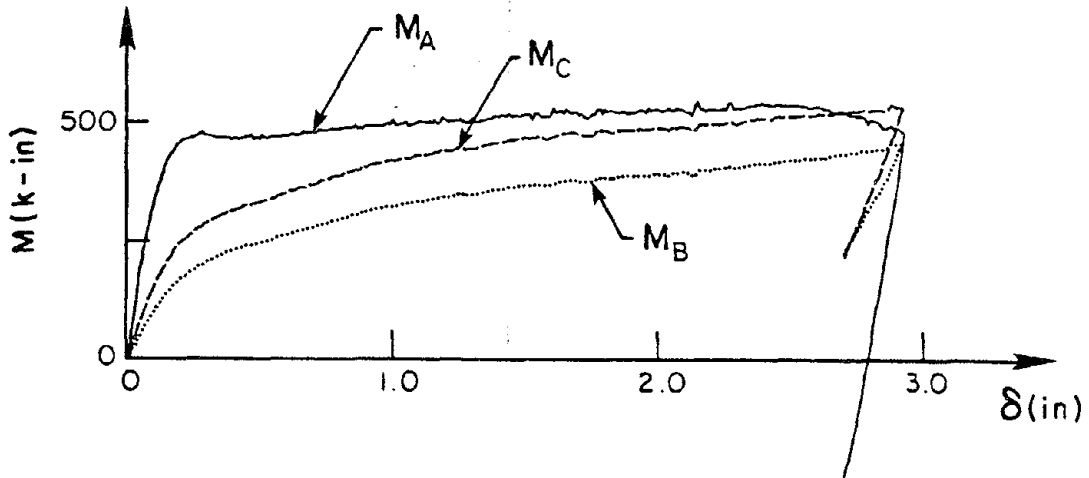
Fig. 6.9   Moment-Displacement Relationship of Specimen 1.
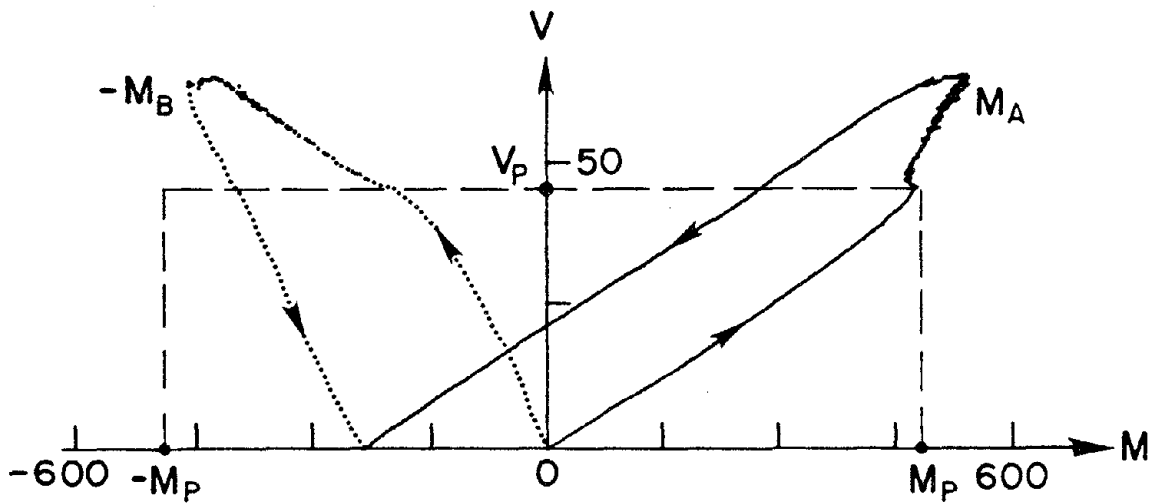
Fig. 6.10   Moment-Shear Relationship of Specimen 1.
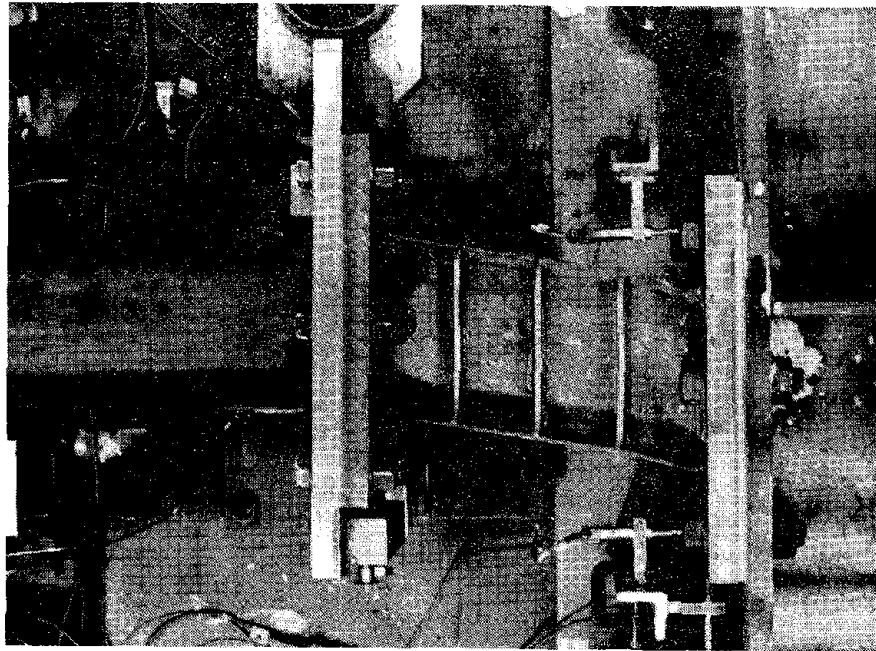
Fig. 6.11   Photo of Specimen at $\delta = 3$ in.
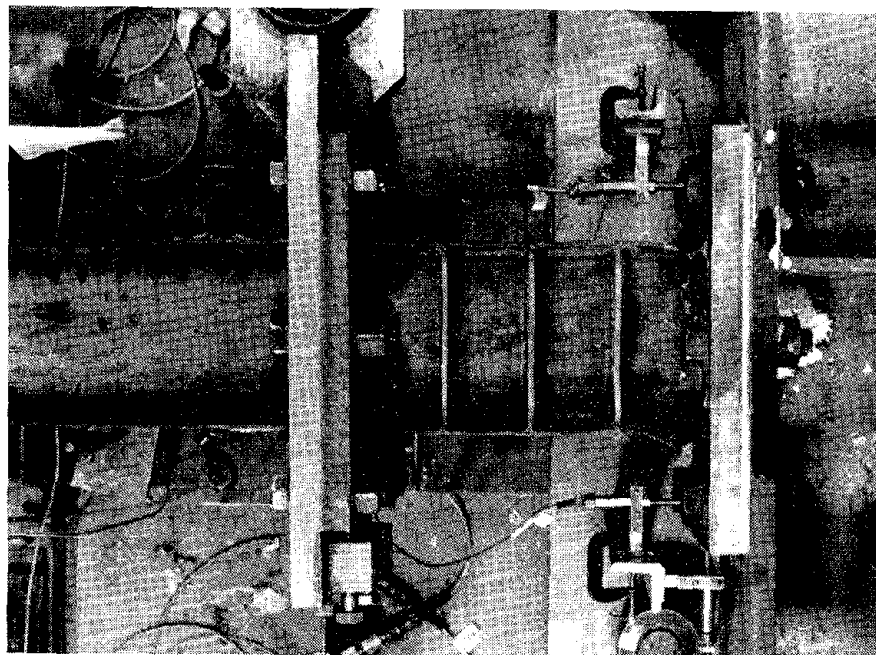
Fig. 6.12   Photo of Specimen Reversed to $\delta = 0$ in.
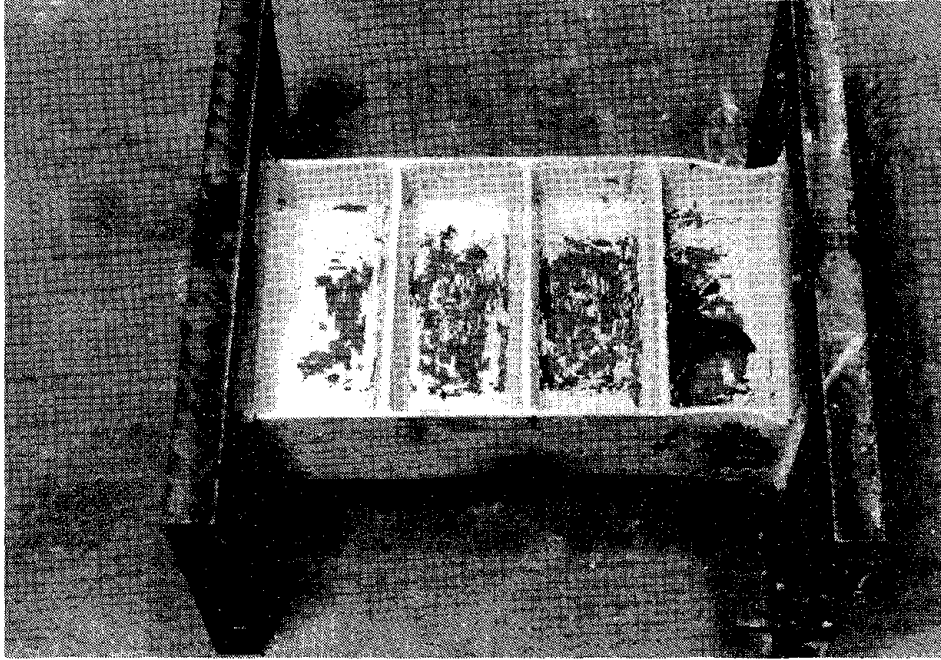
Fig. 6.13   Photo of Specimen 3 at the End of Testing.
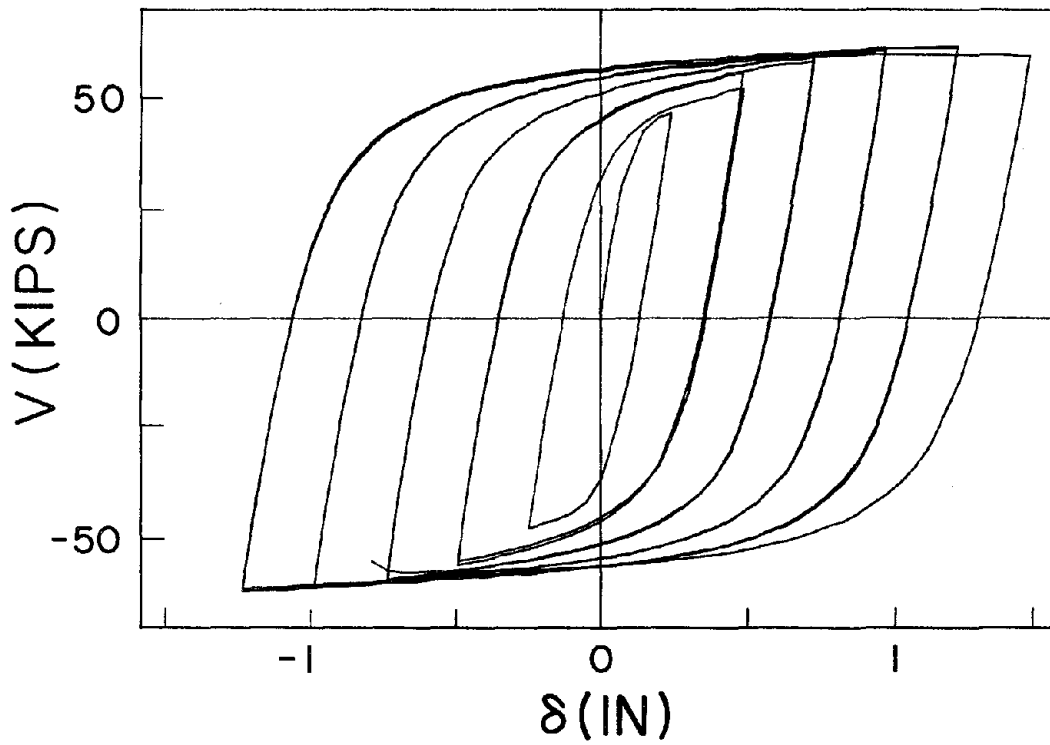
Fig. 6.14   Shear-Displacement Relationship of Specimen 3.
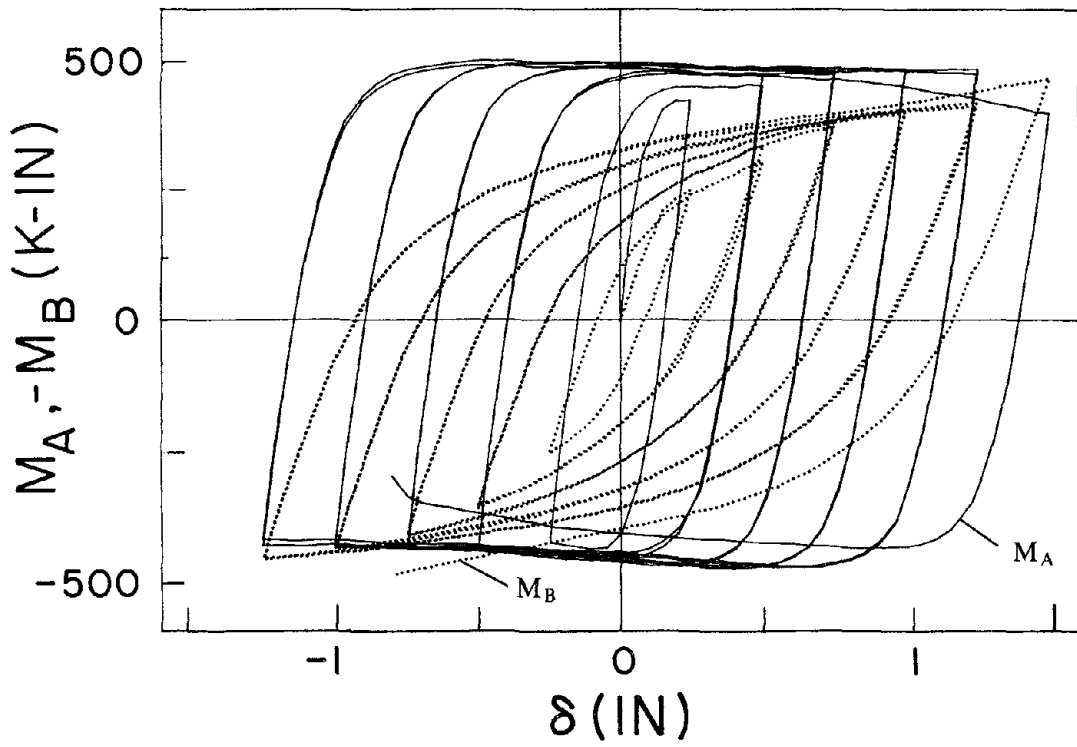
Fig. 6.15   Moment-Displacement Relationship of Specimen 3.
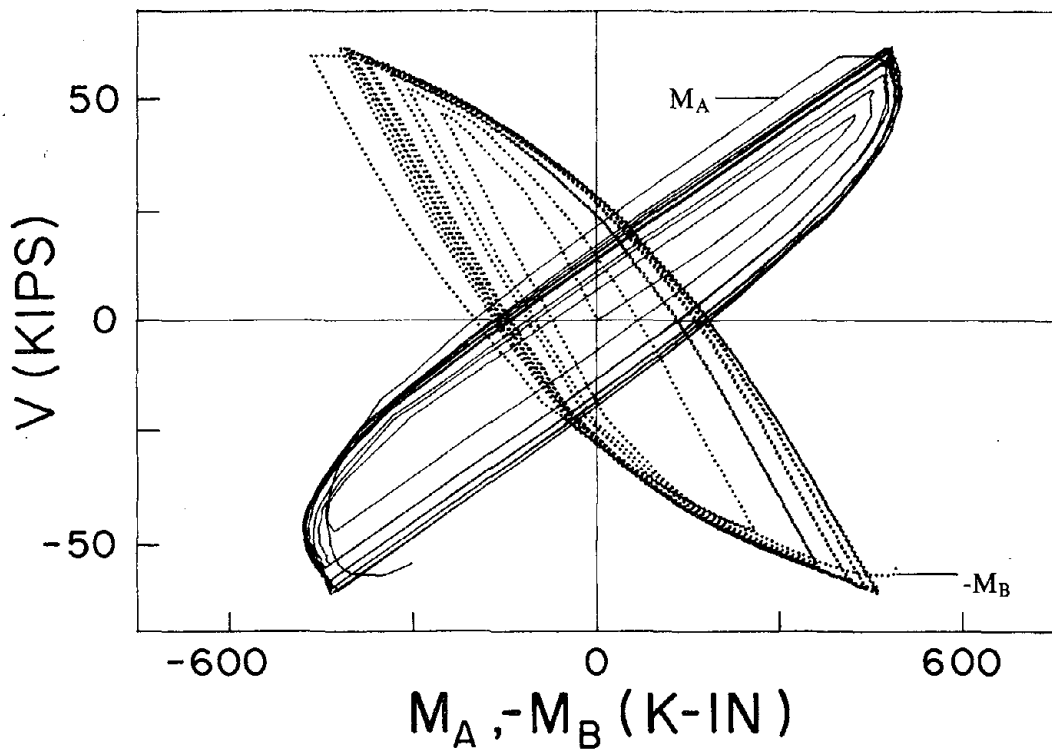
Fig. 6.16   Moment-Shear Relationship of Specimen 3.
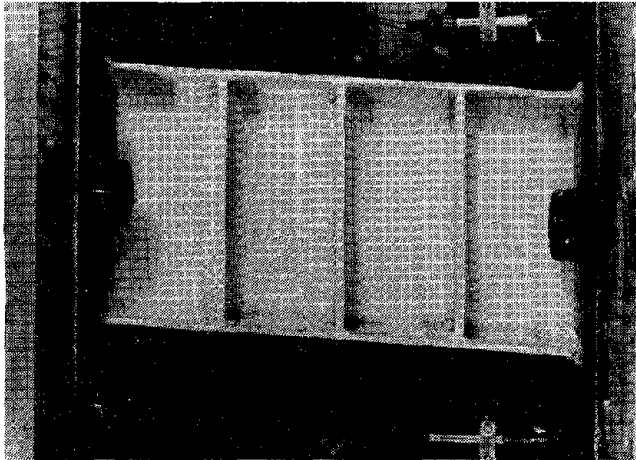
(a) Cycle 6S, at $\delta = 1.0$ in.
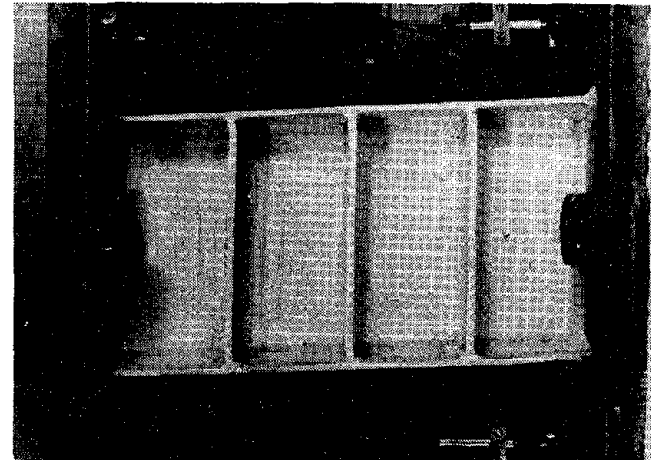
(b) Cycle 8N, at $\delta = -1.25$ in.
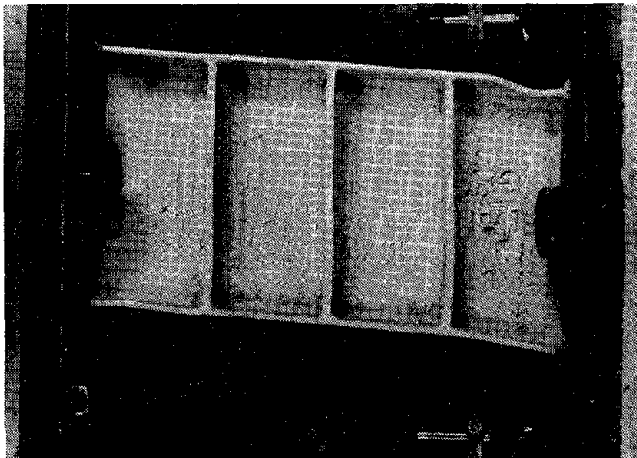
(c) Cycle 10S, at $\delta = 1.5$ in.
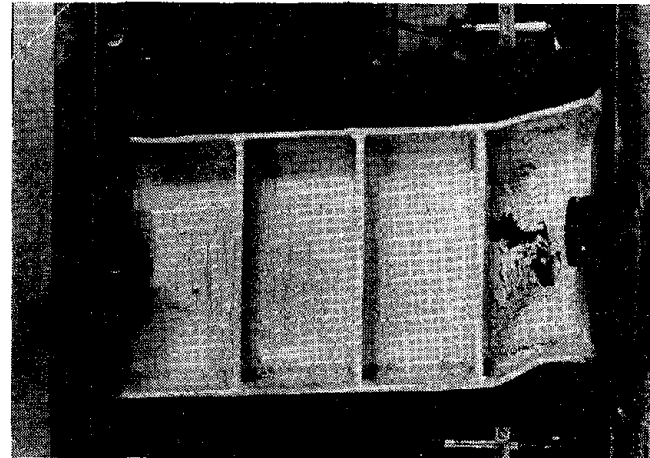
(d) Cycle 10N, at $\delta = -1.5$ in.

Fig. 6.17 Photo of Specimen 3 During Test.
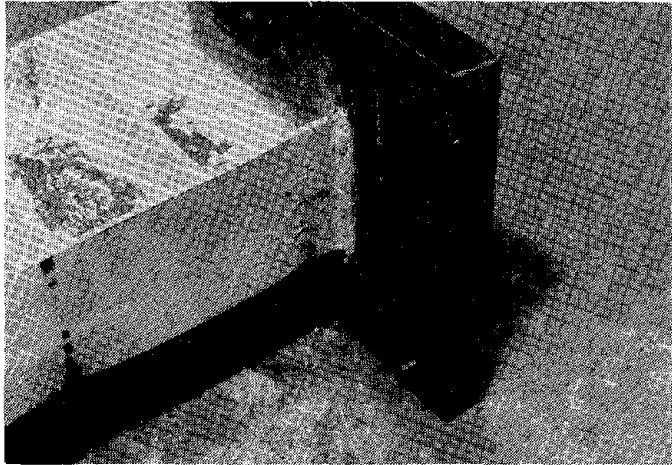
(a) End Region B, South Flange.
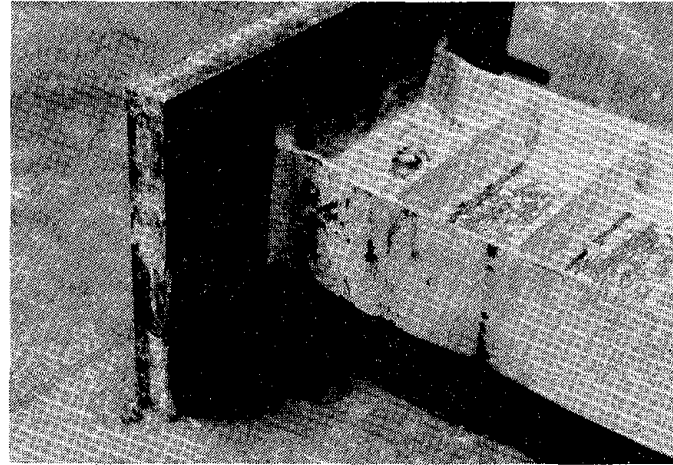
(b) End Region A, South Flange.
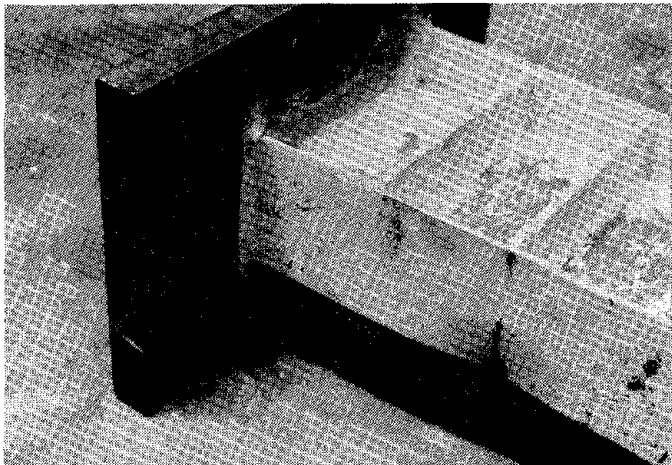
(c) End Region B, North Flange.
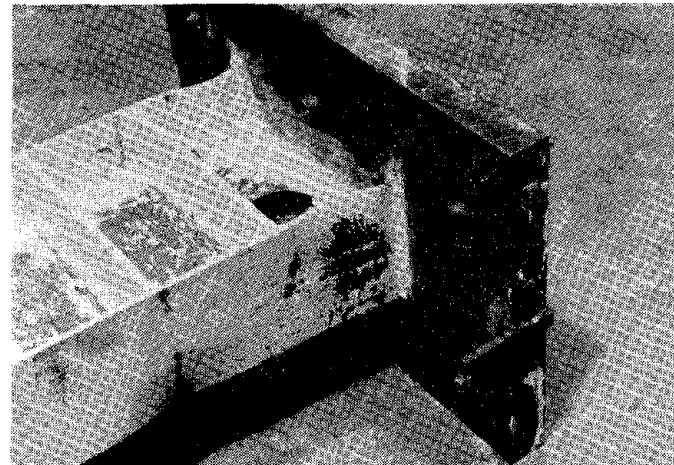
(d) End Region A, North Flange.

Fig. 6.18   Photo of End Regions of Specimen 3 After Test.
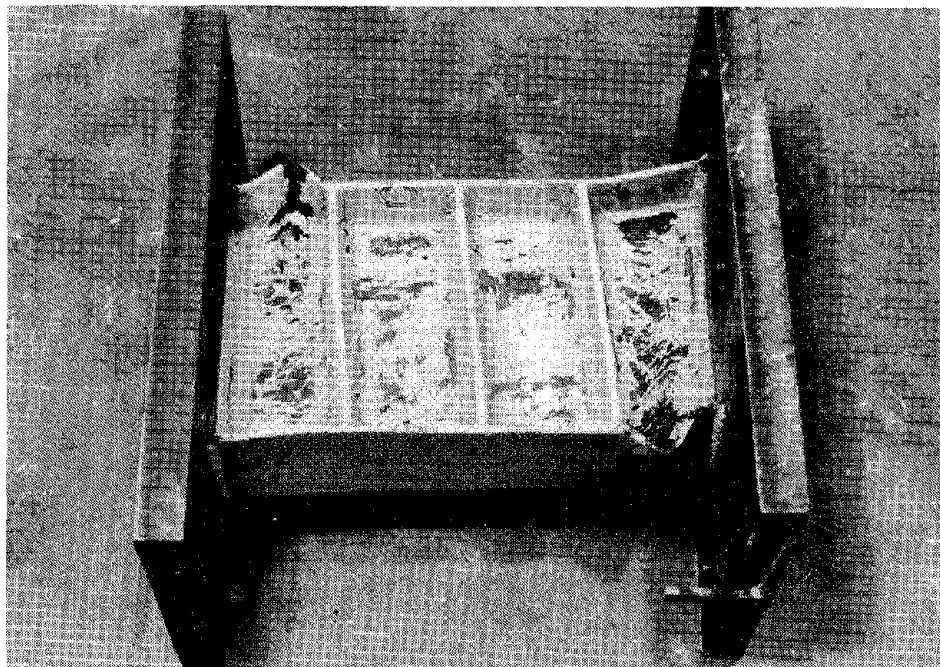
Fig. 6.19   Photo of Specimen 4 at the End of Testing.
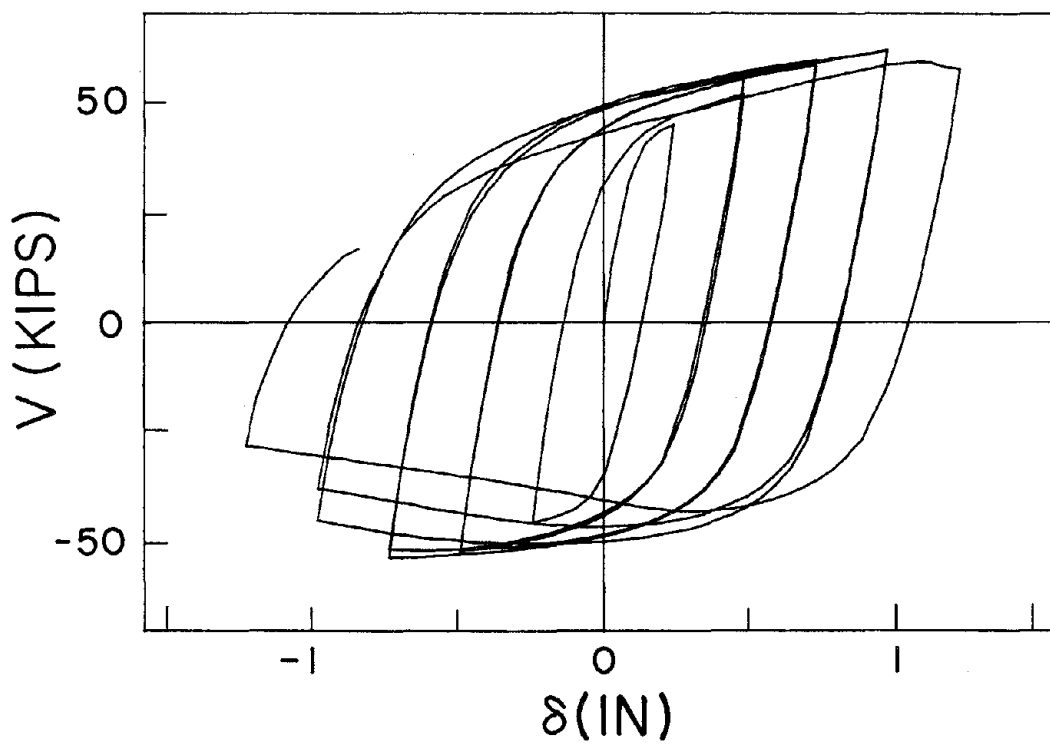
Fig. 6.20   Shear-Displacement Relationship of Specimen 4.
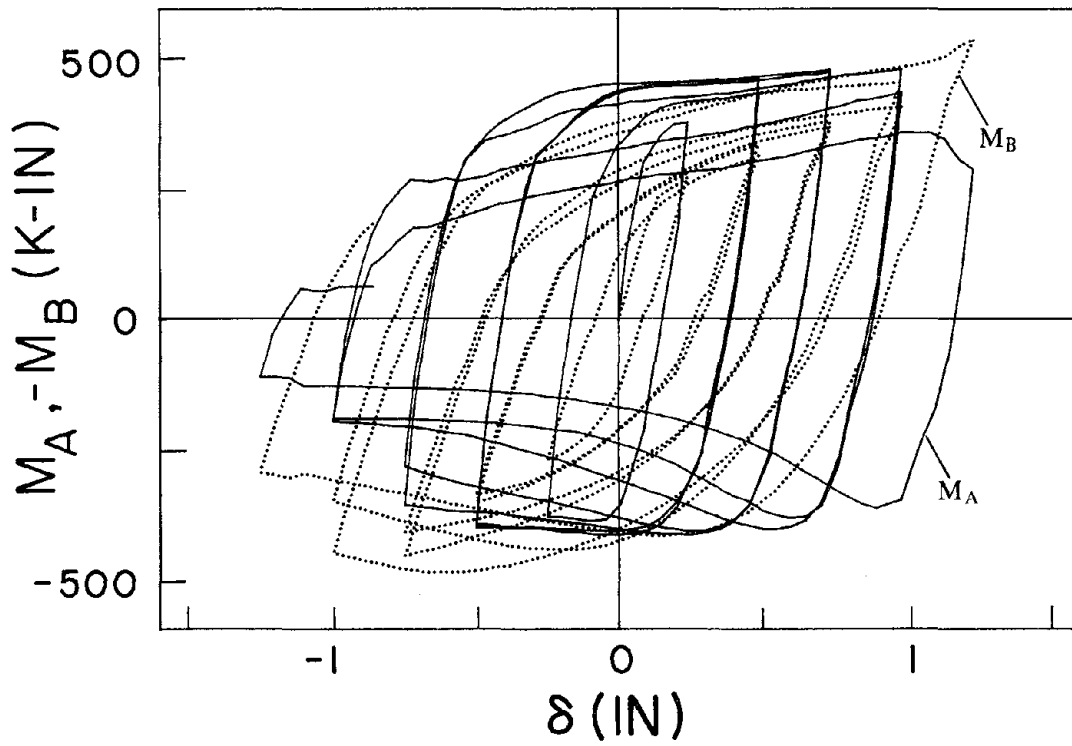
Fig. 6.21   Moment-Displacement Relationship of Specimen 4.
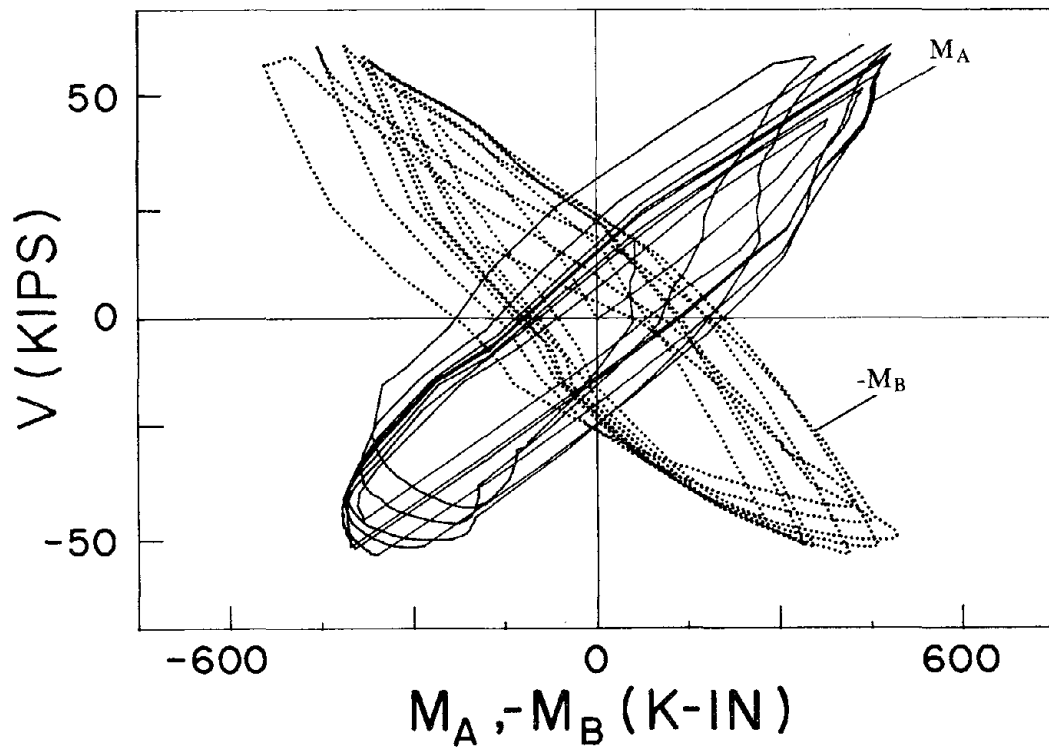
Fig. 6.22   Moment-Shear Relationship of Specimen 4.
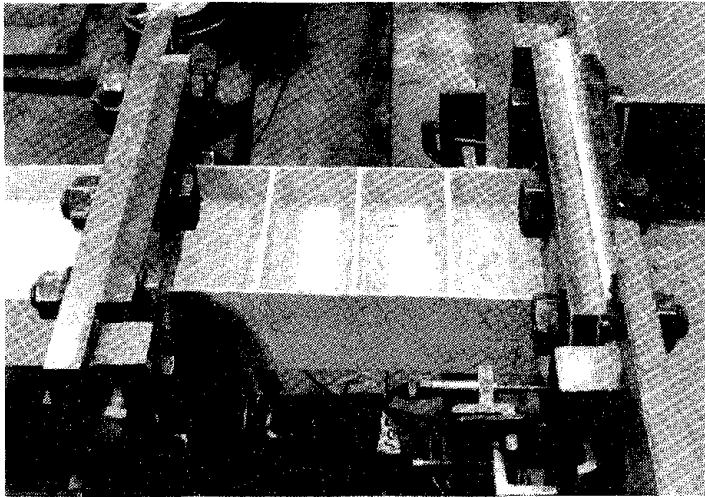
(a) Cycle 3S, at $\delta = 0.75$ in.
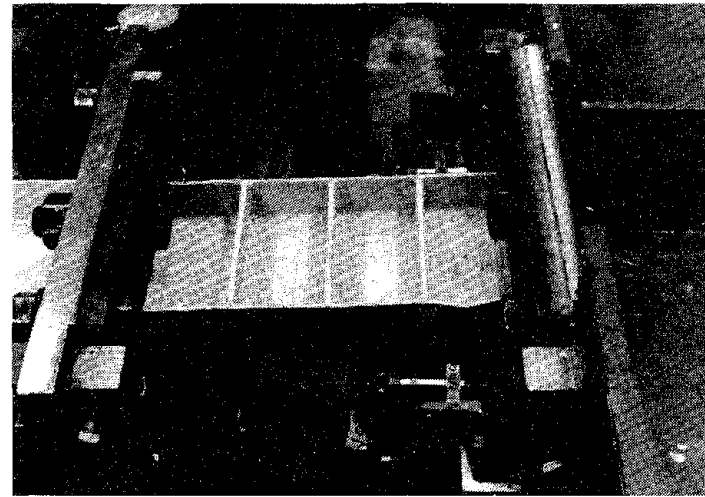
(b) Cycle 3N, at $\delta = -0.75$ in.
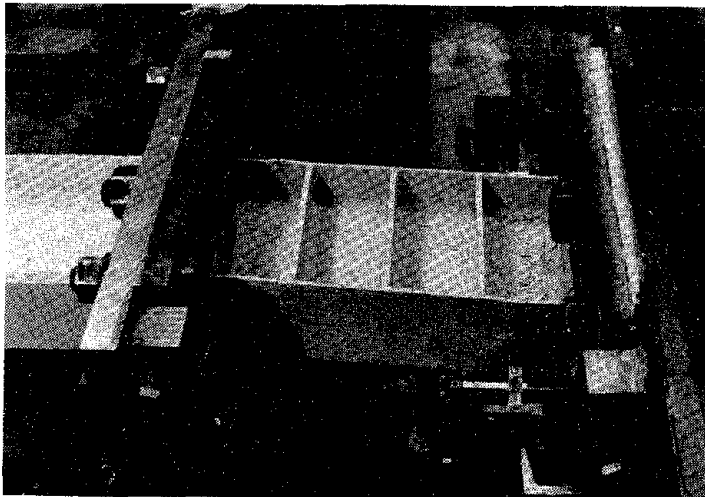
(c) Cycle 8S, at $\delta = 1.25$ in.
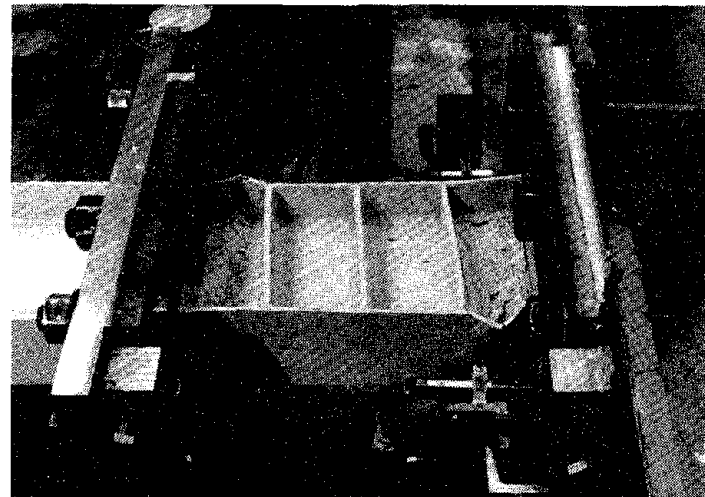
(d) Cycle 8N, at $\delta = -1.25$ in.

Fig. 6.23   Photo of Specimen 4 During Test.
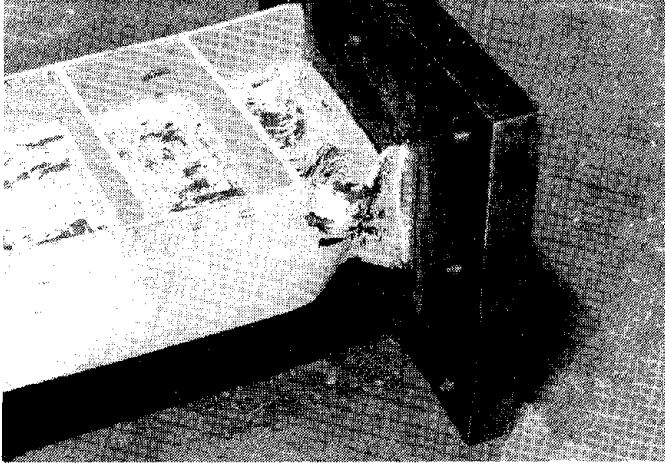
-228-

(a) End Region B, South Flange.
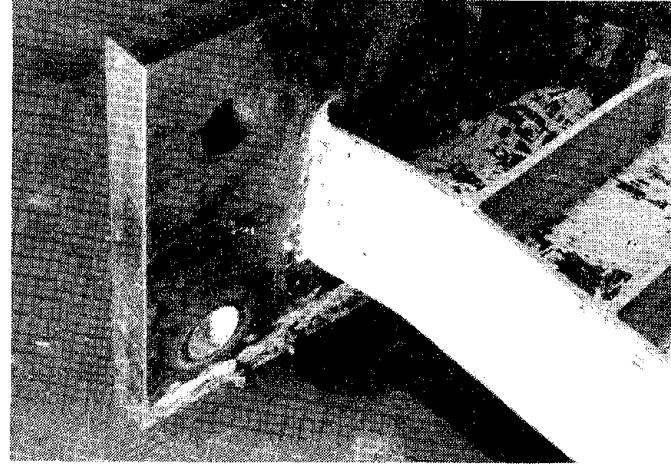
(b) End Region A, South Flange.
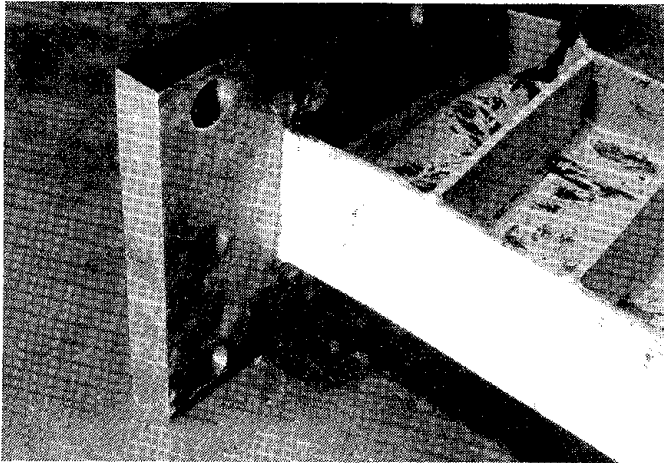
(c) End Region B, North Flange.
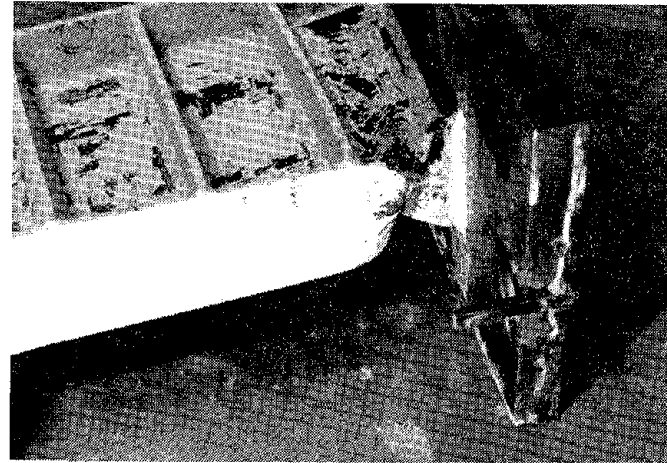
(d) End Region A, North Flange.

Fig. 6.24   Photo of End Regions of Specimen 4 After Test.
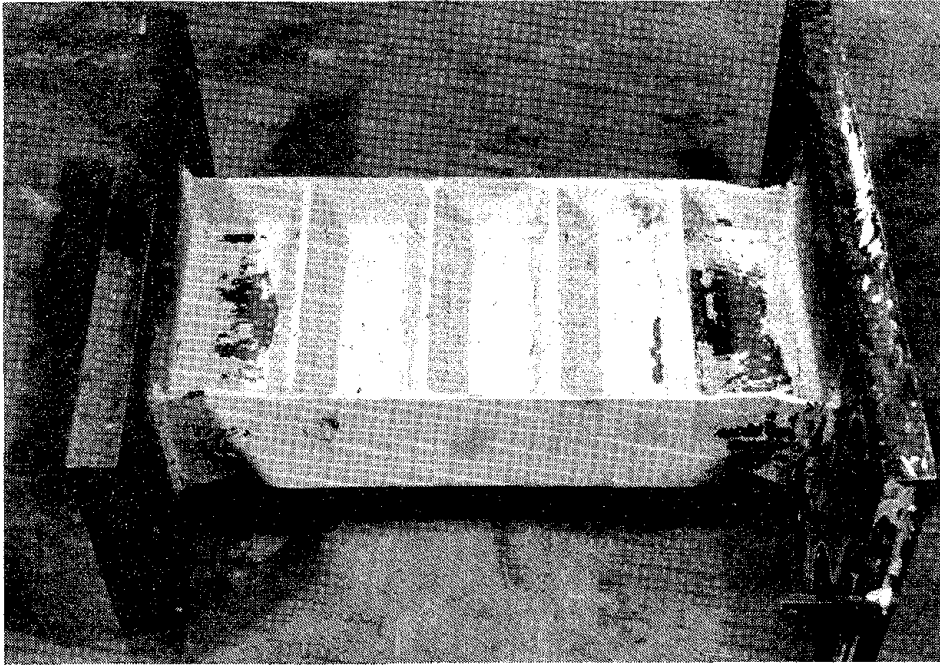
Fig. 6.25   Photo of Specimen 5 at the End of Testing.
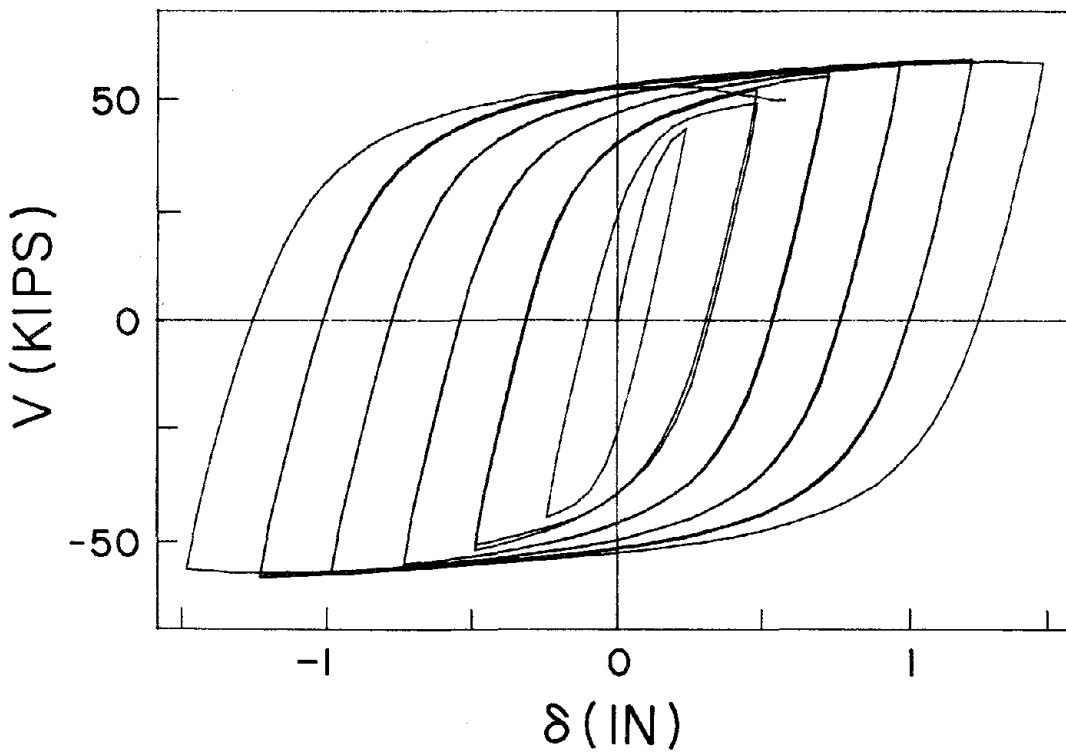
Fig. 6.26   Shear-Displacement Relationship of Specimen 5.
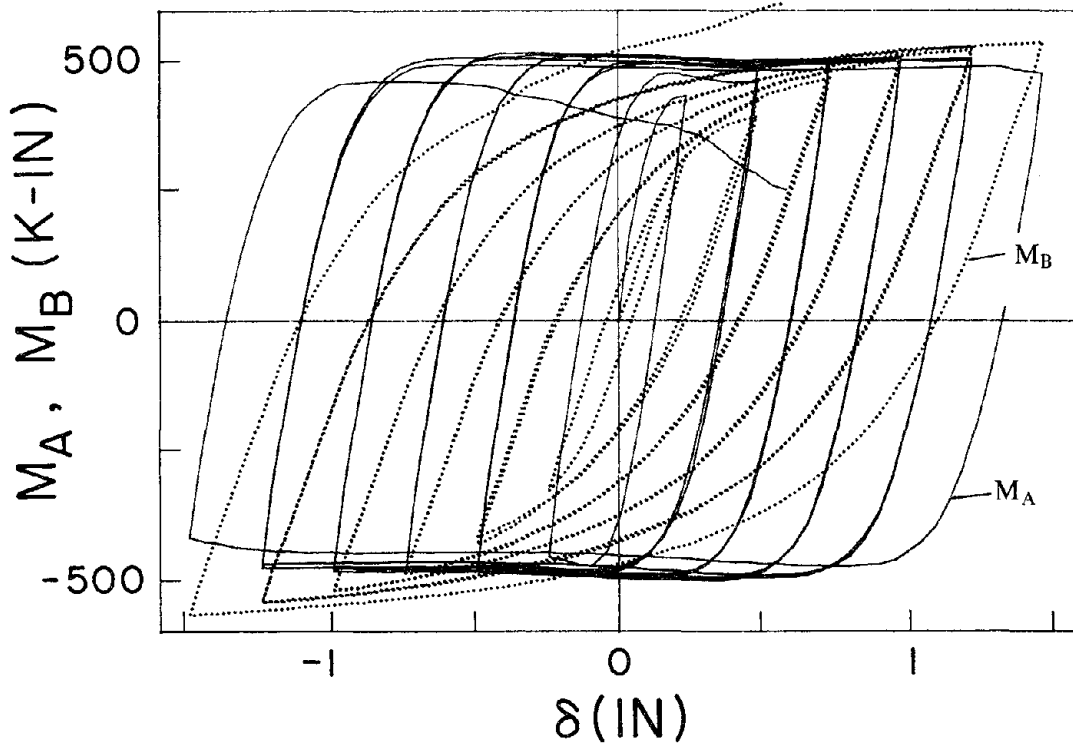
Fig. 6.27   Moment-Displacement Relationship of Specimen 5.
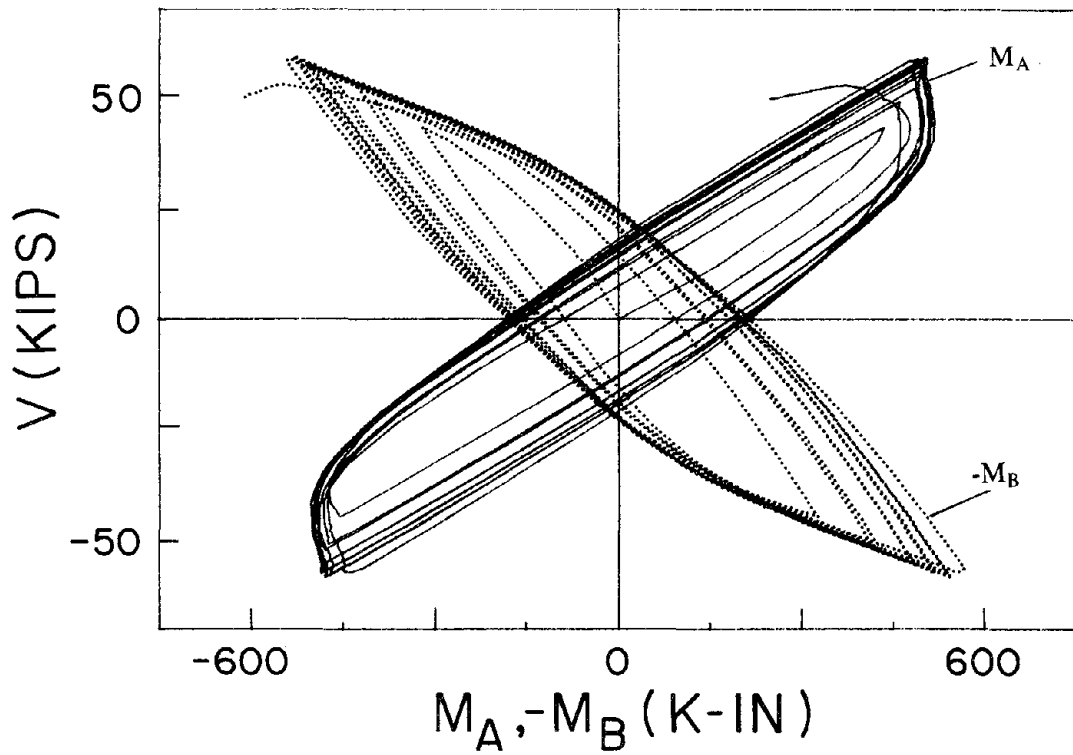
Fig. 6.28   Moment-Shear Relationship of Specimen 5.
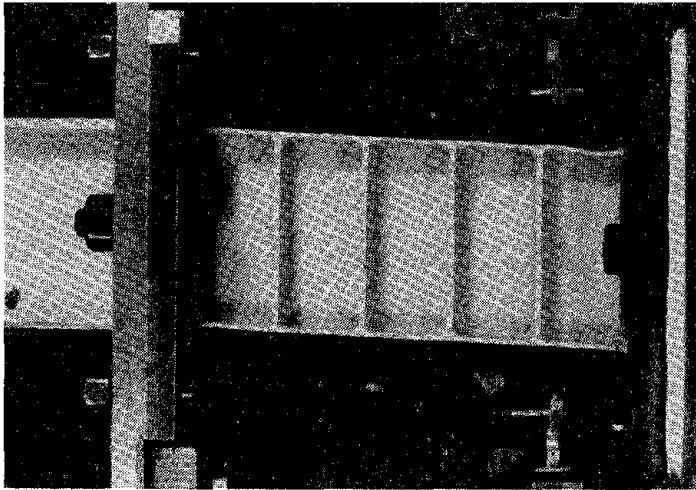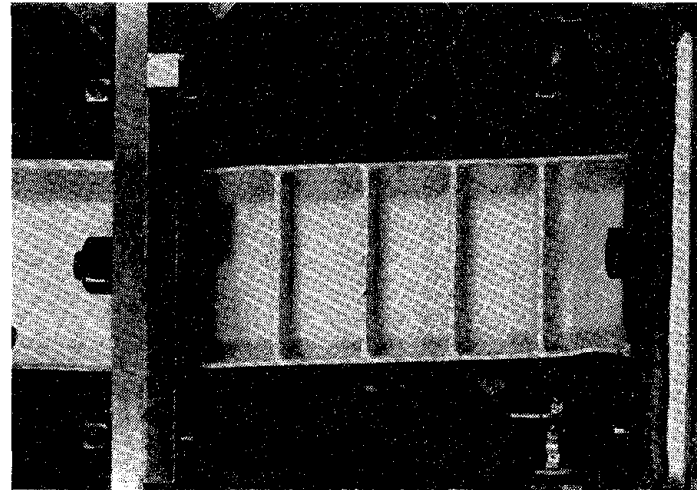
(a) Cycle 6S, at $\delta = 1.0$ in.

(b) Cycle 6N, at $\delta = -1.0$ in.
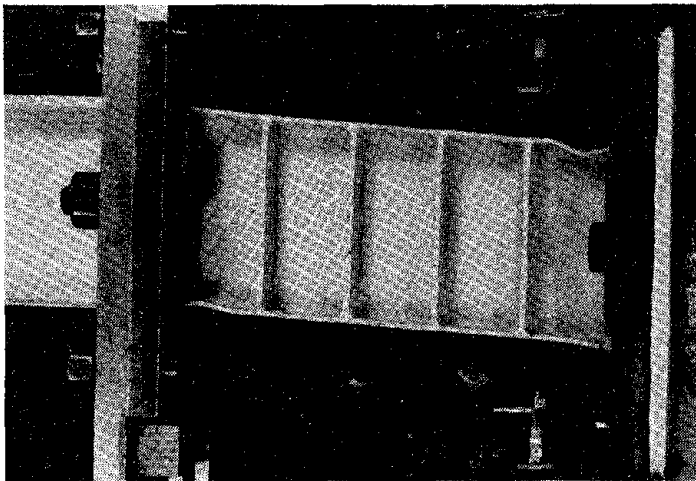
(c) Cycle 10S, at $\delta = 1.5$ in.
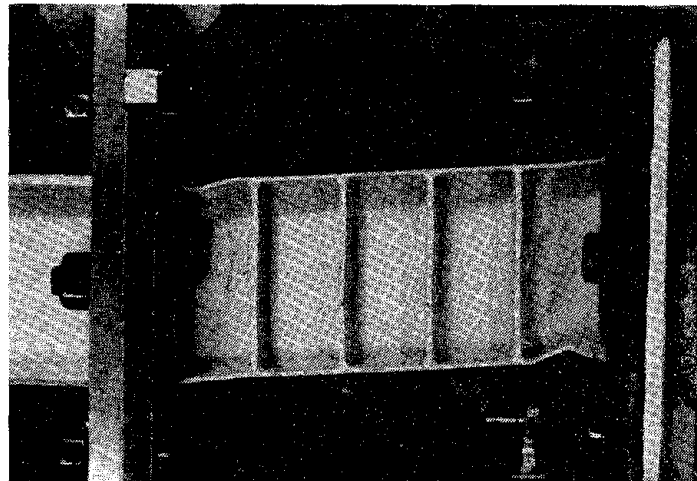
(d) Cycle 10N, at $\delta = -1.5$ in.

Fig. 6.29   Photo of Specimen 5 During Test.
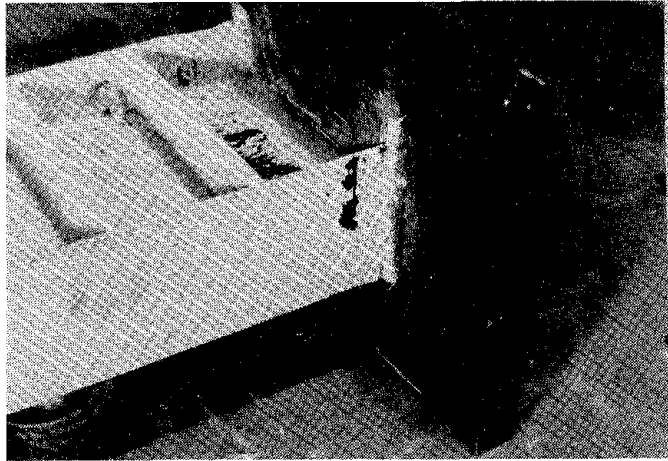
(a) End Region B, South Flange.
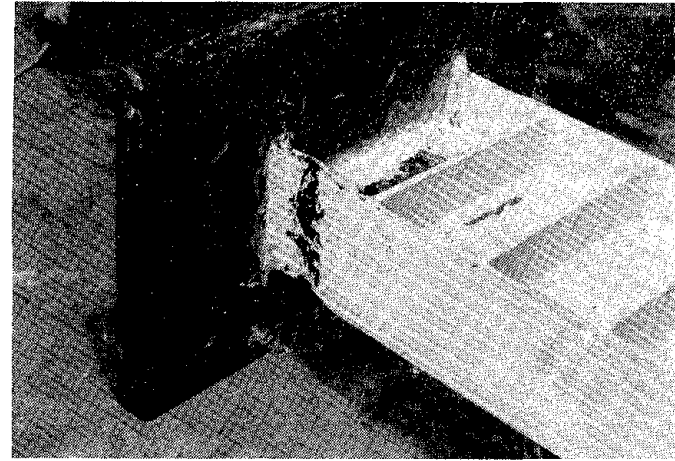
(b) End Region A, South Flange.
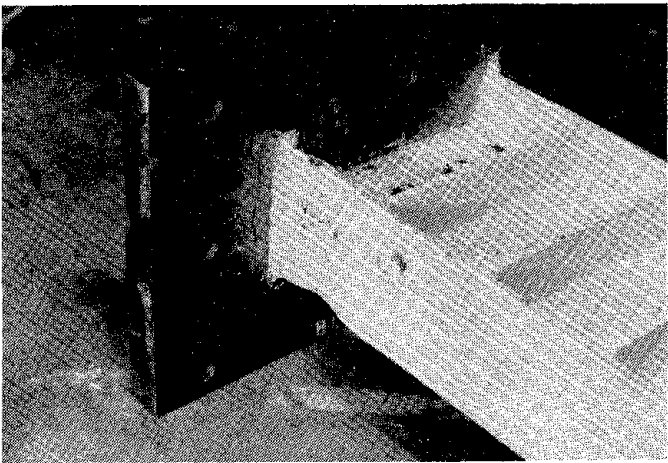
(c) End Region B, North Flange.
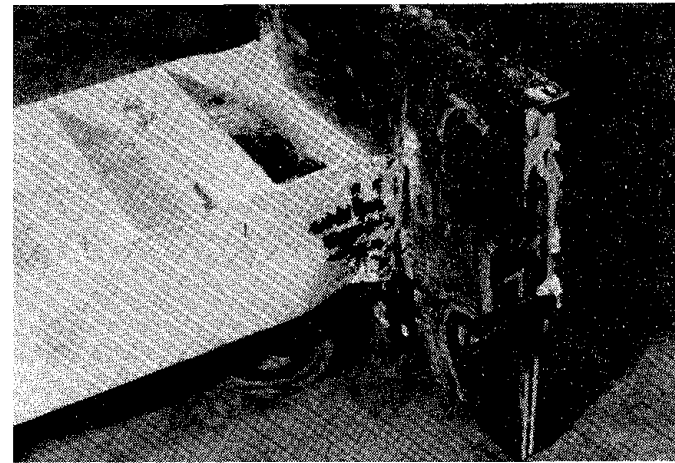
(d) End Region A, North Flange.

Fig. 6.30   Photo of End Regions of Specimen 5 After Test.
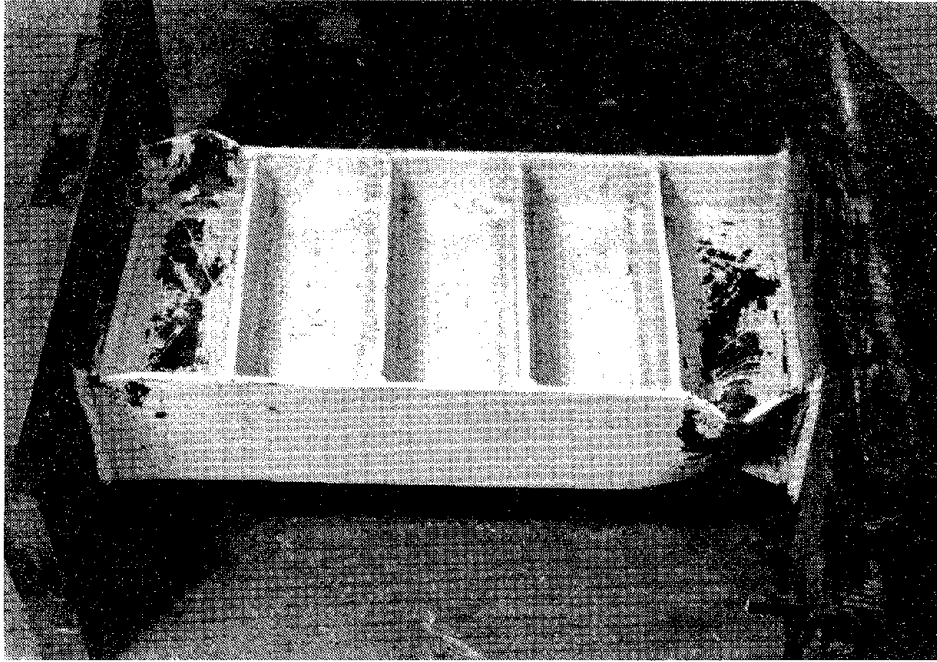
Fig. 6.31   Photo of Specimen 6 at the End of Testing.
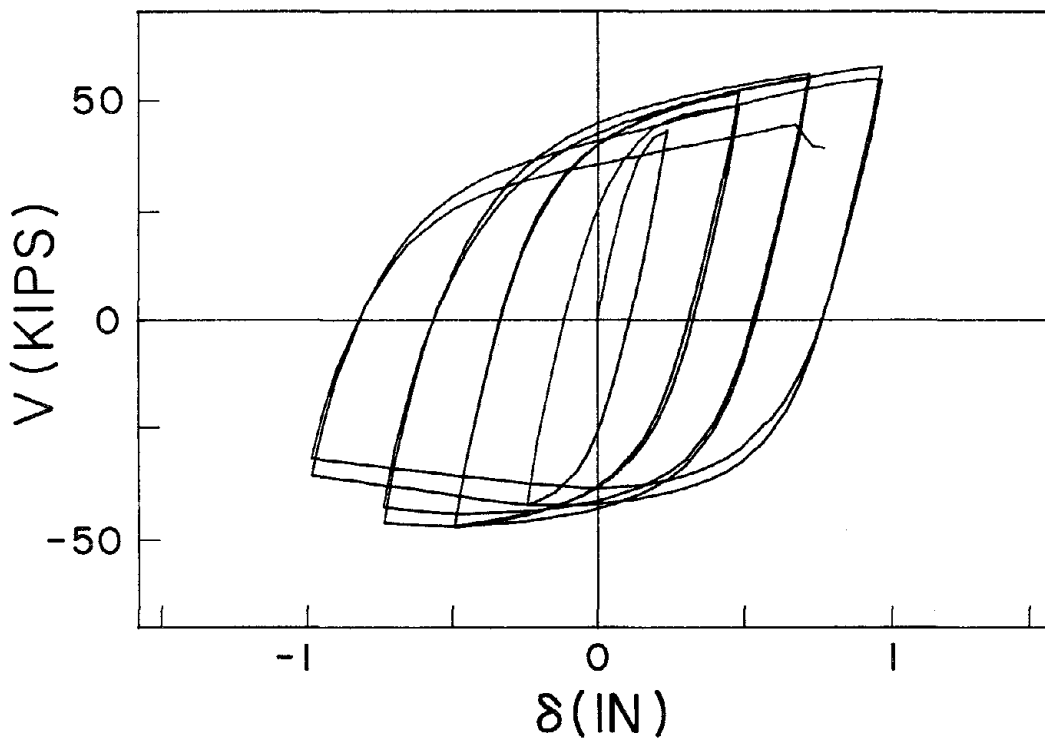
Fig. 6.32   Shear-Displacement Relationship of Specimen 6.
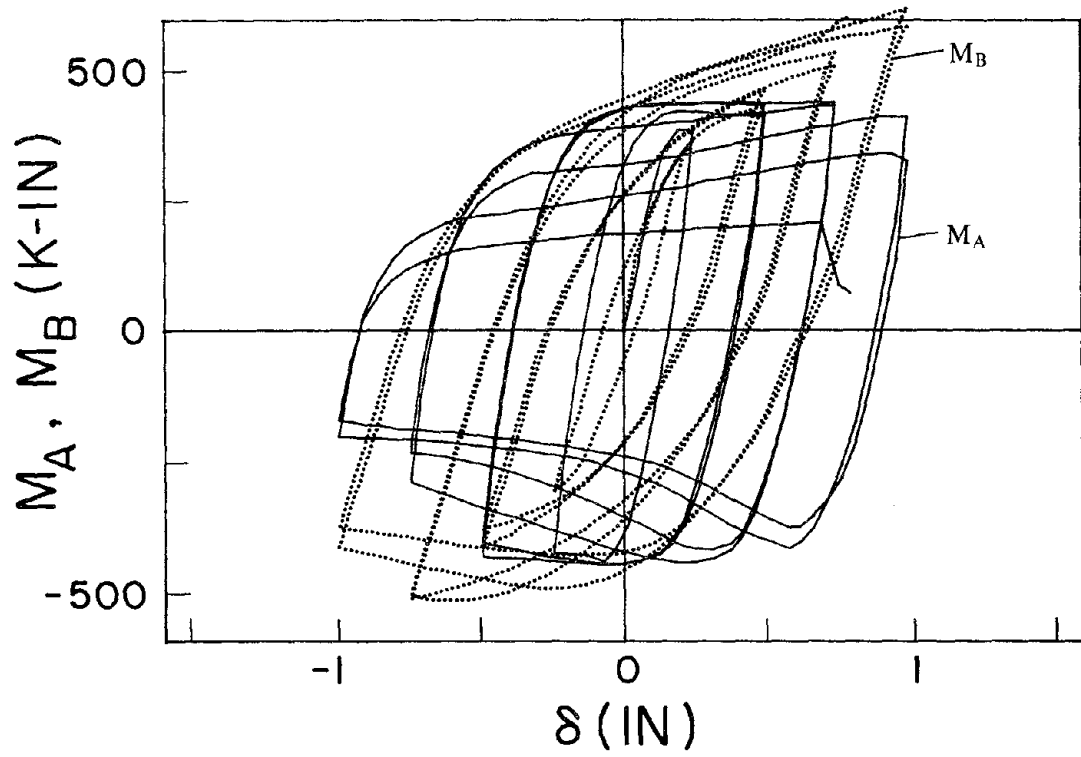
Fig. 6.33   Moment-Displacement Relationship of Specimen 6.
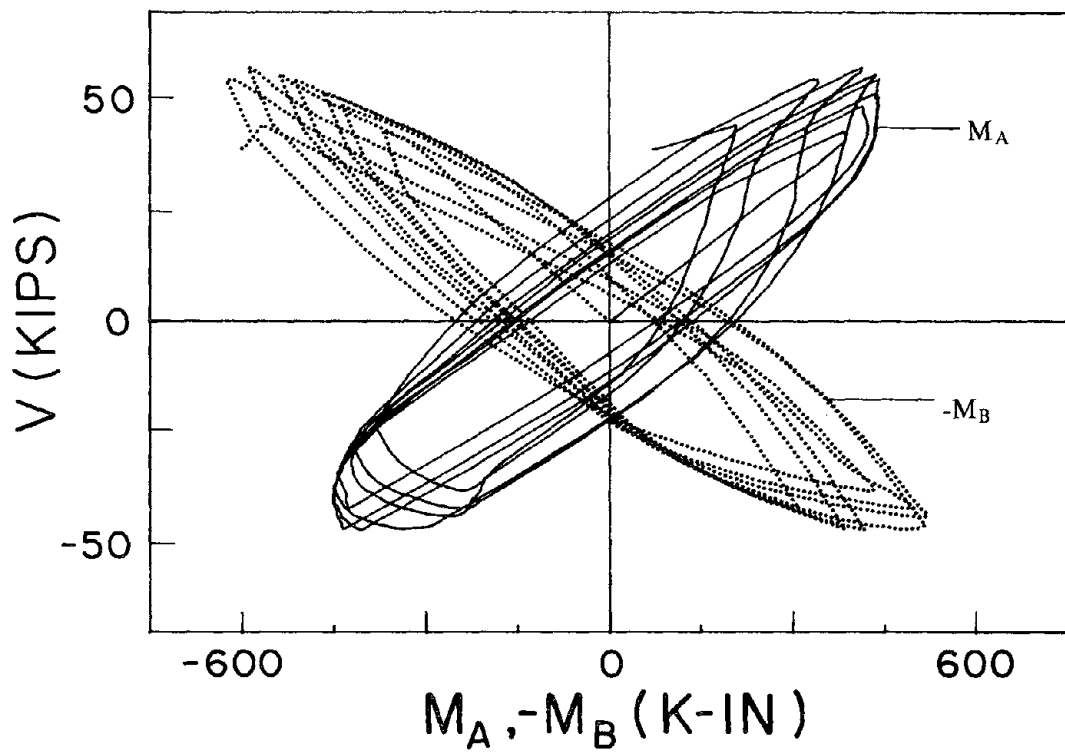
Fig. 6.34   Moment-Shear Relationship of Specimen 6.
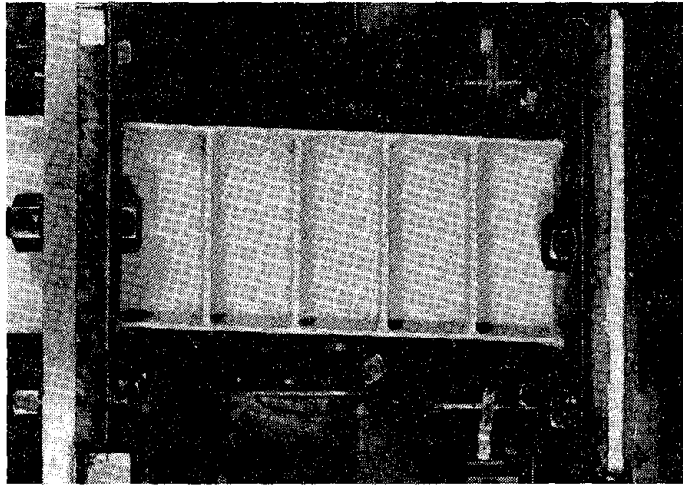
(a) Cycle 4S, at δ=0.75 in.
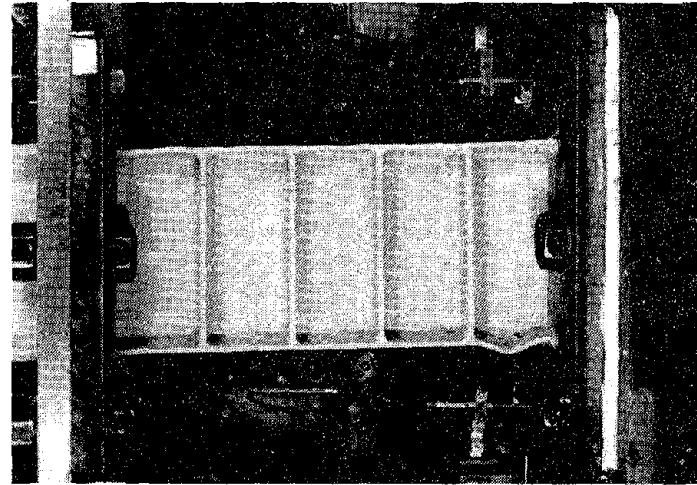
(b) Cycle 4N, at δ=-0.75 in.
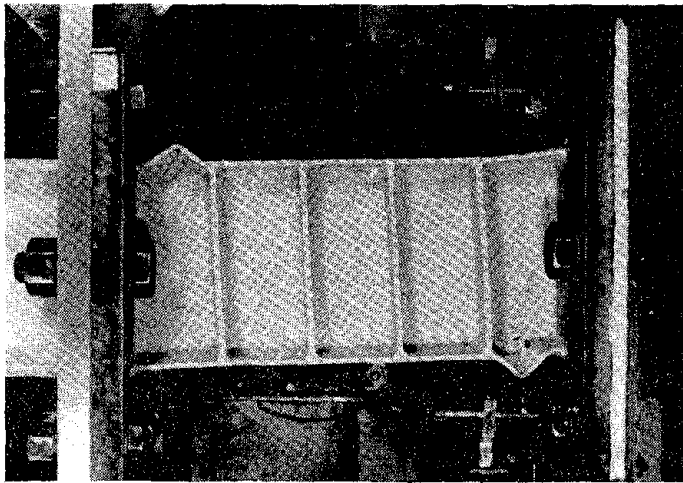
(c) Cycle 6N, at δ=-1.0 in.
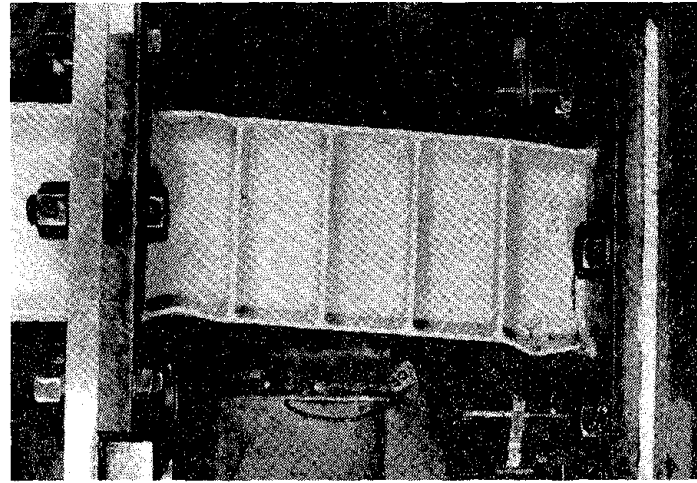
(d) Cycle 7S, at δ=1.0 in.

Fig. 6.35   Photo of Specimen 6 During Test.
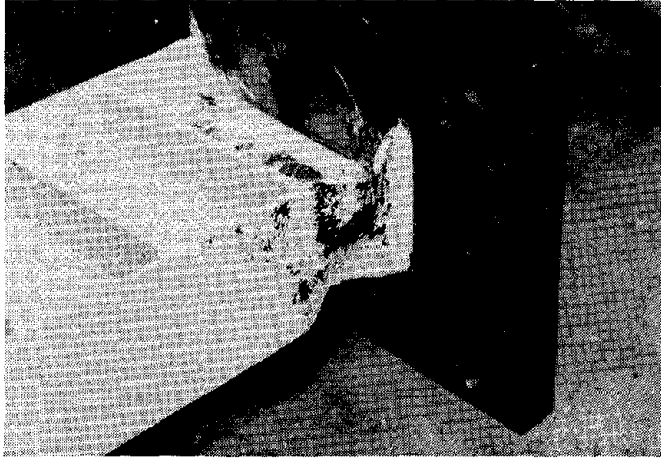
(a) End Region B, South Flange.
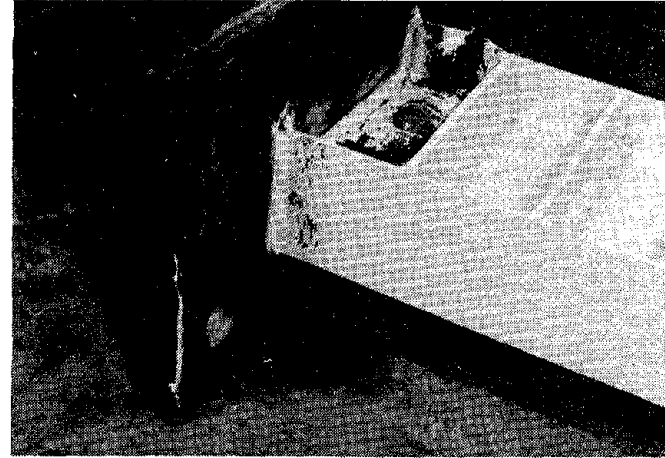
(b) End Region A, South Flange.
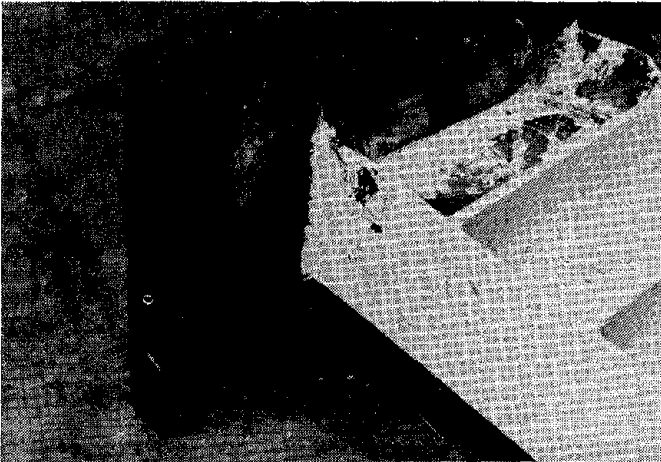
(c) End Region B, North Flange.
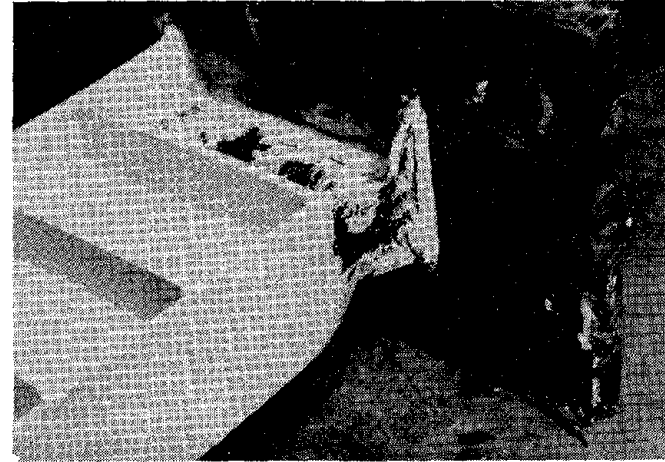
(d) End Region A, North Flange.

Fig. 6.36   Photo of End Regions of Specimen 6 After Test.
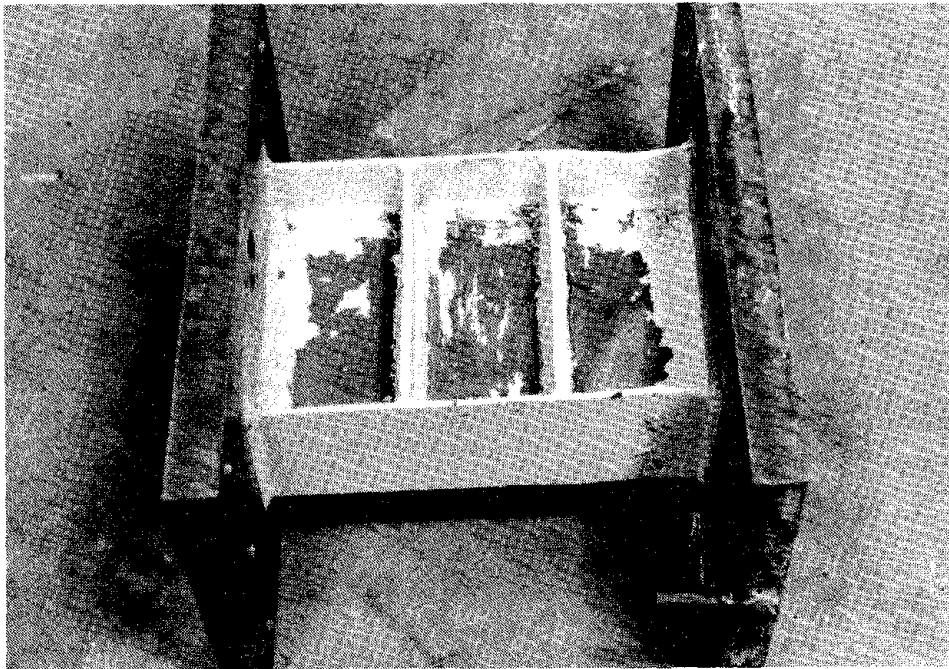
Fig. 6.37   Photo of Specimen 7 at the End of Testing.
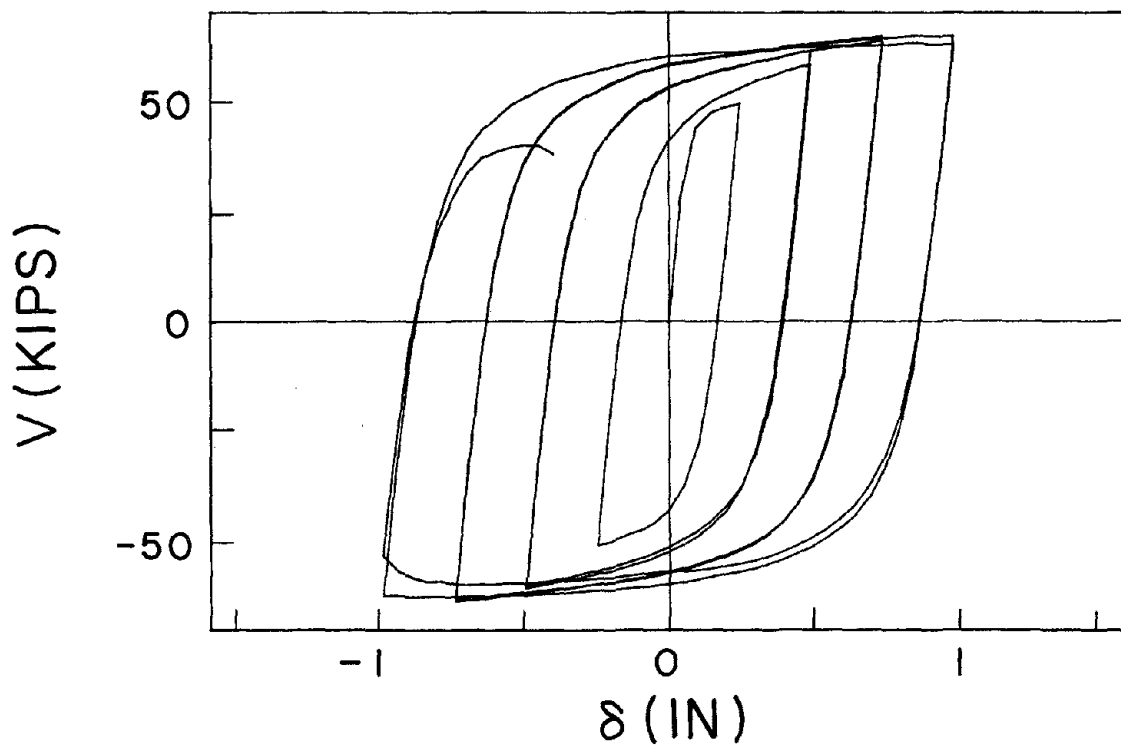
Fig. 6.38   Shear-Displacement Relationship of Specimen 7.
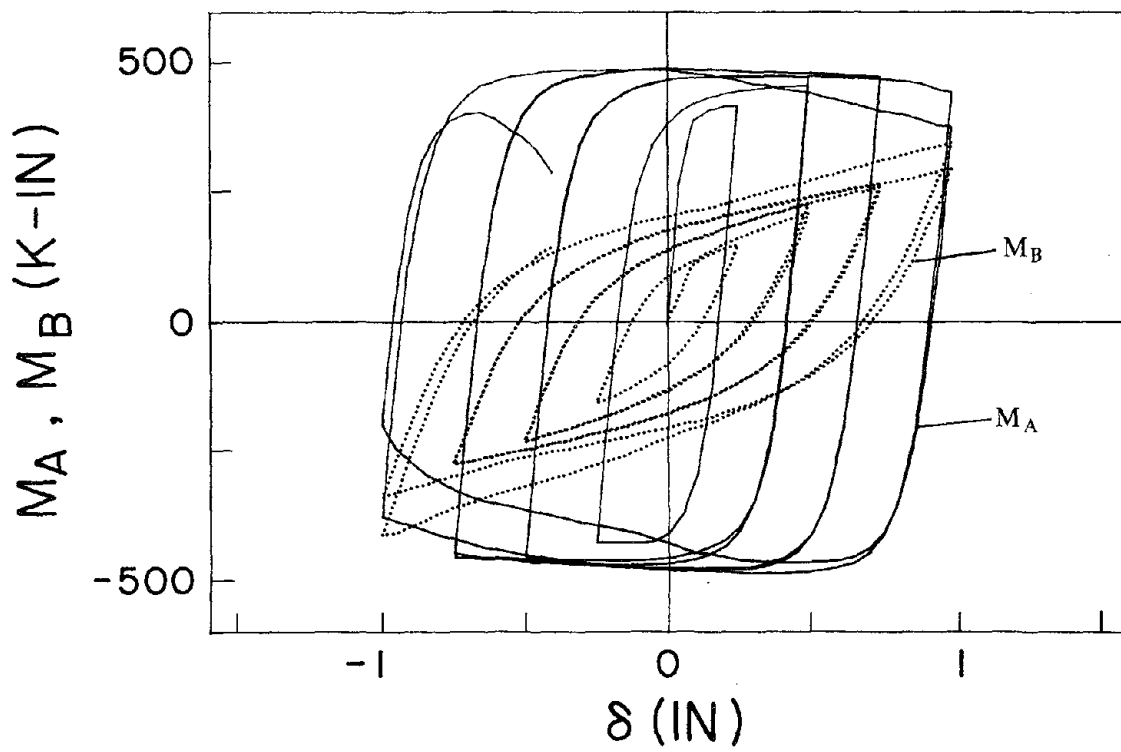
Fig. 6.39   Moment-Displacement Relationship of Specimen 7.
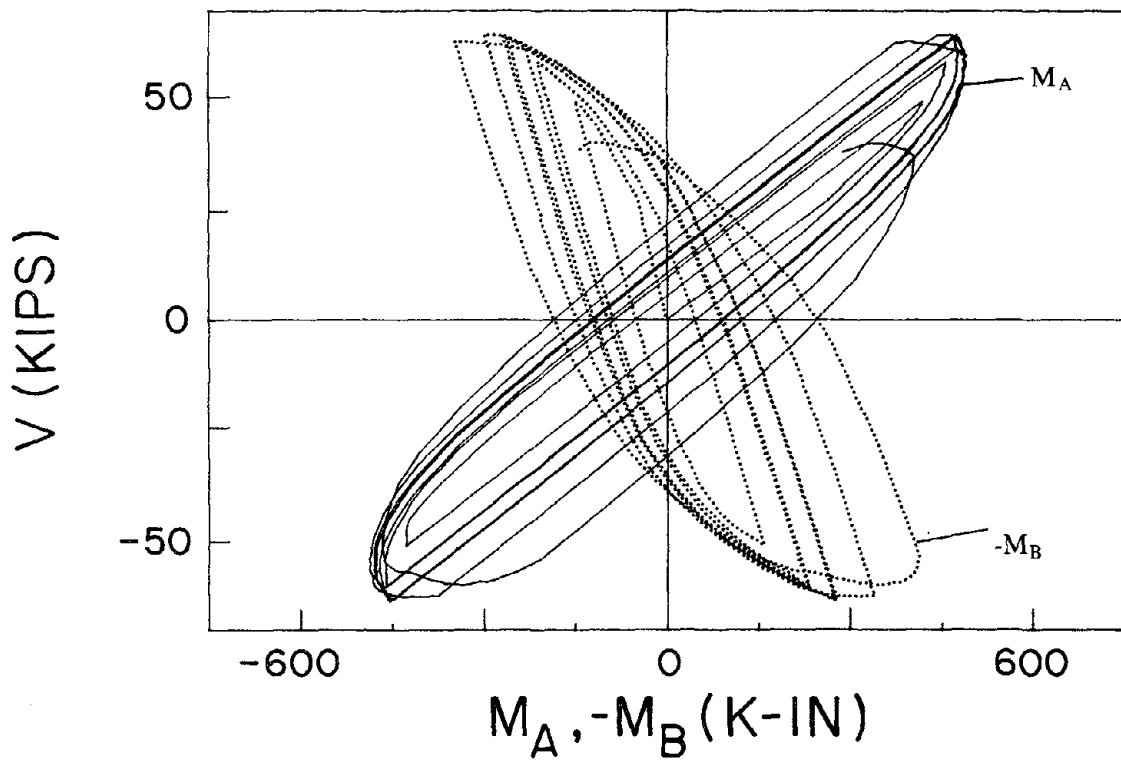
Fig. 6.40   Moment-Shear Relationship of Specimen 7.
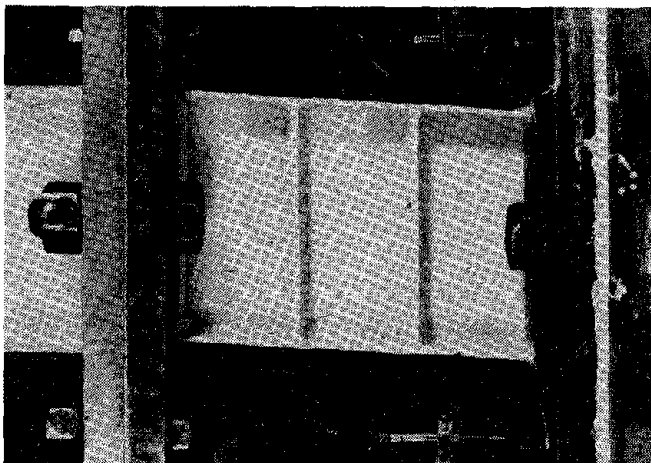
(a) Cycle 4S, at δ=0.75 in.
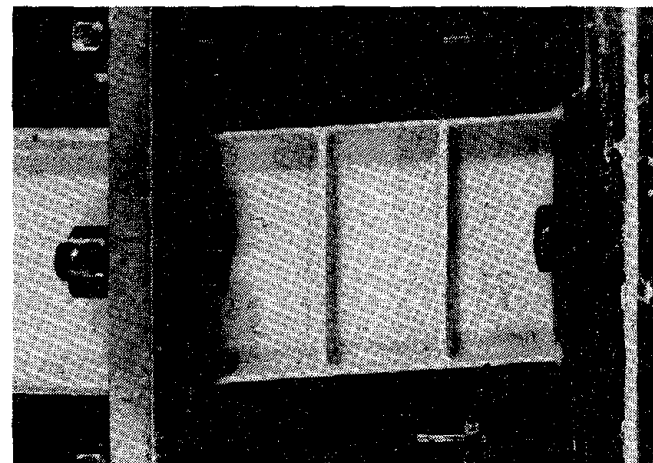
(b) Cycle 4N, at δ=-0.75 in.
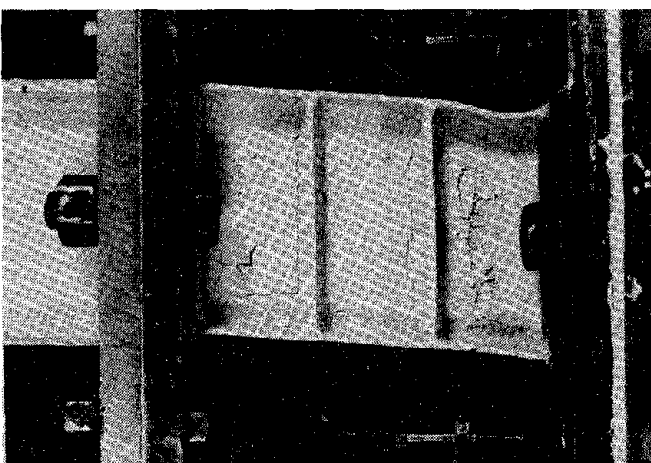
(c) Cycle 6S, at δ=1.0 in.
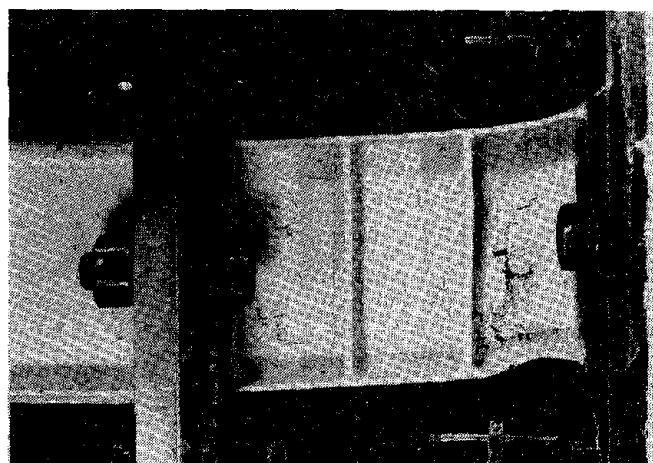
(d) Cycle 7N, at δ=-1.0 in.

Fig. 6.41   Photo of Specimen 7 During Test.
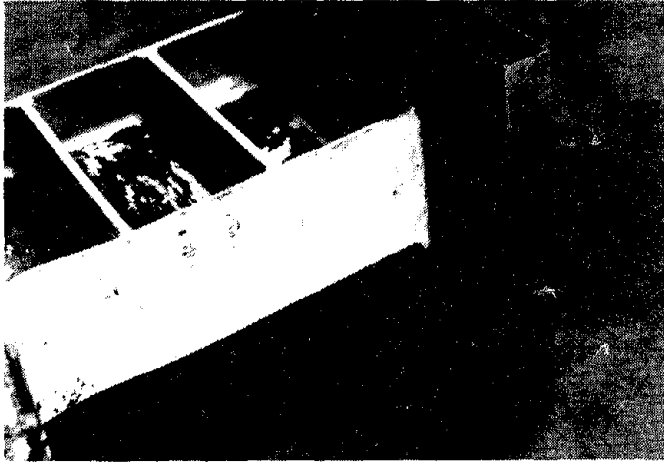
(a) End Region B, South Flange.
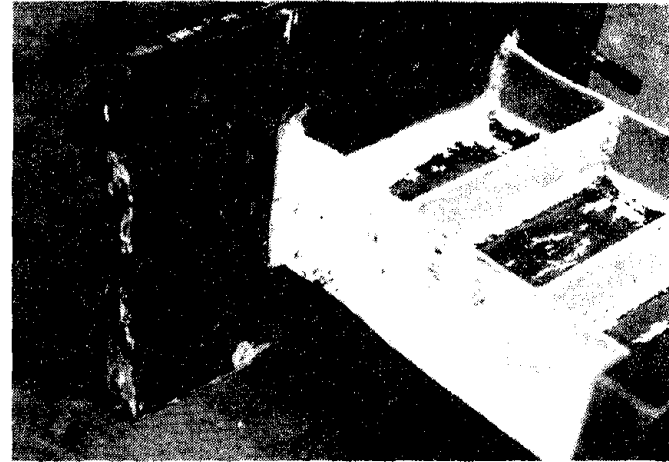
(b) End Region A, South Flange.
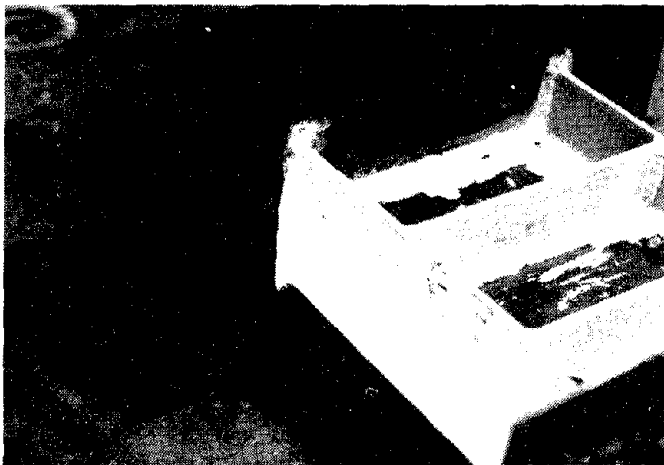
(c) End Region B, North Flange.
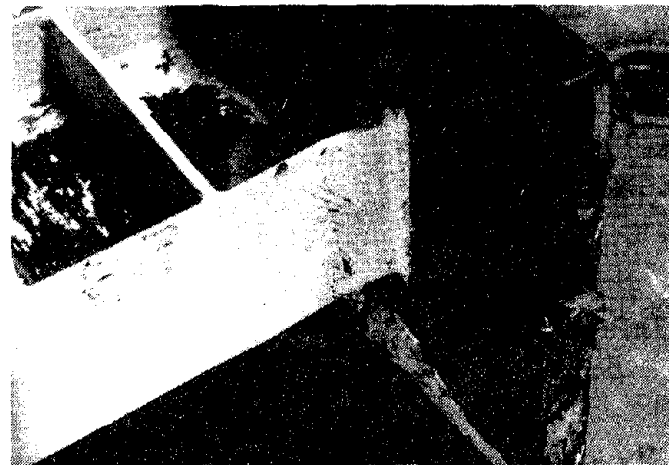
(d) End Region A, North Flange.

Fig. 6.42   Photo of End Regions of Specimen 7 After Test.
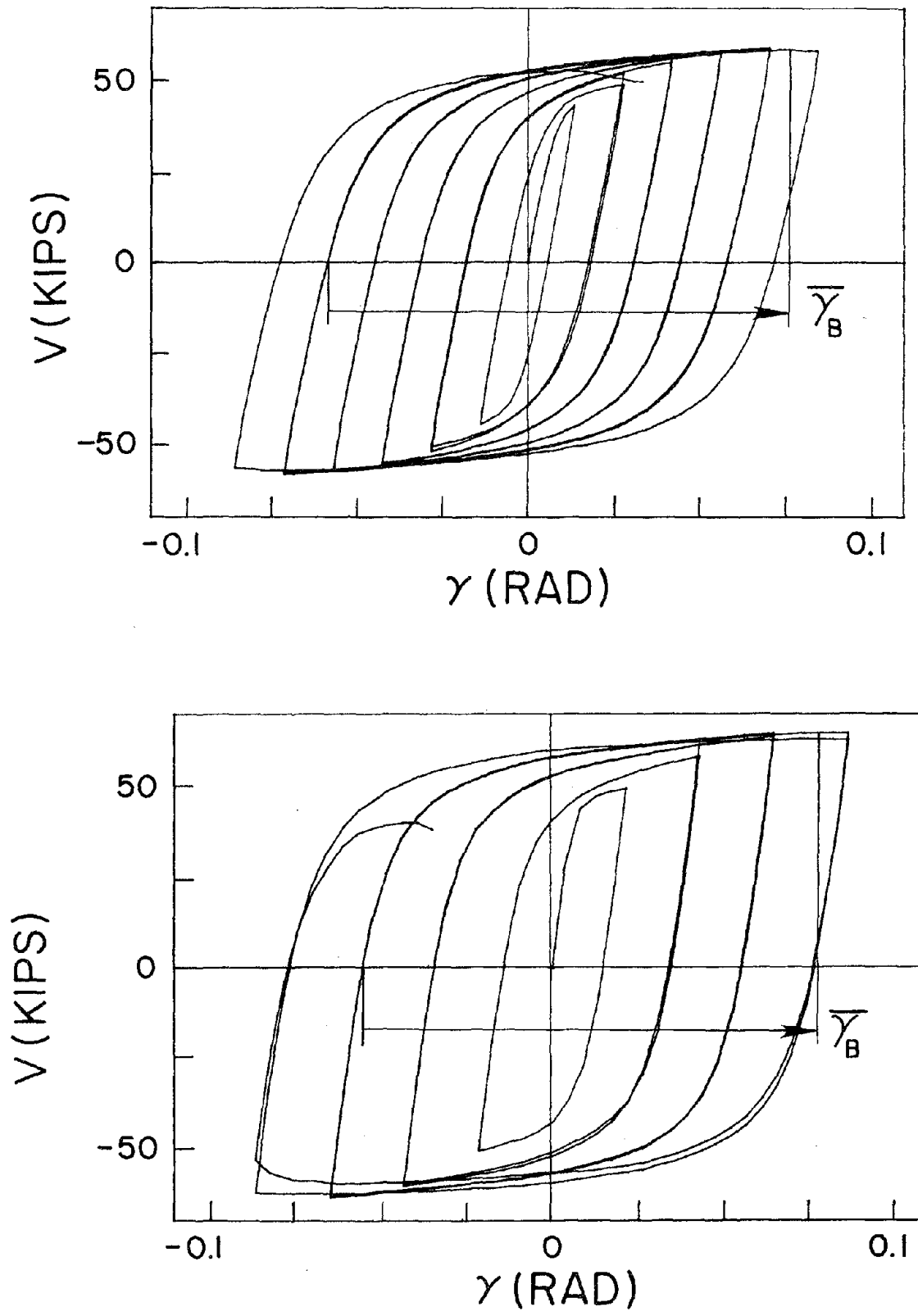
Fig. 6.43 Comparison of $V-\gamma$ History of
(a) Long Shear Link, and (b) Short Shear Link.
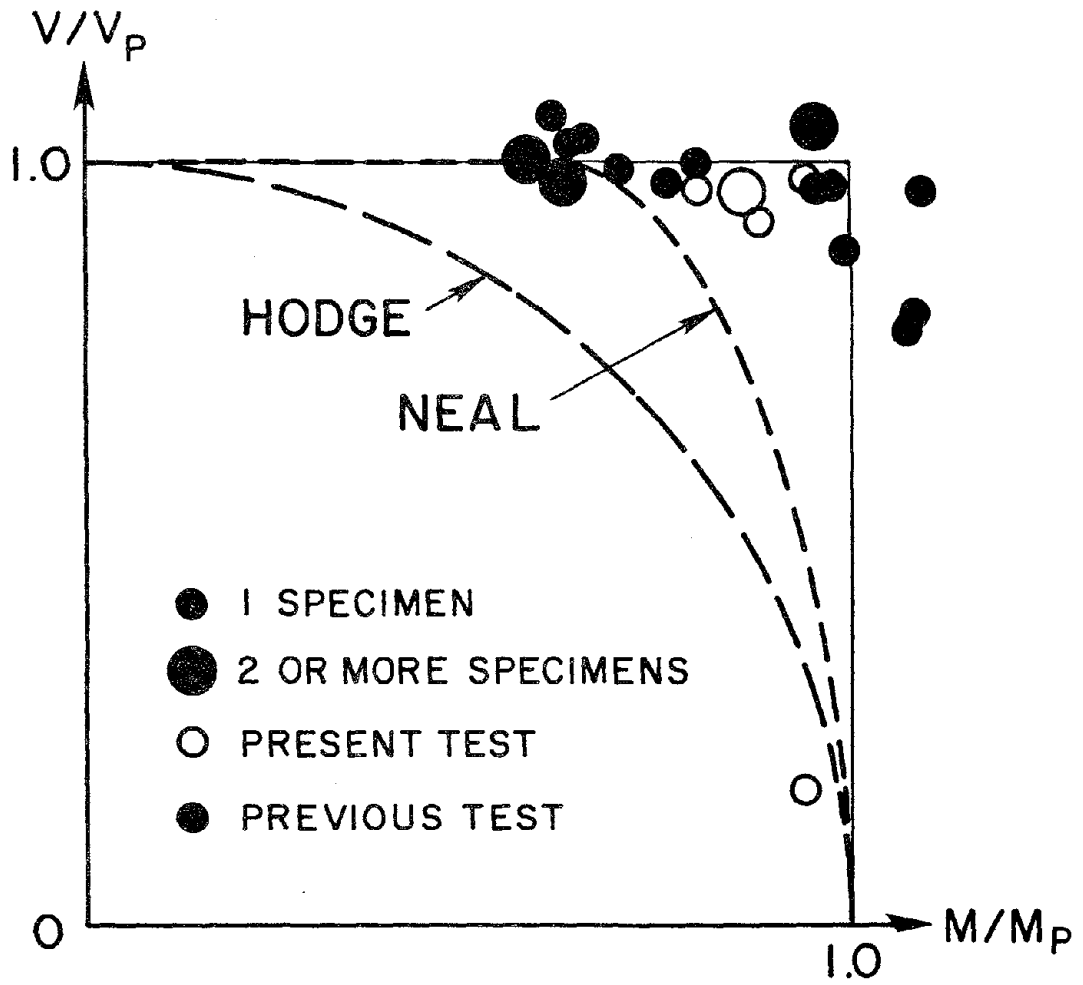
Fig. 7.1   M-V Interaction Plots for 26 Links.
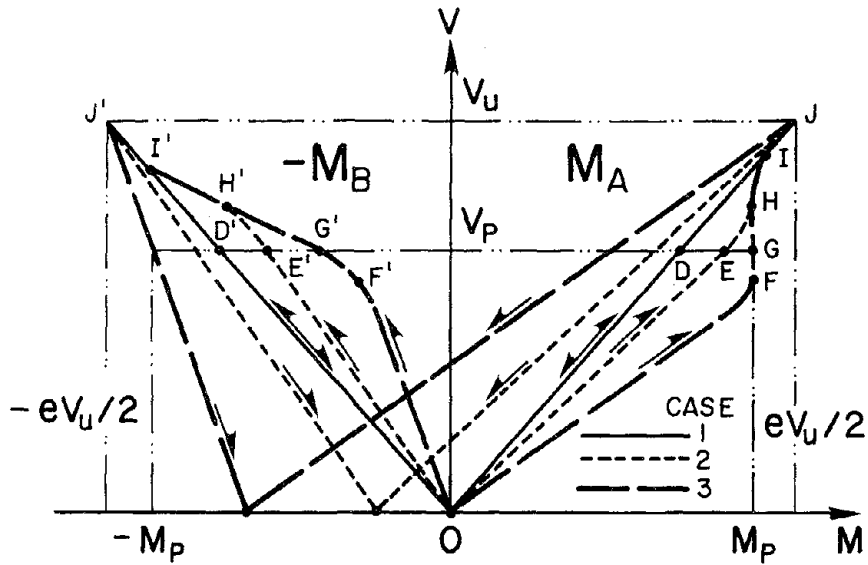
(a)
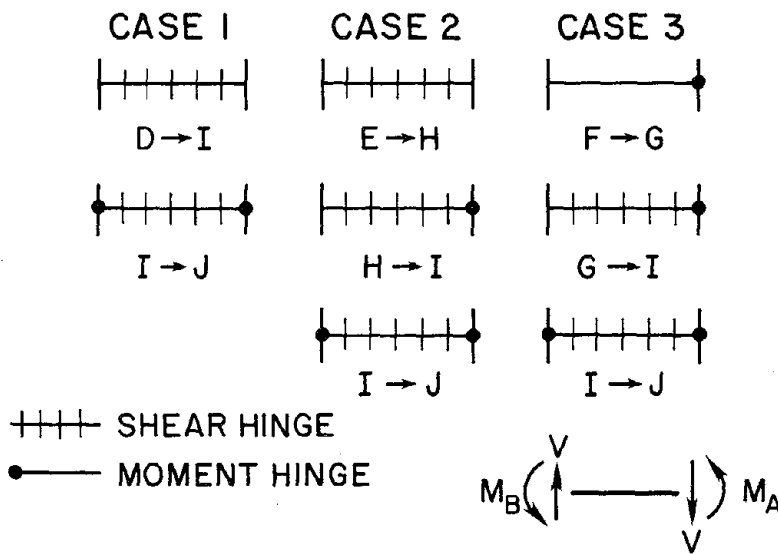
(b)

Fig. 7.2   (a) Idealized M-V Relationships for Links With Initially Equal or Different End Moments, and (b) Sequence of Hinge Formation.
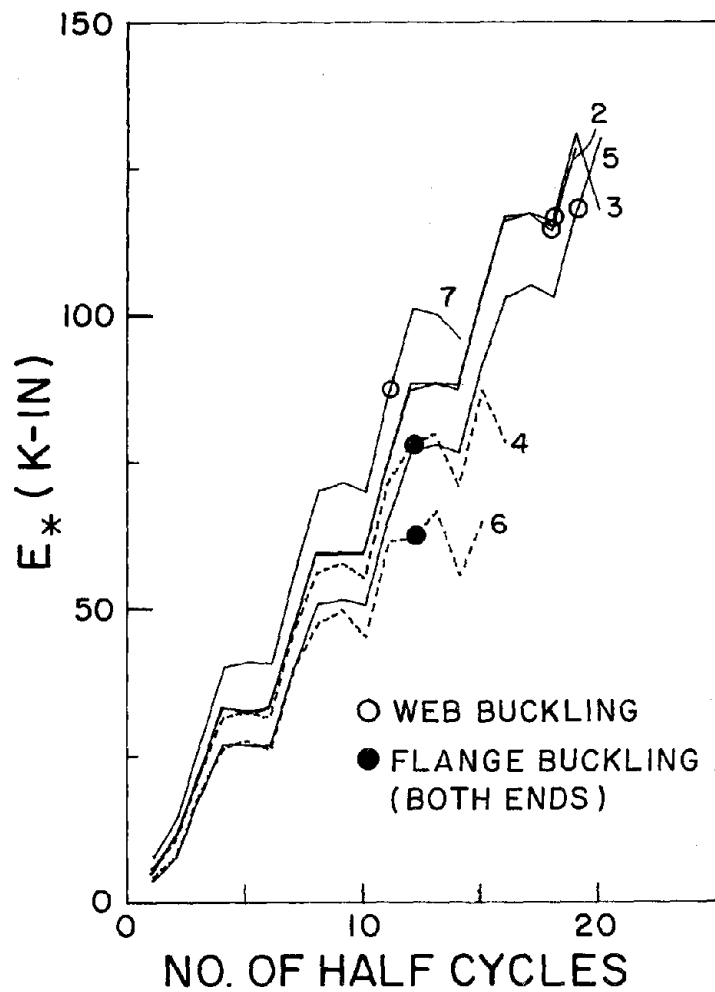
Fig. 7.3　Link Energy Dissipation per Cycle vs. Number of Half Cycles.
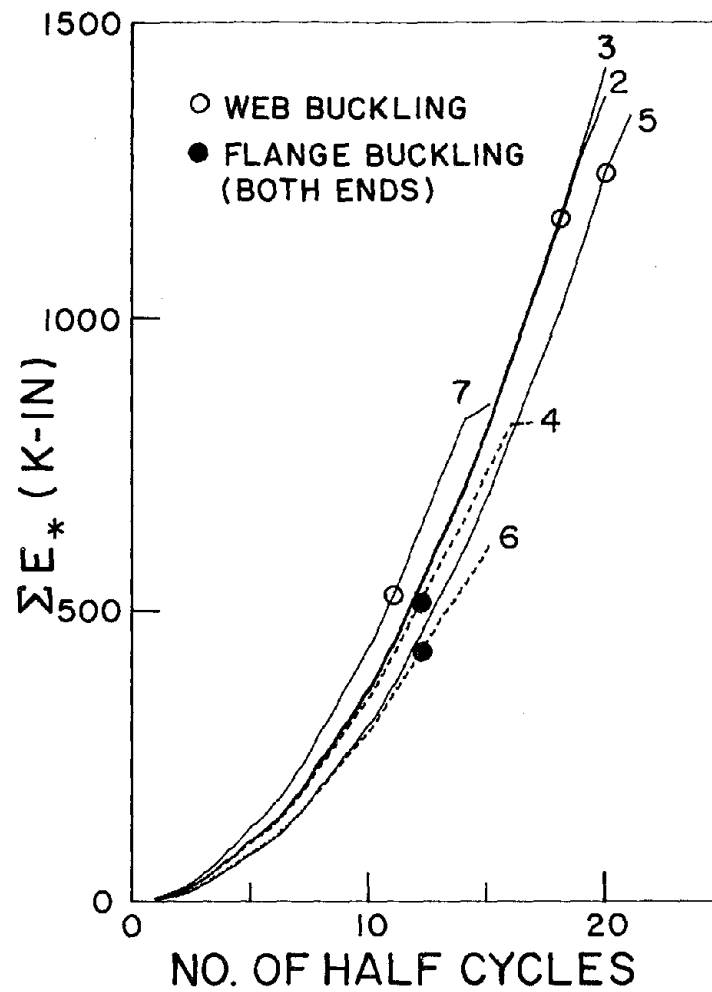
Fig. 7.4　Summation of Link Energy Dissipation vs. Number of Half Cycles.
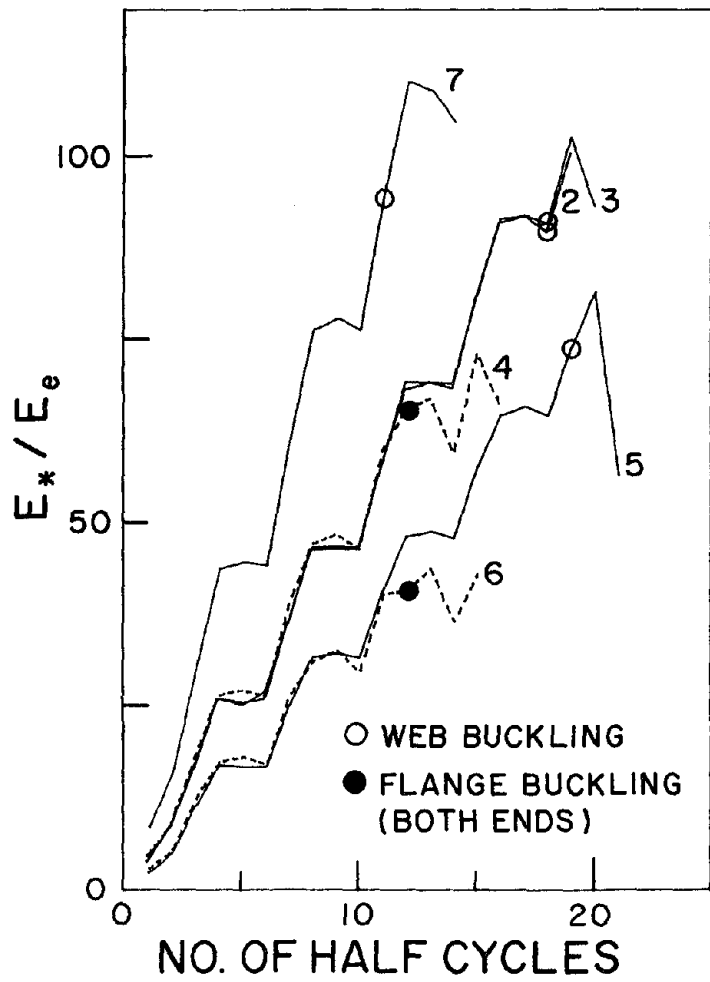
Fig. 7.5   Ratio of E_*/E_e vs. Number of Half Cycles.
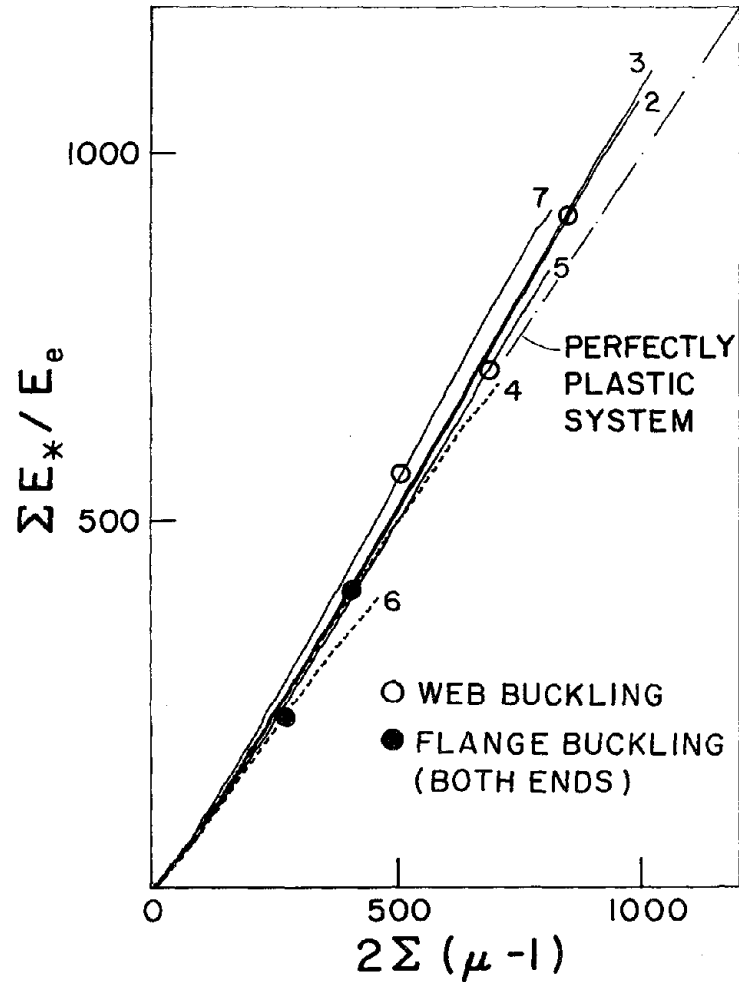
Fig. 7.6   Ratio of $\sum E_*/E_e$ vs. $2\sum(\mu-1)$.
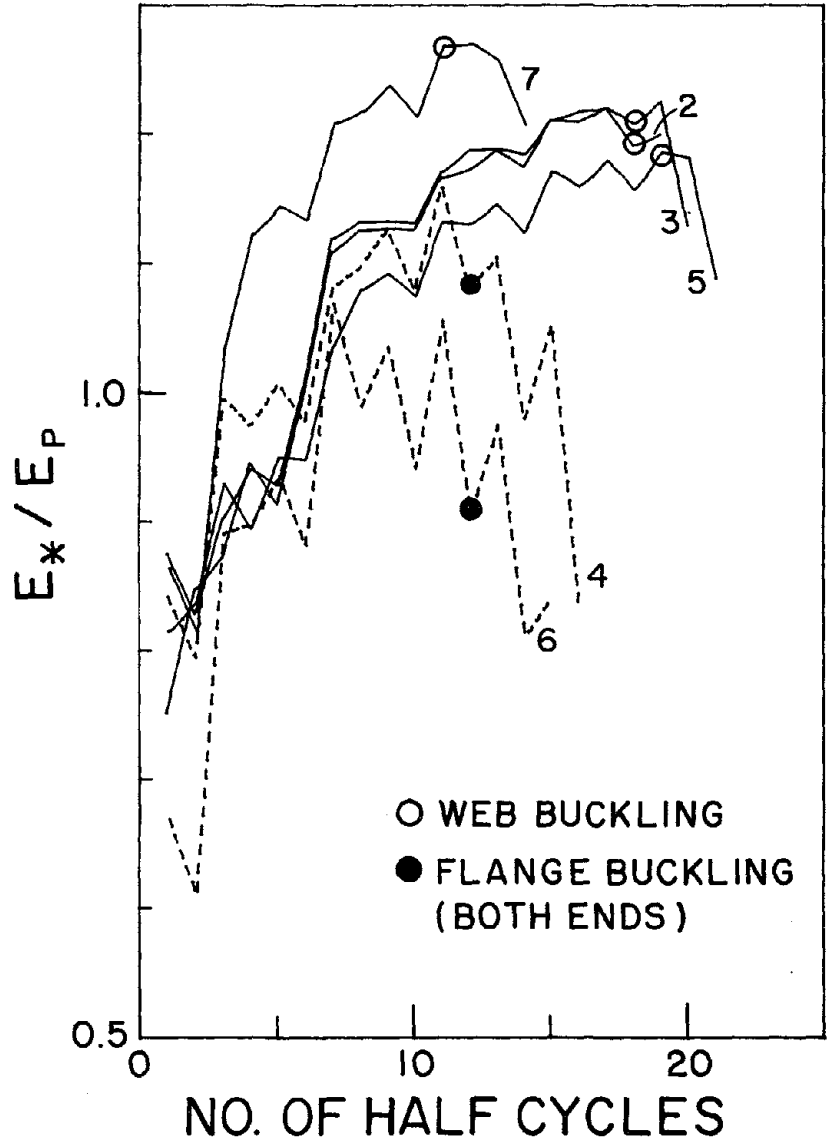
Fig. 7.7   Ratio of E_*/E_p vs. Number of Half Cycles.
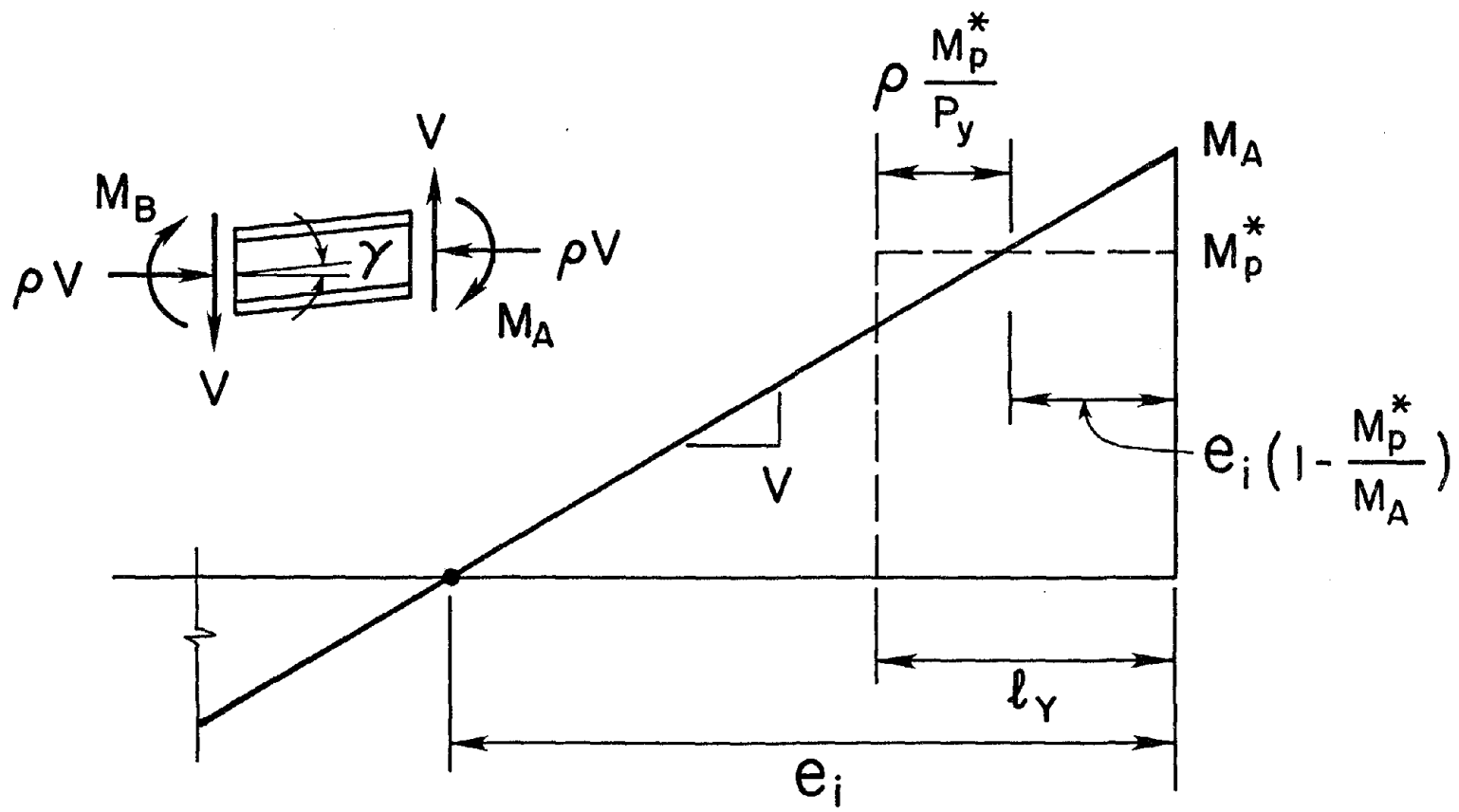
Fig. 7.8   Estimate of Shear Link Flange Yield Zone Length.
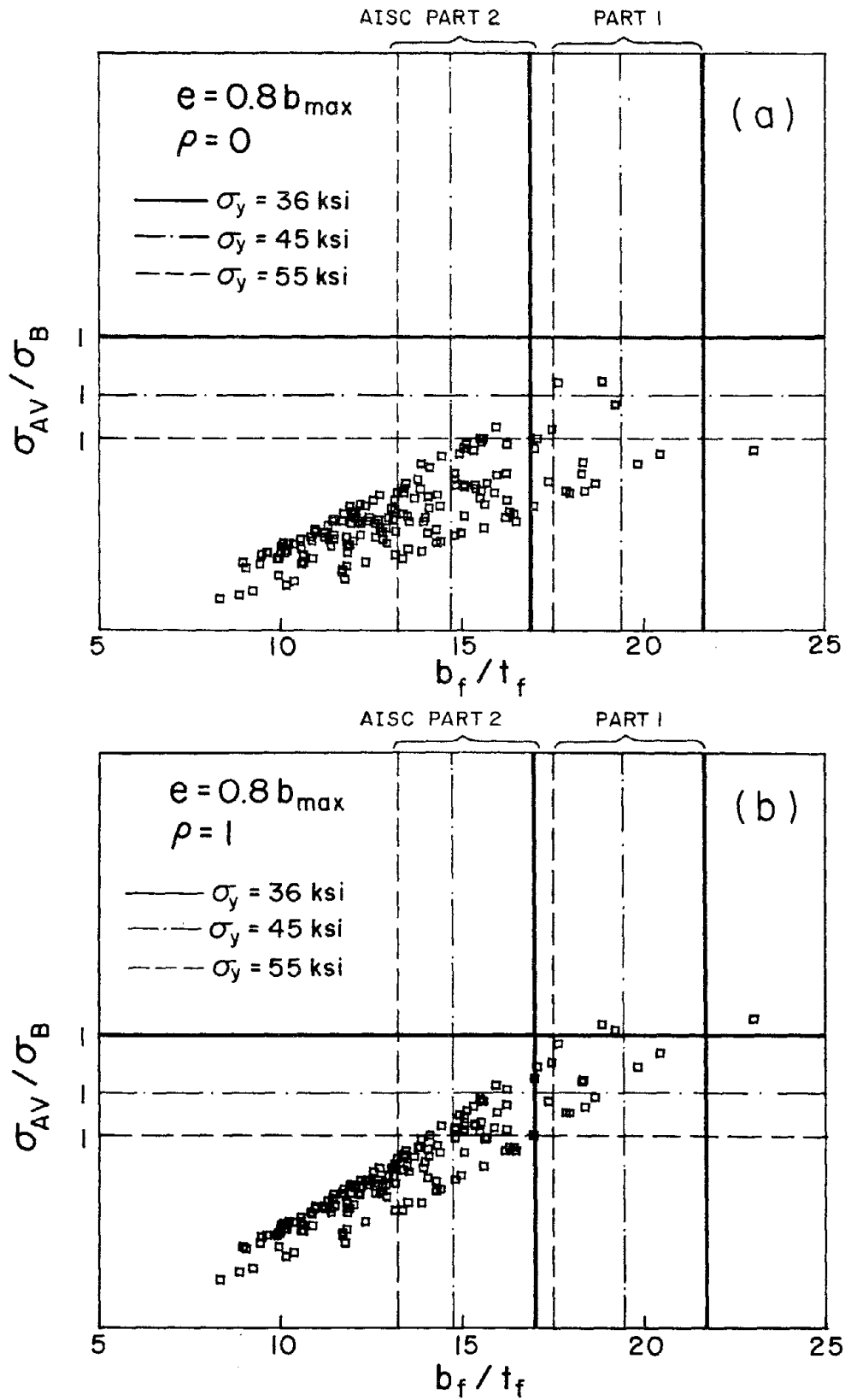
Fig. 7.9   Flange Buckling of 156 Selected Sections for Shear Link having $e = 0.8b_{max}$.
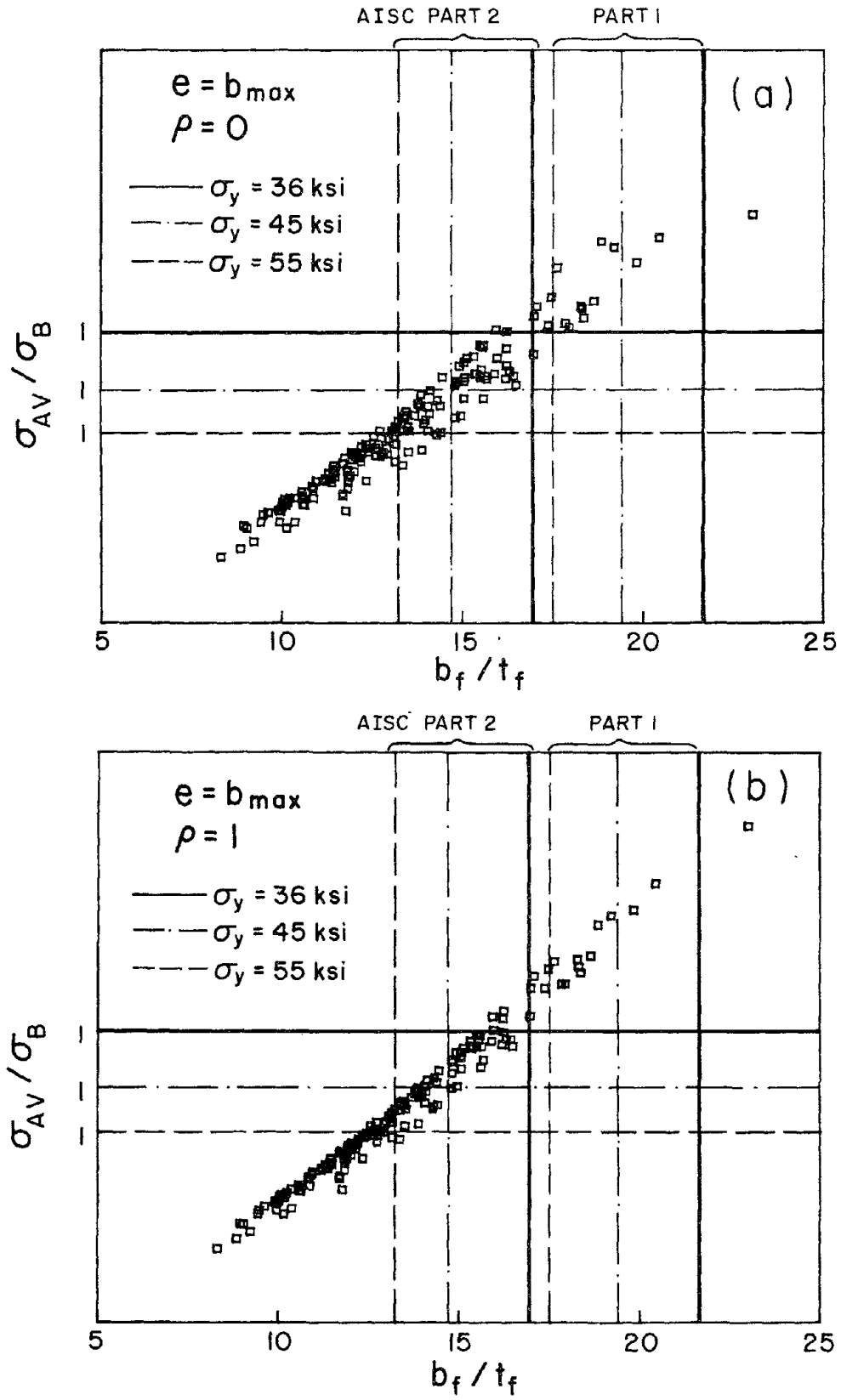
Fig. 7.10   Flange Buckling of 156 Selected Sections for Shear Link having $e = b_{max}$.
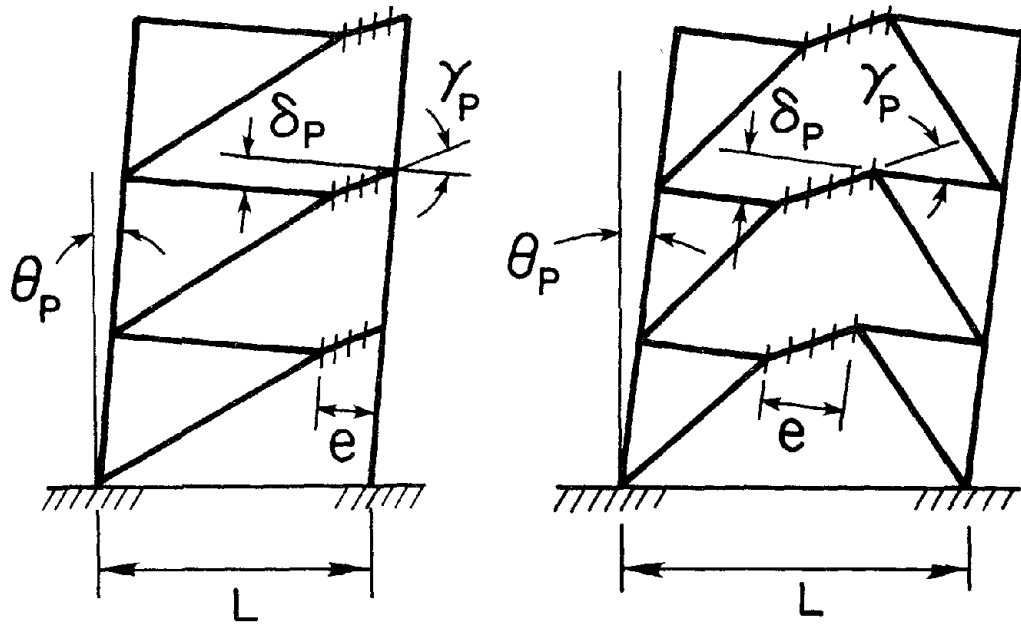
(a)
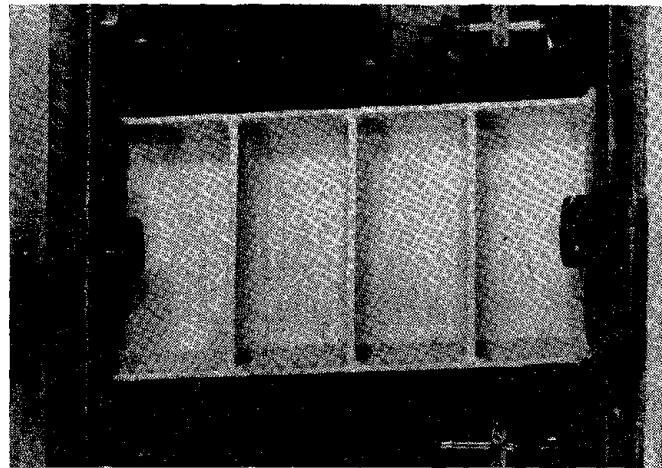
(b)

Fig. 8.1   (a) Typical Energy Dissipation Mechanisms of EBFs at Large Displacement, and
(b) Typical Shear Link Inelastic Deformation (Specimen C3)
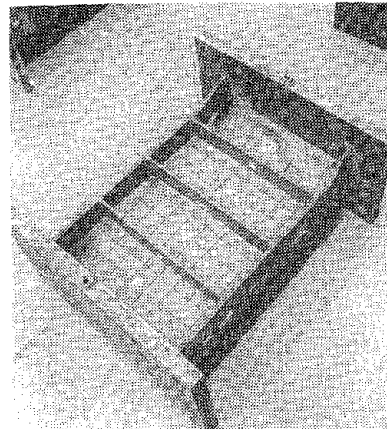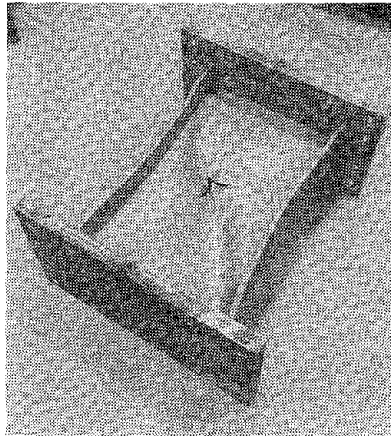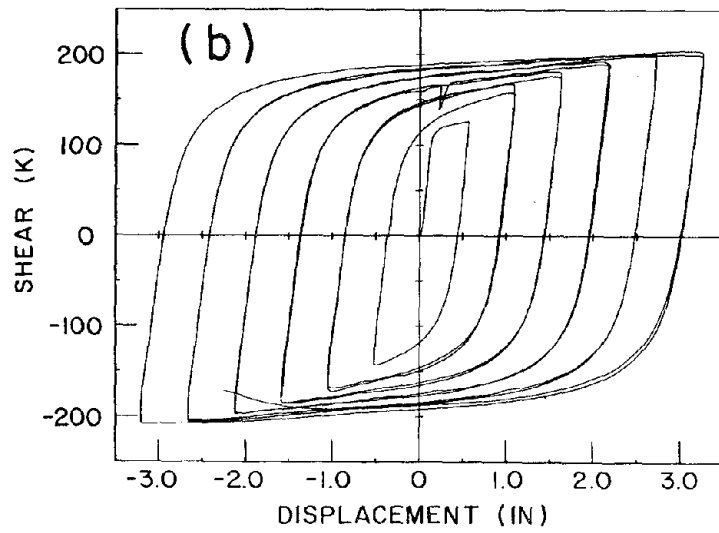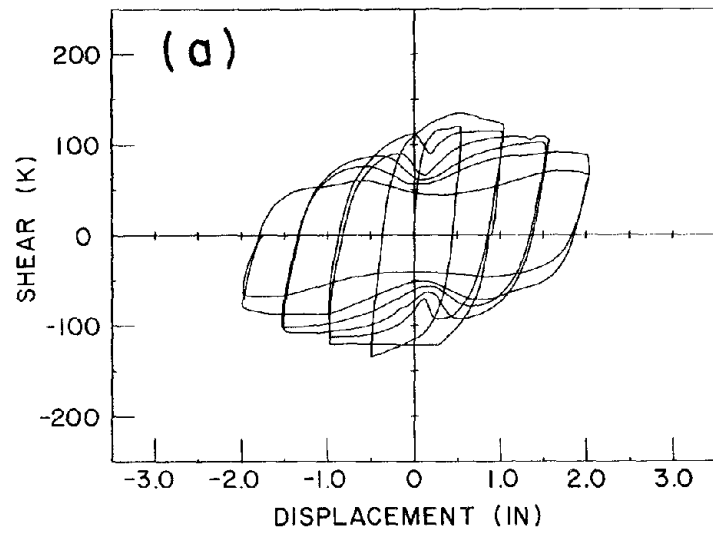
Fig. 8.2   Hysteretic Behavior and Failure Patterns of
(a) Unstiffened Shear Link (Specimen A1), and
(b) Stiffened Shear Link (Specimen A4)

(a)

(b)

(c)
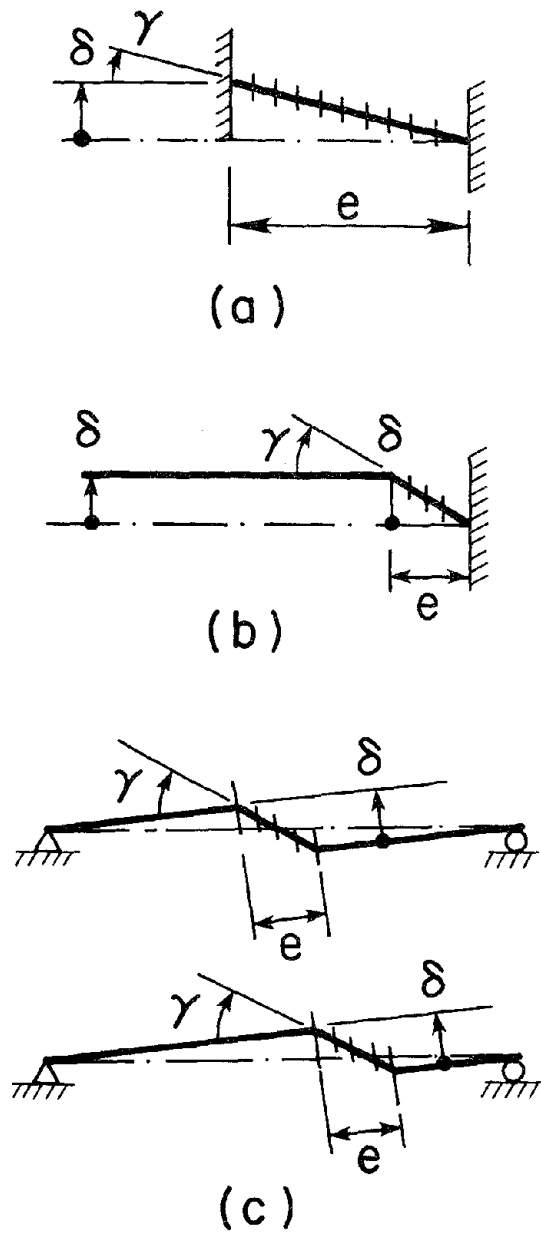
Fig. 8.3   Different Experimental Setups for
Shear Link Tests
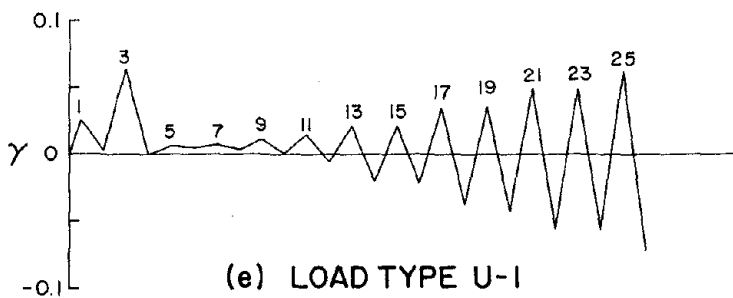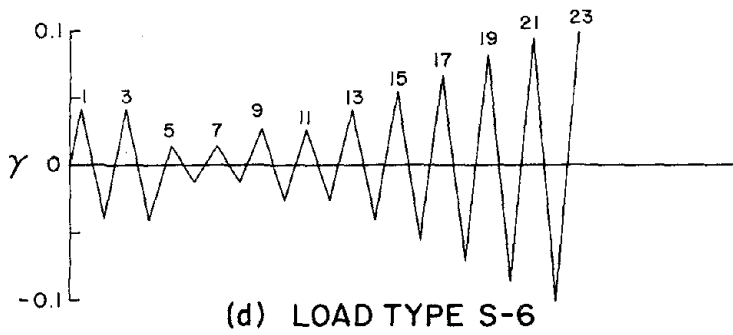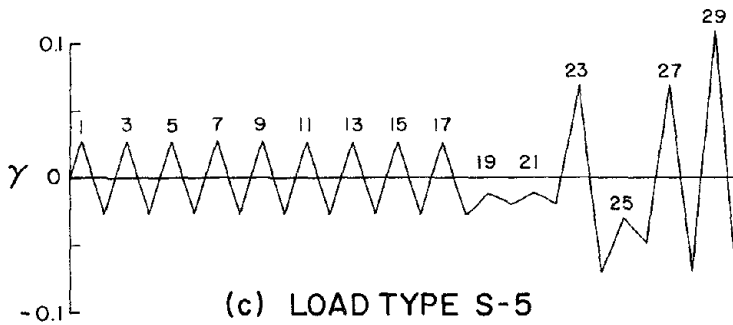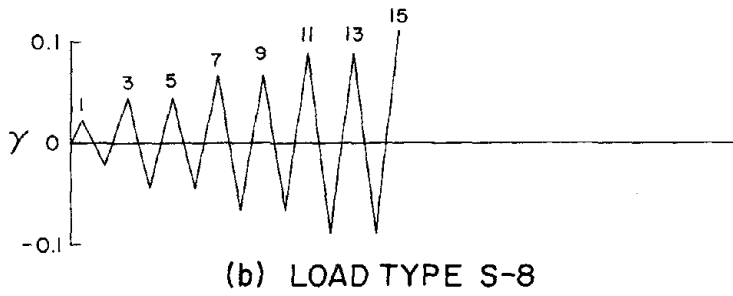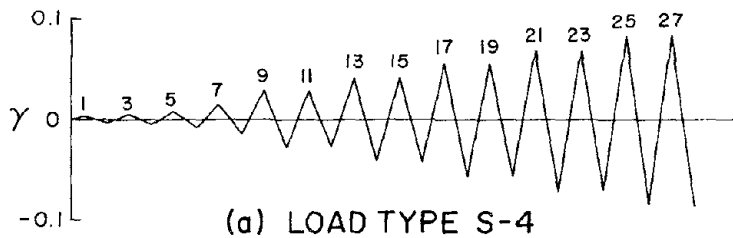
Fig. 8.4   Example of γ-histories Employed for
           Shear Link Tests
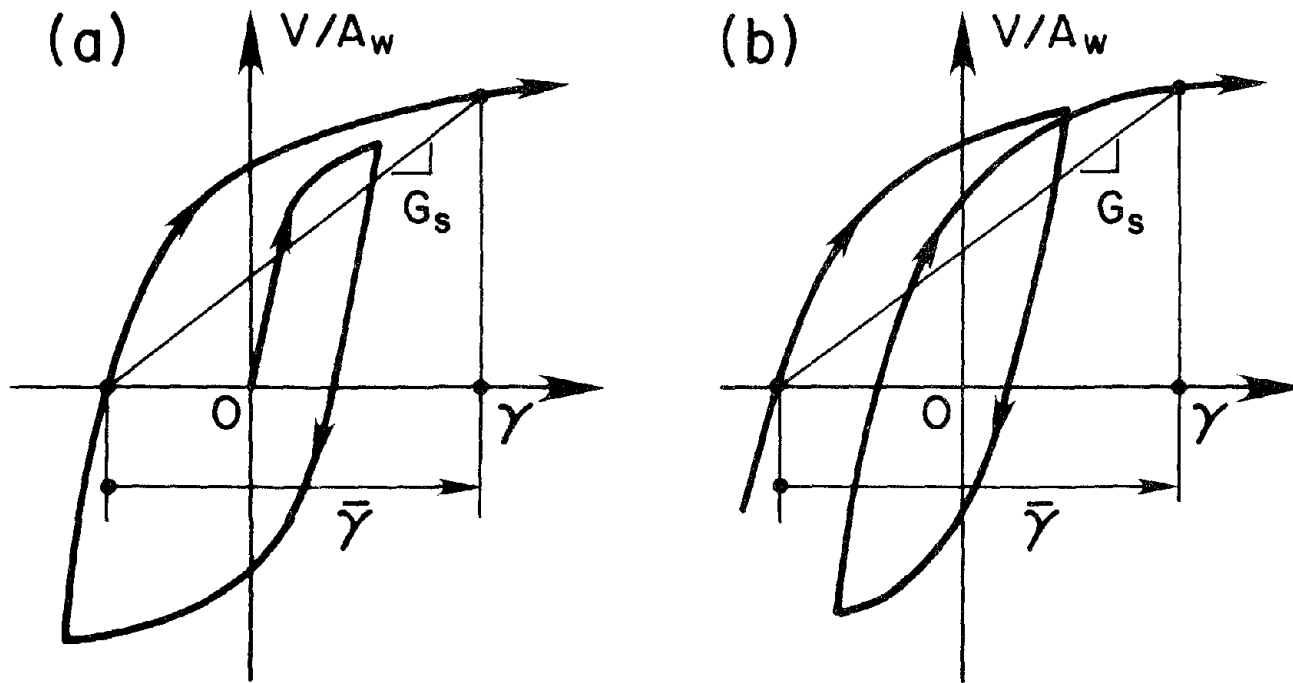
Fig. 8.5   Measure of Link Deformation Angle $\bar{\gamma}$
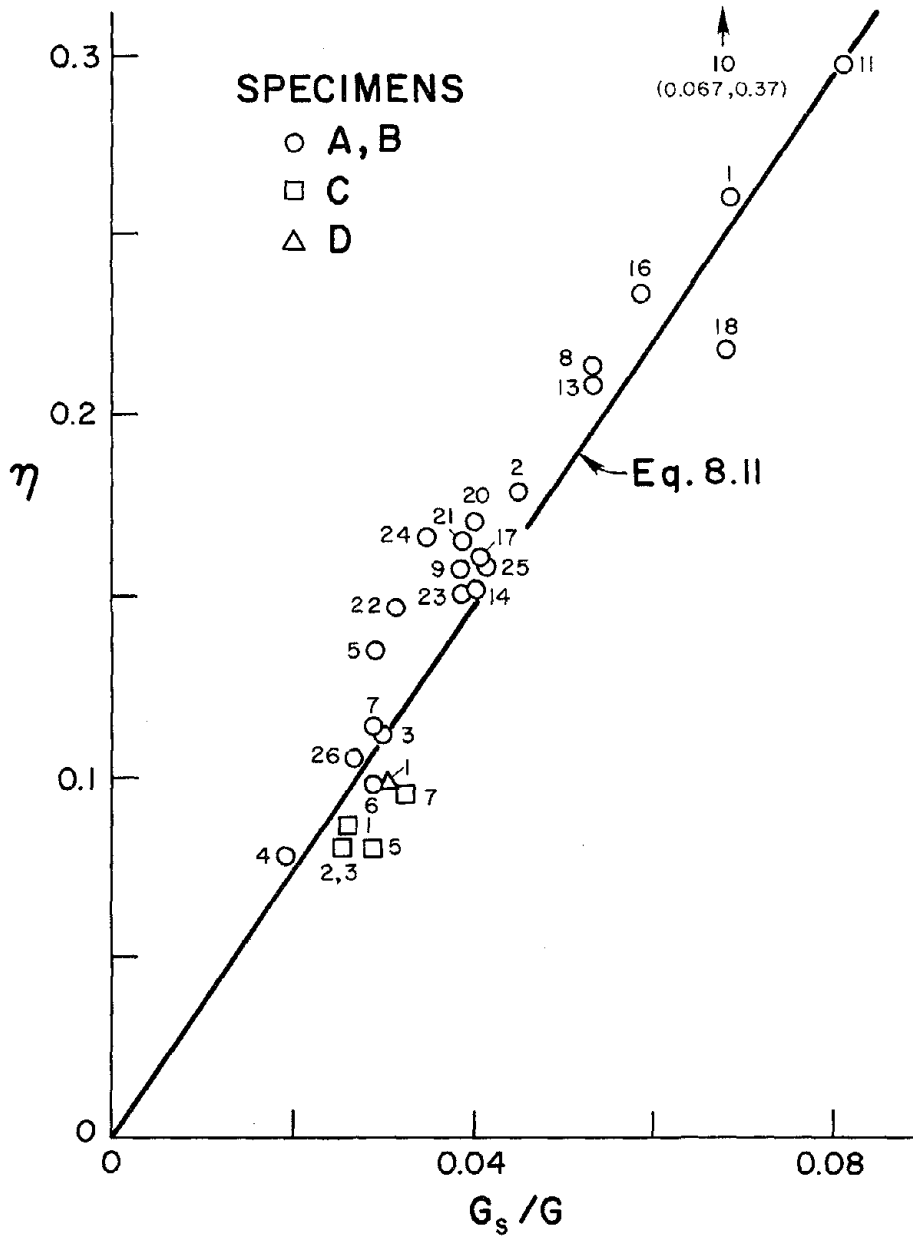
Fig. 8.6   Experimental Relationships Between G_s/G and η
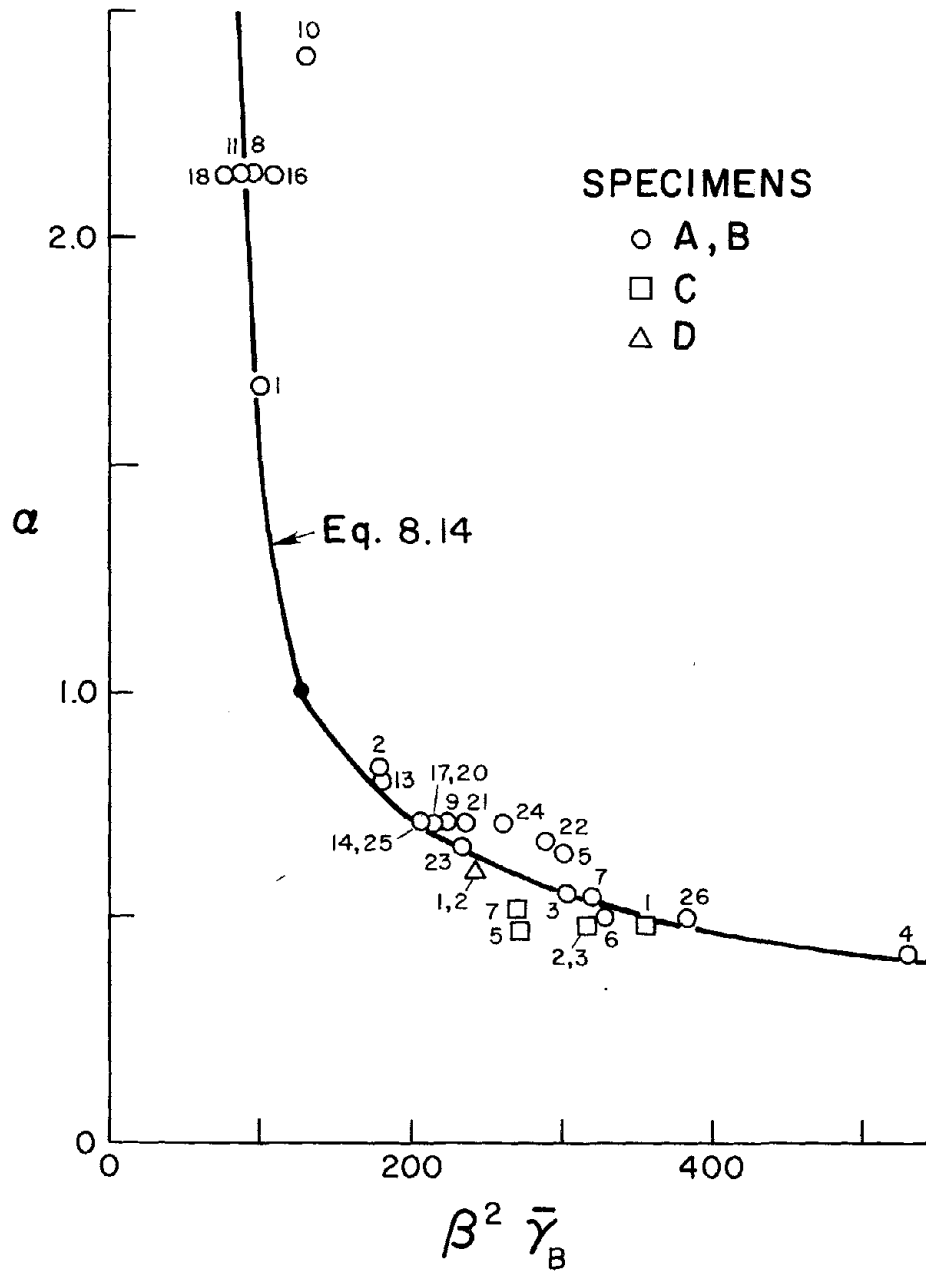
Fig. 8.7   Experimental Relationships Between α and $\beta^2\bar{\gamma}_B$
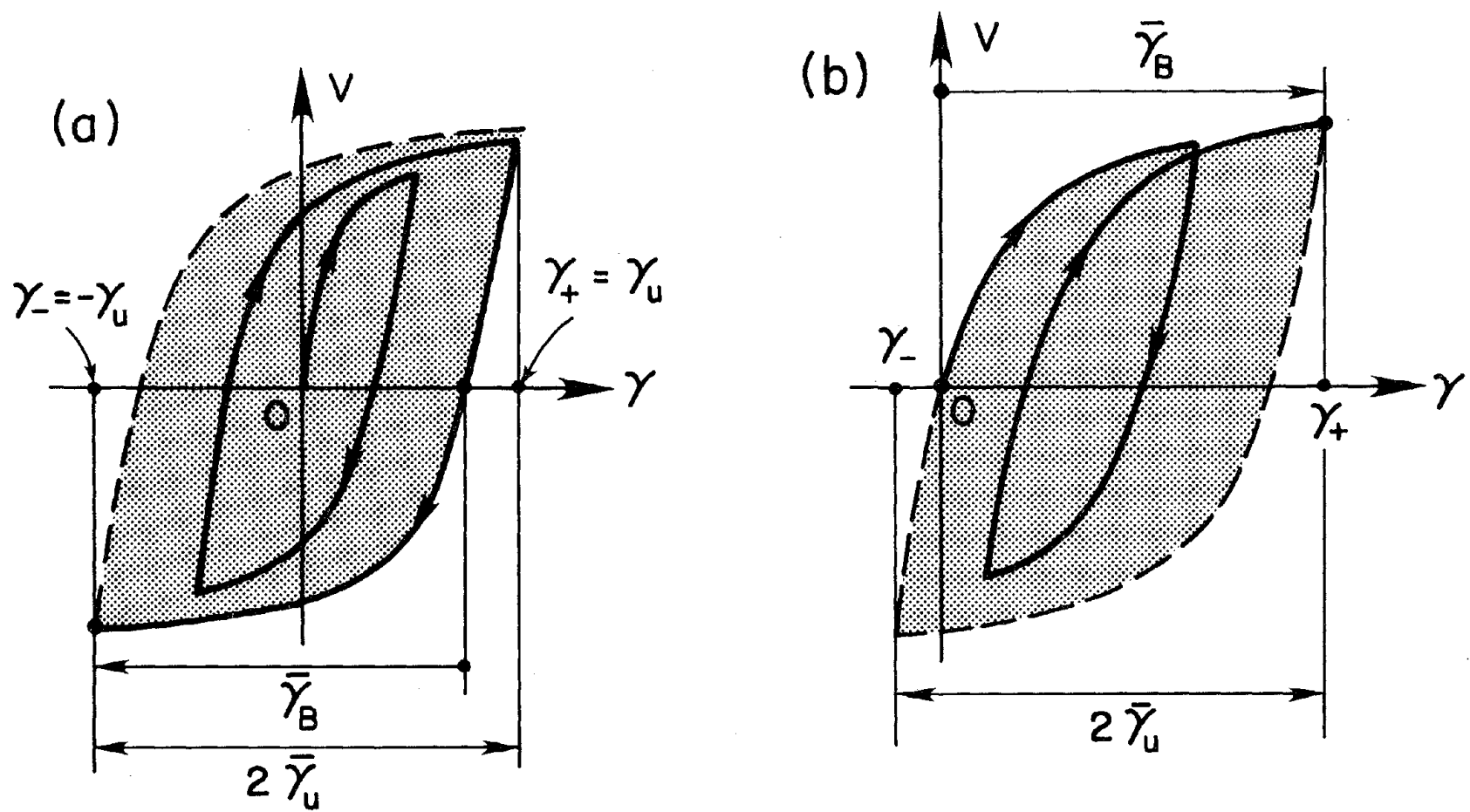
Fig. 8.8   Buckling Hysteretic Loop Envelops for Shear Link
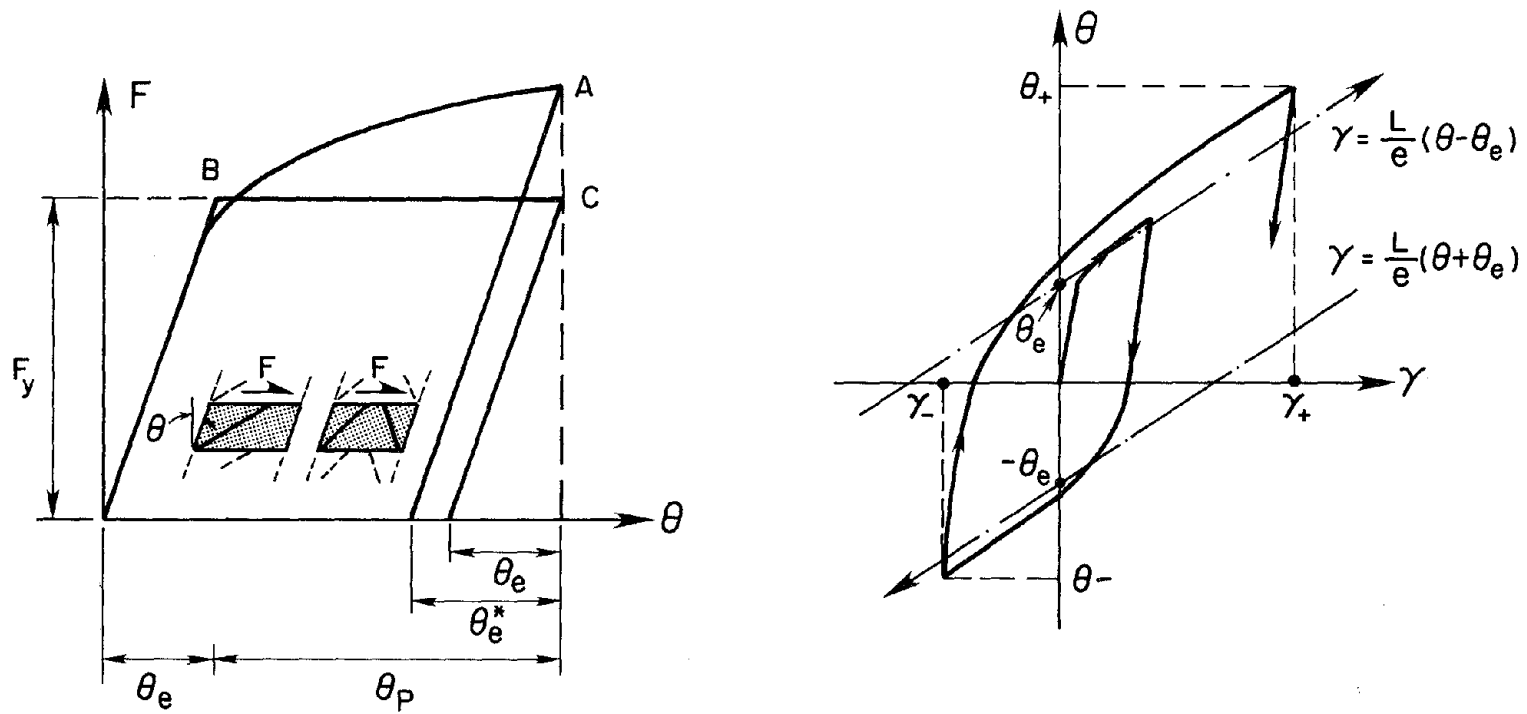
Fig. 8.9   (a) Typical Inelastic Lateral Force-Displacement Relationships for EBF panels, and

(b) Relationships Between EBF Story Drift θ and Link Deformation Angle γ
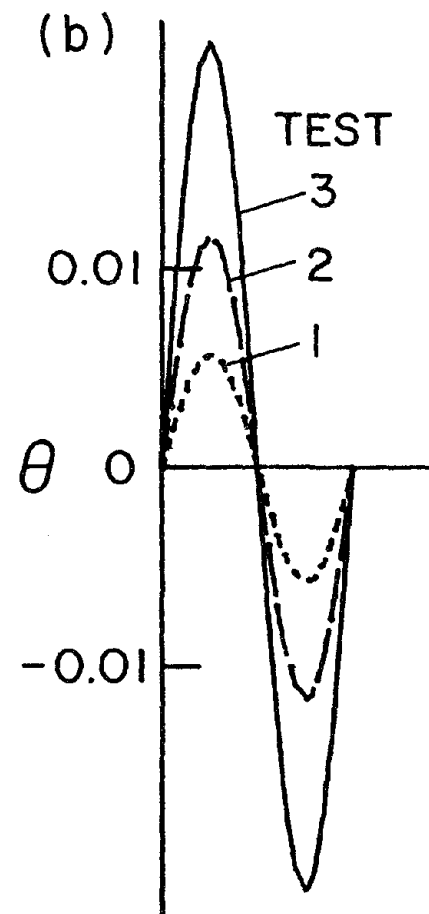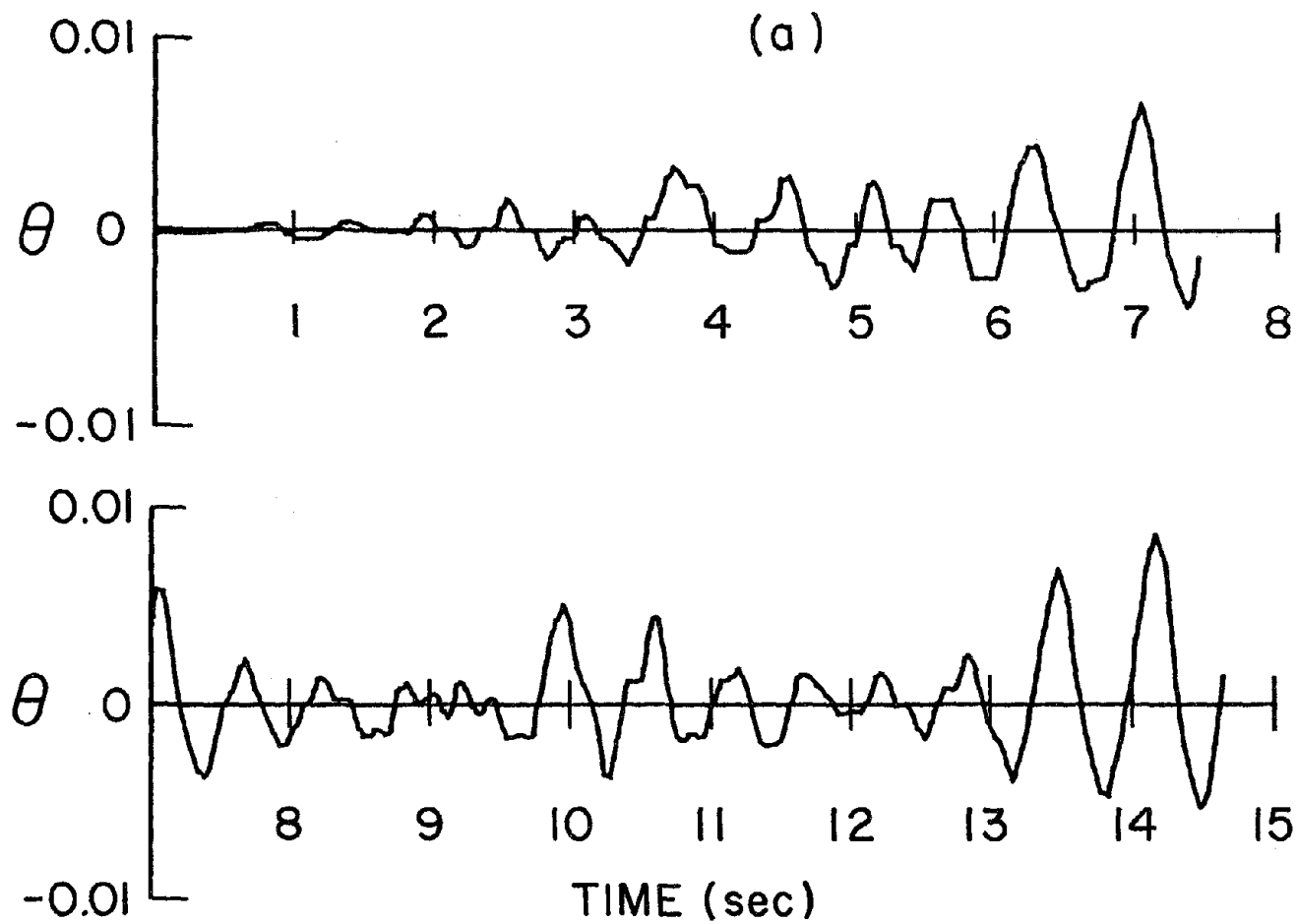
Fig. 8.10   History of 1st Story Drift of Full Scale 6-story Model during
(a) 0.5g Taft Test, and (b) Three Final Tests

APPENDIX

APPENDIX A

ADDITIONAL DETAILS ON

EXPERIMENTAL STUDY

A.1. Support Stiffness of Experimental Setup

As noted in Ref. 32, the tasks in an experimental investigation are first to model as accurately as possible the physical domain of the problem and then to excite the model in a meaningful way. Since it is seldom feasible to model a complete structure due to myriad of technical and economic difficulties, testing of carefully selected subassemblage as a part of the whole structure provides an attractive alternative.

The selected subassemblage in the present experimental investigation (see Chapter 6) was considered to simulate the interaction between the link and an EBF and yet the setup was quite simple. This section comments on the experimental behavior of the link supports which are important parts of the subassemblage for simulating the columns and beams adjacent to the link.

Fig. A.1(a) schematically shows the experimental setup employed. This model was used for preliminary design of the experimental setup and for the development of a nonlinear shear beam element briefly discussed in Appendix B. The spring stiffnesses K_{ϑ_A} and K_{Δ_A} of the support at A express, respectively, the rotational and translational stiffness. The moment of inertia along the beam $\overline{CE}$ varies due to the attachment of flange coverplates (Section 6.3).

A deformed subassemblage is shown in Fig. A.1(b), where ϑ_A, ϑ_B, and ϑ_D are the rotations at A, B, and D, respectively, and Δ_A is the displacement of the link end plate in the direction of the shear force applied to the link. The relationship between these displacements and the corresponding force quantities are shown in Fig. A.2. Fig. A.2(a) shows that the rotational stiffness of the support at link end A is about 9 times that the rotational stiffness provided by the beam at link end B. As noted in Section 6.3, this provides a good model for a typical ratio of a beam stiffness to that of a column for an EBF. Large bolts for connecting the end plates to the support, as shown in Fig. 6.4, were chosen in order to avoid a nonlinear relationship between bolt elongation and bolt axial force due to link end moment. As can be seen from Fig. A.2(a), in this manner the nonlinearity of the rotational springs was successfully kept a minimum.

The end moment at B, in addition to causing the rotation ϑ_B, also caused the rotation ϑ_D. the experimentally obtained elastic ratio between ϑ_B and ϑ_D was 1.7:1. This ratio agreeed very well with the theoretical prediction based on the model shown in Fig. A.1(a).

Fig. A.2(b) shows the relationship between the link shear force V and Δ_A, a translation of the link end A. The Δ_A can be decomposed into two parts: the one is due to the slip of end plates at A, and the other is due to the deformation of the bolts in direct contact with the end plate (see Fig. 6.4). The magnitude of Δ_A was kept under 0.005 in., thus, Δ_A was of negligible magnitude.

A.2. Axial Deformation of Links.

Fig. A.3 shows the axial shortening Δ_a of the link plotted against link transversal displacement δ for the specimens 3, 5, and 7 where no axial force was applied. Due to a relatively large deformation angle δ/e of the link, the

second order effect from such an angle can be recognized. It is interesting to note that without axial force, the link length increased with the number of cyclic excursions. Previously, a similar trend for ordinary beam was reported in Ref. 86. The link elongation was largest in the long link (Specimen 5) where it was about 0.04 in. at $\delta = 0$.

Ref. 54 discussed the second order rigid-plastic mechanism for an EBF. This study attempted to show the second order effect of large link deformation on the stability of an EBF under cyclic loading. The above findings suggest the need of considering the additional effect of link elongation. However, at this stage in research, it is not possible to accurately predict such elongations.

In Fig. A.3, a sudden increase in link shortening in the absence of axial load can be seen at the advanced stages of link loading. This is due to the severe flange buckling induced by the diagonal tension field formed after web buckling occurred. In the link axially loaded, as shown in Fig. A.4, the manner of axial shortening was completely different from that without axial force application. Significant shortening could be noted after severe flange buckling and subsequent web buckling. The shortening was greatest in the long link (Specimen 6), where in the final excursion $\Delta_a \approx 0.7$ in.

It is believed that shortening of the links after severe buckling would be reduced if a concrete slab is attached to the top of a link preventing axial deformation. Such an effect would be beneficial in reducing the deterioration of the link during postbuckling behavior.

APPENDIX B

INELASTIC MODELING OF

CYCLICALLY LOADED LINK

B.1. General

The inelastic response of an EBF is dominated by the behavior of the active link regions. Therefore, the accurate modeling of these elements is of great importance. Many formulations employed in the analysis of structural systems neglect the effect of shear on the structural members at either the elastic or the inelastic state. For an EBF, such modeling is inaccurate since high shear forces act in the active beam regions. Recognizing this, some models for active links were made previously taking into account both elastic and inelastic shear deformation of he beam.

Roeder [84] modeled the shear link as a sandwich beam [69] which assumes that the web resists shear force and the flanges risist moments. Bi-linear approximations of shear force - shear deformation and moment - bending rotation relationships were used to model strain-hardening. The parallel component model consisting of an elastic component and an elastic-perfectly plastic component was utilized. For shear, both isotropic and kinematic hardening effects were considered and their degrees of participation were empirically assigned. For moment, only the kinematic hardening effect was considered. Since moment capacity was defined by considering flange resistance only, it was reported that the model is appropriate only for the case where the link yields

primarily in shear and moments are small.

However, the newly obtained data explained in Chapters 6 and 7 indicate that shear links are generally exposed to both high moment and shear force, and the magnitudes of moment cannot be predicted by considering only flange resistance. Since moment estimates are also of great importance for EBF analysis, this element is not considered to be sufficient for proper EBF analysis. Moreover, some other unreasonable behavior of this element has been recognized.

Yang [98] modeled the active link as an inclined truss element in an effort to represent the shear link behavior including strain-hardening. However, this assumes the pure shear behavior of the link beam and equal end moments at both link ends. As discussed in Chapters 6 and 7, this cannot be the case for general analysis of EBFs.

Hjelmstad [32] developed the finite element model which, based on stress resultant formulation, uses the yield surface similar to the one proposed by Neal [61,62]. This model was used for EBF analysis in Chapters 4 and 5. On using this model for EBF analyses, however, it has been recognized that each link must be discretized into many elements, since the error in estimating moment becomes very large if a small number of elements are used. Obviously this is not an efficient approach for global analysis of EBFs. The element also ignores strain-hardening effect, important for ultimate design and analysis of EBFs.

B.2. Proposed Model

As discussed above, none of the elements were suitable for an efficient and yet accurate prediction of the link random cyclic behavior. One purpose of performing the link tests explained in Chapters 6 and 7 was to obtain basic information to permit simplification of analysis procedures and yet realistic modeling. As stated earlier, the behavior was quite simple in that the interaction between moment and shear is neglected. Being benefited from this simplification, it was decided to use constitutive relations of the link that are as realistic as possible. Accordingly, the simple bi-linear model was not considered, but a nonlinear curve fitting model was considered. Since the active link behavior usually governs the EBF behavior, for correct prediction of EBF behavior, such a constitutive model was considered to be appropriate. Previously, similar general constitutive models were proposed [11,14,15,17,30,38,39,55,56,64,67,75,76,82], among which the Ramberg-Osgood Model [82], Menegetto-Pinto Model [56], Dafalias-Popov Model [14,15], and Petersson-Popov Model [67] may be considered state of the art in this area. However, in order to efficiently match the special numerical algorithm developed for shear link modeling, another constitutive model was developed.

Also, for all nonlinear models, there was a severe limitation on their use for random cyclic constitutive relations, since the unloading-reloading process usually results in a large offset of the load-deflection behavior from the correct one. The models, therefore, were usually used for regular cyclic loading. Many attempts have been made to obtain a good algorithm to realistically simulate random behavior, but they have not been considered satisfactory. As an alternative solution, the author obtained a simplified and quite accurate updating method for the unloading-reloading process. The use of this updating method is

not limited to the nonlinear model developed by the author but also is applicable for the other nonlinear models. Fig. B.1 contrasts the random cyclic behaviors predicted by the previous [11,17] and proposed updating method. Although the size of memory required for both methods was comparable, remarkably better prediction by the latter method can be seen.

In this report, it is not intended to discuss this element in detail. The element is currently being modified for dynamic analysis. For the medium link specimen tested in Chapter 6, analysis by the proposed element was made. Fig. B.2 shows that the element can predict very accurately the cyclic behavior of links.
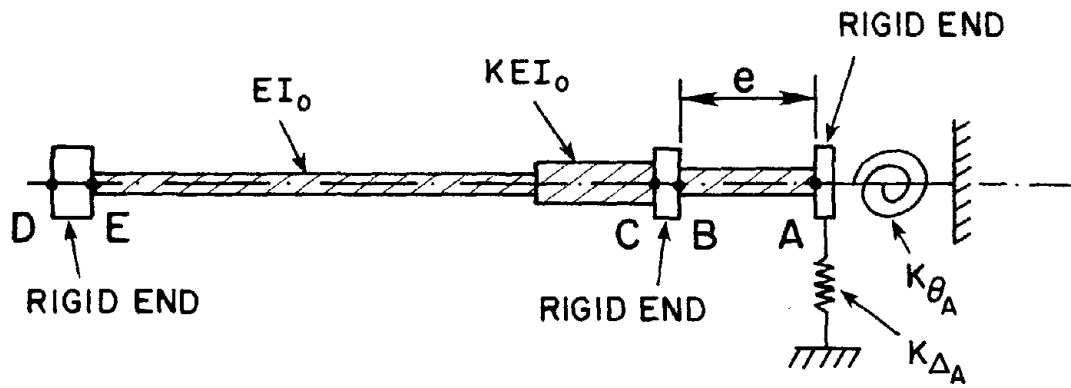
Fig. A.1   (a) Schematic Diagram of Experimental Setup.
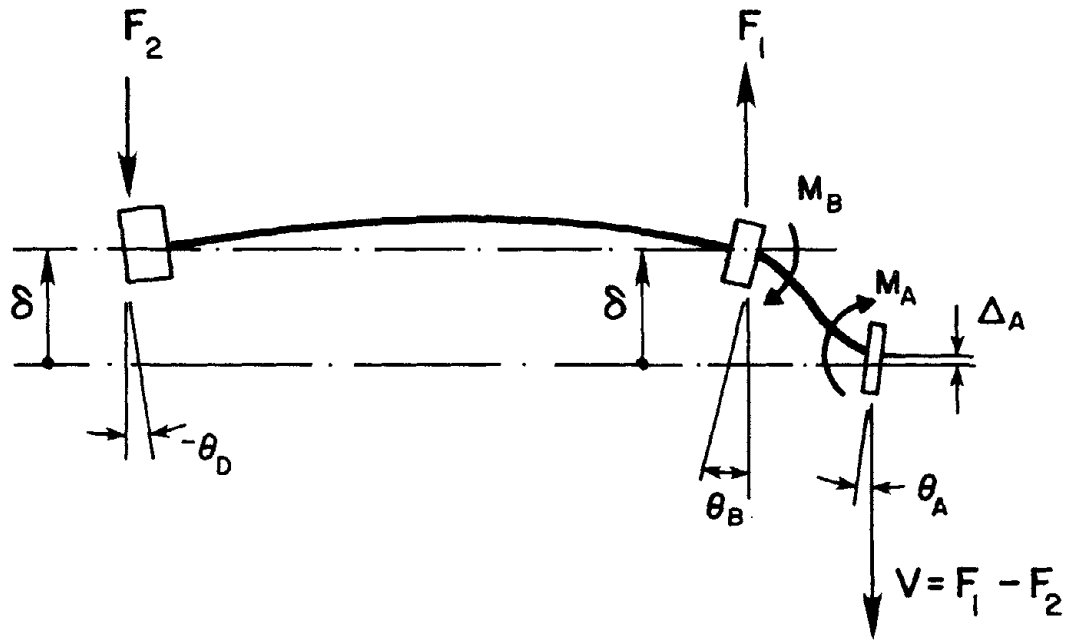
Fig. A.1   (b) Displacements and Rotations of Link Supports.
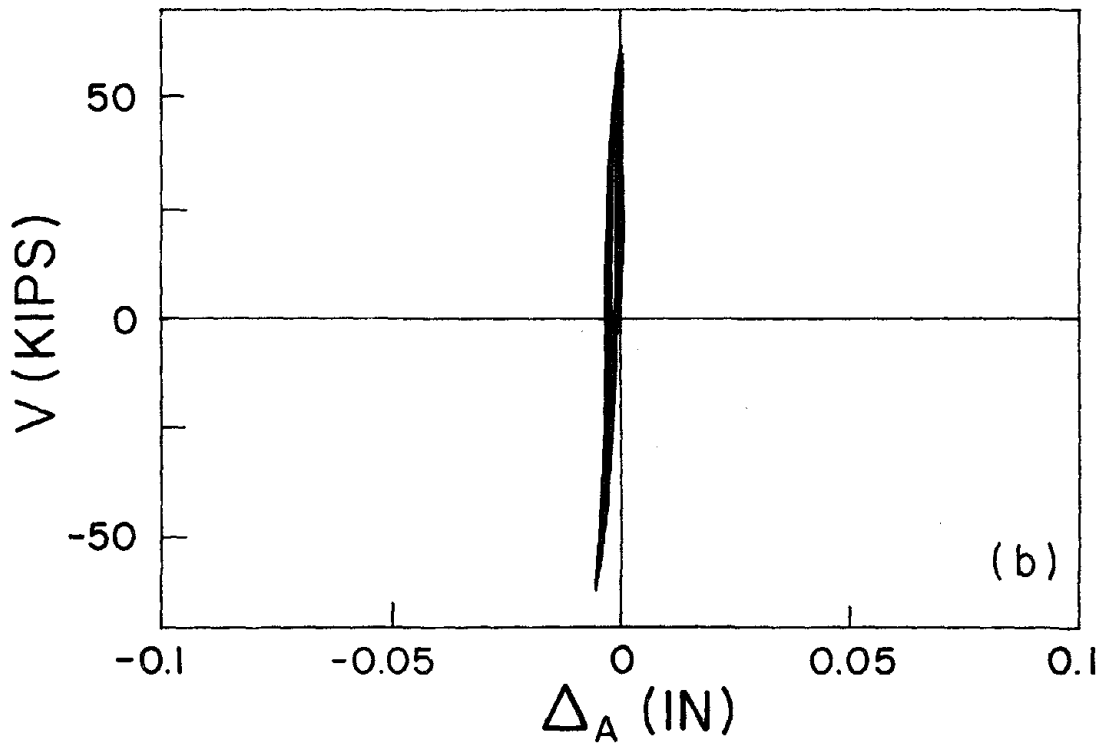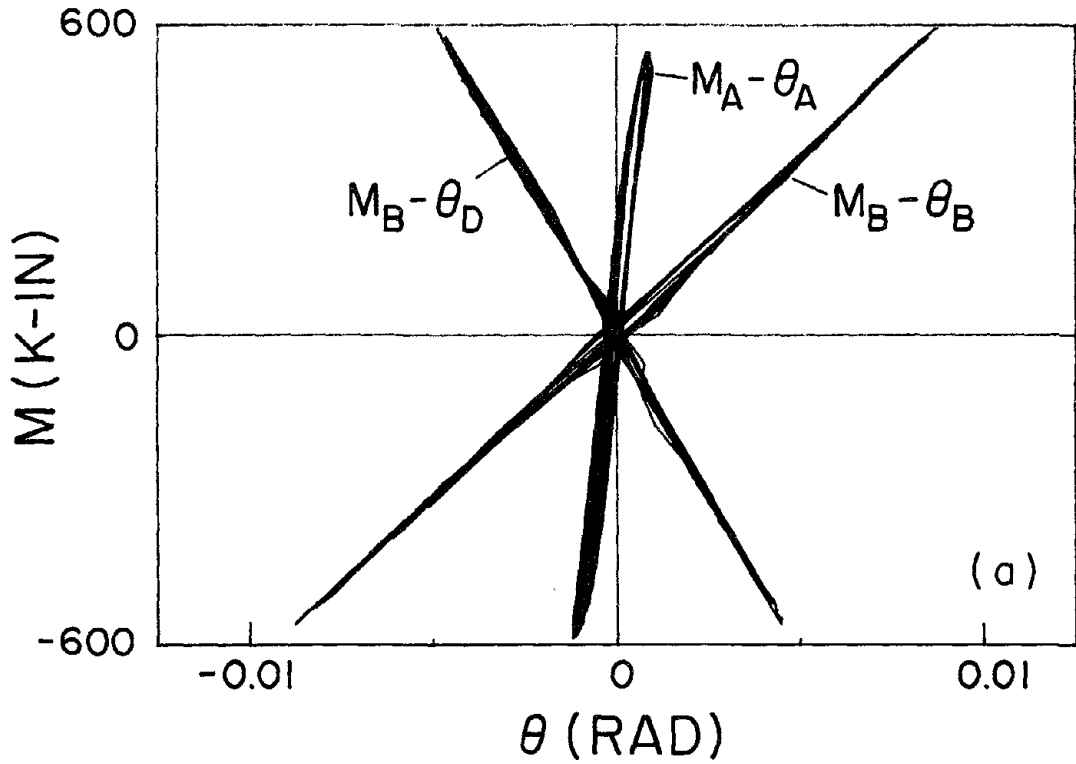
Fig. A.2   (a) Rotation of Link and Beam ends.

(b) In-Plane Movement Δ_A of West End Support.

SPECIMEN 3

SPECIMEN 5

Δ_a in

0.05

δ in

0.5   1.0

O
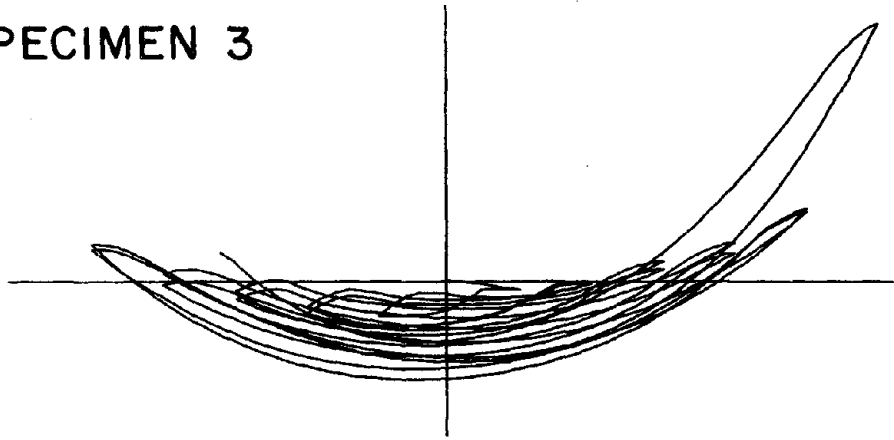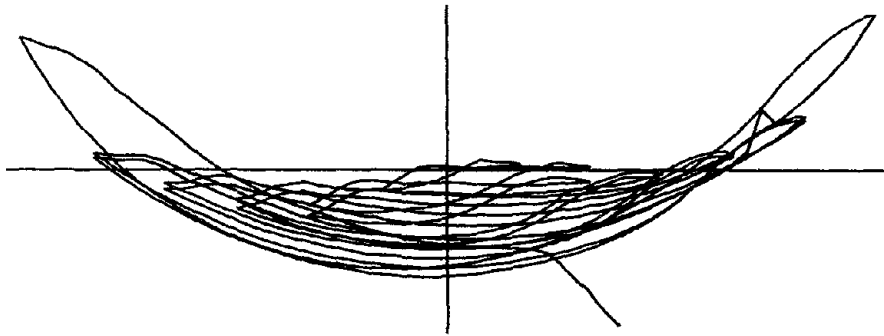
SPECIMEN 7

Fig. A.3   Link Contraction Δ_a vs. Link Lateral Displacement δ for Specimens with No

Axial Force (Specimens 3, 5, and 7).

SPECIMEN 3

SPECIMEN 5

SPECIMEN 7

SPECIMEN 4

Δ_a in

0.25

0

0.5   1.0

δ in
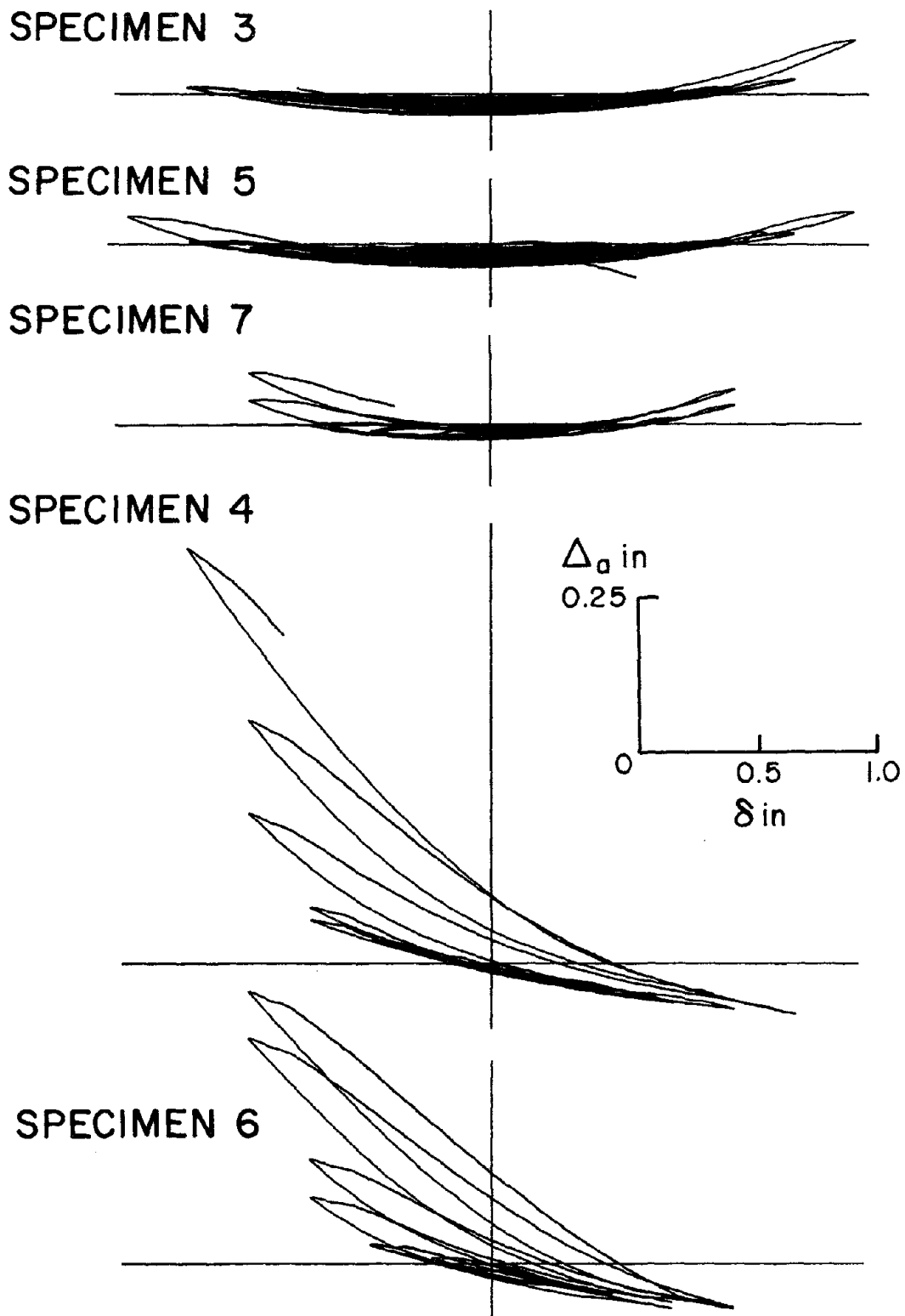
SPECIMEN 6

Fig. A.4   Comparisons of Link Contraction Δ_a vs. Link Lateral Displacement δ between

Specimens with No Axial Force (Specimens 3, 5, and 7) and with Axial Force

(Specimens 4 and 6).
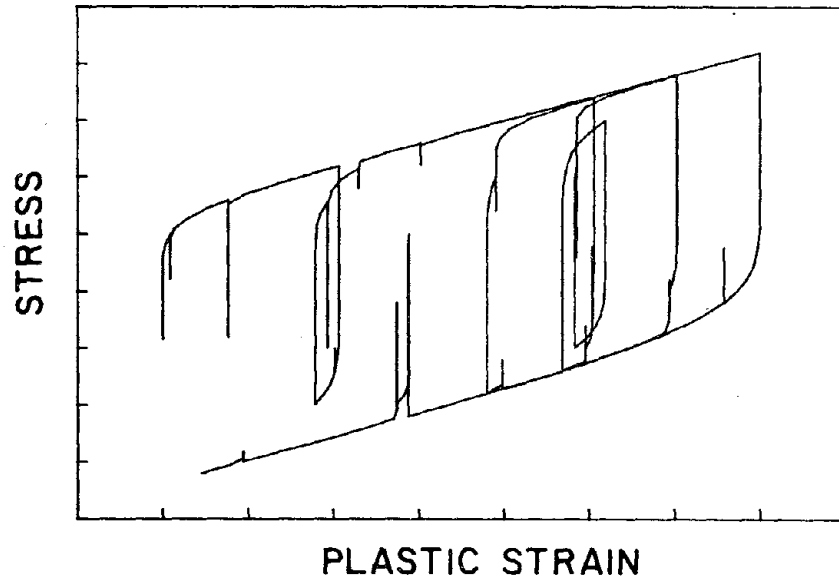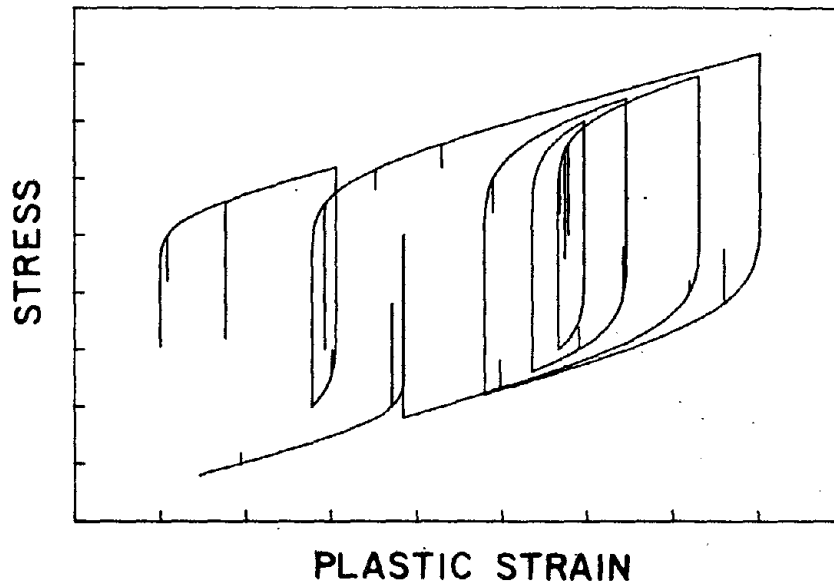
Fig. B.1   Comparison between Previous and Proposed Updating Methods.
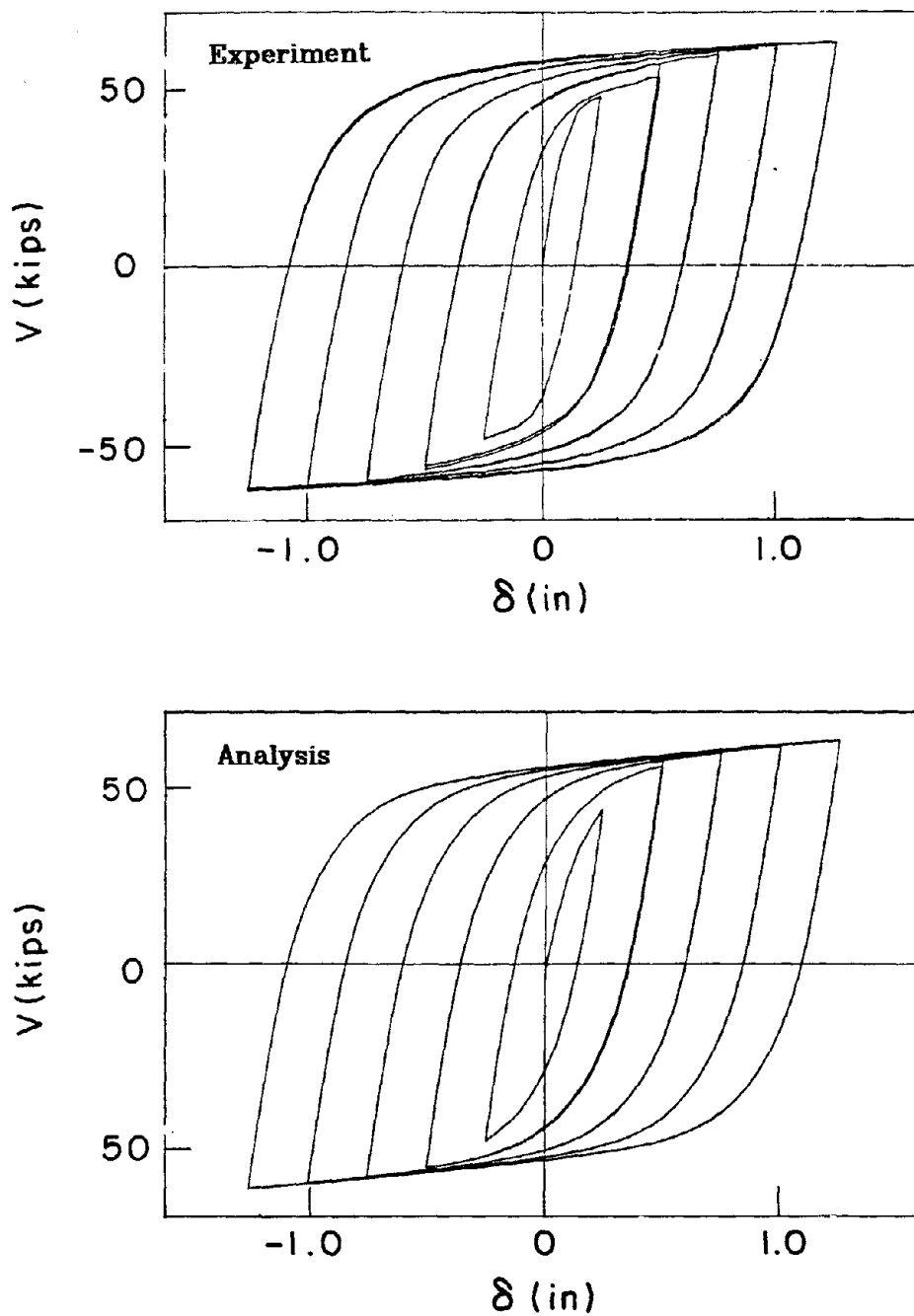
Fig. B.2   Comparison between Experimental Result and Analytical Prediction by Proposed Element.

NOTE: Numbers in parentheses are Accession Numbers assigned by the National Technical Information Service; these are followed by a price code. Copies of the reports may be ordered from the National Technical Information Service, 5285 Port Royal Road, Springfield, Virginia, 22161. Accession Numbers should be quoted on orders for reports (PB --- ---) and remittance must accompany each order. Reports without this information were not available at time of printing. The complete list of EERC reports (from EERC 67-1) is available upon request from the Earthquake Engineering Research Center, University of California, Berkeley, 47th Street and Hoffman Boulevard, Richmond, California 94804.

UCB/EERC-79/01 "Hysteretic Behavior of Lightweight Reinforced Concrete Beam-Column Subassemblages," by B. Forzani, E.P. Popov and V.V. Bertero - April 1979(PB 298 267)A06

UCB/EERC-79/02 "The Development of a Mathematical Model to Predict the Flexural Response of Reinforced Concrete Beams to Cyclic Loads, Using System Identification," by J. Stanton & H. McNiven - Jan. 1979(PB 295 875)A10

UCB/EERC-79/03 "Linear and Nonlinear Earthquake Response of Simple Torsionally Coupled Systems," by C.L. Kan and A.K. Chopra - Feb. 1979(PB 298 262)A06

UCB/EERC-79/04 "A Mathematical Model of Masonry for Predicting its Linear Seismic Response Characteristics," by Y. Mengi and H.D. McNiven - Feb. 1979(PB 298 266)A06

UCB/EERC-79/05 "Mechanical Behavior of Lightweight Concrete Confined by Different Types of Lateral Reinforcement," by M.A. Manrique, V.V. Bertero and E.P. Popov - May 1979(PB 301 114)A06

UCB/EERC-79/06 "Static Tilt Tests of a Tall Cylindrical Liquid Storage Tank," by R.W. Clough and A. Niwa - Feb. 1979 (PB 301 167)A06

UCB/EERC-79/07 "The Design of Steel Energy Absorbing Restrainers and Their Incorporation into Nuclear Power Plants for Enhanced Safety: Volume 1 - Summary Report," by P.N. Spencer, V.F. Zackay, and E.R. Parker - Feb. 1979(UCB/EERC-79/07)A09

UCB/EERC-79/08 "The Design of Steel Energy Absorbing Restrainers and Their Incorporation into Nuclear Power Plants for Enhanced Safety: Volume 2 - The Development of Analyses for Reactor System Piping,""Simple Systems" by M.C. Lee, J. Penzien, A.K. Chopra and K. Suzuki "Complex Systems" by G.H. Powell, E.L. Wilson, R.W. Clough and D.G. Row - Feb. 1979(UCB/EERC-79/08)A10

UCB/EERC-79/09 "The Design of Steel Energy Absorbing Restrainers and Their Incorporation into Nuclear Power Plants for Enhanced Safety: Volume 3 - Evaluation of Commercial Steels," by W.S. Owen, R.M.N. Pelloux, R.O. Ritchie, M. Faral, T. Ohhashi, J. Toplosky, S.J. Hartman, V.F. Zackay and E.R. Parker - Feb. 1979(UCB/EERC-79/09)A04

UCB/EERC-79/10 "The Design of Steel Energy Absorbing Restrainers and Their Incorporation into Nuclear Power Plants for Enhanced Safety: Volume 4 - A Review of Energy-Absorbing Devices," by J.M. Kelly and M.S. Skinner - Feb. 1979(UCB/EERC-79/10)A04

UCB/EERC-79/11 "Conservatism In Summation Rules for Closely Spaced Modes," by J.M. Kelly and J.L. Sackman - May 1979(PB 301 328)A03

UCB/EERC-79/12 "Cyclic Loading Tests of Masonry Single Piers; Volume 3 - Height to Width Ratio of 0.5," by P.A. Hidalgo, R.L. Mayes, H.D. McNiven and R.W. Clough - May 1979(PB 301 321)A08

UCB/EERC-79/13 "Cyclic Behavior of Dense Course-Grained Materials in Relation to the Seismic Stability of Dams," by N.G. Banerjee, H.B. Seed and C.K. Chan - June 1979(PB 301 373)A13

UCB/EERC-79/14 "Seismic Behavior of Reinforced Concrete Interior Beam-Column Subassemblages," by S. Viwathanatepa, E.P. Popov and V.V. Bertero - June 1979(PB 301 326)A10

UCB/EERC-79/15 "Optimal Design of Localized Nonlinear Systems with Dual Performance Criteria Under Earthquake Excitations," by M.A. Bhatti - July 1979(PB 80 167 109)A06

UCB/EERC-79/16 "OPTDYN - A General Purpose Optimization Program for Problems with or without Dynamic Constraints," by M.A. Bhatti, E. Polak and K.S. Pister - July 1979(PB 80 167 091)A05

UCB/EERC-79/17 "ANSR-II, Analysis of Nonlinear Structural Response, Users Manual," by D.P. Mondkar and G.H. Powell July 1979(PB 80 113 301)A05

UCB/EERC-79/18 "Soil Structure Interaction in Different Seismic Environments," A. Gomez-Masso, J. Lysmer, J.-C. Chen and H.B. Seed - August 1979(PB 80 101 520)A04

UCB/EERC-79/19 "ARMA Models for Earthquake Ground Motions," by M.K. Chang, J.W. Kwiatkowski, R.F. Nau, R.M. Oliver and K.S. Pister - July 1979(PB 301 166)A05

UCB/EERC-79/20 "Hysteretic Behavior of Reinforced Concrete Structural Walls," by J.M. Vallenas, V.V. Bertero and E.P. Popov - August 1979(PB 80 165 905)A12

UCB/EERC-79/21 "Studies on High-Frequency Vibrations of Buildings - 1: The Column Effect," by J. Lubliner - August 1979 (PB 80 158 553)A03

UCB/EERC-79/22 "Effects of Generalized Loadings on Bond Reinforcing Bars Embedded in Confined Concrete Blocks," by S. Viwathanatepa, E.P. Popov and V.V. Bertero - August 1979(PB 81 124 018)A14

UCB/EERC-79/23 "Shaking Table Study of Single-Story Masonry Houses, Volume 1: Test Structures 1 and 2," by P. Gülkan, R.L. Mayes and R.W. Clough - Sept. 1979 (HUD-000 1763)A12

UCB/EERC-79/24 "Shaking Table Study of Single-Story Masonry Houses, Volume 2: Test Structures 3 and 4," by P. Gülkan, R.L. Mayes and R.W. Clough - Sept. 1979 (HUD-000 1836)A12

UCB/EERC-79/25 "Shaking Table Study of Single-Story Masonry Houses, Volume 3: Summary, Conclusions and Recommendations," by R.W. Clough, R.L. Mayes and P. Gülkan - Sept. 1979 (HUD-000 1837)A06

UCB/EERC-79/26   "Recommendations for a U.S.-Japan Cooperative Research Program Utilizing Large-Scale Testing Facilities," by U.S.-Japan Planning Group - Sept. 1979(PB 301 407)A06

UCB/EERC-79/27   "Earthquake-Induced Liquefaction Near Lake Amatitlan, Guatemala," by H.B. Seed, I. Arango, C.K. Chan, A. Gomez-Masso and R. Grant de Ascoli - Sept. 1979(NUREG-CR1341)A03

UCB/EERC-79/28   "Infill Panels: Their Influence on Seismic Response of Buildings," by J.W. Axley and V.V. Bertero Sept. 1979(PB 80 163 371)A10

UCB/EERC-79/29   "3D Truss Bar Element (Type 1) for the ANSR-II Program," by D.P. Mondkar and G.H. Powell - Nov. 1979 (PB 80 169 709)A02

UCB/EERC-79/30   "2D Beam-Column Element (Type 5 - Parallel Element Theory) for the ANSR-II Program," by D.G. Row, G.H. Powell and D.P. Mondkar - Dec. 1979(PB 80 167 224)A03

UCB/EERC-79/31   "3D Beam-Column Element (Type 2 - Parallel Element Theory) for the ANSR-II Program," by A. Riahi, G.H. Powell and D.P. Mondkar - Dec. 1979(PB 80 167 216)A03

UCB/EERC-79/32   "On Response of Structures to Stationary Excitation," by A. Der Kiureghian - Dec. 1979(PB 80166 929)A03

UCB/EERC-79/33   "Undisturbed Sampling and Cyclic Load Testing of Sands," by S. Singh, H.B. Seed and C.K. Chan Dec. 1979(ADA 087 298)A07

UCB/EERC-79/34   "Interaction Effects of Simultaneous Torsional and Compressional Cyclic Loading of Sand," by P.M. Griffin and W.N. Houston - Dec. 1979(ADA 092 352)A15

UCB/EERC-80/01   "Earthquake Response of Concrete Gravity Dams Including Hydrodynamic and Foundation Interaction Effects," by A.K. Chopra, P. Chakrabarti and S. Gupta - Jan. 1980(AD-A087297)A10

UCB/EERC-80/02   "Rocking Response of Rigid Blocks to Earthquakes," by C.S. Yim, A.K. Chopra and J. Penzien - Jan. 1980 (PB80 166 002)A04

UCB/EERC-80/03   "Optimum Inelastic Design of Seismic-Resistant Reinforced Concrete Frame Structures," by S.W. Zagajeski and V.V. Bertero - Jan. 1980(PB80 164 635)A06

UCB/EERC-80/04   "Effects of Amount and Arrangement of Wall-Panel Reinforcement on Hysteretic Behavior of Reinforced Concrete Walls," by R. Iliya and V.V. Bertero - Feb. 1980(PB81 122 525)A09

UCB/EERC-80/05   "Shaking Table Research on Concrete Dam Models," by A. Niwa and R.W. Clough - Sept. 1980(PB81122 368)A06

UCB/EERC-80/06   "The Design of Steel Energy-Absorbing Restrainers and their Incorporation into Nuclear Power Plants for Enhanced Safety (Vol 1A): Piping with Energy Absorbing Restrainers: Parameter Study on Small Systems," by G.H. Powell, C. Oughourlian and J. Simons - June 1980

UCB/EERC-80/07   "Inelastic Torsional Response of Structures Subjected to Earthquake Ground Motions," by Y. Yamazaki April 1980(PB81 122 327)A08

UCB/EERC-80/08   "Study of X-Braced Steel Frame Structures Under Earthquake Simulation," by Y. Ghanaat - April 1980 (PB81 122 335)A11

UCB/EERC-80/09   "Hybrid Modelling of Soil-Structure Interaction," by S. Gupta, T.W. Lin, J. Penzien and C.S. Yeh May 1980(PB81 122 319)A07

UCB/EERC-80/10   "General Applicability of a Nonlinear Model of a One Story Steel Frame," by B.I. Sveinsson and H.D. McNiven - May 1980(PB81 124 877)A06

UCB/EERC-80/11   "A Green-Function Method for Wave Interaction with a Submerged Body," by W. Kioka - April 1980 (PB81 122 269)A07

UCB/EERC-80/12   "Hydrodynamic Pressure and Added Mass for Axisymmetric Bodies," by F. Nilrat - May 1980(PB81 122 343)A08

UCB/EERC-80/13   "Treatment of Non-Linear Drag Forces Acting on Offshore Platforms," by B.V. Dao and J. Penzien May 1980(PB81 153 413)A07

UCB/EERC-80/14   "2D Plane/Axisymmetric Solid Element (Type 3 - Elastic or Elastic-Perfectly Plastic) for the ANSR-II Program," by D.P. Mondkar and G.H. Powell - July 1980(PB81 122 350)A03

UCB/EERC-80/15   "A Response Spectrum Method for Random Vibrations," by A. Der Kiureghian - June 1980(PB81122 301)A03

UCB/EERC-80/16   "Cyclic Inelastic Buckling of Tubular Steel Braces," by V.A. Zayas, E.P. Popov and S.A. Mahin June 1980(PB81 124 885)A10

UCB/EERC-80/17   "Dynamic Response of Simple Arch Dams Including Hydrodynamic Interaction," by C.S. Porter and A.K. Chopra - July 1980(PB81 124 000)A13

UCB/EERC-80/18   "Experimental Testing of a Friction Damped Aseismic Base Isolation System with Fail-Safe Characteristics," by J.M. Kelly, K.E. Beucke and M.S. Skinner - July 1980(PB81 148 595)A04

UCB/EERC-80/19   "The Design of Steel Energy-Absorbing Restrainers and their Incorporation into Nuclear Power Plants for Enhanced Safety (Vol 1B): Stochastic Seismic Analyses of Nuclear Power Plant Structures and Piping Systems Subjected to Multiple Support Excitations," by M.C. Lee and J. Penzien - June 1980

UCB/EERC-80/20   "The Design of Steel Energy-Absorbing Restrainers and their Incorporation into Nuclear Power Plants for Enhanced Safety (Vol 1C): Numerical Method for Dynamic Substructure Analysis," by J.M. Dickens and E.L. Wilson - June 1980

UCB/EERC-80/21   "The Design of Steel Energy-Absorbing Restrainers and their Incorporation into Nuclear Power Plants for Enhanced Safety (Vol 2): Development and Testing of Restraints for Nuclear Piping Systems," by J.M. Kelly and M.S. Skinner - June 1980

UCB/EERC-80/22   "3D Solid Element (Type 4-Elastic or Elastic-Perfectly-Plastic) for the ANSR-II Program," by D.P. Mondkar and G.H. Powell - July 1980(PB81 123 242)A03

UCB/EERC-80/23   "Gap-Friction Element (Type 5) for the ANSR-II Program," by D.P. Mondkar and G.H. Powell - July 1980 (PB81 122 285)A03

UCB/EERC-80/24   "U-Bar Restraint Element (Type 11) for the ANSR-II Program," by C. Oughourlian and G.H. Powell
July 1980(PB81 122 293)A03

UCB/EERC-80/25   "Testing of a Natural Rubber Base Isolation System by an Explosively Simulated Earthquake," by
J.M. Kelly - August 1980(PB81 201 360)A04

UCB/EERC-80/26   "Input Identification from Structural Vibrational Response," by Y. Hu - August 1980(PB81 152 308)A05

UCB/EERC-80/27   "Cyclic Inelastic Behavior of Steel Offshore Structures," by V.A. Zayas, S.A. Mahin and E.P. Popov
August 1980(PB81 196 180)A15

UCB/EERC-80/28   "Shaking Table Testing of a Reinforced Concrete Frame with Biaxial Response," by M.G. Oliva
October 1980(PB81 154 304)A10

UCB/EERC-80/29   "Dynamic Properties of a Twelve-Story Prefabricated Panel Building," by J.G. Bouwkamp, J.P. Kollegger
and R.M. Stephen - October 1980(PB82 117 128)A06

UCB/EERC-80/30   "Dynamic Properties of an Eight-Story Prefabricated Panel Building," by J.G. Bouwkamp, J.P. Kollegger
and R.M. Stephen - October 1980(PB81 200 313)A05

UCB/EERC-80/31   "Predictive Dynamic Response of Panel Type Structures Under Earthquakes," by J.P. Kollegger and
J.G. Bouwkamp - October 1980(PB81 152 316)A04

UCB/EERC-80/32   "The Design of Steel Energy-Absorbing Restrainers and their Incorporation into Nuclear Power Plants
for Enhanced Safety (Vol 3): Testing of Commercial Steels in Low-Cycle Torsional Fatigue," by
P. Spencer, E.R. Parker, E. Jongewaard and M. Drory

UCB/EERC-80/33   "The Design of Steel Energy-Absorbing Restrainers and their Incorporation into Nuclear Power Plants
for Enhanced Safety (Vol 4): Shaking Table Tests of Piping Systems with Energy-Absorbing Restrainers,"
by S.F. Stiemer and W.G. Godden - Sept. 1980

UCB/EERC-80/34   "The Design of Steel Energy-Absorbing Restrainers and their Incorporation into Nuclear Power Plants
for Enhanced Safety (Vol 5): Summary Report," by P. Spencer

UCB/EERC-80/35   "Experimental Testing of an Energy-Absorbing Base Isolation System," by J.M. Kelly, M.S. Skinner and
K.E. Beucke - October 1980(PB81 154 072)A04

UCB/EERC-80/36   "Simulating and Analyzing Artificial Non-Stationary Earthquake Ground Motions," by R.F. Nau, R.M. Oliver
and K.S. Pister - October 1980(PB81 153 397)A04

UCB/EERC-80/37   "Earthquake Engineering at Berkeley - 1980," - Sept. 1980(PB81 205 874)A09

UCB/EERC-80/38   "Inelastic Seismic Analysis of Large Panel Buildings," by V. Schricker and G.H. Powell - Sept. 1980
(PB81 154 338)A13

UCB/EERC-80/39   "Dynamic Response of Embankment, Concrete-Gravity and Arch Dams Including Hydrodynamic Interaction,"
by J.F. Hall and A.K. Chopra - October 1980(PB81 152 324)A11

UCB/EERC-80/40   "Inelastic Buckling of Steel Struts Under Cyclic Load Reversal," by R.G. Black, W.A. Wenger and
E.P. Popov - October 1980(PB81 154 312)A08

UCB/EERC-80/41   "Influence of Site Characteristics on Building Damage During the October 3, 1974 Lima Earthquake," by
P. Repetto, I. Arango and H.B. Seed - Sept. 1980(PB81 161 739)A05

UCB/EERC-80/42   "Evaluation of a Shaking Table Test Program on Response Behavior of a Two Story Reinforced Concrete
Frame," by J.M. Blondet, R.W. Clough and S.A. Mahin

UCB/EERC-80/43   "Modelling of Soil-Structure Interaction by Finite and Infinite Elements," by F. Medina -
December 1980(PB81 229 270)A04

UCB/EERC-81/01   "Control of Seismic Response of Piping Systems and Other Structures by Base Isolation," edited by J.M.
Kelly - January 1981 (PB81 200 735)A05

UCB/EERC-81/02   "OPTNSR - An Interactive Software System for Optimal Design of Statically and Dynamically Loaded
Structures with Nonlinear Response," by M.A. Bhatti, V. Ciampi and K.S. Pister - January 1981
(PB81 218 851)A09

UCB/EERC-81/03   "Analysis of Local Variations in Free Field Seismic Ground Motions," by J.-C. Chen, J. Lysmer and H.B.
Seed - January 1981 (AD-A099508)A13

UCB/EERC-81/04   "Inelastic Structural Modeling of Braced Offshore Platforms for Seismic Loading," by V.A. Zayas,
P.-S.B. Shing, S.A. Mahin and E.P. Popov - January 1981(PB82 138 777)A07

UCB/EERC-81/05   "Dynamic Response of Light Equipment in Structures," by A. Der Kiureghian, J.L. Sackman and B. Nour-
Omid - April 1981 (PB81 218 497)A04

UCB/EERC-81/06   "Preliminary Experimental Investigation of a Broad Base Liquid Storage Tank," by J.G. Bouwkamp, J.P.
Kollegger and R.M. Stephen - May 1981(PB82 140 385)A03

UCB/EERC-81/07   "The Seismic Resistant Design of Reinforced Concrete Coupled Structural Walls," by A.E. Aktan and V.V.
Bertero - June 1981(PB82 113 358)A11

UCB/EERC-81/08   "The Undrained Shearing Resistance of Cohesive Soils at Large Deformations," by M.R. Pyles and H.B.
Seed - August 1981

UCB/EERC-81/09   "Experimental Behavior of a Spatial Piping System with Steel Energy Absorbers Subjected to a Simulated
Differential Seismic Input," by S.F. Stiemer, W.G. Godden and J.M. Kelly - July 1981

UCB/EERC-81/10   "Evaluation of Seismic Design Provisions for Masonry in the United States," by B.I. Sveinsson, R.L. Mayes and H.D. McNiven - August 1981 (PB82 166 075)A08

UCB/EERC-81/11   "Two-Dimensional Hybrid Modelling of Soil-Structure Interaction," by T.-J. Tzong, S. Gupta and J. Penzien - August 1981(PB82 142 118)A04

UCB/EERC-81/12   "Studies on Effects of Infills in Seismic Resistant R/C Construction," by S. Brokken and V.V. Bertero - September 1981 (PB82 166 190)A09

UCB/EERC-81/13   "Linear Models to Predict the Nonlinear Seismic Behavior of a One-Story Steel Frame," by H. Valdimarsson, A.H. Shah and H.D. McNiven - September 1981(PB82 138 793)A07

UCB/EERC-81/14   "TLUSH: A Computer Program for the Three-Dimensional Dynamic Analysis of Earth Dams," by T. Kagawa, L.H. Mejia, H.B. Seed and J. Lysmer - September 1981(PB82 139 940)A06

UCB/EERC-81/15   "Three Dimensional Dynamic Response Analysis of Earth Dams," by L.H. Mejia and H.B. Seed - September 1981 (PB82 137 274)A12

UCB/EERC-81/16   "Experimental Study of Lead and Elastomeric Dampers for Base Isolation Systems," by J.M. Kelly and S.B. Hodder - October 1981 (PB82 166 182)A05

UCB/EERC-81/17   "The Influence of Base Isolation on the Seismic Response of Light Secondary Equipment," by J.M. Kelly - April 1981 (PB82 255 266)A04

UCB/EERC-81/18   "Studies on Evaluation of Shaking Table Response Analysis Procedures," by J. Marcial Blondet - November 1981 (PB82 197 278)A10

UCB/EERC-81/19   "DELIGHT.STRUCT: A Computer-Aided Design Environment for Structural Engineering," by R.J. Balling, K.S. Pister and E. Polak - December 1981 (PB82 218 496)A07

UCB/EERC-81/20   "Optimal Design of Seismic-Resistant Planar Steel Frames," by R.J. Balling, V. Ciampi, K.S. Pister and E. Polak - December 1981 (PB82 220 179)A07

UCB/EERC-82/01   "Dynamic Behavior of Ground for Seismic Analysis of Lifeline Systems," by T. Sato and A. Der Kiureghian - January 1982 (PB82 218 926)A05

UCB/EERC-82/02   "Shaking Table Tests of a Tubular Steel Frame Model," by Y. Ghanaat and R. W. Clough - January 1982 (PB82 220 161)A07

UCB/EERC-82/03   "Behavior of a Piping System under Seismic Excitation: Experimental Investigations of a Spatial Piping System supported by Mechanical Shock Arrestors and Steel Energy Absorbing Devices under Seismic Excitation," by S. Schneider, H.-M. Lee and W. G. Godden - May 1982 (PB83 172 544)A09

UCB/EERC-82/04   "New Approaches for the Dynamic Analysis of Large Structural Systems," by E. L. Wilson - June 1982 (PB83 148 080)A05

UCB/EERC-82/05   "Model Study of Effects of Damage on the Vibration Properties of Steel Offshore Platforms," by F. Shahrivar and J. G. Bouwkamp - June 1982 (PB83 148 742)A10

UCB/EERC-82/06   "States of the Art and Practice in the Optimum Seismic Design and Analytical Response Prediction of R/C Frame-Wall Structures," by A. E. Aktan and V. V. Bertero - July 1982 (PB83 147 736)A05

UCB/EERC-82/07   "Further Study of the Earthquake Response of a Broad Cylindrical Liquid-Storage Tank Model," by G. C. Manos and R. W. Clough - July 1982 (PB83 147 744)A11

UCB/EERC-82/08   "An Evaluation of the Design and Analytical Seismic Response of a Seven Story Reinforced Concrete Frame - Wall Structure," by F. A. Charney and V. V. Bertero - July 1982(PB83 157 628)A09

UCB/EERC-82/09   "Fluid-Structure Interactions: Added Mass Computations for Incompressible Fluid," by J. S.-H. Kuo - August 1982 (PB83 156 281)A07

UCB/EERC-82/10   "Joint-Opening Nonlinear Mechanism: Interface Smeared Crack Model," by J. S.-H. Kuo - August 1982 (PB83 149 195)A05

UCB/EERC-82/11   "Dynamic Response Analysis of Techi Dam," by R. W. Clough, R. M. Stephen and J. S.-H. Kuo - August 1982 (PB83 147 496)A06

UCB/EERC-82/12   "Prediction of the Seismic Responses of R/C Frame-Coupled Wall Structures," by A. E. Aktan, V. V. Bertero and M. Piazza - August 1982 (PB83 149 203)A09

UCB/EERC-82/13   "Preliminary Report on the SMART 1 Strong Motion Array in Taiwan," by B. A. Bolt, C. H. Loh, J. Penzien, Y. B. Tsai and Y. T. Yeh - August 1982 (PB83 159 400)A10

UCB/EERC-82/14   "Shaking-Table Studies of an Eccentrically X-Braced Steel Structure," by M. S. Yang - September 1982 (PB83 260 778)A12

UCB/EERC-82/15   "The Performance of Stairways in Earthquakes," by C. Roha, J. W. Axley and V. V. Bertero - September 1982 (PB83 157 693)A07

UCB/EERC-82/16   "The Behavior of Submerged Multiple Bodies in Earthquakes," by W.-G. Liao - Sept. 1982 (PB83 158 709)A07

UCB/EERC-82/17   "Effects of Concrete Types and Loading Conditions on Local Bond-Slip Relationships," by A. D. Cowell, E. P. Popov and V. V. Bertero - September 1982 (PB83 153 577)A04

UCB/EERC-82/18 "Mechanical Behavior of Shear Wall Vertical Boundary Members: An Experimental Investigation," by M. T. Wagner and V. V. Bertero - October 1982 (PB83 159 764)A05

UCB/EERC-82/19 "Experimental Studies of Multi-support Seismic Loading on Piping Systems," by J. M. Kelly and A. D. Cowell - November 1982

UCB/EERC-82/20 "Generalized Plastic Hinge Concepts for 3D Beam-Column Elements," by P. F.-S. Chen and G. H. Powell - November 1982 (PB83 247 981)A13

UCB/EERC-82/21 "ANSR-III: General Purpose Computer Program for Nonlinear Structural Analysis," by C. V. Oughourlian and G. H. Powell - November 1982 (PB83 251 330)A12

UCB/EERC-82/22 "Solution Strategies for Statically Loaded Nonlinear Structures," by J. W. Simons and G. H. Powell - November 1982 (PB83 197 970)A06

UCB/EERC-82/23 "Analytical Model of Deformed Bar Anchorages under Generalized Excitations," by V. Ciampi, R. Eligehausen, V. V. Bertero and E. P. Popov - November 1982 (PB83 169 532)A06

UCB/EERC-82/24 "A Mathematical Model for the Response of Masonry Walls to Dynamic Excitations," by H. Sucuoğlu, Y. Mengi and H. D. McNiven - November 1982 (PB83 169 011)A07

UCB/EERC-82/25 "Earthquake Response Considerations of Broad Liquid Storage Tanks," by F. J. Cambra - November 1982 (PB83 251 215)A09

UCB/EERC-82/26 "Computational Models for Cyclic Plasticity, Rate Dependence and Creep," by B. Mosaddad and G. H. Powell - November 1982 (PB83 245 829)A08

UCB/EERC-82/27 "Inelastic Analysis of Piping and Tubular Structures," by M. Mahasuverachai and G. H. Powell - November 1982 (PB83 249 987)A07

UCB/EERC-83/01 "The Economic Feasibility of Seismic Rehabilitation of Buildings by Base Isolation," by J. M. Kelly - January 1983 (PB83 197 988)A05

UCB/EERC-83/02 "Seismic Moment Connections for Moment-Resisting Steel Frames," by E. P. Popov - January 1983 (PB83 195 412)A04

UCB/EERC-83/03 "Design of Links and Beam-to-Column Connections for Eccentrically Braced Steel Frames," by E. P. Popov and J. O. Malley - January 1983 (PB83 194 811)A04

UCB/EERC-83/04 "Numerical Techniques for the Evaluation of Soil-Structure Interaction Effects in the Time Domain," by E. Bayo and E. L. Wilson - February 1983 (PB83 245 605)A09

UCB/EERC-83/05 "A Transducer for Measuring the Internal Forces in the Columns of a Frame-Wall Reinforced Concrete Structure," by R. Sause and V. V. Bertero - May 1983 (PB84 119 494)A06

UCB/EERC-83/06 "Dynamic Interactions between Floating Ice and Offshore Structures," by P. Croteau - May 1983 (PB84 119 486)A16

UCB/EERC-83/07 "Dynamic Analysis of Multiply Tuned and Arbitrarily Supported Secondary Systems," by T. Igusa and A. Der Kiureghian - June 1983 (PB84 118 272)A11

UCB/EERC-83/08 "A Laboratory Study of Submerged Multi-body Systems in Earthquakes," by G. R. Ansari - June 1983 (PB83 261 842)A17

UCB/EERC-83/09 "Effects of Transient Foundation Uplift on Earthquake Response of Structures," by C.-S. Yim and A. K. Chopra - June 1983 (PB83 261 396)A07

UCB/EERC-83/10 "Optimal Design of Friction-Braced Frames under Seismic Loading," by M. A. Austin and K. S. Pister - June 1983 (PB84 119 288)A06

UCB/EERC-83/11 "Shaking Table Study of Single-Story Masonry Houses: Dynamic Performance under Three Component Seismic Input and Recommendations," by G. C. Manos, R. W. Clough and R. L. Mayes - June 1983

UCB/EERC-83/12 "Experimental Error Propagation in Pseudodynamic Testing," by P. B. Shing and S. A. Mahin - June 1983 (PB84 119 270)A09

UCB/EERC-83/13 "Experimental and Analytical Predictions of the Mechanical Characteristics of a 1/5-scale Model of a 7-story R/C Frame-Wall Building Structure," by A. E. Aktan, V. V. Bertero, A. A. Chowdhury and T. Nagashima - August 1983 (PB84 119 213)A07

UCB/EERC-83/14 "Shaking Table Tests of Large-Panel Precast Concrete Building System Assemblages," by M. G. Oliva and R. W. Clough - August 1983

UCB/EERC-83/15 "Seismic Behavior of Active Beam Links in Eccentrically Braced Frames," by K. D. Hjelmstad and E. P. Popov - July 1983 (PB84 119 676)A09

UCB/EERC-83/16 "System Identification of Structures with Joint Rotation," by J. S. Dimsdale and H. D. McNiven - July 1983

UCB/EERC-83/17 "Construction of Inelastic Response Spectra for Single-Degree-of-Freedom Systems," by S. Mahin and J. Lin - July 1983

UCB/EERC-83/18 "Interactive Computer Analysis Methods for Predicting the Inelastic Cyclic Behaviour of Structural
                Sections," by S. Kaba and S. Mahin - July 1983 (PB84 192 012) A06

UCB/EERC-83/19 "Effects of Bond Deterioration on Hysteretic Behavior of Reinforced Concrete Joints," by F.C. Filippou,
                E.P. Popov and V.V. Bertero - August 1983 (PB84 192 020) A10

UCB/EERC-83/20 "Analytical and Experimental Correlation of Large-Panel Precast Building System Performance," by M.G.
                Oliva, R.W. Clough, M. Velkov, P. Gavrilovic and J. Petrovski - November 1983

UCB/EERC-83/21 "Mechanical Characteristics of Materials Used in a 1/5 Scale Model of a 7-Story Reinforced Concrete
                Test Structure," by V.V. Bertero, A.E. Aktan, H.G. Harris and A.A. Chowdhury - September 1983
                (PB84 193 697) A05

UCB/EERC-83/22 "Hybrid Modelling of Soil-Structure Interaction in Layered Media," by T.-J. Tzong and J. Penzien -
                October 1983 (PB84 192 178) A08

UCB/EERC-83/23 "Local Bond Stress-Slip Relationships of Deformed Bars under Generalized Excitations," by R. Eligehausen,
                E.P. Popov and V.V. Bertero - October 1983 (PB84 192 848) A09

UCB/EERC-83/24 "Design Considerations for Shear Links in Eccentrically Braced Frames," by J.O. Malley and E.P. Popov -
                November 1983 (PB84 192 186) A07

UCB/EERC-84/01 "Pseudodynamic Test Method for Seismic Performance Evaluation: Theory and Implementation," by P.-S. B.
                Shing and S. A. Mahin - January 1984 (PB84 190 644) A08

UCB/EERC-84/02 "Dynamic Response Behavior of Xiang Hong Dian Dam," by R.W. Clough, K.-T. Chang, H.-Q. Chen, R.M.
                Stephen, G.-L. Wang, and Y. Ghanaat - April 1984

UCB/EERC-84/03 "Refined Modelling of Reinforced Concrete Columns for Seismic Analysis," by S.A. Kaba and S.A. Mahin -
                April, 1984

UCB/EERC-84/04 "A New Floor Response Spectrum Method for Seismic Analysis of Multiply Supported Secondary Systems,"
                by A. Asfura and A. Der Kiureghian - June 1984

UCB/EERC-84/05 "Earthquake Simulation Tests and Associated Studies of a 1/5th-scale Model of a 7-Story R/C Frame-Wall
                Test Structure," by V.V. Bertero, A.E. Aktan, F.A. Charney and R. Sause - June 1984

UCB/EERC-84/06 "R/C Structural Walls: Seismic Design for Shear," by A.E. Aktan and V.V. Bertero

UCB/EERC-84/07 "Behavior of Interior and Exterior Flat-Plate Connections subjected to Inelastic Load Reversals," by
                H.L. Zee and J.P. Moehle

UCB/EERC-84/08 "Experimental Study of the Seismic Behavior of a two-story Flat-Plate Structure," by J.W. Diebold and
                J.P. Moehle

UCB/EERC-84/09 "Phenomenological Modeling of Steel Braces under Cyclic Loading," by K. Ikeda, S.A. Mahin and
                S.N. Dermitzakis - May 1984

UCB/EERC-84/10 "Earthquake Analysis and Response of Concrete Gravity Dams," by G. Fenves and A.K. Chopra - August 1984

UCB/EERC-84/11 "EAGD-84: A Computer Program for Earthquake Analysis of Concrete Gravity Dams," by G. Fenves and
                A.K. Chopra - August 1984

UCB/EERC-84/12 "A Refined Physical Theory Model for Predicting the Seismic Behavior of Braced Steel Frames," by
                K. Ikeda and S.A. Mahin - July 1984

UCB/EERC-84/13 "Earthquake Engineering Research at Berkeley - 1984" - August 1984

UCB/EERC-84/14 "Moduli and Damping Factors for Dynamic Analyses of Cohesionless Soils," by H.B. Seed, R.T. Wong,
                I.M. Idriss and K. Tokimatsu - September 1984

UCB/EERC-84/15 "The Influence of SPT Procedures in Soil Liquefaction Resistance Evaluations," by H. B. Seed,
                K. Tokimatsu, L. F. Harder and R. M. Chung - October 1984

UCB/EERC-84/16 "Simplified Procedures for the Evaluation of Settlements in Sands Due to Earthquake Shaking,"
                by K. Tokimatsu and H. B. Seed - October 1984

UCB/EERC-84/17 "Evaluation and Improvement of Energy Absorption Characteristics of Bridges under Seismic
                Conditions," by R. A. Imbsen and J. Penzien - November 1984

UCB/EERC-84/18 "Structure-Foundation Interactions under Dynamic Loads," by W. D. Liu and J. Penzien - November
                1984

UCB/EERC-84/19 "Seismic Modelling of Deep Foundations," by C.-H. Chen and J. Penzien - November 1984

UCB/EERC-84/20 "Dynamic Response Behavior of Quan Shui Dam," by R. W. Clough, K.-T. Chang, H.-Q. Chen, R. M. Stephen,
                Y. Ghanaat and J.-H. Qi - November 1984

UCB/EERC-85/01 "Simplified Methods of Analysis for Earthquake Resistant Design of Buildings," by E.F. Cruz and
A.K. Chopra - Feb. 1985 (PB86 112299/AS) A12

UCB/EERC-85/02 "Estimation of Seismic Wave Coherency and Rupture Velocity using the SMART 1 Strong-Motion Array
Recordings," by N.A. Abrahamson - March 1985

UCB/EERC-85/03 "Dynamic Properties of a Thirty Story Condominium Tower Building," by R.M. Stephen, E.L. Wilson and
N. Stander - April 1985 (PB86 118965/AS) A06

UCB/EERC-85/04 "Development of Substructuring Techniques for On-Line Computer Controlled Seismic Performance
Testing," by S. Dermitzakis and S. Mahin - February 1985 (PB86 132941/AS) A08

UCB/EERC-85/05 "A Simple Model for Reinforcing Bar Anchorages under Cyclic Excitations," by F.C. Filippou - March
1985 (PB86 112919/AS) A05

UCB/EERC-85/06 "Racking Behavior of Wood-Framed Gypsum Panels under Dynamic Load," by M.G. Oliva - June 1985

UCB/EERC-85/07 "Earthquake Analysis and Response of Concrete Arch Dams," by K.-L. Fok and A.K. Chopra - June 1985
(PB86 139672/AS) A10

UCB/EERC-85/08 "Effect of Inelastic Behavior on the Analysis and Design of Earthquake Resistant Structures," by
J.P. Lin and S.A. Mahin - June 1985 (PB86 135340/AS) A08

UCB/EERC-85/09 "Earthquake Simulator Testing of Base Isolated Bridge Deck Superstructures," by J.M. Kelly and
I.G. Buckle

UCB/EERC-85/10 "Simplified Analysis for Earthquake Resistant Design of Concrete Gravity Dams," by G. Fenves and
A.K. Chopra - September 1985

UCB/EERC-85/11 "Dynamic Interaction Effects in Arch Dams," by R.W. Clough, K.-T. Chang, H.-Q. Chen and Y. Ghanaat -
October 1985 (PB86 135027/AS) A05

UCB/EERC-85/12 "Dynamic Response of Long Valley Dam in the Mammoth Lake Earthquake Series of May 25-27, 1980," by
S. Lai and H.B. Seed - November 1985 (PB86 142304/AS) A05

UCB/EERC-85/13 "A Methodology for Computer-Aided Design of Earthquake-Resistant Steel Structures," by M.A. Austin,
K.S. Pister and S.A. Mahin - December 1985 (PB86 159480/AS) A10

UCB/EERC-85/14 "Response of Tension-Leg Platforms to Vertical Seismic Excitations," by G.-S. Liou, J. Penzien and
R.W. Yeung - December 1985

UCB/EERC-85/15 "Cyclic Loading Tests of Masonry Single Piers: Volume 4 - Additional Tests with Height to Width
Ratio of 1," by H. Sucuoglu, H.D. McNiven and B. Sveinsson - December 1985

UCB/EERC-85/16 "An Experimental Program for Studying the Dynamic Response of a Steel Frame with a Variety of Infill
Partitions," by B. Yanev and H.D. McNiven - December 1985

UCB/EERC-86/01 "A Study of Seismically Resistant Eccentrically Braced Steel Frame Systems," by K. Kasai and E.P. Popov -
January 1986